Chitosan-based aerogels and cryogels for wound healing applications

Coraline Chartier

PSL UNIVERSITÉ PARIS

THÈSE DE DOCTORAT
DE L'UNIVERSITÉ PSL

Préparée à Mines Paris - PSL

Chitosan-based aerogels and cryogels for wound healing applications

Aérogels et cryogels à base de chitosane pour le pansement des plaies

Soutenue par
Coraline CHARTIER
Le 17 mars 2023

Dirigée par
Tatiana BUDTOVA
Benjamin NOTTELET

Co-encadrée par
Hélène VAN DEN BERGHE

École doctorale n° 364
Sciences Fondamentales et Appliquées

Spécialité
Mécanique, Numérique et Matériaux

Composition du jury :

Yves, GROHENS Professeur des universités Université Bretagne Sud	*Président*
Audrey, TOURRETTE Maître de conférence Université de Toulouse	*Rapporteur*
Luc, PICTON Professeur, Université de Rouen	*Rapporteur*
Carlos, GARCIA GONZALES Professeur Université de Santiago de Compostella	*Examinateur*
Sytze, BUWALDA Chargé de recherche Cemef – Mines Paris - PSL	*Examinateur*
Hélène, VAN DEN BERGHE Maître de conférence Université de Montpellier	*Examinatrice*
Benjamin, NOTTELET Professeur des universités Université de Montpellier	*Directeur de thèse*
Tatiana, BUDTOVA Directeur de recherche Cemef – Mines Paris - PSL	*Directrice de thèse*

MINES PARIS | PSL

Acknowledgements

En premier lieu j'aimerai remercier mes encadrants : Tania pour sa disponibilité, Benjamin pour son efficacité en réunion, Hélène pour sa gentillesse, et Sytze pour ses qualités de rédaction d'introduction.

I would like to thank the members of my evaluation committee for their comments and the very interesting discussion we had. Thanks to Yves Grohens, Carlos Garcia Gonzales and especially Luc Picton and Audrey Tourette for being my reviewers and writing complete reviews of my manuscript.

I would also like to thank our partners from Utrecht University for the nice work we did together with Tina Vermonden, Martina Viola and Blessing Ilochonwu. The month spent in your lab was a really great experience scientifically and humanly.

Un énorme merci à Christophe pour toute ton aide et toutes les discussions que nous avons eu. Merci pour ton soutien pour toutes les manips qui sortaient de l'ordinaire, la coagulation, l'ex vivo et notre tentative de mise en place de l'in vivo. J'ai énormément appris à tes côtés et tu as été d'un soutien sans faille jusqu'au bout de cette aventure.

Merci Audrey pour tout le temps que tu as passé sur mes manips mais également à me former. Un grand merci pour ta patience et ta gentillesse.

Un grand merci également à tout le personnel du Cemef et Persee pour leur aide et soutien au cours de ces 3 années. Un merci tout particulier à Suzanne pour son aide sur le MEB, à Pierre et Julien pour le séchage supercritique.

Merci à toute l'équipe PHBM de m'avoir si bien accueillie, ces 3 mois à vos côtés ont été un vrai plaisir.

Merci également à Morgane Evin et Pierre Jean Arnoux du LBA à Marseille pour m'avoir donné l'opportunité de faire des tests ex vivo.

Merci également à mes amis et ma famille de m'avoir soutenue.

Table des matières

General introduction

The aging of the population [1] is leading to health problems that are major medical and economic challenges for states [2]. Chronic wounds are one of them, affecting 37 million people worldwide, they represent a growing market of 10 billion dollars in 2019, estimated to reach 16 billion dollars by 2027 [3]. Chronic wound are those that remain in inflammatory stage, showing no sign of healing after 6 weeks, potentially associated with complications such as infections, amputation, and death [4]. Recommendations of treatment are made by the Wound Healing Society [5–9] like using hyperbaric oxygen therapy to reduce the risk of major amputation or select a dressing that manage wound exudate to avoid maceration and wound enlargement, but there is currently no efficient treatment. New wound dressings should be developed to fill these gaps. It should be a dressing which could prevent and/or treat infections, provide a better comfort for the patient and enhance the wound healing process.

Dressings can be developed with improved properties, for example, based on advanced porous materials. A porous material allows gasses such as O_2 and CO_2 to go through, allows to absorb a large amount of exudate from the wound and, depending on the selected material, allows to heal the wound at the same time. In this regard, aerogels and cryogels are appealing materials because they present a high porosity (≥ 90%) which is open and interconnected. These materials are obtained by removing solvent from gels, either by drying with supercritical CO_2 to preserve the structure leading to "aerogel" or *via* freeze-drying to obtain a porous material with macropores named "cryogel". Both types of materials are proposed for wound dressing applications [10,11]. However, considering that dressing colonization by the cells must be prevented to avoid removal of the new cells at each dressing change, aerogels appear as a sounder choice. They present two scales of porosity: mesopores and small macropores, i.e., from 2 nm to few micrometers; such pores sizes are smaller than cell diameter. Aerogels present a low density (< 0.1 g/cm^3) and a high specific surface area (> 100 m^2/g), they can be made with silica [12], synthetic [13] or natural [14,15] polymers. These properties are obtained thanks to drying the aerogel precursors with supercritical CO_2. During this drying, the capillary pressure, that leads to the collapse of the gel pore walls, is theoretically zero, and the structure of the gel is kept intact. This is in contrast with freeze drying where the growth of ice crystals often damages the structure and leads to the formation of large pores with low specific surface area.

Aerogels have been first prepared by sol-gel method by Kistler et al [1] in 1931 from silica gels, using supercritical conditions to remove the solvent. In the last twenty years, a new generation of aerogels was developed: they are based on biomass (bio-aerogels) and are usually based on polysaccharides. Polysaccharides are abundant, inexpensive and most of them are biocompatible making them suitable for various biomedical applications. To make a bio-aerogel the polymer is dissolved, then gelled (this step can be omitted for some polysaccharides); a solvent-exchange step is often necessary to perform a supercritical drying (usually with CO_2). Several polysaccharides have been used to prepare bio-aerogels such as pectin [16], cellulose [17], starch [18], alginate [15] and chitosan [15,19,20].

With the aim to develop a dressing to treat chronic wounds, in this work chitosan was chosen due to unique features compared to most other dressing materials that have a passive role in wound healing. Chitosan has antimicrobial effects, it participates to the healing process through various mechanisms including enhanced hemostatis and easier remodeling during the inflammatory and proliferative phases, and it can be used as a carrier of various drugs of interest for wound healing [21–25]. Chitosan is a pseudo-natural polysaccharide obtained by the deacetylation of chitin. Composed of N-acetyl-D-glucosamine and D-glucosamine units linked by glycosidic bonds in β (1→ 4), its amine groups give it antibacterial, antifungal, and antiviral properties. Porous chitosan is already used in biomedical field as a hemostatic dressing [26,27] in life threatening situations, but was never employed for mid- or long-term treatment of wounds. Research is ongoing to develop porous chitosan dressing

with for examples asymmetric membrane [28] but they present pore size large enough to let the cells colonize it. Complexes with alginate and chitosan [29,30] loaded with usnic acid or chitosan aerogel beads loaded with vancomycin [25] were made to treat infection in chronic wounds but 20 to 50% of the drug is not released and the healing was not improved; no *in vivo* trials were performed. Despite the interest in chitosan aerogels for biomedical application [31], none is commercially available to our knowledge.

The design of a new aerogel dressing improving healing is therefore the topic of the present work that was financed by the CNRS and took place in the framework of a transversal thesis between two laboratories, the Center for Material Forming (CEMEF) of Mines Paris in Sophia Antipolis and the Institut des Biomolécules Max Mousseron (IBMM) of Montpellier university in Montpellier.

The goal of this work is to define a range of targeted properties and then understand the correlation between the process and the final structure/properties to develop a material with adapted characteristics. The most optimal materials have to be tested in relation with the targeted biomedical application first with a drug release and then an *in vitro* study.

The manuscript is divided into five chapters as following:

The first chapter is devoted to literature review on the topic related to the work. It presents different pathways to obtain a dry porous material from a polysaccharide network, and the properties of the final product are described. First, the general pathway to make bio-based aerogels are described and their applications are presented as a function of the polymer used. The second part of this chapter is dedicated to the description of chitosan, its physico-chemical properties, the ways of shaping and the processes to obtain porous dry material based on chitosan. Then, the state of the art of chitosan aero- and cryogels applications in the three main biomedical domains, e.g., tissue engineering, drug delivery and wound dressing, is established. The requirements for each application are detailed. Finally, the skin structure and the wound healing steps are described.

The second chapter describes the materials and experiments. Details on preparation pathways of chitosan aerogels and cryogels are provided. The methods of characterization are specified. The mechanical characterization by Dynamic Mechanical Thermal Analysis (DMTA) and uniaxial compression are described. Finally, the *in vitro* drug release conditions of dexamethasone phosphate and ascorbic acid 2-phosphate are detailed, as well as the conditions used for the biological tests.

The third chapter concerns a study of the coagulation kinetics of chitosan solution using two methods: via optical camera and via DMTA, by following the evolution of the modulus in time. The influence of the chitosan concentration on the coagulation kinetics is evaluated and a model to predict the evolution of the mechanical properties during the coagulation from optical data is proposed. This chapter brings a better understanding of this phenomenon and can gives keys for processing, like 3D printing, with chitosan solutions with non-optimized rheological properties.

The fourth chapter studies the influence of the process parameters on the morphology and properties of the dry porous materials. The parameters of interest include the chitosan concentration in solution, the concentration of NaOH in the coagulating bath, the non-solvent used to be miscible with CO_2 for supercritical drying and the type of drying (with supercritical CO_2 or freeze-drying). We also look more specifically at the mechanical properties of aerogels and cryogels during cycles of uniaxial loading. Finally, the influence of the humidity and of the (an)isotropy of the coagulation front on the mechanical properties is analysed using DMTA.

Chapter five focuses on the biomedical applications of chitosan aerogels and cryogels. The samples are impregnated with dexamethasone phosphate which is an anti-inflammatory agent or with ascorbic acid-2-phosphate, two drugs of interest for wound healing. The release kinetics of the drugs is followed in time and the influence of the chitosan concentration, of the non-solvent used for solvent

exchange, of the type of drying and of the pH of the release medium are evaluated. Finally, biological *in vitro* tests for aerogels loaded with ascorbic acid are presented to demonstrate the absence of cytotoxicity of the dressing and its ability to promote collagen synthesis and wound healing.

The last part of the manuscript concludes on the work performed and shows the perspectives.

The work on aerogels impregnated by dexamethasone phosphate presented in the chapter V was performed within “Aeromed” project (n°44898RA) in the frame of PHC Van Gogh program sponsored by Campus France. We thank all the partners from the Division of Pharmaceutics of the Utrecht Institute for Pharmaceutical Sciences (UIPS) of Utrecht University (Utrecht, The Netherlands) that were involved in the project. We would like to thank Pierre Ilbizan and Julien Jaxel (PERSEE, Mines Paris, France) for drying with supercritical CO_2, Christophe Pradille (Mat Xper, Valbonne, France) for his help on mechanical tests and their analysis, and Audrey Bethry (IBMM, Montpellier, France) for setting up the biological in vitro tests.

Introduction générale

Le vieillissement de la population [1] engendre des problèmes de santé qui constituent des défis médicaux et économiques majeurs pour les Etats [2]. Les plaies chroniques sont l'un d'entre eux, touchant 37 millions de personne dans le monde, elles représentent un marché en croissance de 10 milliards de dollars en 2019 et estimé à 16 milliards de dollars en 2027 [3]. Ce sont des plaies au stade inflammatoire, qui ne présentent aucun signe de cicatrisation après 6 semaines. Elles peuvent entrainer des complications comme des infections, l'amputation du membre, et la mort [4]. La Wound Healing society recommande plusieurs traitements [5–9] comme utiliser l'oxygénothérapie hyperbare pour réduire le risque d'amputation, ou sélectionner un pansement qui adapté à la quantité d'exsudat produit par la plaie pour éviter la macération et l'élargissement de la plaie, mais il n'y a actuellement aucun traitement efficace. De nouveaux pansements doivent être développer pour répondre à ce besoin. Ces pansements devront prévenir et/ou traiter les infections, être confortable pour le patient et améliorer la cicatrisation.

Des pansements avec des propriétés améliorées peuvent être développés, par exemple, sur la base de matériaux poreux de pointe. Un matériau poreux est perméable aux gaz comme l'O_2 et le CO_2, il permet d'absorber de larges quantités d'exsudat de la plaie et, selon le matériau choisi, améliore la cicatrisation en simultané. Dans ce sens, les aérogels et les cryogels sont des matériaux attrayants car ils présentent une haute porosité (≥ 90%) qui est ouverte et interconnectée. Les structures sont obtenues en retirant le solvant des gels, soit par séchage au CO_2 supercritique pour préserver la structure, ce qui donne des « aérogels », soit par lyophilisation pour obtenir des matériaux poreux nommés « cryogels » avec des macropores. Les deux matériaux sont proposés pour des applications de pansement [10,11]. Cependant, la colonisation des pansements par les cellules devant être empêchée pour ne pas détruire les nouvelles cellules à chaque changement de pansement, les aérogels semblent être plus adaptés. Ils présentent deux échelles de porosité : les mésopores et les macropores, avec des tailles de pore, allant de 2 nm jusqu'à quelques micromètres, qui sont inférieures à celui du diamètre des cellules d'environ 10 µm. Les aérogels présentent une faible densité (< 0.1 g/cm^3) et une haute surface spécifique (> 100 m^2/g), ils sont fait de silice [12], polymère synthétiques [13] ou naturels [14,15]. Ces propriétés sont obtenues grâce au séchage des précurseurs d'aérogels avec du CO_2 supercritique. Durant ce séchage, la pression capillaire, qui engendre un écrasement des pores, est théoriquement égale à 0, et la structure du gel est gardé intacte. C'est en contraste avec la lyophilisation pour laquelle lors de l'étape de gélation la croissance des cristaux de glace endommage les structures et mène à la formation de larges pores avec des surfaces spécifiques faible.

Les aérogels ont été pour la première fois préparés avec la méthode de sol-gel par Kistler [1] en 1931 à partir de gels de silice en utilisant les conditions supercritiques pour enlever le solvant. Au cours des vingt dernières années, une nouvelle génération d'aérogels obtenus à partir de la biomasse (bio-aérogels) sont développés ; ils sont généralement faits à partir de polysaccharides. Les polysaccharides sont abondants, bons marchés, et biocompatibles ce qui les rend aptes pour diverses applications biomédicales. Pour faire des bio-aérogels, le polymère est dissout puis gélifié (cette étape peut être omise pour certains polysaccharides) ; une étape d'échange de solvant est souvent nécessaire pour pouvoir réaliser un séchage supercritique (souvent avec du CO_2). Plusieurs polysaccharides ont été utilisés pour préparer des bio-aérogels tel que la pectine [16], la cellulose [17], l'amidon [18], l'alginate [15] et le chitosane [15,19,20].

Avec l'objectif de développer un pansement pour plaie chroniques, le chitosane a été choisi pour ce travail pour ses propriétés uniques par rapport à la plupart des autres matériaux de pansement qui jouent un rôle passif dans la cicatrisation. Le chitosane possède des propriétés antimicrobiennes, il participe à la cicatrisation au travers plusieurs mécanismes tel que l'amélioration de l'hémostase et un remodelage plus facile au cours des phases inflammatoire et proliférative, de plus, il peut être utilisé support pour de nombreux principes actifs pour la cicatrisation [21–25]. Le chitosane est un

polysaccharide pseudo-naturel obtenu par la désacétylation de chitine. Il est composé d'unités de N-acétyle-D-glucosamine et de D- glucosamine liées par une liaison glycosidique en β (1→ 4). C'est son groupe amine qui lui confère des propriétés antibactériennes, antifongiques et antivirales. Le chitosane poreux est déjà utilisé dans le domaine biomédical en tant que pansement hémostatique [26,27] de danger de mort mais jamais utilisé pour des traitements à moyen ou long terme de plaie. Le développement de pansement à base d'aérogels de chitosane est en cours avec par exemple des membranes asymétriques [28] mais elles présente une porosité assez large pour que les cellules colonisent le pansement. Des complexes avec de l'alginate et du chitosane [29,30] chargés d'acide usnique ou des billes d'aérogels chargées avec de la vancomycine [25] ont été développées pour traiter les infections dans les plaies chroniques mais 20 à 50% du médicament est piégé dans le réseau et la cicatrisation n'est pas améliorée et aucun essai *in vivo* n'a été réalisé. Malgré l'intérêt porté aux aérogels de chitosane pour une application biomédicale [31], aucun n'est actuellement commercialisé à notre connaissance.

Le développement de nouveaux pansement basé sur des aérogels améliorant la cicatrisation est donc le sujet de ces travaux qui ont été financés par le CNRS, et réalisés dans le cadre d'une thèse transverse entre deux laboratoires, le Centre de Mise en Forme des Matériaux (CEMEF) à Sophia Antipolis et l'Institut des Biomolécules Max Mousseron (IBMM) à Montpellier.

Pour atteindre cet objectif, nous avons dû définir une gamme de propriété à viser et ensuite comprendre la corrélation entre le procédé et la structure et propriétés finales pour développer un matériau avec des caractéristiques adaptées. Les matériaux les plus optimisés ont été testé pour application biomédicale ciblée, avec en premier la libération de médicament et en second une étude *in vitro*.

Le manuscrit traite de ces aspects au travers 5 chapitres :

Le premier chapitre présente les différentes méthodes pour obtenir un matériaux poreux sec depuis un gel de polysaccharide, et les propriétés des matériaux obtenus sont décrites. Brièvement, le procédé général pour obtenir des aérogels biosourcés est décrit et leurs applications sont présentées en fonction du polymère employé. La seconde partie de ce chapitre est dédiée à la description du chitosane, ses propriétés physico-chimiques, les méthodes de mise en forme et les procédés pour obtenir des matériaux poreux secs fait à base de chitosane. Puis, un état de l'art sur les applications des aérogels et cryogels à base de chitosane dans les trois principales applications biomédicales, c.à.d. l'ingénierie tissulaire, la libération de médicament, et les pansements est dressé. Les prérequis pour chaque application sont détaillés. Enfin, la structure de la peau et les étapes de cicatrisation sont décrites.

Le second chapitre décrit les composés et les méthodes. Les détails sur les méthodes de préparation des aérogels et cryogels de chitosane sont donnés. Les méthodes de caractérisation sont précisées. Les caractérisations mécaniques par DMTA et compression uni-axiale sont décrites. Enfin, les conditions de libération de médicament *in vitro* de dexaméthasone phosphate et d'acide ascorbique 2-phosphate sont détaillées, ainsi que les conditions employées lors des test biologiques.

Le troisième chapitre propose une étude de la cinétique de coagulation des solutions de chitosane suivi par deux méthodes : via caméra optique et via DMTA en suivant l'évolution du module en fonction du temps. L'influence de la concentration de chitosane sur la cinétique de coagulation est évaluée et nous proposons un modèle pour prédire l'évolution des propriétés mécaniques au cours de la coagulation à partir des données optiques. Ce chapitre apporte une meilleure compréhension de la cinétique de coagulation et peut donner les clés pour faciliter la mise en forme, par exemple l'impression 3D avec une solution de chitosane aux propriétés rhéologiques non-optimisées.

Le quatrième chapitre étudie l'influence des paramètres du procédé sur la morphologie et les propriétés du matériau final. Les paramètres étudiés sont la concentration de chitosane en solution, la concentration du bain de coagulation, le non-solvant utilisé pour réaliser le séchage supercritique et le type de séchage. Nous avons également étudié plus spécifiquement les propriétés mécaniques des aérogels et des cryogels durant des cycles de compression uni axial. Enfin, l'influence de l'humidité et du front de coagulation (an)isotrope sur les propriétés mécaniques est mesurée par DMTA.

Le dernier chapitre se concentre sur les applications biomédicales des aérogels et cryogels à base de chitosane. Les échantillons sont imprégnés avec de la dexaméthasone phosphate qui est un anti-inflammatoire ou d'acide ascorbique 2-phosphate, 2 médicaments d'intérêt pour la cicatrisation. La cinétique de libération est suivie en fonction du temps et l'influence de la concentration de chitosane, du non-solvant utilisé pour l'échange de solvant, le type de séchage et le pH du milieu de libération est évaluée. Finalement, les tests biologiques *in vitro* avec des aérogels chargés en acide ascorbique sont présentés pour vérifier l'absence de cytotoxicité du pansement et sa capacité à promouvoir la synthèse de collagène et la cicatrisation.

La dernière partie conclut sur le travail présenté dans ce manuscrit et en montre les perspectives.

Le travail réalisé sur les aérogels imprégnés de dexaméthasone phosphate a été réalisé dans le cadre du projet « Aeromed » (n°44898RA) du programme PHC Van Gogh financé par Campus France et le CNRS. Nous remercions tous les partenaires du département pharmaceutique de Utrecht Institute for Pharmaceutical Sciences (UIPS) de l'université d'Utrecht (Utrecht, Pays Bas) qui ont été impliqué dans ce projet. Nous voudrions également remercier Pierre Ilbizan et Julien Jaxel (du laboratoire PERSEE, Mines Paris, France) pour la réalisation des séchages supercritiques, Christophe Pradille (Mat Xper, Valbonne, France) pour son aide pour la réalisation et l'analyse des essais mécaniques, et Audrey Bethry (IBMM, Montpellier, France) pour la mise en place des essais biologiques *in vitro*.

References

[1] Population et structure par âge dans le monde - Données annuelles 2020, Insee. (2021). https://www.insee.fr/fr/statistiques/2381482.

[2] S.R. Nussbaum, M.J. Carter, C.E. Fife, J. DaVanzo, R. Haught, M. Nusgart, D. Cartwright, An Economic Evaluation of the Impact, Cost, and Medicare Policy Implications of Chronic Nonhealing Wounds, Value Health. 21 (2018) 27–32. https://doi.org/10.1016/j.jval.2017.07.007.

[3] Chronic wound care market size, share & COVID-19 impact analysis, by type(diabetic ulcers, pressure ulcers, venous ulcers and arterial ulcers), by product (advanced wound dressings, wound care devices, active therapy and others), by end user (Hospitals & wound care centers, and homecare settings & others), an regional forecast 2022-2029, Fortune Buisness Insights. (2022). https://www.fortunebusinessinsights.com/industry-reports/chronic-wound-care-market-100222.

[4] S. Bowers, E. Franco, Chronic Wounds: Evaluation and Management, Am. Fam. Physician. 101 (2020) 159–166.

[5] L.A. Lavery, K.E. Davis, S.J. Berriman, L. Braun, A. Nichols, P.J. Kim, D. Margolis, E.J. Peters, C. Attinger, WHS guidelines update: Diabetic foot ulcer treatment guidelines, Wound Repair Regen. 24 (2016) 112–126. https://doi.org/10.1111/wrr.12391.

[6] D.G. Federman, B. Ladiiznski, A. Dardik, M. Kelly, D. Shapshak, C.M. Ueno, E.N. Mostow, N.A. Richmond, H.W. Hopf, Wound healing society 2014 update on guidelines for arterial ulcers, Wound Repair Regen. 24 (2016) 127–135. https://doi.org/10.1111/wrr.12395.

[7] W. Marston, J. Tang, R.S. Kirsner, W. Ennis, Wound healing society 2015 update on guidelines for venous ulcers, Wound Repair Regen. 24 (2016) 136–144. https://doi.org/10.1111/wrr.12394.

[8] L. Gould, M. Stuntz, M. Giovannelli, A. Ahmad, R. Aslam, M. Mullen-Fortino, J.D. Whitney, J. Calhoun, R.S. Kirsner, G.M. Gordillo, Wound healing society 2015 update on guidelines for pressure ulcers, Wound Repair Regen. 24 (2016) 145–162. https://doi.org/10.1111/wrr.12396.

[9] R.S. Kirsner, The wound healing society chronic wound ulcer healing guidelines update of the 2006 guidelines—blending old with new, Wound Repair Regen. 24 (2016) 110–111. https://doi.org/10.1111/wrr.12393.

[10] T. Ferreira-Gonçalves, C. Constantin, M. Neagu, C.P. Reis, F. Sabri, R. Simón-Vázquez, Safety and efficacy assessment of aerogels for biomedical applications, Biomed. Pharmacother. 144 (2021) 112356. https://doi.org/10.1016/j.biopha.2021.112356.

[11] B. Akin, M.M. Ozmen, Antimicrobial cryogel dressings towards effective wound healing, Prog. Biomater. 11 (2022) 331–346. https://doi.org/10.1007/s40204-022-00202-w.

[12] S.S. Kistler, Coherent Expanded Aerogels and Jellies, Nature. 127 (1931) 741–741. https://doi.org/10.1038/127741a0.

[13] L. Zuo, Y. Zhang, L. Zhang, Y.-E. Miao, W. Fan, T. Liu, Polymer/Carbon-Based Hybrid Aerogels: Preparation, Properties and Applications, Materials. 8 (2015) 6806–6848. https://doi.org/10.3390/ma8105343.

[14] T. Budtova, D.A. Aguilera, S. Beluns, L. Berglund, C. Chartier, E. Espinosa, S. Gaidukovs, A. Klimek-Kopyra, A. Kmita, D. Lachowicz, F. Liebner, O. Platnieks, A. Rodríguez, L.K. Tinoco Navarro, F. Zou, S.J. Buwalda, Biorefinery Approach for Aerogels, Polymers. 12 (2020) 2779. https://doi.org/10.3390/polym12122779.

[15] F. Quignard, R. Valentin, F. Di Renzo, Aerogel materials from marine polysaccharides, New J. Chem. 32 (2008) 1300. https://doi.org/10.1039/b808218a.

[16] S. Groult, T. Budtova, Tuning structure and properties of pectin aerogels, Eur. Polym. J. 108 (2018) 250–261. https://doi.org/10.1016/j.eurpolymj.2018.08.048.

[17] N. Buchtová, T. Budtova, Cellulose aero-, cryo- and xerogels: towards understanding of morphology control, Cellulose. 23 (2016) 2585–2595. https://doi.org/10.1007/s10570-016-0960-8.

[18] C.A. García-González, M. Alnaief, I. Smirnova, Polysaccharide-based aerogels—Promising biodegradable carriers for drug delivery systems, Carbohydr. Polym. 86 (2011) 1425–1438. https://doi.org/10.1016/j.carbpol.2011.06.066.
[19] C. López-Iglesias, J. Barros, I. Ardao, P. Gurikov, F.J. Monteiro, I. Smirnova, C. Alvarez-Lorenzo, C.A. García-González, Jet Cutting Technique for the Production of Chitosan Aerogel Microparticles Loaded with Vancomycin, Polymers. 12 (2020) 273. https://doi.org/10.3390/polym12020273.
[20] S. Takeshita, S. Yoda, Chitosan Aerogels: Transparent, Flexible Thermal Insulators, Chem. Mater. 27 (2015) 7569–7572. https://doi.org/10.1021/acs.chemmater.5b03610.
[21] A. Muxika, A. Etxabide, J. Uranga, P. Guerrero, K. de la Caba, Chitosan as a bioactive polymer: Processing, properties and applications, Int. J. Biol. Macromol. 105 (2017) 1358–1368. https://doi.org/10.1016/j.ijbiomac.2017.07.087.
[22] M. Dash, F. Chiellini, R.M. Ottenbrite, E. Chiellini, Chitosan—A versatile semi-synthetic polymer in biomedical applications, Spec. Issue Biomater. 36 (2011) 981–1014. https://doi.org/10.1016/j.progpolymsci.2011.02.001.
[23] J.-U. Park, E.-H. Song, S.-H. Jeong, J. Song, H.-E. Kim, S. Kim, Chitosan-Based Dressing Materials for Problematic Wound Management, in: H.J. Chun, K. Park, C.-H. Kim, G. Khang (Eds.), Nov. Biomater. Regen. Med., Springer Singapore, Singapore, 2018: pp. 527–537. https://doi.org/10.1007/978-981-13-0947-2_28.
[24] G.M. Guebitz, A. Pellis, G.S. Nyanhongo, Delivery of Biomolecules Using Chitosan Wound Dressings, in: R. Jayakumar, M. Prabaharan (Eds.), Chitosan Biomater. IV, Springer International Publishing, Cham, 2021: pp. 447–467. https://doi.org/10.1007/12_2021_95.
[25] C. López-Iglesias, J. Barros, I. Ardao, F.J. Monteiro, C. Alvarez-Lorenzo, J.L. Gómez-Amoza, C.A. García-González, Vancomycin-loaded chitosan aerogel particles for chronic wound applications, Carbohydr. Polym. 204 (2019) 223–231. https://doi.org/10.1016/j.carbpol.2018.10.012.
[26] A.E. Pusateri, J.B. Holcomb, B.S. Kheirabadi, H.B. Alam, C.E. Wade, K.L. Ryan, Making Sense of the Preclinical Literature on Advanced Hemostatic Products:, J. Trauma Inj. Infect. Crit. Care. 60 (2006) 674–682. https://doi.org/10.1097/01.ta.0000196672.47783.fd.
[27] K. Inaba, B.C. Branco, P. Rhee, B. Putty, O. Okoye, G. Barmparas, P. Talving, D. Demetriades, Long-term preclinical evaluation of the intracorporeal use of advanced local hemostatics in a damage-control swine model of grade IV liver injury:, J. Trauma Acute Care Surg. 74 (2013) 538–545. https://doi.org/10.1097/TA.0b013e31827d5f5f.
[28] F.-L. Mi, S.-S. Shyu, Y.-B. Wu, S.-T. Lee, J.-Y. Shyong, R.-N. Huang, Fabrication and characterization of a sponge-like asymmetric chitosan membrane as a wound dressing, Biomaterials. 22 (2001) 165–173. https://doi.org/10.1016/S0142-9612(00)00167-8.
[29] M.P. Batista, V.S.S. Gonçalves, F.B. Gaspar, I.D. Nogueira, A.A. Matias, P. Gurikov, Novel alginate-chitosan aerogel fibres for potential wound healing applications, Int. J. Biol. Macromol. 156 (2020) 773–782. https://doi.org/10.1016/j.ijbiomac.2020.04.089.
[30] N.A. Gorshkova, O.S. Brovko, I.A. Palamarchuk, K.G. Bogolitsyn, Influence of the Structure of Alginate-Chitosan Materials on the Kinetics of Usnic Acid Release, Appl. Biochem. Microbiol. 58 (2022) 110–117. https://doi.org/10.1134/S0003683822020089.
[31] M.E. El-Naggar, S.I. Othman, A.A. Allam, O.M. Morsy, Synthesis, drying process and medical application of polysaccharide-based aerogels, Int. J. Biol. Macromol. 145 (2020) 1115–1128. https://doi.org/10.1016/j.ijbiomac.2019.10.037.

Articles and communications

This work has been published and submitted as articles and presented at international conferences.

Articles

Chartier, C.; Buwalda, S.; Van Den Berghe, H.; Nottelet, B.; Budtova, T. Tuning the Properties of Porous Chitosan: Aerogels and Cryogels. Int. J. Biol. Macromol. 2022, 202, 215–223. https://doi.org/10.1016/j.ijbiomac.2022.01.042.

Chartier, C.; Buwalda S.; Ilochonwu B.C.; Van Den Berghe H.; Vermonden T.; Viola M.; Nottelet B.; Budtova T. Release kinetics of dexamethasone phosphate from porous chitosan: comparison of aerogels and cryogels. Submitted to Biomacromolecules.

Oral communications

Chartier C., Buwalda S., Budtova T.
'Influence of processing conditions on chitosan aerogel structure and properties', Online Seminar on Aerogels
16-18th September 2020 – online

Chartier C., Bethry A., Bouvard J.L., Pradille C., Van Den Berghe H., Buwalda S., Nottelet B., Budtova T.
'Tunable structure and properties of chitosan aerogels', American Chemical Society Spring 2021
5-16th April 2021 – online

Chartier C., Bethry A., Van Den Berghe H., Buwalda S., Nottelet B., Budtova T.
'Tuning structure and properties of chitosan aerogels and cryogels for controlled drug release', 7th International Polysaccharide conference of the European Polysaccharide Network of Excellence (EPNOE)
11-15th September 2021 – Nantes (France)

Chartier C., Buwalda S., Van Den Berghe H., Nottelet B., Budtova T.
'Kinetics of ascorbic acid 2-phosphate release from chitosan aerogels in view of potential wound dressing applications', American Chemical Society Spring 2022
20-24th March 2022 – Hybrid, San Diego (USA)

Chartier C., Buwalda S., Van Den Berghe H., Nottelet B., Budtova T.
'Release of ascorbic acid 2-phosphate from chitosan aerogels and cryogels in view of potential wound dressing applications', 17th days of Groupement Français d'Etude et d'Applications des Polymères (GFP) Méditerranée
7-8th April 2022 – Marseille (France)

Chartier C., Ilochonwu B., Viola M., Vermonden T., Buwalda S., Van Den Berghe H., Nottelet B., Budtova T.
'Kinetics of ascorbic acid 2-phosphate and dexamethasone phosphate release from chitosan porous materials in view of wound dressing applications', 5th EPNOE junior scientist meeting
8-9th September 2022 – Aveiro (Portugal)

Chartier C., Pradille C., Buwalda S., Van Den Berghe H., Nottelet B., Budtova T.
'From solution to aerogel: study of chitosan coagulation kinetics', 6th international seminar on aerogels

28-30th September 2022 – Hambourg (Germany)

Posters

Chartier C., Bouvard J.L., Pradille C., Buwalda S., Budtova T.
'Influence of processing conditions on chitosan aerogel structure and properties', EPNOE junior online scientist meeting
3rd-4th January 2021 – online

Chartier C., Ilochonwu B., Viola M., Vermonden T., Buwalda S., Van Den Berghe H., Nottelet B., Budtova T.
'Release of ascorbic acid 2-phosphate and dexamethasone phosphate from chitosan aerogels and cryogels in view of potential wound dressing applications', AFPM
1st-3rd June 2022 – Sophia Antipolis (France)

Chapter I. State of the art on porous chitosan for biomedical applications

List of abbreviations:

ABTS: 2,2'-azino-bis(3-ethylbenzothiazoline-6-sulfonic acid)

AgNP: silver nanoparticles

BJH Analysis: Barrett-Joyner-Halenda

BSA: Bovine serum albumin

CA: cellulose acetate

CECS: N-carboxyethyl chitosan

CF: Chitosan/fibroin

CHT-C: Chitosan/Cloisite 30B

CHT-LDH: composite of chitosan with Mg-Al-PO_4-LDH (layer double hydroxide)

CMC: carboxymethyl chitosan

CNF: cellulose nanofibers

CS: chitosan

CS/CaP: Calcium phosphate-containing chitosan-based composites

HPS-X: CS/HAP in different ratio 100/0, 90/10, 80/20, 70/30, 60/40, 50/50 and 40/60

DA: degree of acetylation

DEAAm: N, N'-diethyl acrylamide

DMAEMA: 2-(dimethylamino)ethyl methacrylate

DMEM: Dulbecco's Modified Eagle Medium

DMF: dimethyl formamide

DPBS: Dulbecco's phosphate buffer saline

DPPH assay: 2,2-diphenylpicrylhydrazyl

EC50: half maximal effective concentration

ECM: Extracellular matrix

EGDMA: ethylene glycol dimethacrylate

FITC-BSA: Fluorescein isothiocyanate labelled bovine serum albumin

FTIR: Fourier transform infrared

G: gelatin

GA: gallic acid

GPTMS: chitosan-3-glycidoxypropyl trimethoxysilane

GTA: Glutaraldehyde

HAC: hydroxyapatite-alginate-chitosan

HAP: hydroxyapatite

HEMA: 2-hydroxyethyl methacrylate

HP-β-CD : 2-hydroxypropil-β-cyclodextrin

Ibu: ibuprofen

IPN: interpenetrating network

LCST: lower critical solution temperature

MIC: Minimum inhibitory concentration

MTT: (3-(4, 5-dimethylthiazolyl-2)-2, 5-diphenyltetrazolium bromide) assay

NC: chitin nanocrystals

NF: Chitin nanofibers

NGF: Neuron growth factor

NIR laser: Near infrared laser

NMNS: amino-functionalized molybdenum disulfide nanosheets

NSAID: non-steroidal anti-inflammatory

PBS: Phosphate buffer saline

PCL: poly(ε-caprolactone)

PDEAAm poly (N, N'-diethyl acrylamide)

PEC: Polyelectrolyte complexes

PPG: porous polyglycolide

PGA: poly(γ-glutamic acid)

pI: isoelectric point

PS: Polystyrene

PVA: Polyvinyl alcohol

PVD: DMAEMA grafted on PVA

PVP: polyvinylpyrrolidone

QPVD: Quaternized PVD

rBMSC: rat bone marrow-derived mesenchymal stem cells

$scCO_2$: Supercritical CO_2

SEM: Scanning electron microscopy

TEOS: Tetraethyl orthosilicate

UA: usnic acid

WVTR: water vapor transmission rate

Zn-UHANWs: Chitosan scaffolds with zinc-containing, nanoparticle-decorated, ultralong hydroxyapatite nanowires

α-Ais: α-Amylase inhibitors

Content

Introduction

Chitosan aerogels present interesting properties making them promising biobased materials for adsorption [1], catalysis [2], thermal insulation [3] or biomedical applications [4]. The material structure strongly influences the properties and thus the efficiency regarding the applications, hence a good comprehension of the correlation between the process and the final structure is needed.

This chapter is a review of the state of the art on porous chitosan materials for biomedical applications focusing on how the properties of the material are tuned to efficiently answer to a medical problem. In this chapter we will not consider membranes, foams or non-wovens as they present an "added" porosity.

- The first part of this chapter is dedicated to aerogels, the differences between the porous materials and the main properties and applications of a recent category of aerogels: the bio-aerogels.
- The second part is dedicated to chitosan with first the structure and physico-chemical properties of chitosan, the different ways of shaping chitosan and how to prepare porous chitosan.
- Then, state of the art concerning the use of porous chitosan in the three main biomedical applications - tissue engineering, drug release and wound dressing - will be made. The most important properties for each application will be detailed.
- Finally, the skin structure is described, and the several stages of wound healing are detailed.

The goal of this chapter is to highlight the interest of aerogels' properties in biomedical applications and review what is done in the literature to propose a new dressing with tunable properties that improve healing.

Résumé

Les aérogels de chitosane présentent des propriétés intéressantes ce qui en fait des matériaux prometteurs pour l'absorption [1], la catalyse [2], l'isolation thermique [3] ou des applications biomédicales [4]. La structure du matériau influence fortement les propriétés et donc les performances pour les différentes applications, il est donc essentiel de comprendre de manière approfondie la relation entre le procédé et la structure finale obtenue.

Ce chapitre est une revue de l'état de l'art sur les matériaux poreux à base de chitosane pour les applications biomédicales. L'accent est mis sur la façon dont les propriétés des matériaux peuvent être modifiées pour répondre efficacement à un problème médical. Dans ce chapitre, nous n'aborderont pas les membranes, mousses ou des matériaux non-tissés car ils présentent une porosité « ajoutée ».

- La première partie de ce chapitre est dédiée aux aérogels, les différences entre les matériaux poreux et les principales propriétés et applications d'une catégorie récente d'aérogel : les bio-aérogels.
- La seconde partie est dédiée au chitosane avec en premier la structure et les propriétés physico-chimiques du chitosane, les différentes méthodes de mise en forme du chitosane et comment préparer du chitosane poreux.
- Puis, un état de l'art sur l'utilisation du chitosane poreux dans les 3 principales applications biomédicales – ingénierie tissulaire, libération de principe actif et pansement – est faite. Les propriétés les plus importantes pour chaque application seront détaillées.
- Finalement, la structure de la peau est décrite, et les différentes étapes de cicatrisation sont détaillées.

Le but de ce chapitre est de mettre en avant l'intérêt des propriétés des aérogels dans les applications biomédicales et d'avoir un regard d'ensemble sur la littérature pour proposer un nouveau pansement avec des propriétés ajustables et qui améliore la cicatrisation.

1. Aerogels

1.1. Porous material: drying methods

The simplest ways of evacuation of a liquid from a polymer solution or gel are ambient pressure or low-vacuum drying. However, it usually gives rather dense materials with almost no porosity due to the capillary pressure (Figure I.1). Because of the capillary pressure, which develops during evaporation of a liquid, pores are usually closing, resulting in materials with low porosity. The pressure can be described with the Young-Laplace equation (eq. I.1). Small pore's radius, high surface tension and high wettability of the liquid induce higher pressure.

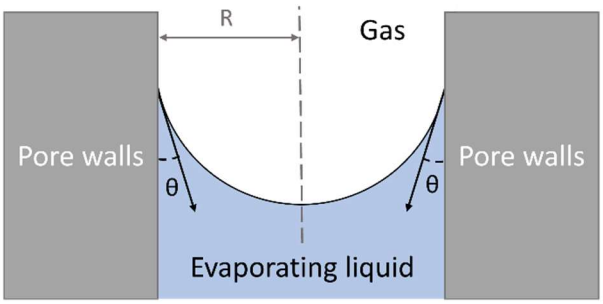

Figure I.1: Schematic representation of capillary forces

$$\Delta p = \frac{2\,\gamma \cos\theta}{R} \qquad \text{I.1}$$

with Δp the capillary pressure, R the radius of the meniscus, γ the surface tension between the gas and the liquid and θ the contact angle. The pressure can be strong enough to induce cracks in the material or collapse of the pores. The materials obtained by this method will be called ***"xerogels"***. There are different ways to make pores in such a non-porous material, for example, mixing with a surfactant, or foaming, or adding a sacrificial component that is leached out. Chitosan materials with "added" porosity will not be considered here as the thesis is devoted to intrinsically porous chitosan.

Another way to remove a liquid from the pores of a gel is to perform freeze-drying, the materials are called "***cryogels***" or "***cryostructurates***" [5]. The most common freeze-drying way is when water is in the pores of the network. The formation and growth of ice crystals strongly deform pore walls; this way of drying usually does not preserve the structure of the network (see an example of freeze-dried chitosan hydrogel in [6]). Such materials usually present a low specific surface area and high porosity (usually above 90%). It should be noted that if using specific conditions of freeze-drying which allow suppression of the growth of ice crystals (for example, using tert-butanol/water mixture [7]), materials with high porosity and high surface area can be obtained.

The best way to preserve the morphology of a gel and limit the shrinkage is to use drying in supercritical conditions as no capillary pressure exists either by suppressing the liquid-gas surface tension or make meniscus angle close to 90° by chemical treatment of the pore surface. In the majority of cases, CO_2 is used thanks to its mild supercritical conditions (P_c = 72.8 bars and T_c = 31°C). The liquid in the pores of the network before drying must be miscible with CO_2. The ***"aerogels"*** obtained present a low density (< 0.2 g/cm^3), high porosity (> 90%) and a high specific surface area (> 100 m²/g). The Figure I.2 shows the different drying methods and the state of the fluid during the drying.

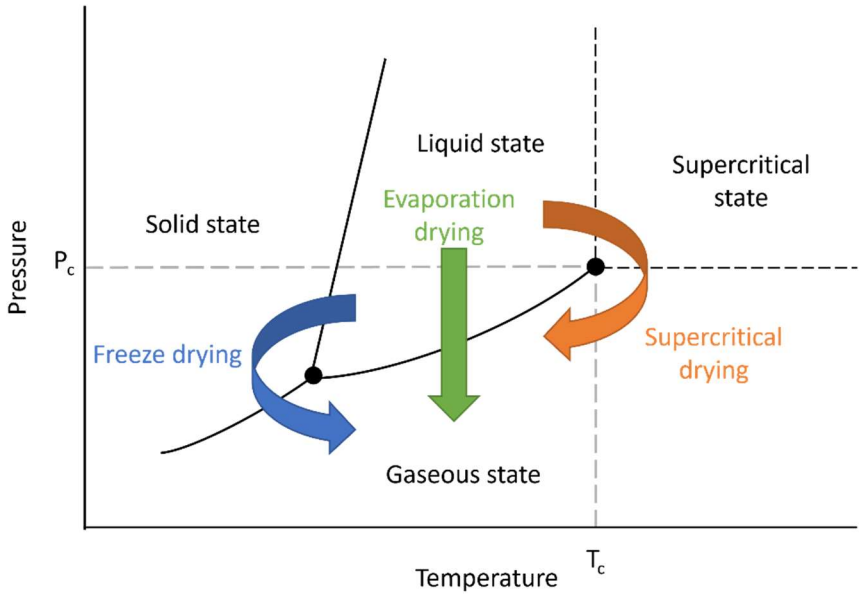

Figure I.2: Schematic representation of the drying routes on a phase diagram. T_c and P_c are the critical temperature and critical pressure point, respectively.

1.2. Bio-based aerogels

Aerogels were first discovered by Kistler in 1931 [8] who obtained transparent silica aerogels from silica gel by supercritical CO_2. Another paper a year later [9] describes aerogels made with alumina, tungstic oxide, ferric oxide, stannic oxide, nickel tartrate and also bio-based polymers like cellulose, gelatin, agar, egg albumin and rubber, but the properties were not detailed. Technological constraint limited the development of this method, and it was not until the 1970's that silica aerogels had a renewed interest especially as thermal super-insulators (below the thermal conductivity of air: 0.025 C/m/K). In the end of the XXth century, aerogels based on synthetic polymers were made from polyurethane [10], polyimide [11], and polyamide [12]. These aerogels presented improved mechanical properties compared to the brittle silica aerogels, and new applications were considered such as catalysis [13].

In the last 20 years, a new class of aerogels was developed: the bio-aerogels. Made from bio-based polymers, polysaccharides or proteins, they often present several advantages compared to the inorganic aerogels such as biocompatibility or environmental friendliness. Here only polysaccharide-based aerogels will be considered. The properties of bio-aerogels strongly depend on the polysaccharide and on the processing steps, but they all present a low density (< 0.2 g/cm^3) and a specific surface area of several hundreds of m²/g.

The bio-aerogels preparation shown on Figure I.3 starts with the dissolution of the polymer, most of them are water soluble. The second step is solution gelation to obtain a gel, but this step is not mandatory and depends on the polymer. In this step, a network is created either via chemical or physical (i.e. ionic bonds) crosslinking. Another way is formation of a polymer network via coagulation (non-solvent induced phase separation) when put in contact with a non-solvent. For bio-based aerogels, the drying is always performed with supercritical CO_2 because the supercritical conditions for other fluids like water (P_c = 22 MPa and T_c = 374°C) are degrading the biopolymers. To perform supercritical drying, the solvent to remove must be miscible with the supercritical fluid; as water is not miscible with CO_2, it is replaced generally by ethanol, acetone, isopropanol, or hexane. The exchange should be performed gradually to limit the shrinkage of the samples.

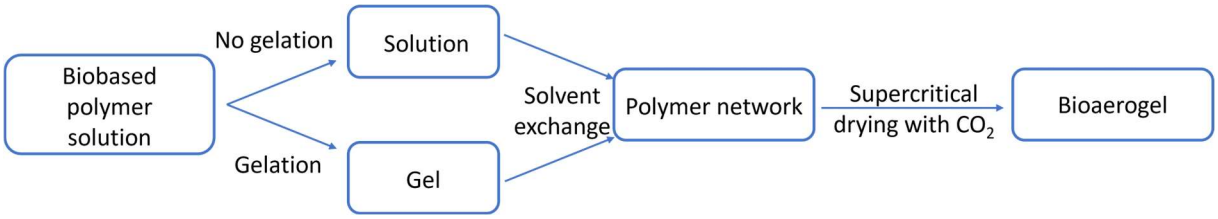

Figure I.3: Schematic presentation of bio-aerogel preparation.

The most common polysaccharides used to make aerogels are cellulose, alginate, chitosan, starch and pectin [14]. Recently, protein based aerogels were developed [15–17] but they are not widespread. The main polysaccharide-based aerogels are briefly presented below, except chitosan, which will be widely discussed in the next part as it is the polymer of interest in this thesis.

Cellulose is the most abundant natural polymer being the main constituent of vegetal cell walls. The polymer is composed of D-glucose units linked by β (1→4) bonds forming linear chains. It was widely used to make aerogels, either using the cellulose I [18], or cellulose II [19], nanocellulose [20] forming nanofibers or crystals, or modified cellulose like cellulose ester [21] or cellulose-inorganic composites [22]. The application of cellulose-based aerogels depends on the type of cellulose used as it influences the characteristics of the final aerogel. Cellulose aerogels are biocompatible opening the field of the biomedical applications [23], they can be used as absorbent of pollutants [21]. Nanocellulose aerogels can be used in various applications such as absorbent, insulating materials, scaffold or as drug delivery system for biomedicals applications, or carbon precursor in electrical device [24]. Bacterial cellulose is also a form of nanocellulose; aerogel made of it present a very low density of 0.008 g/cm^3 thanks to the very limited shrinkage of 7% [25] compared to other bio-aerogels with a shrinkage from 30 – 90%, 20% and 95%, 40-80% for chitosan [26–29], alginate and carrageenan [28], and for pectin [30] respectively.

Alginate is a marine polysaccharide produced by brown algae. Alginate is composed of (1→4) linked β-D-mannuronic and α-L-gluconic. Valentin et al. made one of the first alginate aerogel [31]. Typically, ionic gelation occurs with divalent cations as Ca^{2+}, described by the egg-box model [32]. The gelation can occur with Cu^{2+} [33] or a cationic polymer such as chitosan [34]. Quignard et al. [28] studied various marine polysaccharides: they prepared alginate aerogel beads with a maximum specific surface of 570 m²/g to be used as catalytic support. Drug delivery from alginate aerogels was also widely studied with encapsulation of ketoprofen (anti-inflammatory) and benzoic acid (manages urea cycle disorder) [35] or ibuprofen [36].

Starch is serving as the energy storage of plants; it is composed of amylose (linear chain of D-glucopyranose linked in α(1→4)) and amylopectin (ramified α-D-glucopyranose linked in α(1→4)), present in different ratios depending on the starch's source. This ratio has an important influence on the final properties of the aerogels as shown by Garcia-Gonzalez [37] and Druel et al [38]. Starch aerogels present super-insulating properties with thermal conductivity between 0.021 to 0.023 W/m/K [38]. Starch aerogel beads can be used as a drug delivery system of ketoprofen [35,39] or vitamin E and K_3 [40].

Pectin is mainly found in vegetables and fruits. It is composed of D-galacturonic acid linked in α(1→4) with different degree of methyl esterification of carboxyl group depending on the preparation process. Pectin aerogels can be prepared with or without gelation leading to aerogels with different properties but always very high specific surface area from 300 to 650 m²/g and density between 0.06 and 0.12 g/cm^3 [30]. Pectin aerogels were the first bio-aerogels to present impressive properties for thermal insulation [41] with a minimal conductivity of 0.0015 W/m/K which can be tuned by the preparation methods [42], making super-insulating materials with a non-brittle mechanical behavior [43]. As the above-mentioned bio-aerogels, biomedical applications were also proposed as drug

delivery of theophylline [44], ketoprofen or benzoic acid [35] or nicotinic acid [45]. TiO_2 nanoparticles inside a pectin network improve the mechanical, thermal and antimicrobial properties of the aerogel, making it a promising material for thermally sensitive food packaging [46].

2. Generalities on chitosan, its shaping and ways to make porous materials

2.1. Generalities on chitosan

Chitosan is a semi-natural polymer synthetized from chitin which comes from crustacean shells and some fungi. Chitin and chitosan are linear copolymers of D-glucosamine and N-acetyl-D-glucosamine linked by β (1→4) glycosidic bonds [47], as shown in Figure I.4.

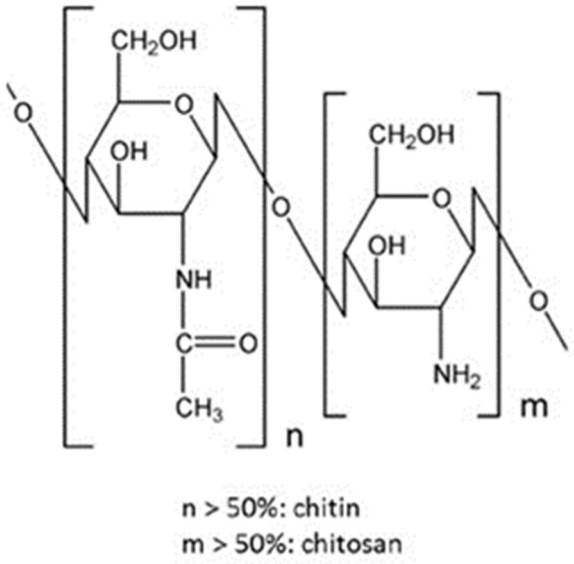

Figure I.4: Structural formula of chitin and chitosan. Reprinted with modifications from [47]

Chitin is the second most abundant natural biopolymer; it exists in 3 polymorphic forms (α, β and γ-chitin) organized in microfibrils. Chitin, due to its high crystallinity, is not soluble in common solvents and can only be solubilized in strong acids, organic solvents and in hot aqueous solutions with a high concentration of salt (LiCNS, $Ca(CNS)_2$, CaI_2, $CaBr_2$, $CaCl_2$).

In order to obtain chitosan from chitin, acetyl groups are partly removed. To achieve this, two processes are usually applied. One is the process developed by Broussignac [48]: chitin is mixed with potassium hydroxide, ethanol, and monoethyleneglycol, and the whole is heated. The other is the process developed by Kurita [49]: under a nitrogen stream, a suspension of chitin in an aqueous sodium hydroxide solution is heated to high temperature. In both cases the time of reaction depends on the desired degree of acetylation (DA). The reaction is stopped by precipitating chitosan in aqueous NaOH, chitosan is subsequently filtered, washed and dried.

α and β chitin do not undergo deacetylation in the same way; α-chitin has chains stacked in anti-parallel configuration, with deacetylation occurring only in the amorphous parts leading to a block distribution of the N-glucosamine and N-acetyl glucosamine units in chitosan. The β-chitin has chains stacked in parallel direction; after deacetylation chitosan becomes fully amorphous with statistically distributed glucosamine groups.

Chitosan has a DA below 50%. It is insoluble in water at neutral pH, in alkaline solutions and organic solvents, but can be solubilized in acidic media. Chitosan is the only pseudo-natural cationic polymer. Thanks to its amino function, chitosan has antiviral, antibacterial and antifungal properties [50]. The antimicrobial activity is due to two mechanisms: the first one is the interaction between

anionic groups at the surface of the cells with the cationic groups of the polymer chain which leads to an alteration in the permeability of the bacterial membrane. The other mechanism is induced by the bonding between chitosan and cellular DNA via the amino groups, resulting in an inhibition of the synthesis of the microbial RNA. This antimicrobial activity of the chitosan depends on its molecular weight, DA, the presence and concentration of the cationic NH_3^+ group.

Chitosan is also a hemostatic agent as it stimulates the formation of a blood clot [51]. The amine functions are protonated in a physiological environment and interact with the red blood cells which are negatively charged, resulting in clotting. This property is already exploited in commercial wound dressings as HemCon® and Thermoguard® used to stop hemorrhages.

Importantly, chitosan-based materials are biocompatible, biodegradable, and non-allergenic. Chitosan also presents bioactivity by speeding up wound healing, stimulating the immune system and decreasing the cholesterol level.

The β-1,4-linkage between D-glucosamine units or between N-acetyl-D-glucosamine and D-glucosamine units can be hydrolyzed by chitosanases (EC 3.2.1.132, [52]) named chitosan N-acetylglucosaminohydrolases. In the human body, lysozyme and colonic bacterial enzyme can also degrade chitosan. An enzymatic activity has been demonstrated for some human glucosidases [53] as well as proteases [54] and they can degrade chitosan to various degrees. During the degradation of chitosan, N-acetyl-β-D-glucosamine is formed which is helping wound healing by stimulating the proliferation of fibroblasts and the formation of collagen as well as hyaluronic acid. It induces the activation of macrophages that will inhibit the abnormal growth of tissues, which decreases the risk of scare. Chitosan is a suitable biomaterial for tissue regeneration as it can be used as a matrix for growing new cells.

The presence of hydroxyl, amino and N-acetyl groups allows for intra- and intermolecular hydrogen bonds which leads to the formation of chitosan aggregates with a high crystallinity. The crystallinity [55,56] depends on the DA and molecular weight, for example, maximum crystallinity is achieved for fully deacetylated chitosan due to the high chemical regularity. For example, the degree of crystallinity for a chitosan of 400 000 g/mol (in powder) and a DA of 12% is around 57% [57], whereas the degree of crystallinity of chitosan fibers of molecular weight of 150 – 300 KDa is in the range of 35-50% [58]. High crystallinity decreases the degradation rate of chitosan [59].

Chitosan monomer units possess several functions such as a primary amine as well as a primary and secondary hydroxyl function which can be chemically modified without decreasing the degree of polymerization [60,61]. These chemical modifications can increase the hydrophilicity of chitosan and improve the properties of chitosan-based materials for drug delivery and chelation of metal ions. Phosphorylation is possible on all the mentioned functions whereas thiolation can be done on the amine function. Crosslinking of chitosan is possible through the amine function with aldehydes like glutaraldehyde or through the primary hydroxyl group with chlorine compounds like epichlorohydrin. Grafting of acrylonitrile or methyl methacrylate onto chitosan was performed using a radical initiator [62] (such as azobisisobutyronitrile or potassium persulfate), or a redox system [63] (like Fenton's agent, Fe^{2+}/H_2O_2) or Ce(IV)).

2.2. Shaping of chitosan

Chitosan can be processed into different shapes for biomedical applications: monoliths, films, beads, fibers, etc., and it can be kept in a "wet" state (usually, hydrogel with water in the pores) or dried, using various drying routes. Similar to the processing of cellulose, the first step is to dissolve chitosan as degradation occurs before melting. Chitosan can be crosslinked or not; in the latter case immersion precipitation (or non-solvent induced phase separation) is applied to "regenerate" chitosan from solution.

The classical shapes of chitosan materials are films and fibers made by film casting optionally followed by solvent evaporation (Figure 2a) [64] and wet spinning [65,66], respectively (Figure 2b). Chitosan nanofibers can be made by electrospinning (Figure 2c) [67,68].

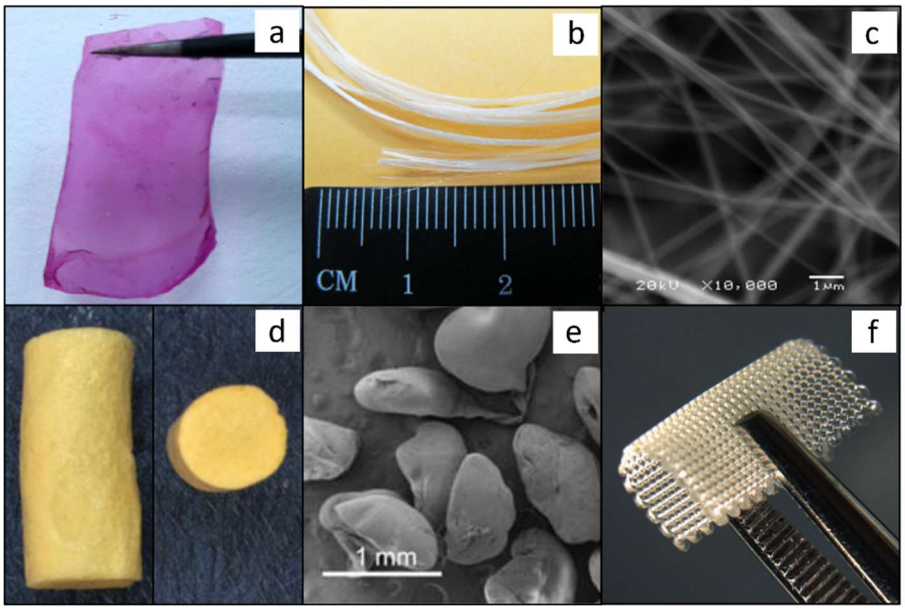

Figure I.5: Photos of differently shaped chitosan biomaterials:
(a) O-carboxymethyl chitosan/Tannic acid/1,4-benzenediboronic acid hydrogel film stained with rhodamine [69] Adapted with permission from H. Geng et al., ACS Appl. Bio Mater. 3 (2020) 1258–1266. Copyright 2023 American Chemical Society.;
(b) Chitosan fibers obtained by wet spinning [65], Reprinted from Acta Biomaterialia, Vol 44, Gossla et al., Electrostatic flocking of chitosan fibres leads to highly porous, elastic and fully biodegradable anisotropic scaffolds, Pages 267-276., Copyright 2023, with permission from Elsevier;
(c) SEM picture of chitosan nanofibers obtained by electrospinning [67], Reproduced with permission from Springer Nature;
(d) freeze dried chitosan graft-poly(acrylic acid)/Hydroxyapatite nanocomposite scaffolds [70] Adapted with permission from Asadian-Ardakani et al., journal of biomedical materials research part A (2016), Vol.104, Issue 12, Pages 2992-3003. Copyright 2023, with permission from John Wiley & Sons;
(e) SEM image of chitosan aerogel beads obtained by jet cutting. Adapted from [71];
(f) Chitosan scaffold obtained by 3D printing [72], Adapted with permission from Heuzey et al., Advanced Biosystems (2017), Vol.1, Issue 6. Copyright 2023, with permission from John Wiley & Sons.

Chitosan materials can also take 3D shapes: monoliths, beads and complex forms made by 3D printing. To make monoliths, chitosan is often crosslinked to form a gel; to prevent the collapse of the pores and preserve gel shape during drying, either freeze-drying or drying with supercritical CO_2 is applied (Figure 2d) [6,73,74]. Beads can be made using classical ways of making gel particles (atomization, prilling, jet-cutting) via dropping chitosan solution into a coagulant (for example, NaOH-water) or into crosslinker bath (for example, sodium tripolyphosphate solution) (Figure 2e) [71,75]. Recently, additive manufacturing started to be used for making chitosan scaffolds for tissue engineering (Figure 2f) [72].

2.3. Preparation of porous chitosan materials

As stated in the Introduction, we will focus on intrinsically porous 3D chitosan materials. To make such materials, whatever are their shapes, chitosan must be first dissolved (Figure I.6). Usually, an acidic medium is used so that the amine functions are protonated (pKa = 6.2). Chitosan can be crosslinked to form a gel [27,73], or a non-solvent can be added to form a network of coagulated polymer with non-solvent in the pores [71,76]. In the latter case aqueous NaOH is often used. The presence of a basic non-solvent results in deprotonation of the cationic groups decreasing chitosan solubility. In both cases, either after chemical crosslinking or non-solvent induced phase separation, chitosan 3D network is formed from which the liquid should be evacuated if willing to make a dry

material. Chitosan materials with "added" porosity will not be considered as the thesis is devoted to intrinsically porous chitosan.

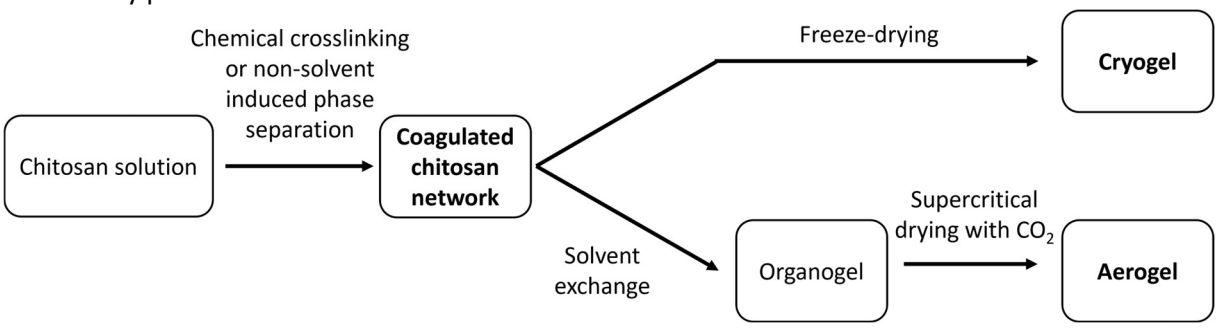

Figure I.6: Schematic representation of the preparation of porous chitosan materials: cryogels and aerogels.

Uncommon options of freeze-drying, can be applied directly to chitosan solution which is frozen, placed in coagulation bath and dried at ambient pressure [77]. Additional pores can be created from air bubbles that are made, for example, by sonication [78].

Despite some shrinkage of chitosan network during solvent exchange, supercritical drying allows a reasonably good preservation of the gel structure. This pathway can be applied to chemically crosslinked chitosan gels and to networks obtained via non-solvent induced phase separation. Chitosan materials with high porosity (> 90%) and very high internal pores surface area (> 200 m^2/g), aerogels, are obtained [3,4,26,29,75,79–81].

In this chapter, two types of intrinsically porous chitosan materials for bio-medical applications will be considered: aerogels and cryogels, that we define as follows:

- A cryogel is a dried gel presenting a high porosity (> 80%), a low density and low specific surface area (usually around few to few tens of m^2/g) due to very large macropores (> 1 µm). Such materials are usually obtained using freeze-drying.
- An aerogel is a dried gel presenting a high porosity (> 80%), low density, and high specific surface area (> 100 m^2/g) due to pore sizes in the region from micropores to small macropores. In most cases these properties are reached thanks to drying with supercritical CO_2, however, freeze-drying or even ambient pressure drying may also lead to such unique properties.

3. Biomedical applications of chitosan aero- and cryogels

Statistics concerning published articles and patents on porous chitosan materials for different biomedical applications are shown in Figure I.7A and B. Research has mainly focused on tissue engineering, as presented in Figure I.7A. Figure I.7B shows that in comparison with scientific papers, a relatively high proportion of patents deals with wound healing. Very few patents concern porous chitosan as a drug carrier. These data clearly show that porous chitosan is a very attractive material for biomedical applications, constituting a rather new research field as it has only been explored for the past 20 years. Figure I.7C shows the number of patents distinguishing three types of porous structure as determined above: aerogels, cryogels and xerogels. The number of patents clearly increases over the years, showing the interest of industry for these materials. It is worth noting that because of not well-established terminology (for example, IUPAC determines aerogels as microporous materials only [82] which is now not accepted in the community of aerogel researchers [83]), the number of patents shown in Figure I.7C is underestimated, and search with keywords for articles does

not give a representative result. This absence of clear terminology by the scientific community also demonstrates the novelty of these materials and their broad spectrum of tunable properties.

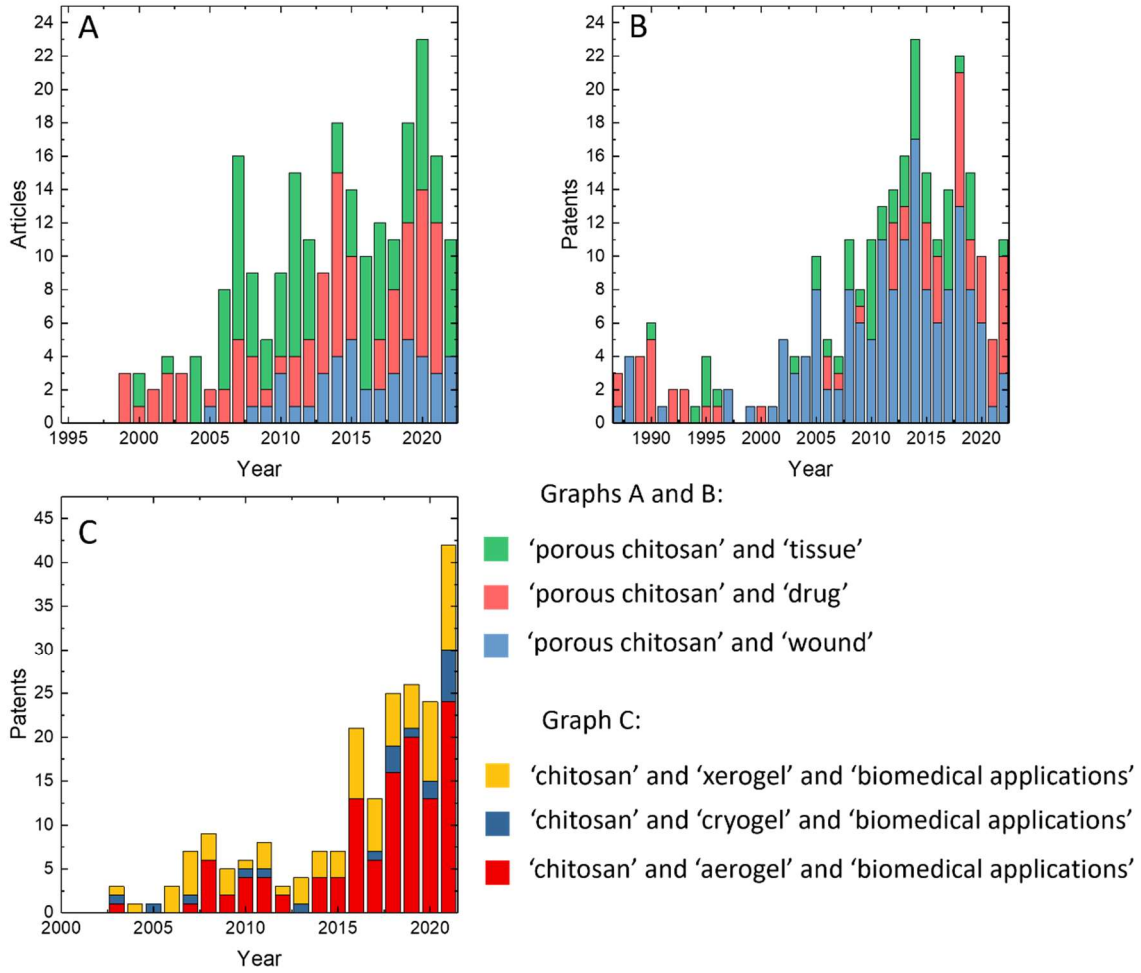

Figure I.7: Histograms of (A) published articles and (B) patents concerning chitosan materials over the years for the 3 main biomedical applications with keywords "tissue", "drug" and "wound"; (C) patents concerning chitosan materials for biomedical applications for the 3 main preparation methods of porous materials: "xerogels", "cryogels" and "aerogels". Statistics gathered with Scopus in December 2022 using the combination of the indicated keywords.

This chapter focuses on 3 biomedical applications of porous chitosan materials: tissue engineering, drug delivery and wound dressings, each categorized by material property, i.e. "cryogel" and "aerogel".

Irrespective of the biomedical application, a biomaterial must present acceptable biocompatibility [84] with no cytotoxicity, little sensitization and little irritation or intracutaneous reactivity. Depending on the application as well as the nature and duration of the contact with the human body, the biomaterial may also have to fulfill other requirements. All essential properties are listed in ISO 10993, [85]. The most important expected properties for each application are detailed in the beginning of the following sections.

3.1.1. Porous chitosan for tissue engineering

(1) Expected properties

Porous materials for tissue engineering are expected to facilitate cell ingrowth by guiding them through or over a polymer network. Ideally, they present dual porosity with pores larger than 100 µm [86,87] to favor cell infiltration and smaller pores (≤ 10 µm) to help cell attachment and increase the

surface area available for tissue growth [88]. A porosity higher than 70% is also recommended to allow an extracellular matrix distribution (ECM) similar to native tissues [89]. Contrary to wound dressings, cells should grow into the material. Stem cells can be added to the material to enhance the cell growing [90] by maintaining the homeostasis and cells' differentiation toward the targeted phenotype. Also, bioactive molecules such as drugs and growth factors are frequently incorporated in the scaffolds to evoke the desired biological response.

Materials used for tissue engineering should present good bioabsorption [91] and biodegradation properties [92]: once the material has started to be colonized by the cells, the polymer network should degrade slow enough to maintain a scaffold for the growing cells but fast enough to be gradually replaced by cells. One other major requirement is a good implantation of the scaffold without causing inflammation.

(2) Chitosan cryogels for tissue engineering

Cryogels are more often used for tissue engineering purposes, as the growth of ice crystals during freezing often provides a pore size in the order of tens of micrometers, which is suitable for efficient cell colonization and growth.

For example, porous polyglycolide (PPG)/chitosan matrices were developed for tissue engineering [93]. PPG was solubilized in DMSO and chitosan in acetic acid. The solutions were mixed in two weight ratios, namely PPG:CS 7:3 (named P/CS-1) and 3:7 (named P/CS-2). The mixtures were frozen and immersed in NaOH to neutralize acidity and precipitate chitosan. The samples were then washed with PBS to obtain a neutral pH and limit the degradation of PPG. Lastly the samples were dried at 25°C. Control samples without PPG were prepared as well. Interconnected pores from 10 to 200 µm could be observed for P/CS-1 matrices and from 10 to 100 µm for chitosan and P/CS-2 matrices. The porosity was 89, 77 and 64% for P/CS-1, chitosan and P/CS-2 respectively. The Young's modulus increased with an increase of the PPG concentration, reaching values of 0.15, 1.16 and 9.13 kPa for chitosan, P/CS-2 and P/CS-1 respectively. As a stronger network better resists extension to absorb liquid, the swelling ratio in PBS decreased with the increase of PPG content: 410%, 360% and 310% for chitosan, P/CS-2 and P/CS-1 matrices, respectively. The degradation of the matrices after 35 days in PBS was 40% for chitosan and 61% for matrices with PPG. In the PPG-containing materials, most of the weight loss is due to the degradation of PPG. The fibroblast cell density increased with time for the 3 scaffolds in ascending order P/CS-2, chitosan and P/CS-1. However, the cell activity decreased with time for all the cryogels, authors did not comment on this result, which questions the material for tissue engineering.

A scaffold of porous chitosan was made for hepatocyte culture, with the ultimate goal of fabricating artificial liver to compensate the lack of organs donors [94]. Chitosan was dissolved in an acetic acid solution. The mixture was coagulated with a NaOH solution and freeze dried. The cryogels were then immersed in sodium alginate solution or heparin solution to induce crosslinking, forming a polyelectrolyte complex thanks to the ionic bonds between the NH_3^+ groups of chitosan and the COO^- or SO_3^{2-} groups of the additional polymer. If chitosan was complexed with alginate or heparin, a second freeze drying was done. The cryogels were immersed in ethanol to sterilize them, washed with water and subsequently with PBS. Lastly, the scaffolds were air-dried and sterilized by UV. The scaffolds presented a porosity around 90% and a pore size ranging from 50 to 200 µm. In the presence of alginate, the surface became granular and the pore walls were textured. Rat hepatocytes were seeded within the scaffolds, which could attach to the pore walls thanks to the positive charges of chitosan and the negative charges of the cell membranes. They also adopted a spherical shape, similar to the in vivo situation. The presence of alginate or heparin improved the albumin and urea secretion over time, confirming the good differentiation in liver cells. Heparin had the most important effect due to its

covalent bonds with a core protein through a serine group: GAGs, attached to the core protein, can bind to the hepatocytes improving the cell adhesion molecules and matrixes.

Kim et al. [95] developed cryogel composites made from bacterial cellulose and chitosan. Bacterial cellulose pellicles were obtained from *Glucobacter xylium*. These pellicles were immersed in chitosan dissolved in acetic acid and after some time taken out of the solution, followed by removal of the excess liquid. The pellicles were then freeze dried. SEM images showed an interconnected porous structure. An increase of the chitosan content resulted in a decrease of the Young's modulus from 6 to 1.8 GPa. Fibroblast cells seeded on the cryogel showed a good cell attachment with spreading and the formation of pseudopodia.

Polyelectrolyte complexes (PEC) of chitosan and hyaluronic acid (HA) were fabricated to be used as scaffold for dental pulp regeneration [96]. Both polymers were solubilized in acetate buffer. The solutions were mixed in a ratio HA:CS 2:1. PEC formed thanks to the ionic bonds between the cationic amine group of chitosan and the anionic acid group of HA. The non-complexed chains were washed out with water and the PEC were freeze dried. The swelling ratio in PBS at 37°C reached a high value of 1222%, indicating a hydrophilic character of the PEC. Degradation was evaluated under the same conditions for 5 weeks. Gels lost 35% of their weight in 3 weeks due the dissolution of weakly bound chains. After this period the degradation stopped as only strong ionic bonds remain. SEM showed interconnected macropores from 1 to 5 µm and a high porosity. Mesenchymal stem cells adhered to the scaffold and developed filopodia after 24h. The cell viability was around 95% after 24h and decreased to 70% after 72h confirming the non-toxicity of the scaffold.

Chitosan/hydroxyapatite (HAP) scaffolds were made to control cell differentiation in bone repair [86]. Chitosan was solubilized in acetic acid. Calcite and urea phosphate were added to the solution to synthesize the HA. The ratios CS/HAP were 100/0, 90/10, 80/20, 70/30, 60/40, 50/50 and 40/60, named HPS-0, HPS-1, HPS-2, HPS-3, HPS-4, HPS-5 and HPS-6, respectively. The samples were frozen and neutralized by immersing them in a solution of ethanol and sodium hydroxide, resulting in the gelation of chitosan. The gel was then dried at room temperature. SEM images showed interconnected pores and a clear influence of the concentration of HAP as shown in Figure I.8. Higher is the quantity of HAP, lower is the pore size. The porosity ranged from 84 to 91%. The swelling ratio was determined in Dulbecco's phosphate buffer saline (DPBS) at 37°C after 24h. Higher is the amount of HAP, lower is the swelling ratio, with values between 2330 and 1360 %. According to the authors, this decrease is due to the formation of a HAP barrier, limiting the water permeation into the scaffold. The Young's modulus decreased with the increase of HAP content from 6.6 kPa to 3.5 kPa going from HPS-1 to HPS-4. The presence of HAP particle agglomerates, due to the high amount of HAP, weakens the network as they are weak load-bearing points in the material. HPS-5 formed an exception, presenting a porosity of 73%, a Young's modulus of 4.7 kPa and a swelling ratio of 1750%. HPS-6 was too brittle to perform a compression test. The largest pores were observed for HPS-4, which could explain the low Young's modulus and the low water uptake. Cell cultures of mouse MC2T3-E1 preosteoblasts showed a good biocompatibility with cells proliferating up to 7 days. The presence of HAP favored cell colonization of the scaffold; however, HPS-5 showed a lower cell number at primary adhesion stage compared to the other scaffolds with HAP which can be attributed to its lower porosity.

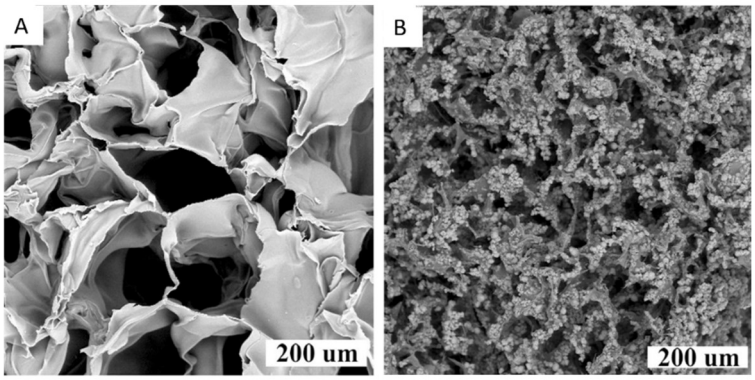

Figure I.8: SEM images of cross section of (a) HPS-0 and (b) HSP-5 scaffold after 24h of DPBS immersion [86]. Reproduced with permission from Springer Nature.

Lyophilized polyelectrolyte complex were prepared for applications as an in vitro cell culture model mimicking organization and function of pancreatic cancers [97]. Chitosan and poly(γ-glutamic acid) (PGA) in different ratios were solubilized in acetic acid and freeze dried, forming a polyelectrolyte complex (PEC) named PEC-CS:PGA with CS and PGA the ratio of polymer. Pure chitosan cryogels were also prepared and crosslinked via ionic bonds using sodium tripolyphosphate. The cryogels showed pore sizes ranging from 50 to 200 µm; a smaller pore size was observed for PEC cryogels than for pure chitosan cryogels. Higher was the concentration of PGA, lower was the absorption of PBS, from 1900% to 1100%, due to the increasing ionic strength resulting in a higher stiffness of the network. Mechanical properties were obtained on cryogels in swollen state in PBS at 37°C. The compression modulus of pure chitosan scaffolds was lower than that of PEC scaffolds, respectively 1.7, 2.5 and 2.2 kPa for pure chitosan, PEC-80:20 and PEC-70:30 due to the increase of ionic strength. The samples presented a good thickness recovery from 89 to 95% with a better recovery for pure chitosan. Cell viability and proliferation of mouse fibroblasts were also assessed. The cell proliferation was approximately 70% after 14 days. SEM images showed cells with a spherical morphology forming clusters, indicative of a poor cell adhesion. The reason may be that the substrate is too soft to promote cell spreading.

Chitosan scaffolds were loaded with magnesium gluconate to help tissue remodeling and development as this element plays an important role in the ECM [98]. Chitosan was dissolved in acetic acid and carboxymethyl chitosan (CMC) in water at 2, 4 and 5wt% and the solutions were mixed in 1:1wt ratio. CMC is negatively charged allowing for stable network formation via complexation with chitosan. Magnesium gluconate was solubilized in water at 5, 10 or 20% relative to the total weight of chitosan and CMC in the scaffold. Solutions were mixed, casted in the wells of cell culture plates and freeze dried. Excess of acetic acid was neutralized by immersing the scaffold in sodium hydroxide solution. SEM images showed a uniform and interconnected porosity with a pore size ranging from 150 to 250 µm and from 50 to 150 µm, respectively, for 2% and 4 - 5% of chitosan. The presence of magnesium did not influence the pore size. Higher was the concentration of chitosan and magnesium, lower was the water sorption with values of 2600 and 1200% for 2% chitosan and 5% chitosan, respectively, both containing 20% Mg. Mechanical properties were evaluated via compression tests. As expected, higher was the concentration of chitosan, higher was the compressive modulus with values ranging from 0.45 to 3.2 MPa. An increase of the modulus upon the addition of magnesium was observed, with a minimal value of 5.2 MPa. Between 5 and 10% of magnesium there was no evolution of the modulus, but an important increase was observed between 10 and 20% to 7 MPa. The release profile of Mg^{2+} in PBS at 37°C was studied as well. A quick release was observed during the first 10 hours up to 50% of cumulative release, after which it stabilized around 75% after 160 hours. Higher was the amount of magnesium in the scaffold, faster was the release. The cytotoxicity of the scaffold was evaluated with fibroblast and osteoblast cells. After 3 days, scaffolds showed a cell viability ranging from 88 to 95% compared to the control cryogel without magnesium, demonstrating the absence of

cytotoxicity. With osteoblast cells, the cell viability ranged from 119 to 101% for 5% Mg to 20% Mg, showing that scaffolds promote osteoblast development.

Kurup and Sumayya [92] prepared a hydroxyapatite-alginate-chitosan (HAC) blend for tissue engineering. Alginate was dissolved at 5%w/v in water and hydroxyapatite was added. A solution of 3%w/v chitosan in 2%v/v of acetic acid was added to the alginate solution. Condensation between the OH groups of chitosan and the COOH groups of alginate and ionic interactions between the amine groups of chitosan and COOH groups of alginate occurred, and hydroxyapatite (HAP) was physically trapped in the network. After homogenization, 3% Na_2HPO_4 and 2% $CaCl_2$ were added to crosslink the chitosan and the alginate respectively. The scaffold obtained was cast, dried overnight and crosslinked again with 10% $CaCl_2$ solution for 30 min. The scaffold was washed to remove residual sodium acetate and $CaCl_2$ and finally freeze dried. Fucoidan, an anionic polysaccharide obtained from brown seaweeds, was incorporated in the scaffolds by adding it to the alginate solution prior to crosslinking. It has an anti-inflammatory effect and improves the cellular activity for tissue regeneration. The scaffold presented a pore size of 74 and 95 µm and a porosity of 65 and 77% without and with fucoidan respectively, indicating an effect of the drug on the network creation which can be explained by hydrogen bond formation between the HAP and the drug. The cryogels presented a water absorption ratio of 290 and 360%, respectively, in 30 minutes without and with the drug. Fucoidan induces a higher hydrophilicity of the material potentially facilitating nutrient transport and cell growth. Both materials exhibited degradation in DMEM and PBS over 30 days, but the drug loaded scaffold degraded slower than HAC. An MTT test did not show any cytotoxicity and the hemocompatibility was confirmed. The absence of inflammatory markers (TNF-α, IL-6 and NF-κB) allowed to conclude that the material does not induce an inflammatory response. These properties make HAC scaffolds loaded with fucoidan interesting materials for tissue engineering applications, with a better physiological acceptation.

Calcium phosphate-containing chitosan-based composites [99] were made by unidirectional freeze drying with the aim of mimicking the properties of living bone. Chitosan was solubilized in acetic acid and mixed in different weight ratios with a dispersion of hydroxyapatite (CS/CaP): 56/3.75, 56/14 and 56/26.3. The solution was then unidirectionally frozen and freeze dried. SEM images showed a pore size ranging from 20 to 50 µm. The CaP content did not influence the porosity, which ranged from 80.1 to 84.6%. This porosity is similar to the one found in cancellous bone tissue. The sample showed no crystallinity despite the semi-crystalline nature of chitosan and the presence of CaP. The absence of crystallinity for chitosan was ascribed to the presence of acetic acid, hindering the formation of inter- and intramolecular hydrogen bonds, thus limiting the organization in the material. The absence of crystallinity for CaP was explained by its amorphous nature. The biocompatibility of the composite was assessed using two cell lines: premyoblasts and preosteoblasts. Higher is the amount of CaP, better is the biocompatibility after 7 days. At a low concentration of CaP, the cells showed a round morphology indicating a poor adhesion to the material. For an elevated concentration of CaP, a high density of cells growing on the surface and inside the scaffold was observed.

Chitosan/fibroin (CF) cryogels with hydroxyapatite (HAP) [100] were prepared for cell transplantation and tissue engineering purposes. Fibroin is a natural biopolymer, which has good mechanical properties and blood compatibility. HAP was dispersed in acetic acid solution and chitosan was added. Fibroin in aqueous solution was added to the mixture of HAP and chitosan with a weight ratio of 0.2 fibroin/chitosan. The ratio CF/HAP was varied from 100/0 to 30/70. The solutions were freeze dried and then dried again under vacuum to eliminate residual solvents. Higher was the amount of HAP, higher was the density (with values from 0.81 to 1.20 g/cm^3) and lower was the porosity (with values from 98% to 94.4%). IR spectroscopy demonstrated the presence of hydrogen bonds between the amino groups of chitosan and the hydroxyl groups of HAP as well as chelation of glucosamine amino groups by Ca^{2+}. SEM images near the surface showed an interconnected porosity with pores from 40 to 200 µm. The pore size decreased with an increasing HAP content. SEM images deeper inside

the material revealed an oriented porosity, according to the authors the internal apertures correspond to the morphology of solvent crystals. A protein permeation test with FITC-BSA showed a better permeation of cryogels with a balanced amount of HAP, as the cumulative release after 24h was 1 and 10 µg/mm² for cryogels with CF/HAP ratios of 80/20 and 50/50, respectively.

Chitosan scaffolds with enhanced mechanical properties were made via a compression method [101]. An acidic chitosan solution was frozen and immersed in a saturated NaCl solution at -20°C for 48h, inducing screening of the chitosan NH_3^+ groups by Cl^-. After thawing the gel was compressed at different strains and simultaneously immersed in a NaOH/NaCl solution to induce coagulation. The obtained gel was washed and stored in PBS. The scaffolds presented a porosity from 55 to 92% and a pore size from 30 µm to 60 µm, whereby the porosity and the pore size decreased with increasing compression ratios. The materials exhibited an elastic modulus from 2 to 500 kPa which could be controlled via the initial polymer concentration and the compression ratio. The absence of cytotoxicity was shown and a good adhesion of human adipose-derived stem cells was observed. Higher was the compression ratio, higher was the density of adherent cells and the cells were colonizing the pores as demonstrated by confocal micrograph images.

Scaffolds of chitosan with nanochitin were prepared to support the growth of human adipose stem cells [89]. Chitosan was dissolved in acetic acid and genipin was added to crosslink NH_2 groups. Chitin nanofibers (NF) or chitin nanocrystals (NC) were added as nanofiller in several chitosan/nanochitin ratios (1/0, 1/0.5, 1/1 and 1/2) and the mixtures were freeze dried. Higher was the concentration of nanochitin, higher were the porosity and pore size; porosity values were 67%, 97% and 94% and pore size values were 90 µm, 300 µm and 400 µm for scaffolds without nanochitin, 1/2 NC scaffolds and 1/2 NF scaffolds, respectively. The authors explained this increase by a lower degree of crosslinking between chitosan and genipin due to the presence of nanochitin. This pore size is adequate for nutrient and oxygen diffusion. SEM images showed macropores with a rough surface due to the presence of nanochitin. The compressive modulus increased with the amount of NC and NF, from 0.16 MPa for scaffolds without chitin to 0.96 MPa and 0.92 MPa for 1/2 NC and 1/2 NF scaffolds respectively. The strain recovery after 72 hours was 23%, 32% and 28% for materials without chitin, 1/2 NC composites and 1/1 NF composites respectively. The presence of nanochitin reinforced the network; the NF showed generally better mechanical properties than NC indicating a stronger entanglement with the chitosan. Chitosan cryogels exhibited a water sorption of 97%. Higher is the amount of chitin, lower is the swelling, 45% and 49% respectively for 1/2 NC and 1/2 NF scaffolds. The cryogels showed a low water uptake compared to other gels in the literature due to the crosslinking. Murine fibroblasts and hematopoietic stem cells (hASC) were used to investigate the cytotoxicity and the cell adhesion. The cell viability varied from 73% to 92% with fibroblasts and 82% to 100 with hASC. Higher is the amount of NC or NF, lower is the cell viability, due to a higher release of chitin, according to the authors. SEM images showed hASC cells attached to the cryogels, developing cytoplasmic projections.

Chitosan scaffolds with resolvin D1 were prepared for *in vivo* bone healing [102]. Resolvin controls neutrophil recruitment and differentiation of macrophages, thereby facilitating bone healing. Chitosan was dissolved in acetic acid and freeze dried. The material was cut in cylinders and sterilized by immersion in ethanol. After washing with distilled water, the gel was freeze dried a second time. Resolvin was dissolved in ethanol and added dropwise onto the scaffold and then freeze dried. A rat femoral bone defect model was used to evaluate the healing capacity in vivo. Cryogels were implanted in the defect with or without resolvin. Histological sections of the femur performed 2 months after implantation showed a layer of newly formed bones being thicker in the presence of resolvin. Identification of collagen fibers was done with the picrosirius-polarization method in transmitted and polarized light. Animals with an implant containing resolvin developed more collagen type I fibers and the ratio Coll I/Coll III was higher than the animals that received scaffolds without resolvin. Evaluation

of bone formation was done by micro-computed tomography. It showed a higher ratio bone volume/tissue volume and a thicker trabecular compared to scaffold without drug. It indicates a high strength of the bone, and it is an important factor for the success of implant-supported rehabilitation as the healing occurs at the interface of the bone and the implant.

Chitosan scaffolds with zinc-containing, nanoparticle-decorated, ultralong hydroxyapatite nanowires (Zn-UHANW) were prepared for application in bone defects [103]. Zinc was incorporated as it has important roles in bone metabolism such as promoting cell proliferation, inhibiting osteoclast differentiation and enhancing osteogenic response of osteoblast. To synthetize Zn-UHANW, sodium hydroxide, $ZnCl_2$, $CaCl_2$, NaH_2PO_4, methanol and oleic acid were mixed in water. The resulting suspension was heated to 180°C and washed with ethanol and water. The formed meshes were then dispersed in water. Control UHANWs were prepared without Zn nanoparticles. The scaffolds were prepared by dissolving chitosan in an acetic acid solution, followed by addition of the nanowire suspension with a ratio UHANW/chitosan of 8:2. The mixture was freeze dried, immersed in sodium hydroxide, washed with water and ethanol and dried at 37°C. The chitosan monoliths presented a higher shrinking compared to the composite monoliths, indicating that the UHANW improve the mechanical properties as they increase the resistance to swelling. The presence of UHANW induced a higher pore size, with values between 50 and 170 µm, 100 and 260 µm and 120 and 430 µm for chitosan, UHANW/Cs and Zn-UHANW/Cs cryogels, respectively (Figure I.9). Scaffolds with nanowires presented a rough surface with entangled fibers of UHANW of several hundreds of micrometers in length. The scaffolds exhibited a high porosity, between 90 and 95%, which is in the range of human cancellous bone. Swelling ratios in water of 1365, 868 and 929% were found for Cs, UHANW/Cs and Zn-UHANW/Cs cryogels, respectively. The lower swelling ratio of the cryogels with nanowires can be explained by the ability of the networks to better resist deformation compared to the CS cryogels. Mechanical tests confirmed that nanowires reinforced the network as the Young's modulus ranged from 5.5 kPa for the CS scaffold to 12.5 kPa and 10.8 kPa for UHANW/Cs and Zn-UHANW/Cs cryogels, respectively. The hierarchical fabric-like pore wall with a strong adhesion between chitosan and UHANW explains the improved mechanical properties. SEM images showed rat bone marrow-derived mesenchymal stem cells (rBMSC) with cytoplasmic extensions on UHANW/Cs and Zn-UHANW/Cs cryogels, indicating a good adhesion and proliferation of the cells in comparison with the Cs scaffold where just a few spherical cells were observed (Figure I.9C and F). This indicates that the presence of nanowires improves the biocompatibility. Cell proliferation experiments confirmed the previous observations. After 14 days, with UHANW/Cs and Zn-UHANW/Cs scaffolds, the rBMSCs showed an enhanced expression of 4 osteogenesis-related genes, indicative of a higher osteoinductive ability. These results were confirmed by *in vivo* bone regeneration tests showing a better regeneration of the bone after 8 weeks for cryogels with UHANW.

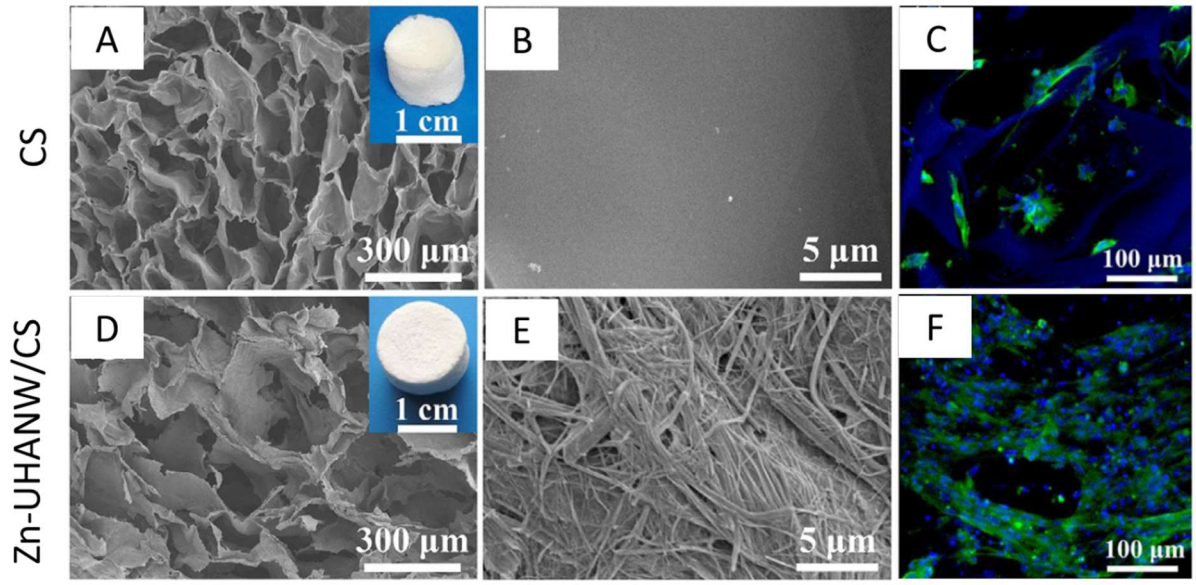

Figure I.9: SEM images of the (A and B) chitosan porous scaffold; (D and E) the Zn-UHANW/Cs porous scaffold. Cytoskeleton staining of rBMSCs cells on the (C) chitosan scaffold and (F) Zn-UHANW/Cs scaffold after 7 days of culture. [103]. Adapted with permission from Sun et al., Chemistry - A European Journal (2018), Vol.24, Issue 35, pages 8809-8821. Copyright 2023, with permission from John Wiley & Sons.

Mahanda et al. [104] developed hybrid chitosan scaffolds for bone tissue engineering. Two types of nanofillers were used: Mg-Al-PO_4-LDH (layer double hydroxide) and an organically modified nanoclay (Cloisite 30B). The resulting composite materials were named CHT-LDH and CHT-C respectively. 5% wt of nanofiller was dispersed in 0.1M acetic acid with dissolved chitosan at concentrations from 1 to 6%w/v, followed by freeze-drying. The presence of nanofiller modified the hydrophilicity of the scaffold according to its nature with CHT-C cryogels being more hydrophobic and CHT-LDH cryogels being more hydrophilic than pure chitosan cryogels as shown by the different swelling ratios after immersion for 5 min in water: 2200, 2700 and 2300%, respectively. Scaffolds with nanofiller presented a higher compressive modulus than pure chitosan scaffolds with values of 23, 30 and 65 kPa for chitosan, CHT-C and CHT-LDH, respectively, making the composite scaffolds structurally more stable to withstand in vivo mechanical stresses. The higher modulus of CHT-LDH can be explained by the hydrogen bonds formed between the OH groups of LDH and the NH_2 groups of chitosan, while only Van Der Waals bonding occurs between clay and chitosan. A broad-spectrum antibiotic, tetracycline hydrochloride, was encapsulated in the scaffold at 6 and 10%wt. The incorporation of nanofiller decreased the drug release rate as 90, 69 and 56% of drug was released in 15h from pure chitosan, CHT-C and CHT-LDH scaffolds, respectively. This is ascribed to the nanofillers acting as barrier to the drug diffusion. The antibacterial activity in vitro against *E. Coli* was assessed and an inhibition zone was observed for all scaffolds. The MTT test showed the absence of cytotoxicity and proliferation tests showed clusters of cells proliferating on the scaffold but also inside the pores. Bone healing efficiency was assessed in a bone defect model in rats. After 8 weeks, only bones treated with CHT-LDH showed a complete healing of the bone, whereas the other materials demonstrated partial healing. Bones treated with CHT-LDH presented a higher number of osteoblast cells and no inflammation in the surrounding tissues was observed.

Chitosan/agarose scaffolds containing extracellular matrix (ECM) extracted from human nose were developed to mimic nasal cartilage [74]. Thanks to the presence of collagen, ECM enhances cellular adhesion and chondrogenesis. Agarose was dissolved in water and chitosan in acetic acid. Chitosan and agarose solutions of different concentrations were mixed in equivalent volumes and ECM was added to the mixture. Glutaraldehyde was used as crosslinker. The samples were washed with water, immersed in 0.1M of glycine and freeze dried. The cryogels were then sterilized using ethanol

and UV. The compressive modulus increased with increasing agarose content and decreasing chitosan content. The presence of ECM decreased the modulus from 0.77 MPa to 0.18 Mpa for ECM concentrations of 0 and 0.75%wt/v respectively. According to the authors, ECM is physically included in the network, thereby decreasing the interactions between chitosan and agarose. The mean pore size varied from 65 to 258 µm, which corresponds to the optimal pore size for the growth of cartilage cells (70 – 120 µm). The cell viability of mesenchymal stromal cells varied from 37 to 98% after 5 days. The degradation of the gels was evaluated for 19 days at 37°C in PBS at pH 7.4. It was found that 12 – 30 % of the gel remains, with a more pronounced degradation for materials without ECM. The optimal scaffold composition selected by the authors for nasal cartilage applications was at a chitosan/agarose/ECM ratio of 0.75/1/1 which offers a compromise between mechanical properties (modulus of 0.569 Mpa), pore size (109 µm), cell viability (98%) and good adhesion of the cells on the cryogel. For this composition, the scaffold exhibited a swelling ratio of 1400% at 37°C in PBS at pH 7.4.

Chitosan cryogels reinforced with electrospun fibers composed of cellulose acetate (CA) and poly(ε-caprolactone) (PCL) [105] were developed for bone tissue engineering. Fibrous mats were electrospun from CA/PCL hexafluoroisopropanol solutions and dried in vacuum. After coagulation with ethanol the mats were cut into small pieces. Ball milling was used to grind the nanofibers, which were then dispersed in a solution of 1%w/v chitosan in 1%v/v acetic acid. The mixture was subsequently injected into a 48-well culture plate and freeze dried. The mean diameter of fibers in the cryogels was 1.5 µm. The presence of nanofibers decreased the average pore size from 17 µm for pure chitosan cryogels to 11 µm for composite cryogels. The presence of fibers enhanced the compressive modulus from 12.5 kPa for chitosan cryogels to 45, 35 and 23 kPa for composite cryogels with 13, 15 and 17 mL of chitosan solution, respectively. A higher fiber concentration induced a higher stiffness. However, the achieved moduli are lower than the mechanical properties of bone, indicating that the stiffness of the proposed scaffolds needs to be further improved. The absence of cytotoxicity was shown and the presence of fibers in the cryogels facilitated cell adhesion and infiltration. Immunohistochemistry demonstrated a faster collagen I production and more markers of osteogenic differentiation for cells in contact with composite cryogels.

Chitosan cryogels with cellulose nanofibers (CNF) [106] were prepared using a crosslinker-free approach to be used as scaffolds for tissue engineering. Four percent by weight of CNF was homogenized in distilled water. Chitosan was dissolved at 5%wt in 1% acetic acid solution. The CNF dispersion and the chitosan solution were mixed in different ratios (60/40 CNF-CS and 40/60 CNF-CS) followed by freeze drying of the mixture. 60/40 CNF-CS and 40/60 CNF-CS cryogels presented a density in between those of the pure cellulose and pure chitosan cryogels, with values of 0.043, 0.111, 0.0081 and 0.141 g/cm^3, respectively. An increase in the chitosan concentration increased the density and the mechanical strength of the scaffolds. 40/60 CNF-CS cryogels presented a slightly enhanced hardness compared to the hardness of pure chitosan cryogels (0.3946 N/mm² and 0.38113 N/mm² respectively) probably due to interactions between the nanofibers and chitosan. As expected, the porosity followed the inverse order of the density with values of 91, 93, 97 and 99% for chitosan, 40/60 CNF-CS, 60/40 CNF-CS and CNF cryogels, respectively. The water sorption for both CNF-CS cryogels was lower than the water sorption for pure CNF cryogels due to the decreasing affinity with the water due to chitosan presence. Pure CNF cryogels induced a 0-log reduction of *E. coli* and *S. aureus* whereas 40/60 CNF-CS cryogels presented a 2-log reduction like pure chitosan cryogel, highlighting the antibacterial properties of chitosan.

(3) Chitosan aerogels for tissue engineering

Chitosan-gelatin aerogels [73] were prepared for bone tissue engineering. Chitosan (CS) and gelatin (G), separately dissolved in acetic acid solution, were mixed in different proportions (CS/G: 1/1, 1/4 and 4/1). Thanks to the interactions between the cationic charge of chitosan and the anionic charge

of the acidic functions of gelatin the gelation is facilitated. Glutaraldehyde (GTA) was used to crosslink amines groups of chitosan and gelatin. Solvent exchange with ethanol was performed and the gels were dried using supercritical CO_2. SEM images showed a homogeneous and nanoporous structure with no significant difference between the CS/G ratios. The specific surface area ranged from 225 to 254 m^2/g. The release of unreacted GTA from samples was followed by UV/Vis in PBS at pH 7.4 with 0.1M glycine. Higher is the amount of chitosan in the composite aerogel, higher is the amount of released GTA with values of 0.31, 2.10 and 2.32 ppm for CS/G ratios of 1/4, 1/1 and 4/1, respectively, due to a higher affinity of gelatin with GTA compared to chitosan. 3 ppm is the toxicity limit above which cell growth is inhibited. The Young's modulus of CS/G, around 173 kPa, was higher than the modulus of single component aerogels, 120 kPa and 54 kPa for chitosan and gelatin respectively, suggesting that an interpenetrating polymer system formed with ionic interactions between chitosan and gelatin chains. These composite aerogels are promising for bone tissue engineering thanks to their Young's moduli suitable for bone regeneration (above 150 kPa).

Silica (SiO_2)/chitosan (CS) composite aerogels were proposed by Perez-Moreno et al. [107] as bioactive scaffolds for bone tissue regeneration. A heterogenous solution of TEOS (tetraethyl orthosilicate) in aqueous HCl was mixed with a HCl solution of chitosan in different ratios to obtain 1.7, 6.5 and 10.3 % of chitosan in the gel. Hydrogen bonding between the OH groups of silica and the NH_2 groups of chitosan was shown by FTIR. The gels were aged in ethanol for 28 days and finally dried with supercritical CO_2. Uniaxial compression revealed a viscoelastic behavior with a Young's modulus decreasing with increasing CS content, with values of 11.6 and 0.7 MPa for SiO_2 aerogels and composite aerogels with 10 % chitosan, respectively, due to the lower modulus of pure chitosan. Fickian diffusion of water inside the aerogel could be observed. After immersion in PBS for 4 weeks, hydroxyapatite crystallites formed at the surface of the cryogel (Figure I.10), having a Ca/P ratio of 2 which is similar to the value of tetracalcium phosphate used in cement for bone repair. Human osteoblasts placed in contact with the scaffold survived for a short period (98% of cell viability after 48h) but the material presented cytotoxicity after 1 week with only 64% of living cells left. The authors did not give any explanation for this cytotoxicity; clearly this issue needs to be solved as the biomaterial is intended for long term application i.e. bone tissue engineering.

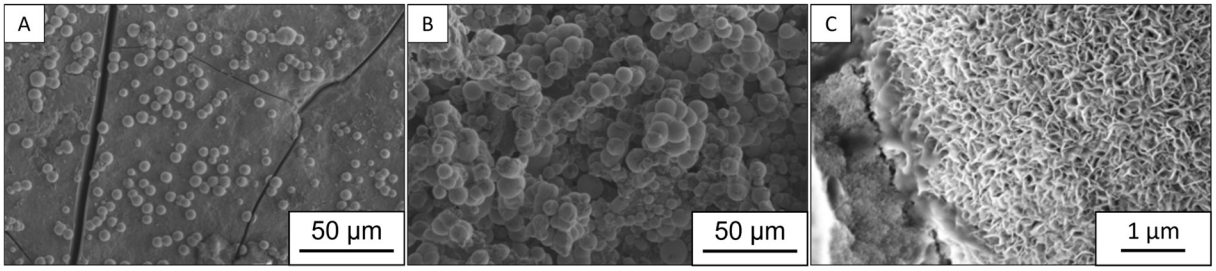

Figure I.10: SEM images of a 6.5% chitosan-silica aerogel after (a) two weeks and (b) four weeks. Picture (c) shows the needle-like surface crystallites of spherulite. Adapted from [107].

Reyes-Peces et al. [108] prepared chitosan-3-glycidoxypropyl trimethoxysilane (GPTMS)-silica aerogels via a sol-gel method for bone tissue engineering. A suspension of TEOS in aqueous HCl was mixed with a GPTMS-containing solution of chitosan in acetic acid, resulting in gelation via hydrogen bond formation between TEOS and chitosan. The gels were left aging for 10 days at 50°C and the solvent was replaced by ethanol, followed by supercritical drying with CO_2. The final chitosan concentration was between 1.7%wt and 10.3 %wt. A decrease in the TEOS/CS ratio from 150 to 30 generally resulted in a decrease of the density from 0.38 to 0.17 g/cm^3. Despite a decrease of the density and an increase of the porosity with decreasing TEOS/CS ratio, the specific surface area decreased suggesting the pore size increased, which was corroborated by BJH measurements. The compressive modulus could be tuned from 1.9 to 50.3 MPa by increasing the GMTPS/CS ratio.

Hydroxyapatite spherulites formed after 7 days on the aerogel immerged in SBF. Osteoblasts were able to adhere and divide on the aerogel, showing the potential of this material for bone tissue reparation.

To the best of our knowledge, no porous chitosan biomaterial for tissue engineering has been commercialized yet.

Research on porous chitosan for tissue engineering mostly targets bone and conjunctive tissues (Figure I.11). The incidence of bone fractures is increasing due to the aging of the population [109]. Depending on the fracture area, the treatment is different. For example, a fracture of the ulna or radius can be treated with classical methods such as fracture reduction and casts for external fixation. However, for example for tibia, ankle, scapula, or humerus fractures, healing can be delayed or result in a non-union without surgical treatment. For these fractures, a porous chitosan material could improve healing by providing a support for cell growing.

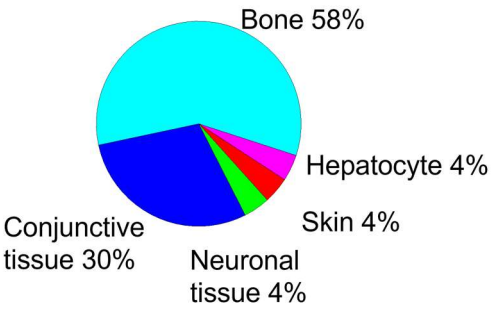

Figure I.11: Pie chart of the different applications targeted for porous chitosan scaffolds in tissue engineering.

Figure I.12 shows the range of porosity (A) and modulus (B) values as a function of the pore size for porous chitosan biomaterials developed for tissue engineering. All these properties can be tuned by adapting the chitosan concentration, by changing the type of drying, by adding other components allowing crosslinking (such as genipin) or by making a hybrid material (with for example hydroxyapatite). Most of the materials present a high porosity (>60 %) with a pore size ranging from 10 µm to 400 µm, which is the pore size to target for osteoconduction. The modulus ranges from 1 kPa to 100 MPa which can provide different support for cell growth depending on the cell type.

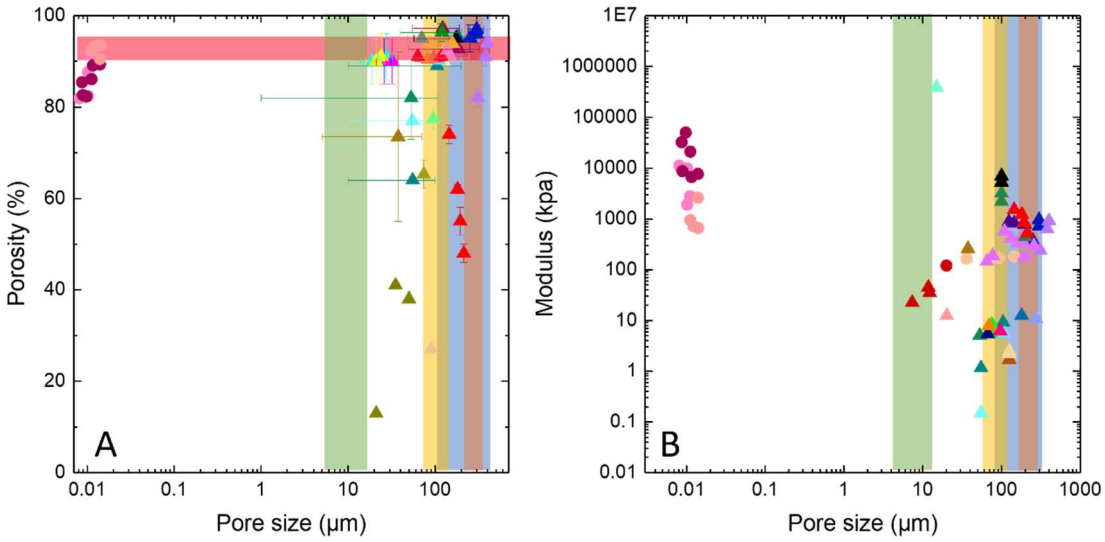

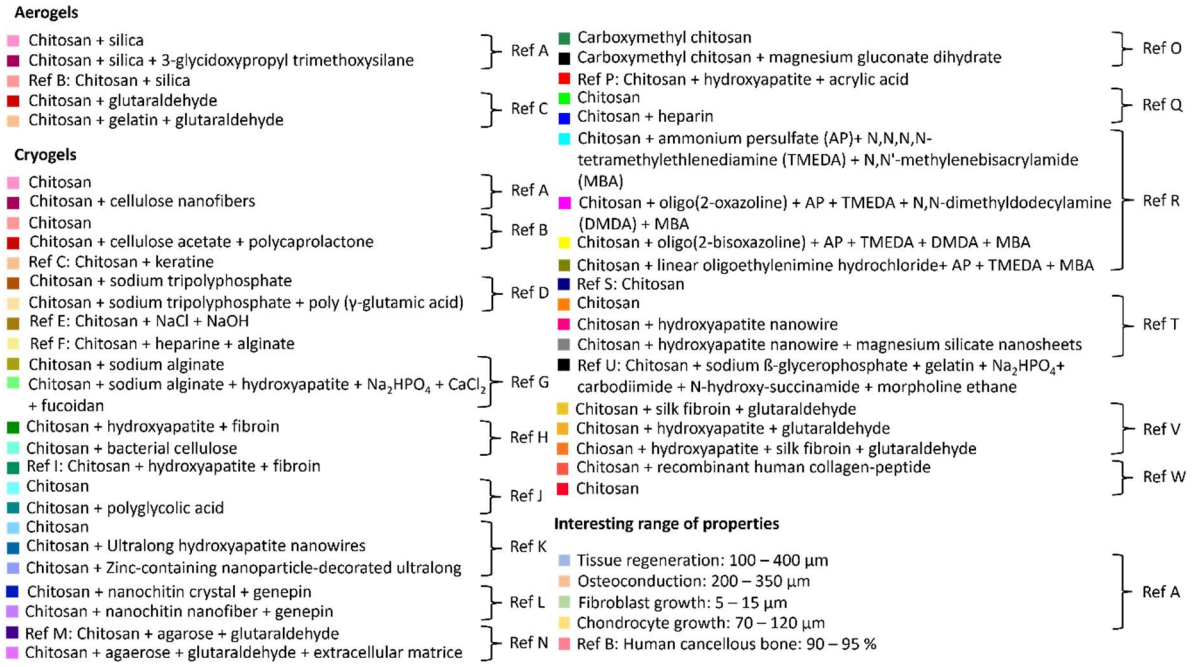

Figure I.12: Variation of the porosity (A) and the modulus (B) as a function of the pore size. Methods of drying are represented by triangles for freeze drying and circles for supercritical drying. The colored bands indicate ranges of interesting properties to aim for.

Correspondence letter-reference figure i.12 :
***Aerogel**: Ref A:[108]; Ref B:[107] * porosity calculated with $\rho_{skeletal}$ = 2.09 g/cm³ [110]; Ref C:[73]*
***Cryogel**: Ref A:[106]; Ref B:[105]; Ref C:[111]; Ref D:[97]; Ref E:[101]; Ref F:[94]; Ref G:[92]; Ref H:[100]; Ref I:[95]; Ref J:[86]; Ref K:[93]; Ref L:[103]; Ref M:[89]; Ref N:[74]; Ref O:[98]; Ref P :[70] ; Ref Q :[112]; Ref R :[113]; Ref S :[78]; Ref T :[114]; Ref U :[115]; Ref V :[116]; Ref W :[117]*
Interesting range of properties *: Ref A: [86], Ref B: [103]*

Chitosan scaffolds for tissue engineering can be prepared with the desired properties depending on the targeted tissue to regenerate. It should be noted that aerogels usually present a pore size too small for most of the tissue engineering applications, cryogels pore sizes are much larger and thus more adequate material for these applications. The modulus of these materials is generally lower than the one of the tissues, so improvements have to be made to approach mechanical tissue properties.

3.1.2. Porous chitosan for drug delivery

(1) Expected properties

In controlled drug delivery, a drug is delivered locally or systemically at a predetermined rate for a specific period of time. Controlled drug delivery facilitates keeping a drug level within a desired range, optimizes drug utilization, allows for fewer administrations, and may increase patient compliance.

Potential disadvantages include toxicity of the used material, undesirable by-products from degradation, the necessity for surgery to implant or remove the device, possible discomfort for the patient from the delivery device, and higher costs compared to classical drug administration. To prevent these drawbacks, the ideal drug delivery system should be inert, biocompatible, mechanically strong, comfortable for the patient, easy to administer and remove and straightforward to prepare and sterilize. The drug release should be controlled, ideally following a zero order release i.e. independent of the drug concentration [118], thereby avoiding a burst in drug concentration which

may lead to toxic effects for surrounding cells. At the same time, the device should release a sufficient amount of drug to achieve the minimum effective concentration.

Specific requirements for drug delivery systems depend on the route of administration, the targeted site and the minimum effective concentration.

The drug carrier, here the porous chitosan, should be able to accommodate and release the drug. Parameters that influence drug release include the carrier porosity, drug-polymer interactions, temperature, pH and degradation/erosion of the matrix. Porosity seems to play an important role: for example, macropores promote drug diffusion resulting in a fast release rate [26].

(2) Chitosan cryogels for drug delivery

Drug release of teicoplanin and vancomycin from crosslinked chitosan beads was studied. Chitosan was dissolved in acetic acid, glutaraldehyde was added as a crosslinker, and the solution was dropped into a sodium hydroxide solution and left 15min to crosslink and gel. The chitosan beads [119] were collected and immersed either in vancomycin hydrochloride solution or in teicoplanin solution. Both drugs have antibacterial properties. The beads of a few millimeters were then freeze dried. Prolonging the time of immersion significantly increased the time to achieve 50% of teicoplanin release, but this was not the case for vancomycin. The time to release 50% of antibiotic load was shorter for vancomycin (Mw= 1449 g/mol) than for teicoplanin (Mw= 1879 g/mol), which can be explained by the higher electrostatic and hydrogen binding capacity of teicoplanin thanks to more lipophilic groups, according to the authors.

Hybrid cryogels of chitosan-*g*-glycolic acid and Au-Fe_3O_4 nanoparticles [120] were synthetized by Singh et al. for controlled delivery and tissue engineering applications. Glycolic acid and an anti-cancer drug, cyclophosphamide, were added to an aqueous chitosan dispersion. Au-Fe_3O_4 nanoparticles were also included with the aim of controlling the drug release. Glycolic acid was grafted on chitosan through the formation of amide bonds between the amine groups of chitosan and the acidic function of the glycolic acid. The solution was cast onto tissue culture plates and freeze dried. The pore size was 3.4 – 4.9 µm. Scaffolds dissolved completely in acidic media within 3.5 h, but were stable in basic or neutral solutions. The acidic solution protonated the amine functions of chitosan and solubilized the polymer. The drug release in 0.1M phosphate buffer at 37 °C was fast in the first hours as the drug present on the surface of the sample was released. Later on, the release slowed down as the drug located deep inside the pores was released. The proliferation of fibroblast cells on the scaffold was evaluated by an MTT assay. No cytotoxic effect was observed as the cell growth was almost 100% after 70h compared to a control without chitosan.

Thermo- and pH-responsive, poly (N,N'-diethyl acrylamide) (PDEAAm) coated chitosan-collagen cryogels [121] were prepared for the controlled delivery of therapeutic agents. Chitosan and collagen were dissolved in acetic acid solution. Bovine serum albumin (BSA) or ibuprofen (Ibu) were added, and the solution was freeze-dried. The cryogel was crosslinked by reaction of the amine functions with glutaraldehyde to varying extents via saturated supercritical CO_2. PDEAAm was polymerized in situ using supercritical CO_2 containing the monomer DEAAm, the cross-linking agent N, N'-methylenebisacrylamide and the initiator the 2,2'-azobis(isobutyronitrile). PDEAAm is a thermo-sensitive polymer with a lower critical solution temperature (LCST) around 34°C. Below this temperature the polymer forms a swollen gel in aqueous solution, above this temperature the gel dehydrates and collapses. The cryogels exhibited a porosity between 54 and 92%, a Young's modulus between 1.8 and 20.6 MPa and a degradation by lysozymes between 15 and 71 % after 40 days of incubation. Porosity and Young's modulus increased with increasing gluturaldehyde concentration whereas the degradation became less pronounced. The matrix becomes more hydrophobic due to the crosslinking and hence has more affinity with $scCO_2$, leading to a higher porosity. The pore size (10 – 37 µm) decreased in the presence of PDEAAm, as the polymer covered uniformly the walls of the

scaffold. Swelling properties were determined at different temperatures and for different pH and glutaraldehyde concentrations. Increasing the pH or the temperature decreased the swelling ratio, which had values between 150 and 750%. At pH 5, the amino group of chitosan is protonated, resulting in increased hydrophilicity and swelling. Below its LCST, PDEAAm establishes hydrogen bonds with water, transforms into a swollen gel and makes the scaffold permeable which results in a high swelling ratio. When the temperature is above the LCST of PDEAAm the gel collapses leading to a decrease in the swelling ratio. An increase in the crosslinker concentration decreases the ratio due to the increase of stiffness. The mass loss of the cryogels in 40 days via enzymatic degradation in PBS by lysozyme decreased with increasing crosslinking degree. The PDEAAm coating did not seem to have an influence on the degradability. The cytotoxicity of PDEAAm solutions was assessed on fibroblast cells, the cell viability decreased to 40% for high concentration (10 mg/mL) and 70% for low concentrations (0.1 and 1 mg/mL) compared to fresh medium. The solutions are therefore considered cytotoxic according to the ISO standard [85]. A high crosslinking degree led to a slow drug release profile, as expected. Increasing the pH increased the drug release rate. At pH 5.5, collagen (pI ≈ 7.8) and chitosan (pKa = 6.2) are protonated whereas BSA (pI ≈ 4.8) and Ibu (pKa = 4.8) are deprotonated, resulting in electrostatic interactions and slow drug release. At pH 7.4, all the molecules are deprotonated, so there are no more interactions and the drug release is faster. Ibu release was faster than BSA release due to the smaller molecular weight of Ibu. The coating of PDEAAm on the cryogel provided an on/off character regarding drug release which could be controlled via the temperature. Below the LCST there was a burst in the drug release, at a temperature above the LCST the release was almost zero.

Chitosan-graft-poly(acrylic acid)/nano-hydroxyapatite cryogels were prepared by Asadian-Ardakani et al. for application as drug-releasing bone tissue engineering scaffolds [70]. The non-steroidal anti-inflammatory (NSAID) drug naproxen sodium was selected as a water-soluble model drug. Poly(acrylic acid) was grafted on chitosan via free radical polymerization in a solution of chitosan with potassium persulfate as initiator and N,N'-methylene-bis-acrylamide as crosslinker. Heating the mixture resulted in the formation of a free radical on the chitosan C_3, initiating the polymerization of acrylic acid. Hydroxyapatite (HAP) powder was added in various amounts (1:0.25, 1:0.5, 1:0.75, and 1:1 chitosan/n-HAP ratio) to the blend and was trapped in the network. The polymerization and crosslinking were stopped before the gelation point and the suspension was dried in an oven. The obtained powder was then dissolved in acetic acid, cast in a mold and freeze dried. The gelation percentage was estimated between 12 and 27% depending on the concentration of HAP. The naproxen was incorporated by soaking the scaffolds in a drug solution. The scaffold, containing interconnected pores ranging from 145 to 213 µm, had a porosity between 48 and 74%, SEM images are shown Figure I.13. The increase of the ratio of HAP decreases the percentage of acrylic acid grafted onto chitosan and of HAP trapped inside the network. The pore size decreases and the porosity increases with the increase of HAP content, authors suggest that higher crystallinity of the network was the reason. HAP also influenced the mechanical properties such as the elastic modulus, which increased from 0.52 GPa to 1.52 GPa with an increase in HAP concentration. This was ascribed to ionic interactions with the polymers, resulting in physical crosslinking strengthening the network. According to the authors, the formation of hydrogen bonds and ionic interactions during the graft polymerization and the addition of HAP lead to a decrease of the crystallinity of chitosan and therefore to a lower compressive modulus, which ranged between 1.65 and 5.85 MPa. Mechanical properties were similar to those of trabecular bone. The swelling ratio (30 – 78%) decreased with an increase in HAP concentration. Higher amounts of HAP induced a higher loading capacity (22 – 34%) and encapsulation efficiency (45 – 69%), which was explained by the increase in porosity and the increased possibility of electrostatic and hydrogen interactions with the drug through ionic groups such as Ca^{2+}, PO^{3-} and OH^-. The drug release was controlled by Fick diffusion. On the first day, a burst release was observed with 20 – 33% of the cumulative release, which was followed by a relatively constant release up to 40 – 70% on the 14^{th} day.

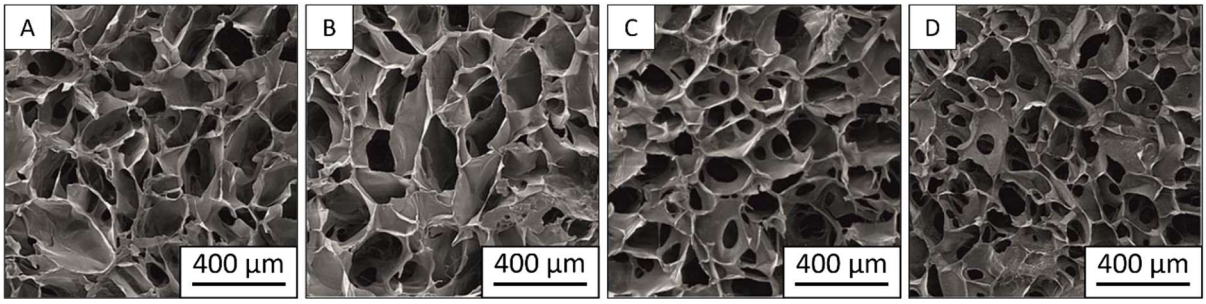

Figure I.13: SEM images of the nanocomposite scaffolds with chitosan/HAP ratio of (A) 1:0.25; (B) 1:0.5; (C) 1:0.75 and (D) 1:1 [70]. Reproduced with permission from Asadian-Ardakani et al., Journal of biomedical materials research part A (2016), Vol.104, Issue 12, pages 2992-3003. Copyright 2023, with permission from John Wiley & Sons.

Chitosan-alginate cryogels [122] were made for postprandial glucose management via the release of α-Amylase inhibitors (α-AIs). An acetic acid solution of chitosan and calcium chloride was mixed with an aqueous solution of sodium alginate. Gelation occurred via ionic interactions; the obtained hydrogels were washed several times with water and freeze dried. α-AIs was incorporated via impregnation of the networks in an aqueous drug solution. The loaded gels were subsequently freeze dried a second time. The drug-loaded aerogels presented a density of 0.274 g/cm^3 with a specific surface area of 105 m²/g. In vitro studies showed that placing the cryogels for 2h in simulated gastric fluid results in inhibition of α-AIs activity. However, after moving the networks to simulated intestinal fluid the α-AIs became active and exhibited a high inhibition rate of 80%. This drug carrier was tested on rats via intragastric administration and showed a high potential to limit hypoglycemia with an increase of postprandial blood glucose levels of 11.5 mg/dL instead of 30 mg/dL for a control formulation.

(3) Chitosan aerogels for drug delivery

Chitosan aerogel microparticles [75] for pulmonary drug delivery were prepared by adding an aqueous solution of chitosan dropwise to an aqueous solution of sodium tripolyphosphate to induce ionic interactions between NH_3^+ groups of chitosan and O^- groups of tripolyphosphate anions. Water was replaced by ethanol to facilitate supercritical CO_2 drying. Salbutamol, a bronchodilator, was incorporated in the chitosan microparticles by dispersing the drug in the ethanol prior to the drying process. The size of the particles was between 8 and 240 µm and the density ranged between 0.07 and 0.32 g/cm^3. Increasing the concentration of chitosan increased the particle size and density. The specific surface area for aerogels based on chitosan with a molecular weight of 250 kDa was around 102 m²/g and according to the authors, total pore volume was 0.29 cm^3/g. Lower values were found for aerogels made from chitosan with a lower molecular weight (16 kDa): 73 m²/g and 0.20 cm^3/g, respectively. The values of the specific surface area are relatively low for aerogels, but no explanation was proposed. The release of salbutamol into PBS was controlled by diffusion and erosion of the polymeric matrix, as shown by the Korsmeyer-Peppas model, except for low concentrations of crosslinker where only Fick diffusion took place. The aerogels demonstrated a good stability over time as 3 months of storage did not affect their properties.

An emulsification-gelation method was used to prepare chitosan-alginate nanoporous carriers loaded with cisplatin to treat lung cancer [123]. An oil phase composed of paraffin oil and 4% of sorbitane trioleate as a surfactant. After homogenization, an aqueous 2% chitosan (13 kDa) solution was added to the oil phase. One percent of an aqueous alginate solution was added, resulting in polymer complexation thanks to positive amine groups of chitosan and negative carboxylic acid groups of alginate. The hydrogel microparticles were then dried with supercritical CO_2 and supercritically impregnated with cisplatin. Particles of 430 nm in diameter were obtained; they presented a specific surface area of 86 m²/g and a pore size of 13 nm. Cisplatin was partially released (60%) in 2 h in PBS

(pH 7.4) at 37°C. Cisplatin is known to induce nephrotoxicity, hepatic toxicity, and lung toxicity. *In vivo* studies on rats showed a reduction of the lung toxicity and of the mortality rate when the drug is carried by the chitosan-alginate aerogel particles. A reduction of the toxicity is needed to pursue a biomedical application.

Diosa et al. [124] developed a chitosan-silica hybrid material support for antimicrobial peptide KR-12 loading and delivery. Sodium silicate was dissolved in sodium acetate solution and the pH of the mixture was adjusted to 6, 7 or 8 with acetic acid. Chitosan, dissolved in acetic acid, was added to the silica mixture. The pH of the system was re-adjusted to the original value, left reacting, washed with water and dried in open air. Chitosan-silica materials were subsequently soaked in a solution of KR-12 (25 mg/L – 1000 mg/L) in phosphate buffer at pH 8. The specific surface area decreased with increasing solution pH from 745 m²/g to 345 m²/g. The high specific surface area was explained by the absence of a chitosan pore-templating effect implying that chitosan and silica species are randomly associated during the gelation, according to the authors. SEM images showed a material composed of nanoparticles (100 nm) and their agglomerates (583 – 766 nm). BJH analysis demonstrated pore diameters around 3 nm, corresponding to the interstices between the nanoparticles. KR-12 peptide adsorbed as a monolayer on chitosan materials prepared at pH 6 following the Langmuir model thanks to the large specific surface area and total pore volume (0.58 g/cm^3). In contrast, materials prepared at pH 7 or 8 followed the Freundlich model with adsorption of KR-12 as multilayers on the surface, as these materials are less porous and quickly saturated. The release profiles of KR-12 showed a burst during the 1st hour. A higher pH of the initial solution resulted in a faster release confirming that electrostatic interactions are more implied in the adsorption. The MIC against *S. aureus* increased with the pH of the initial solution from 128 to 256 µg/mL. The monolayer of drug formed at pH 6 on a large surface area made the drug more available to interact with bacteria compared to small surface areas with multiple layers of drug formed at higher pH values.

An aqueous sodium alginate solution and an acetic acid chitosan solution were mixed to prepare alginate – chitosan IPEC [125]. After solvent exchange and supercritical CO_2 drying, the aerogel was impregnated with levomycetin in an aqueous solution. The IPEC presented a specific surface area of 260 m²/g with an average pore size of 16 nm. The morphologies obtained are illustrated on Figure I.14. Absorption of PBS at pH 5.5, 6.4 and 8.5 was evaluated at 20, 30 and 35 g/g respectively. In 5 h, 95% of levomycetin was released into PBS. First order kinetics as well as the Higuchi model were used to describe the release.

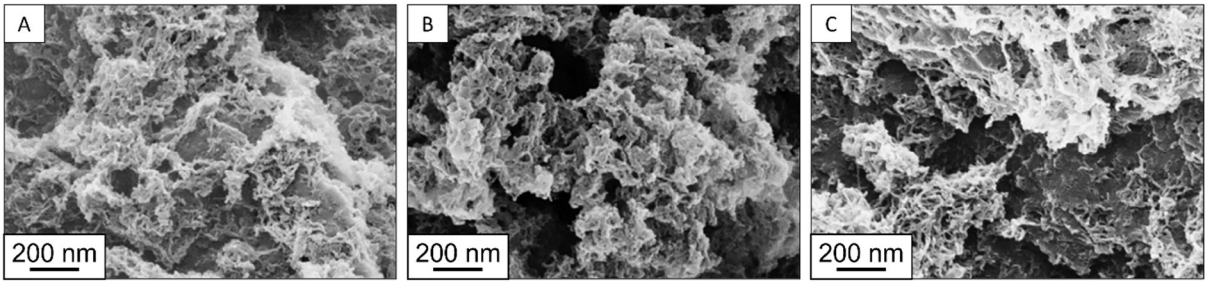

Figure I.14: SEM images of aerogels of alginate/chitosan in different ratios (A) 0.8, (B) 1.0 and (C) 1.2 [125]. Adapted with permission from Gorshkova et al., Polymers for Advanced Technologies (2021), Vol.32, Issue 9, pages 3474-3482. Copyright 2023, with permission from John Wiley & Sons.

To the best of our knowledge, no commercial drug delivery system based on porous chitosan exists.

Most of the drugs that have been incorporated in porous chitosan have antibiotic or anti-inflammatory properties (Figure I.15A). Chitosan is not only employed as drug carrier, most of the time,

its mechanical and absorption properties are exploited for wound healing applications or for tissue engineering, for example to enhance new tissue formation or prevent infection. To compare the systems with each other, the drug release rate was used: it is the maximum release achieved by a system divided by the time needed to reach this release. For example, a system which has a maximum release of 80% in 2 h will have a drug release rate of 40%/h. A high specific surface area is generally associated with a lower drug release rate (Figure I.15B). Figure I.15C shows two distinct groups for drug release rates: cryogels with a large pore diameter in the micrometer range and aerogels with a pore diameter below 100 nm. However, despite the small pore size exhibited by aerogels, the drug release is faster compared to cryogels which is surprising. An adequate comparison between cryogels and aerogels can only be done when the materials are from the same precursor and present the same density. An important parameter, that is not considered here, is the possible interactions and the affinity of the drug with the matrix, possibly slowing down the drug release.

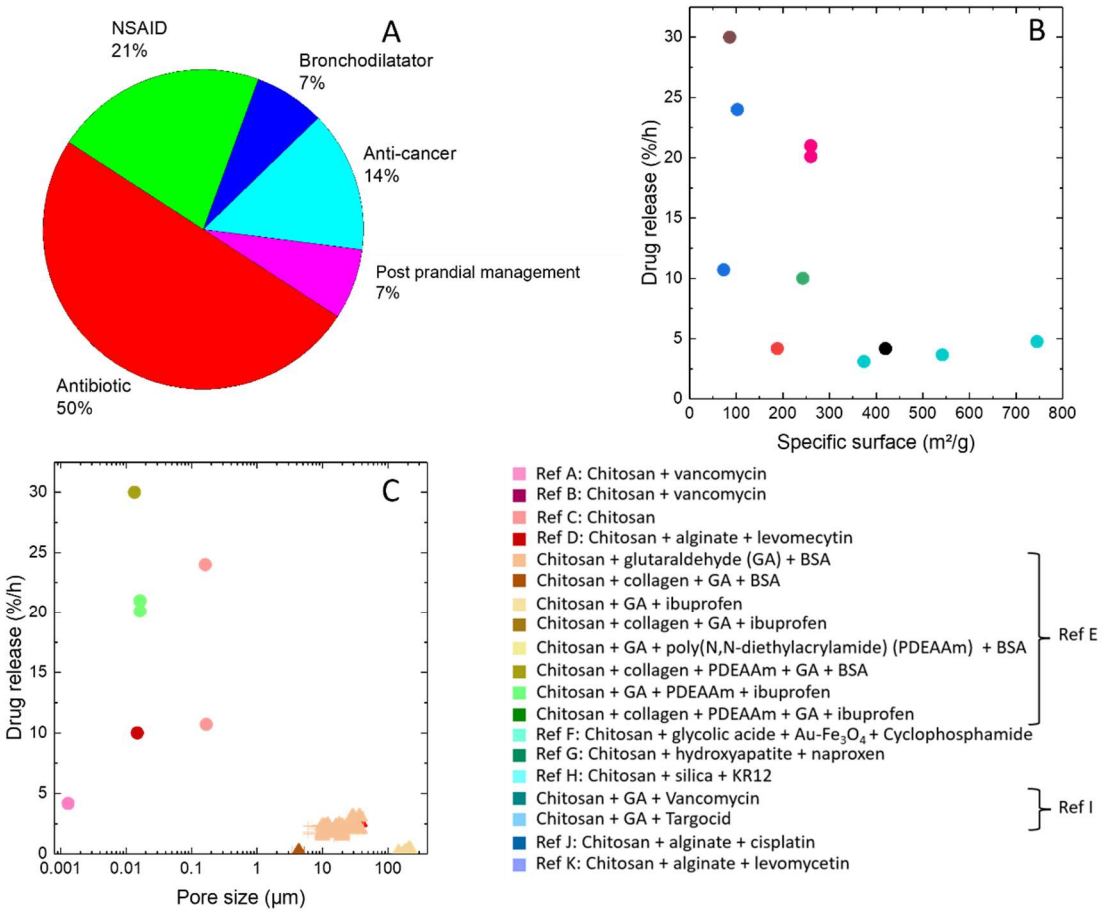

Figure I.15: (A) Circle chart of different drug types incorporated in chitosan aerogels and cryogels. (B) Drug release rate vs specific surface area for chitosan aerogels and cryogels reported in literature and (C) drug release rate vs pore size for chitosan aerogels and cryogels reported in literature. Triangles represent the cryogels and circles aerogels. The error bars indicate the variation in drug release/specific surface area/pore size reported in the articles.

Correspondence letter-reference Figure I.15:
Ref A: [26]; Ref B: [71]; Ref C: [75]; Ref D: [126]; Ref E: [121]; Ref F: [120]; Ref G: [70]; Ref H: [124]; Ref I: [119]; Ref J: [123]; Ref K: [125]

3.1.3. Wound dressings

(1) Expected properties

Although wound dressings have been used since 2000 BC, it was not until 1962 that Winter [127] proved that wound healing is more efficient in moist conditions. Under such circumstances, there is no scabbing, the wound is not dehydrated, and wound healing is twice as effective. There are many types of wounds, each of which is very specific depending on the etiology, the location of the wound, the patient, and the stage of healing. There is no universal dressing and, consequently, each dressing needs to be adapted to the situation. Nonetheless, several general requirements can be defined for wound dressings. The ideal wound dressing [128] is described as a dressing that creates conditions which promote wound healing, including a moist wound environment and the possibility for gas exchanges. This dressing should absorb the exudate, increase the temperature at the wound site, be impervious to liquids and bacteria, be comfortable and sterile. It should not stick to the wound and not degrade being on the wound. New cells should not be able to colonize the dressing to ensure an atraumatic removal. The dressing should also be adaptable to the shape of the wound, absorb the odour of the wound and be cost effective [129]. Pusateri and al. [130] described the ideal hemostatic dressing for prehospital use. The dressing should be easy to use with minimal training and not require any preparation or mixing. A dressing safe to use with no risk of injury for the tissue nor bacterial or viral transmission is needed. The dressing should be lightweight, durable, stable between 10°C and 55°C, and inexpensive. Its most important quality is to be able to stop, within 2 minutes, large-vessel arterial and venous bleeding.

Ideal values for several important dressing-related properties, which facilitate an efficient and safe use, have been identified and will be discussed below.

The water vapor transmission rate (WVTR) [131] is 204 g/m²/day for intact skin, but for an injured skin it can go from 279 g/m²/day for a first degree burn to 5138 g/m²/day for a granulated wound. To maintain ideal moist conditions, the rate for a dressing should be around 2500 g/m²/day to allow for sufficient drying to avoid bacterial proliferation; at this value, excessive drying, which may favor the formation of scab, is avoided. To facilitate the absorption of wound exudate, material porosity should be in between 60 to 90% [132]. As dressings are directly in contact with the wound, they must be compatible with red blood cells, to prevent interference with hemostatic activity. Materials with hemolysis values lower than 5% can be safely used, according to ISO 10993-4 [133]. The pH of the wound during healing varies from 8.9 in a chronic wound, to 6 in an epithelized wound, to 5 for intact skin. The pH variation should not induce the release of toxic compounds from the dressing into the wound; ideally the dressing should be 'smart' and adapt its properties to the state of healing to always have optimal properties. According to the French High Authority of Health (Haute Autorité de Santé [134]) the sorption properties of hydrocellular primary dressings, composed of polymers, must be superior or equal to 30 g/100cm²/24h for films and three-dimensional shapes and 8 g/g/24h for dressings intended for filling cavity wounds.

(2) Chitosan cryogels for wound dressings

Most of the cryogels for wound dressing applications reported in literature are composite materials to obtain better mechanical properties compared to pure chitosan.

Cryogels consisting of a semi-interpenetrating network (IPN) [135] were prepared by UV polymerization after mixing two solutions in various ratios: N-carboxyethyl chitosan (CECS) and 2-hydroxyethyl methacrylate (HEMA) aqueous solutions, the latter containing a UV photoinitiator and the crosslinker (ethylene glycol) dimethacrylate (EGDMA). A free radical polymerization took place via the double bonds of HEMA and of EGDMA. The xerogel was washed and dried under vacuum. The maximum swelling ratio in water was achieved in 25 h for all semi-IPNs; it was from 65% up to 85% for semi-IPNs containing a lower concentration of crosslinker, leading to a more loosely crosslinked

network. SEM images showed a porosity of a few micrometers. Markedly, the pores did not collapse during the drying thanks to the solid network formed after crosslinking. The semi-IPNs showed a lower in vitro cytotoxicity than pure chitosan and CECS.

A genipin-containing porous chitosan-collagen-gelatin scaffold [136] was prepared by blending an aqueous solution of gelatin and collagen with an aqueous solution of chitosan. Genipin at different concentrations was added as crosslinker to the aqueous blend and the degree of crosslinking between collagen and chitosan -OH groups was respectively 7%, 13% and 28%. The samples were subsequently freeze-dried. A higher degree of crosslinking resulted in a higher porosity (values were between 25 and 45 %) and a larger cross-sectional area of the pores (values between 187 and 1066 µm²) shown on Figure I.16. The swelling properties were investigated as function of the genipin concentration and the composition of the absorbed fluid. The presence of genipin resulted in a higher swelling (2400 – 2760%) compared to non-crosslinked cryogels (2000%) because of weak mechanical properties of the non-crosslinked scaffold leading to an unstable 3D structure. Increasing the concentration of genipin decreased the swelling ratio. The composition of the absorbed fluid also had an influence on the swelling ratio: for a sample crosslinked with 0.5% of genipin the absorption of water was around 6250% whereas a medium with a salt composition similar to wound exudate resulted in a swelling ratio of 2760%. A higher concentration of genipin allowed for a better stability in wound exudate (23 – 33% of dissolution in 120 h). An enzymatic degradation of 6% in 168h was induced by lysozyme. The concentration of genipin did not influence the WVTR which was around 410 g/m²/day for every sample. The cryogel showed better anti-oxidative properties than commercial wound dressings (alginate hydrocolloid dressing and cotton gauze dressing). The presence of genipin did not induce cytotoxicity.

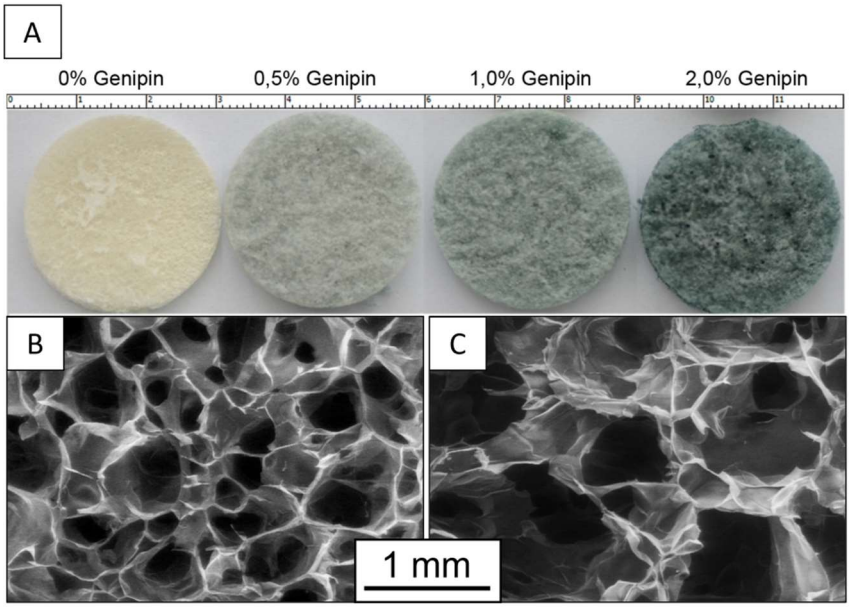

Figure I.16: (A) Pictures of the chitosan-protein scaffold crosslinked with different degree of genipin. (B) Cross sectional SEM images of the chitosan-protein scaffold with (B) no crosslinking and (C) 2% of genipin [136]. Reprinted from Carbohydrate Polymers, Vol 102, Gorczyca et al., Preparation and characterization of genipin cross-linked porous chitosan–collagen–gelatin scaffolds using chitosan–CO_2 solution, Pages 901-911., Copyright 2023, with permission from Elsevier.

A porous cryogel of chitosan and keratin [137] was prepared to accelerate wound healing and skin regeneration. Chitosan was dispersed in a keratin aqueous solution and was freeze-dried. The concentration of chitosan was varied from 50 to 1000 µg/mL and the properties of the cryogels were compared with those of pure chitosan and keratin. SEM images showed a porous material (70 – 90%) with a pore diameter between 80 and 125 µm. The cryogel hydrophilicity could be tuned via the concentration of chitosan as shown by the water contact angle which increased from 60° to 100° with

an increase of the chitosan concentration. The swelling properties were reported in between 120 – 220%. The mass loss in PBS and in lysozyme solution was respectively 20 – 50% and 25 – 50% after 30 days. Higher was the concentration of chitosan, lower were the swelling ratio and the mass loss, which was explained respectively by the decrease of the hydrophilicity and the poor degradation properties of chitosan. Pure chitosan material showed a higher swelling ratio and lower or equivalent contact angle in comparison with the composites. Antibacterial properties were assessed in vitro against *S. aureus* and *E. Coli*. All composite scaffolds presented better antibacterial properties than pure keratin but lower antibacterial activity than pure chitosan. It is supposed that the NH_3^+ groups of chitosan are complexed by the anionic charges of the keratin and therefore not available to interact with bacterial walls. The antibacterial properties improved with higher chitosan concentrations. The cytocompatibility was investigated with MTT assays on fibroblast cells and evaluated at the 1st and 3rd day. The cell growth between the 1st and 3rd day was between 50 and 230% whereas a cell viability up to 95% was observed.

Chitosan-based silver nano-biocomposites [138] were synthesized with different concentrations of chitosan and $AgNO_3$ via a solution plasma process. Two electrodes placed side by side in the solution, delivered a discharge of plasma to disperse silver nanoparticles (AgNP). The solution was freeze-dried and crosslinked by UV irradiation. The viscosity of the solution increased with the concentration of chitosan. The cryogels presented a pore size in the range of 6 – 150 µm. The AgNP were homogeneously dispersed in the material and exhibited a diameter of 2.5 – 27.5 nm. The cryogels showed good antimicrobial properties against several bacteria and fungi including *E. coli*, *P. aeruginosa*, *Vibrio vulnificus*, *Vibrio parahaemolyticus*, *S. aureus*, *Bacillus cereus*, *Candida albicans* and *Aspergillus parasiticus*. MIC for several pathogens were determined, a higher AgNp concentration induced a higher MIC. At high concentration, the AgNP were more agglomerated, decreasing the effective surface to interact with micro-organisms.

A matrix composed of chitosan and a N-propylphosphonic acid chitosan derivative was prepared starting from aqueous solutions saturated with gaseous CO_2 [139]. The pure chitosan and modified chitosan were solubilized at 1% and 2%, mixed in different ratios and freeze-dried. The cryogels presented a relatively high porosity (55 -77%) and high swelling (3000%) in media similar to wound exudate. Some degradation (6 -11%) was observed after 7 days in these media. Mechanical properties could be tuned via the composition of the initial solution. Increasing the concentration of chitosan increased the hardness (2 – 65 kPa). The flexibility first increased with the concentration of chitosan up to 0.65 and then decreased, starting from 1% w/w of chitosan, to a flexibility of 0.15. For equivalent hardness (55 kPa), the sample flexibility decreased when the amount of chitosan derivative increased. The antioxidant activity was assessed by 3 tests: DPPH, ABTS and metal (Fe^{2+}) chelating activity. The EC50 was in the mg/mL range, which indicates a relatively low free radical scavenging capacity compared to natural antioxidants which have EC50 values in the µg/mL range. Antimicrobial properties were evaluated against 2 bacteria, *E. coli* and *S. aureus*, and one fungus, *C. albicans*. All cryogels showed a reduction of the antimicrobial activity superior to 88% compared to non-modified chitosan cryogels. Pure chitosan did not show any antimicrobial properties in neutral pH. MTT assays showed 50-80% growth of fibroblasts in the presence of the solution before freeze-drying. According to the authors this indicates that fibroblasts kept their capacity to proliferate; however, cryogels exerted a cytotoxic effect for a low concentration of modified chitosan according to ISO 10993-5[85].

Polyelectrolyte-complex multilayer membranes [140] composed of alternating layers of chitosan and alginate were reported by Sun et al. A 2%wt alginate solution was poured into a mold, after which a 2%wt chitosan solution was poured onto the alginate layer. This operation was repeated to obtain materials with 3, 5, 7 or 9 layers. After freeze drying, the material was immersed in a calcium chloride/ethanol solution to crosslink. The crosslinked material was then dried in open air. Thanks to their high porosity (75-93%) and their large pores (50 – 200 µm), cryogels reached their maximum

swelling (1750 – 2250%) in 40 minutes. Good antimicrobial properties against *E. Coli* were confirmed which improved when the number of layers of chitosan increased. The cryogels showed a stimulating effect on in vitro cell proliferation.

Chitosan cryogels with amino-functionalized molybdenum disulfide nanosheets (CS/NMNS) were prepared by Zhang et al. [141] as a photothermal antibacterial agent. Chitosan was solubilized in acetic acid solution and freeze dried. NaOH solution was used to neutralize the excess of acid and the NaOH was washed away with water. The neutralized and purified gel was then immersed in NMNS solutions and freeze dried again. The cryogels presented a large pore size, around 10µm, with a porosity of 82 %. Under NIR laser exposition, the cryogel temperature increased up to 60°C. Higher is the concentration of NMNS and longer is the exposition time, higher is the achieved temperature. This conversion of NIR light into thermal energy provides an antibacterial effect, which was confirmed for high NMNRS concentrations on two strains: *E. Coli* and *S. aureus*. An *in vivo* study was conducted on mice with circular wounds infected by *S. aureus*. Wounds were covered by the cryogel and a NIR laser was applied. After 10 days, a faster healing was observed for laser-irradiated composite cryogels in comparison with CS/NMNS or CS and histology revealed almost no inflammatory cells as well as a better organization of the tissues.

Cryogels made of chitosan and chondroitin sulfate [142] were applied on an open transmetatarsal amputation of the forefoot of a person with diabetes. Chitosan and chondroitine sulfate were solubilized in water and freeze dried. The wound was cleansed with saline and treated with the antibacterial betain polyhexanide for 10 min before applying the cryogel. A secondary dressing was used to keep the cryogel in place. The cryogel was renewed twice a week. By taking pictures of the wound at regular intervals, it was possible to evaluate its closure. The initial wound area of 38 cm^2 encountered in this study is the largest wound on which this team applied the cryogels, previous studies were on wounds of 2 to 6 cm^2 [143]. The surgical wound area was 50% closed after 28 days. A complete closure was achieved after 94 days with a well-structured epithelial tissue and favorable cosmetic results. No complications were encountered and no additional surgery was required. The total costs of the dressing for the 3 months of treatment were only $30, suggesting a good cost-effectiveness. This clinical case shows promising results, but it needs to be repeated on larger groups of patients to further prove its effectiveness and applicability.

Cryogels based on chitosan and modified PVA (polyvinyl alcohol) were prepared for wound dressing applications offering an accelerated wound healing and protection against bacterial infection [144]. 2-(dimethylamino)ethyl methacrylate (DMAEMA) was grafted on PVA via potassium persulfate-initiated free radical polymerization in water. The final product was named PVD. Quaternized PVD (QPVD) was obtained by dissolving PVD in DMSO and adding 1-bromobutane. QPVD was dissolved in water and chitosan was dissolved in acetic acid, followed by mixing of these solutions, freeze drying and crosslinking using glutaraldehyde vapor. SEM images showed an open, interconnected porosity. Thanks to their high porosity, around 80%, the cryogels presented high PBS absorption values, from 1300% to 2300%, for high ratios of QPVD. Antibacterial activity against *E. coli* and *S. aureus* was confirmed with a minimum of 88% of the bacteria eliminated. The presence of QPVD greatly increased this activity compared to CS cryogels thanks to its disruptive effect on bacterial cell membranes. The hemolysis ratio was around 0.8%, demonstrating a good blood compatibility, and the materials presented no cytotoxicity.

Cryogels generally exhibit a high swelling capacity and a good biocompatibility. However, the main drawback of these materials is the large size of the pores which is often above 10 µm. This allows for colonization of the dressing by cells, and removing the material may damage the newly formed tissue and induce pain.

(3) Chitosan aerogels for wound dressings

Chitosan aerogels for biomedical applications is a very recent approach, only few articles are dedicated to wound healing.

Valchuk et al. [126] developed aerogel materials based on polyelectrolyte complexes composed of sodium alginate and chitosan. Chitosan and sodium alginate were dissolved in acetic acid solution and water, respectively. After mixing the solutions in equimolar proportion, physical crosslinking by complexation of the anionic carboxylic acid groups of the alginate and the cationic amine groups of the chitosan resulted in a PEC gel. The aqueous phase was substituted by acetone and the samples were dried using supercritical CO_2. The aerogel was subsequently impregnated with an aqueous solution of the antibiotic agent levomycetin. The maximum drug release was achieved in 5 h but represented only 70% of the drug absorbed by the aerogel. The average pore size of 15 nm seems adapted to limit cell colonization during wound healing. The swelling degree in water vapor was around 180%wt, indicating a high sorption capacity for exudate, which also suggests potential application as wound dressing.

López-Iglesias et al. [26] prepared chitosan aerogel beads as drug delivery system to prevent infections in chronic wounds. The selected drug was vancomycin hydrochloride, which is highly soluble in water (> 100 mg/mL) but poorly soluble in ethanol. It is a glycopeptide antibiotic used against Gram-positive bacteria, especially methicillin-resistant *S. aureus*, and administered parenterally or locally. Chitosan was dissolved in acetic acid and vancomycin hydrochloride was dissolved in the chitosan solution at different concentrations. This solution was added dropwise through a syringe to a NaOH bath in which chitosan underwent non-solvent induced phase separation, resulting in transformation of the droplets into beads. These beads were left in the bath for different ageing times ranging from 0.5 h to 24 h. Solvent exchange was carried out by replacing water with ethanol and the beads were then dried with supercritical CO_2. Nitrogen adsorption-desorption analysis revealed a specific surface area of 479 m^2/g and SEM images showed a high porosity (>95%). Pores were bounded by intertwined bundles of polysaccharide fibers. Different scales of porosity could be observed: mesoporosity (2-50 nm) and macroporosity (> 50 nm). The vancomycin release profile from chitosan aerogels was investigated in PBS at pH 7.4 and 37 °C. For the first hour, a fast release of the vancomycin was observed, which concerns drug that is weakly bonded to the aerogel. This phase was followed by a slower release during the next 48 h reaching a plateau, which concerns vancomycin that interacts with the polymer chains via hydrogen bonds. This last part of the release followed first order kinetics. The release was not complete as 20% to 50% of the initial vancomycin remained in the bead. The antimicrobial activity of the beads was tested against *S. aureus* in simulated body fluid (pH 7.35-7.45, 37°C) in contact with the vancomycin loaded aerogels. The amount of bacteria decreased after 6 h of incubation for each medium containing vancomycin, showing a time-dependent survival rate for bacteria in contact with vancomycin. No bacteria could be observed after 48 h of incubation for all tested drug loadings. As expected, formulations with free vancomycin reached the MIC faster than the controlled release formulations of vancomycin-loaded chitosan aerogels. Chitosan aerogels without vancomycin showed no antimicrobial effect despite the reported antimicrobial properties of chitosan, which may be ascribed to the low amount of cationic NH_3^+ groups at this pH. A small increase of the collagenase activity was recorded in the presence of chitosan beads, but it was not significant, leading the authors to conclude that the chitosan aerogels do not hinder wound healing. The PBS absorption was studied at pH 6, 7 and 8. The weight of chitosan aerogel beads increased 200% - 300% and 300% - 400% at pH 6 and pH 7-8, respectively, after 30 min in contact with PBS. With this high absorption, the material meets an indispensable criterium for dressings for exuding wounds. Aerogels presented a good cytocompatibility (85% to 99% fibroblast viability after 48 h).

The same group produced vancomycin-loaded chitosan aerogel microparticles [71] via jet cutting for wound dressing purposes. Chitosan dissolved in acetic acid was extruded through a nozzle and the filament was cut by a disc. The droplets were collected in a coagulant bath containing ethanol and NH_3 and left aging for 1h, followed by solvent exchange to ethanol and supercritical CO_2 drying. A high porosity (96 %) and large specific surface area (188 m^2/g) led to a significant exudate sorption capacity, up to 900% in 24 h. The particles and the internal structure are shown on Figure I.17. This was explained by the physical crosslinking allowing the loose network to swell considerably in water. The hemolytic activity of -7.7% showed that microparticles are fully hemocompatible, even preventing the destruction of red blood cells. Vancomycin HCl was dissolved in the initial chitosan solution. The entrapment efficiency in chitosan aerogel microparticles was only 25%, which was ascribed to drug loss during the solvent exchange from water to ethanol. Vancomycin release tests were carried out in PBS and the particles were applied as layer to simulate an application on a wound. In 4h, the microparticles released 50% of the drug payload, whereas complete release was observed after 24h. Concentrations of vancomycin were above the MIC (2 µg/mL) during a short time, which was confirmed by an antimicrobial test performed in simulated body fluid (SBF) against *S. aureus*. Vancomycin-loaded aerogels showed an antimicrobial effect, inhibiting the bacterial growth completely in 6h; this inhibition was maintained up to 48 h. Non-loaded aerogels did not present any antimicrobial activity, due to the pH of SBF (7.4) which is above the pKa of the chitosan amino function (pKa NH_2 = 6.2). The microparticles, thanks to their small diameter (0.7-0.9 µm), could be in contact with the entire surface of a wound even in a restricted space, which could favor healing. Furthermore, the particles cannot go through the main biological barriers such as the skin and the blood brain barrier and remain at the location of interest, which favors local drug delivery instead of systemic delivery, avoiding a possible toxic effect. The results in [71] and [26] demonstrate that vancomycin-loaded chitosan aerogel microparticles hold great promise for wound healing applications.

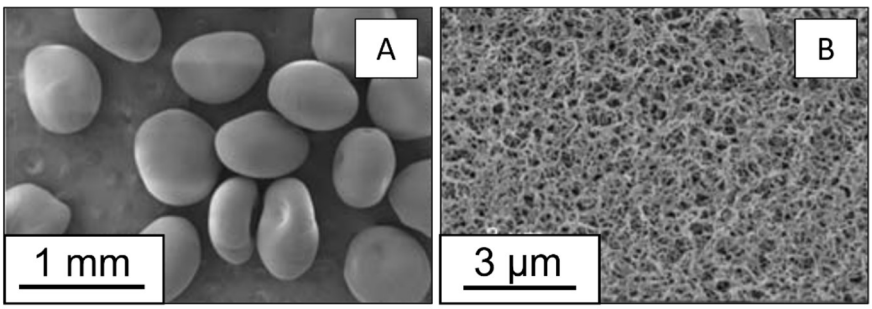

Figure I.17: SEM images of (A) chitosan aerogels particles processed with a nozzle diameter of 500 µm at 4000 rpm and (B) the associated structure. Adapted from [71].

Gurikov and coworkers prepared hybrid aerogel fibers based on chitosan and alginate [145]. A water in oil emulsion was made with the aqueous phase containing alginate and the oil phase containing a surfactant. An acidic solution of chitosan was slowly added to the emulsion to form a hybrid hydrogel. The ratio of alginate/chitosan was varied as well as the molecular weight of chitosan. After purification, solvent exchange and supercritical drying, a fibrillar structure was obtained with a specific surface area between 162 and 302 m^2/g. The material presented no cytotoxicity and exhibited an antibacterial effect from 60% to 90% of initially present bacteria on *S. aureus* and *K. pneumoniae*. During a scratch test, wounds covered with aerogels presented a wound closure around 80% which is better than the control (60%).

Wound dressings based on aerogel IPNs of chitosan and alginate were developed by Gorshkova et al. [146]. An aqueous solution of sodium alginate and a solution of chitosan dissolved in acetic acid were mixed. The gel was dried via supercritical drying after solvent exchange with acetone. The antibacterial agent usnic acid (UA) was incorporated via impregnation of the organogel. The

aerogels presented a mesoporous structure with a specific surface area of 260 m²/g and an average pore diameter of 16 nm. Aerogels presented a high-water absorption ratio of 4500%. Antibacterial activity against the most common bacteria responsible for wound infection (*E. coli*, *S. aureus* and *B. subtilis)* was confirmed. In 5 h 60% of the UA was released from aerogels. Analysis of these kinetics using the Korsmeyer-Peppas model revealed that anomalous transport predominates.

Chitosan aerogels for biomedical applications present the same interesting properties as cryogels but they have a smaller pore size (< 1 µm), which limits cell colonization. This could avoid tissue detachment and, consequently, pain during removal of the wound dressing.

Figure I.18A shows that aerogels have a porosity above 80% and that their absorption values are generally below 1000%. Cryogels have a variable porosity from 25% up to 98% and present the higher values of absorption, between 2000 and 3000%. However, the trend of fluid sorption vs porosity is not very clear as fluid sorption depends not only on porosity but on the intrinsic swelling properties of each polymer, and in the majority of cases discussed above chitosan is mixed with another component. In addition, the "second" polymer may be soluble in water which should create additional porosity which increases in time. Supercritically dried gels present a pore size below 1 µm (Figure I.18B) which is also the case for a few cryogels (these are, however, exceptions in their class). Most of the cryogels have pore diameters above 10 µm and present higher absorption values than aerogels, which can be attributed to their higher porosity. Here again, the comparison between different materials is not simple as the majority are composites.

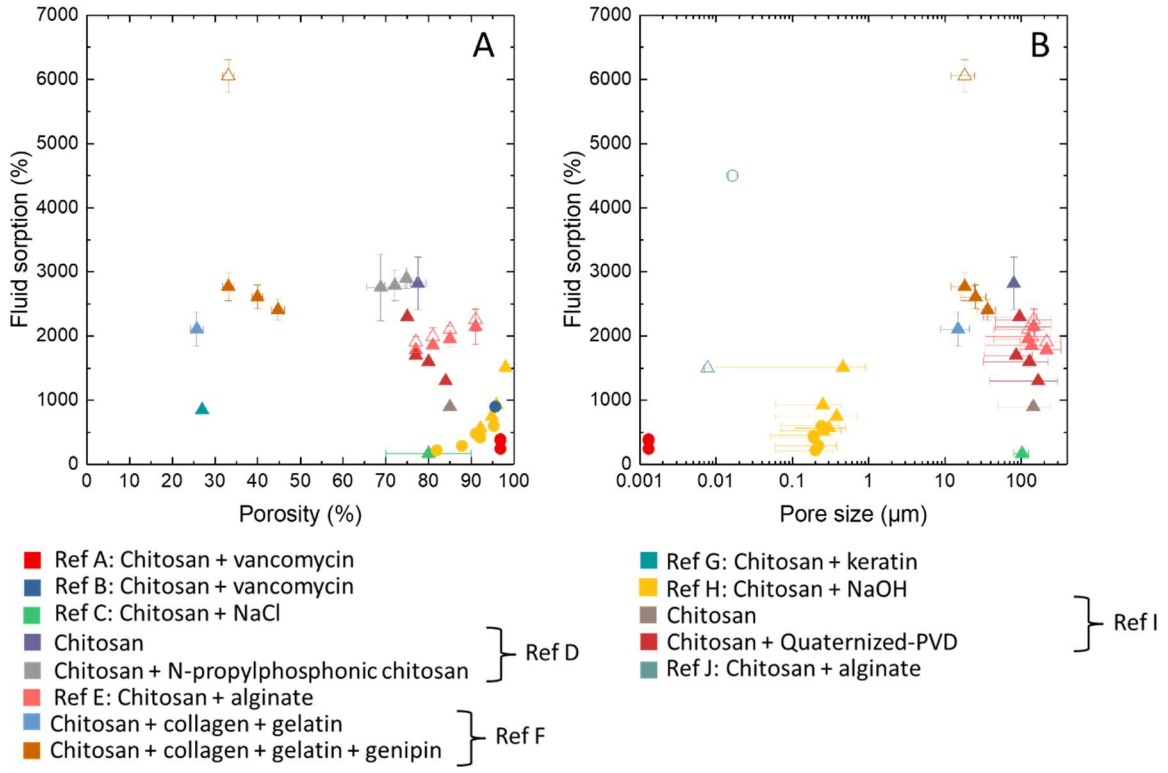

Figure I.18: Influence of the porosity and the pore size on the fluid sorption (summary of data collected from literature). Open symbols represent water, closed symbols represent PBS, exudate or another salt solution, triangles represent cryogels and circles represent aerogels.
Correspondence letter-reference of Figure I.18:
A: [26]; B: [71]; C: [101]; D: [139]; E: [140]; F: [136]; G: [111]; H: [29]; I: [144]; J: [146].

(4) Commercial dressings

Commercial wound dressings based on chitosan are available, which are mainly used for their antithrombotic properties: Chitoseal™ [147], HemCon® [51,130], QuickClot® [130], Celox® [148] and Thermoguard®. They were all developed for first line use on the battlefield. Another application is for dermis regeneration (Vulnosorb® and Chotodine®). Most of them are either non-woven materials or made by freeze-drying. However, these dressings have several disadvantages such as ingrowth of regenerating cells inside the pores, destruction of the newly formed tissue upon removal of the dressing and pain for the patient. None of the commercial chitosan-based dressings is recommended for infected wounds.

4. Wound healing

The skin is the largest organ of the human body. It has a surface from 1.5 to 2 m² and its thickness is around 2 mm [149]. The skin is a physical protection of organs and tissues against the outside environnement, mechanical agressions, UV radiations, heat, cold and microorganisms. This organ is in constant renewal as cells from the deepest layer migrate to surface in 45 days and peel off. Skin is composed of three layers (from the surface to the interior): epidermis, dermis and hypodermis, completed with skin appendages: the dander (hair and nails) and the sebaceous and apocrine glands as shown in Figure I.19.

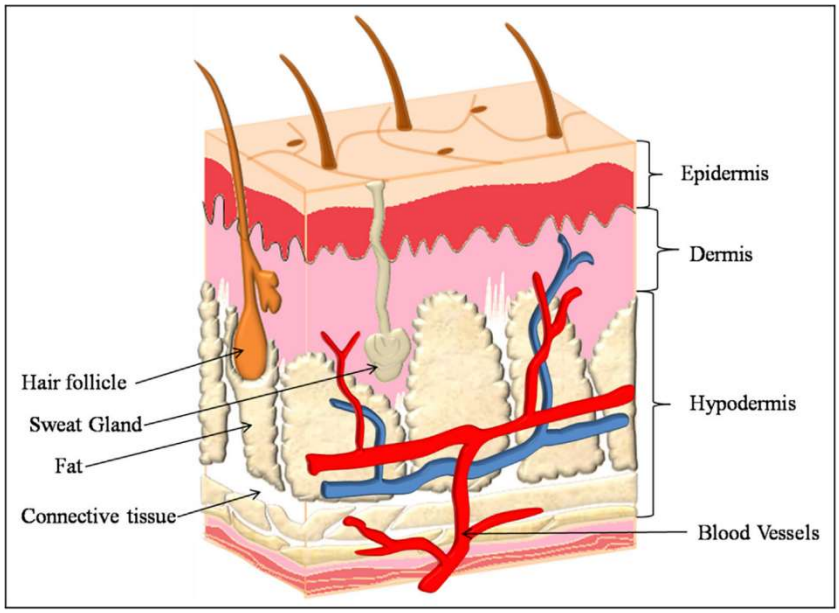

Figure I.19: Structure of the human skin [150]. Reprinted from European Polymer Journal, Vol 117, Rushikesh S. Ambekar and Balasubramanian Kandasubramanian, Advancements in nanofibers for wound dressing: A review, Pages 304-336., Copyright 2023, with permission from Elsevier

The epidermis helps to maintain the body temperature and is mainly composed of keratinocytes and then melanocytes, langerhans and merkel cells. This layer is composed of stratified and squamous epithelium in constant renewal. The epidermis can be divided into 5 layers (from surface to depth): stratum corneum, stratum lucidum, stratum granlosum, stratum spinosum and stratum germinativum.

The dermis is a vascularized and innervated connective tissue, it protects the body from external stress and strain. It is composed of fibroblasts, mastocytes, macrophages, dermal dendritic cells and fundamental substances made up of polysaccharides, including hyaluronic acid and proteins. Fibers are also present as elastin, collagen and reticulin.

The hypodermis is a subcutaneous tissue constituted of fibroblasts, macrophages and adipocytes. It assists in coupling of dermis with bone and muscles. Hypodermis protects the body from the external temperature by an insulating mechanism. The main function of the hypodermis is the lipogenesis, which consists of storing energy in form of lipids.

The nerves in the skin allow the body to perceive different sensations such as touch, vibration, temperature, pressure or pain through different receptors. The high vascularisation plays an important role in thermoregulation and nutrition. The epidermis is covered by bacteria, *e.g.* non-harmful *Staphylococci* species can be found in low numbers. However, gram-negative bacteria can be harmful and in case of ruptured skin can cause infection. As soon as the integrity of the skin is ruptured the wound healing process starts.

Wound healing can be divided in 4 stages [150] as shown in Figure I.20:

- The hemostasis stage,
- The inflammation stage,
- The proliferation stage,
- The remodeling stage.

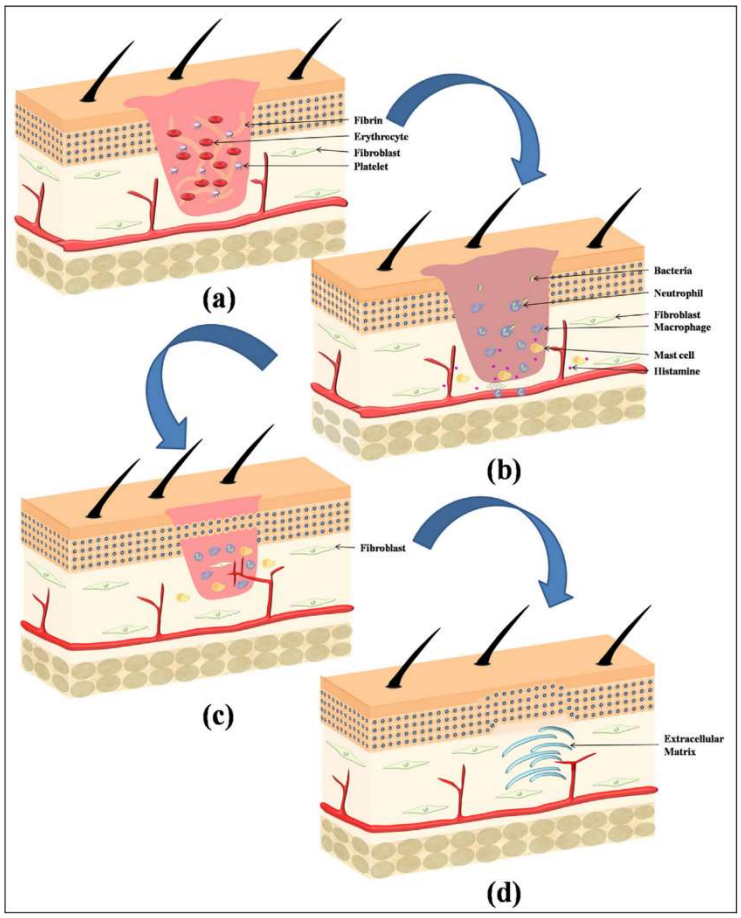

Figure I.20: Wound healing stages: (a) Hemostasis stage, (b) Inflammation stage, (c) Proliferation stage, (d) Remodeling stage. [150]. Reprinted from European Polymer Journal, Vol 117, Rushikesh S. Ambekar and Balasubramanian Kandasubramanian, Advancements in nanofibers for wound dressing: A review, Pages 304-336., Copyright 2023, with permission from Elsevier.

The hemostasis stage is an immediate response towards a skin injury. The main goal is to stop the blood loss to assure that other organs can maintain their function despite the wound.

Thrombocytes and inflammatory cells will accumulate in the extracellular matrix (ECM) and bind with structural proteins (such as collagen). Vasoconstriction also occurs to decrease blood loss. Thrombocytes secrete clotting factors, that help with post-hemostasis and ensure the stability of temporary scaffolds by stimulating the deposition of a fibrin matrix. It creates a suitable environment for the next stages of wound healing.

The inflammation stage lasts 3 days. During the first 24 h-48 h, mediators and chemotactic factors, coming partly from thrombocytes, attract leukocytes in the injury. Redness is caused by the dilatation of blood vessels; this dilatation is due to the presence of enzymes, like histamine, coming from mast cells by exocytosis. Neutrophils migrate efficiently towards the injury thanks to the vasodilatation. These neutrophils clean the wound by phagocytosis of foreign and dead cells as well as pathogens. Neutrophils also release proteinases and antimicrobial substances. After 48 h, granulation tissue formation starts. Macrophages and cytokines produce growth factors which are used later for the proliferation of fibroblast and endothelial cells.

The proliferation stage consists of transforming the temporary scaffolding into a permanent tissue by combining different processes as angiogenesis, granulation tissue formation, re-epithelialization and wound contraction. This stage begins with the migration of fibroblasts and myofibroblasts and it lasts 7 days. After this step, the accumulation of ECM can support the migration of the cells. Endothelial cells start angiogenesis which consists of the restoration of new arterioles. This process is important because the new arterioles bring nutrients and oxygen to the wound site that are used for the formation of granulation tissue and the onset of re-epithelialization. Wound contraction is the wound closing process by bringing the wound edges together using a combination of fibroblasts and myofibroblasts.

The final stage, remodelling, starts two weeks after the injury and can last over a year. All the processes initiated in the inflammation and proliferation stages are going to terminate. Small arterioles aggregate into larger vessels, that induce a diminution of the metabolic activity of wound healing. Macrophages, endothelial cells and myofibroblasts undergo apoptosis or leave the wound site. Reticular collagen (type III) in the ECM is replaced by fibrillar collagen (type I) which increases the tensile strength of the new tissues up to 80% relative to unwounded tissue. A lack of anchoring between the epidermis and the dermis leads to scarring. A proper balance between synthesis and degradation can avoid scar formation. After serious wound damage, sweat glands and hair follicles do not have the ability to heal.

Healing of an acute wound takes about 14 days followed by a remodeling step of approximately a year. However, in some cases the wound healing is delayed by factors coming from the wound or elsewhere in the patient. When a wound does not show signs of healing after 4 to 6 weeks, it is a chronic wound [151]. Chronic wounds are a major public health problem, affecting 37 million people worldwide and generating very high costs for their treatment.

In a chronic wound, the wound healing remains in the inflammatory stage. A chronic wound can have different etiologies like: diabetic foot wounds, amputation stumps, burns with extensive healing, pressure ulcers (bedsores) and leg ulcers. Despite different causes of these wounds, there are common characteristics like excessive levels of pro-inflammatory cytokines, proteases, aging cells and the existence of cells susceptible to infection. A high level of protease degrades the ECM and growth factors. Aging cells are not able to proliferate anymore.

As wound healing is a complicated process, it is necessary to help protecting the wound and promote healing: dressings have been developed for this purpose. However, nowadays there is no recommended dressing for chronic wound ensuring a complete healing process.

5. Expected properties of the dressing and solutions adopted in this work

In order to develop an effective dressing to treat chronic wounds, constraints and needs have been identified and the solutions adopted to address them in this work are detailed in the table below.

Table I.1: Summary of the constraints and needs identified for a dressing design treating chronic wounds and solutions adopted in this work to address them.

Constraints	Needs	Solutions
Prevention and treatment of infections	Antibacterial material or addition of drugs	Chitosan based material
Absorption of exudate	Porous hydrophilic material	Aerogels and cryogels
No colonization of the dressing by the cells	Pore size below 10 µm	Aerogels
Improvement of healing for chronic wound by going further the inflammatory state	Induce collagen synthesis, Decrease the inflammation	Addition of ascorbic acid 2-phosphate (AAP) to induce collagen synthesis, Addition of dexamethasone phosphate (Dex-P) to reduce the inflammation
Mechanical properties close to the one of the skin for a better adaptation and control	Modulus close to 1 MPa, Elasticity around 10%	Elasticity coming from the material (Tune on the process and formulation, addition of a crosslinker) and/or from the object structure (3D printing)

Conclusions

The main focus of this chapter was on intrinsically porous chitosan materials for biomedical applications. These recent materials are very attractive, and their development and optimization are ongoing.

First, a brief overview of bio-based porous materials, aerogels and cryogels, was presented. Then the main properties of chitosan, its shaping, the specificities of the different ways to prepare porous chitosan and the properties of the final material were described.

An overview of porous chitosan developed for tissue engineering, drug delivery and wound dressing were widely reviewed, and the commercial products were mentioned, if any. The main properties needed for each application were discussed. A large range of properties can be reached thanks to the different processes such as mixing, physical or chemical interactions or chemical modifications. Some proposed materials are with good results in vitro, but only few reach the *in vivo* stage, and they are only cryogels. The main parameters to tune the structure are the polymer concentration, the drying method and the possible crosslinking or association with another material. For this thesis, we decided to work with pure non-crosslinked chitosan. The following chapters will be dedicated to a better understanding of the correlations between the process and the properties of chitosan porous materials. A particular attention will be given to the coagulation step in which the network is created.

Chitosan cryogels has several advantages compared to other porous materials used for wound dressings, such as biocompatibility, bioactivity, and capacity of high absorption of aqueous media. Chitosan aerogels possess all these properties but also provide high specific surface area and allow tuning material pore size from few tens of nanometers to few microns. Thus, chitosan aerogels can be used not only as wound dressings but also as a drug delivery system at the same time. Their high porosity, large specific surface area and possibility of functionalization allow the impregnation and release of the drug in a controlled way and the material can be simultaneously used as exudate absorbent. The open and interconnected pores allow gases to go through the dressing to obtain an optimal condition for the wound site. As demonstrated in this chapter, the development of chitosan aerogels for wound healing is at the very beginning of a long way to do.

In the final section, the skin structure and the steps of wound healing were described. The understand the problematic of a chronic wounds is on-going. They are one of the major health problems. They are painful with an acute risk of infection. Healthcare related to chronic wounds is expensive due to the long duration of its application. Existing dressings are not always adapted to the wound but still are applied despite the absence of data demonstrating effectiveness. Few research papers propose dedicated dressings but none of them reach the *in vivo* stage. Chronic wounds need wound dressings which can treat at the same time the etiology and the inflamed wound. To improve patient care and wound healing, new dressings must be developed.

References

[1] X. Chang, D. Chen, X. Jiao, Chitosan-Based Aerogels with High Adsorption Performance, J. Phys. Chem. B. 112 (2008) 7721–7725. https://doi.org/10.1021/jp8011359.

[2] A. Ricci, L. Bernardi, C. Gioia, S. Vierucci, M. Robitzer, F. Quignard, Chitosan aerogel: a recyclable, heterogeneous organocatalyst for the asymmetric direct aldol reaction in water, Chem. Commun. 46 (2010) 6288. https://doi.org/10.1039/c0cc01502d.

[3] S. Takeshita, S. Yoda, Chitosan Aerogels: Transparent, Flexible Thermal Insulators, Chem. Mater. 27 (2015) 7569–7572. https://doi.org/10.1021/acs.chemmater.5b03610.

[4] K. Rinki, P.K. Dutta, A.J. Hunt, D.J. Macquarrie, J.H. Clark, Chitosan Aerogels Exhibiting High Surface Area for Biomedical Application: Preparation, Characterization, and Antibacterial Study, Int. J. Polym. Mater. 60 (2011) 988–999. https://doi.org/10.1080/00914037.2011.553849.

[5] V.I. Lozinsky, I.Yu. Galaev, F.M. Plieva, I.N. Savina, H. Jungvid, B. Mattiasson, Polymeric cryogels as promising materials of biotechnological interest, Trends Biotechnol. 21 (2003) 445–451. https://doi.org/10.1016/j.tibtech.2003.08.002.

[6] S.K. Lee, M. Wang, J.H. Lee, J. Suhr, Development of reversibly compressible feather-like lightweight Chitosan/GO composite foams and their mechanical and viscoelastic properties, Carbon. 157 (2020) 191–200. https://doi.org/10.1016/j.carbon.2019.10.019.

[7] A. Borisova, M. De Bruyn, V.L. Budarin, P.S. Shuttleworth, J.R. Dodson, M.L. Segatto, J.H. Clark, A Sustainable Freeze-Drying Route to Porous Polysaccharides with Tailored Hierarchical Meso- and Macroporosity, Macromol. Rapid Commun. 36 (2015) 774–779. https://doi.org/10.1002/marc.201400680.

[8] S.S. Kistler, Coherent Expanded Aerogels and Jellies, Nature. 127 (1931) 741–741. https://doi.org/10.1038/127741a0.

[9] S.S. Kistler, Coherent Expanded-Aerogels, J. Phys. Chem. 36 (1932) 52–64. https://doi.org/10.1021/j150331a003.

[10] A. Rigacci, J.C. Marechal, M. Repoux, M. Moreno, P. Achard, Preparation of polyurethane-based aerogels and xerogels for thermal superinsulation, J. Non-Cryst. Solids. 350 (2004) 372–378. https://doi.org/10.1016/j.jnoncrysol.2004.06.049.

[11] M.A.B. Meador, C.R. Alemán, K. Hanson, N. Ramirez, S.L. Vivod, N. Wilmoth, L. McCorkle, Polyimide Aerogels with Amide Cross-Links: A Low Cost Alternative for Mechanically Strong Polymer Aerogels, ACS Appl. Mater. Interfaces. 7 (2015) 1240–1249. https://doi.org/10.1021/am507268c.

[12] J.C. Williams, M.A.B. Meador, L. McCorkle, C. Mueller, N. Wilmoth, Synthesis and Properties of Step-Growth Polyamide Aerogels Cross-linked with Triacid Chlorides, Chem. Mater. 26 (2014) 4163–4171. https://doi.org/10.1021/cm5012313.

[13] M.A. Aegerter, N. Leventis, M.M. Koebel, M.-A. Aegerter, International Sol-Gel Society, eds., Aerogels handbook, Springer, New York, NY Heidelberg, 2011.

[14] M.A. Aegerter, N. Leventis, M. Koebel, S.A. Steiner III, Handbook of Aerogels, 2nd edition, Springer Nature Switzerland, 2023.

[15] M. Betz, C.A. García-González, R.P. Subrahmanyam, I. Smirnova, U. Kulozik, Preparation of novel whey protein-based aerogels as drug carriers for life science applications, J. Supercrit. Fluids. 72 (2012) 111–119. https://doi.org/10.1016/j.supflu.2012.08.019.

[16] M.A. Marin, R.R. Mallepally, M.A. McHugh, Silk fibroin aerogels for drug delivery applications, J. Supercrit. Fluids. 91 (2014) 84–89. https://doi.org/10.1016/j.supflu.2014.04.014.

[17] I. Selmer, C. Kleemann, U. Kulozik, S. Heinrich, I. Smirnova, Development of egg white protein aerogels as new matrix material for microencapsulation in food, J. Supercrit. Fluids. 106 (2015) 42–49. https://doi.org/10.1016/j.supflu.2015.05.023.

[18] N. Lavoine, L. Bergström, Nanocellulose-based foams and aerogels: processing, properties, and applications, J. Mater. Chem. A. 5 (2017) 16105–16117. https://doi.org/10.1039/C7TA02807E.

[19] T. Budtova, Cellulose II aerogels: a review, Cellulose. 26 (2019) 81–121. https://doi.org/10.1007/s10570-018-2189-1.

[20] R.J. Moon, A. Martini, J. Nairn, J. Simonsen, J. Youngblood, Cellulose nanomaterials review: structure, properties and nanocomposites, Chem. Soc. Rev. 40 (2011) 3941. https://doi.org/10.1039/c0cs00108b.

[21] A. Tripathi, G.N. Parsons, O.J. Rojas, S.A. Khan, Featherlight, Mechanically Robust Cellulose Ester Aerogels for Environmental Remediation, ACS Omega. 2 (2017) 4297–4305. https://doi.org/10.1021/acsomega.7b00571.

[22] A. Demilecamps, C. Beauger, C. Hildenbrand, A. Rigacci, T. Budtova, Cellulose–silica aerogels, Carbohydr. Polym. 122 (2015) 293–300. https://doi.org/10.1016/j.carbpol.2015.01.022.

[23] H. Maleki, L. Durães, C.A. García-González, P. del Gaudio, A. Portugal, M. Mahmoudi, Synthesis and biomedical applications of aerogels: Possibilities and challenges, Adv. Colloid Interface Sci. 236 (2016) 1–27. https://doi.org/10.1016/j.cis.2016.05.011.

[24] L. Zuo, Y. Zhang, L. Zhang, Y.-E. Miao, W. Fan, T. Liu, Polymer/Carbon-Based Hybrid Aerogels: Preparation, Properties and Applications, Materials. 8 (2015) 6806–6848. https://doi.org/10.3390/ma8105343.

[25] F. Liebner, E. Haimer, M. Wendland, M.-A. Neouze, K. Schlufter, P. Miethe, T. Heinze, A. Potthast, T. Rosenau, Aerogels from Unaltered Bacterial Cellulose: Application of scCO $_2$ Drying for the Preparation of Shaped, Ultra-Lightweight Cellulosic Aerogels: Aerogels from Unaltered Bacterial Cellulose: Application of scCO $_2$ Drying …, Macromol. Biosci. 10 (2010) 349–352. https://doi.org/10.1002/mabi.200900371.

[26] C. López-Iglesias, J. Barros, I. Ardao, F.J. Monteiro, C. Alvarez-Lorenzo, J.L. Gómez-Amoza, C.A. García-González, Vancomycin-loaded chitosan aerogel particles for chronic wound applications, Carbohydr. Polym. 204 (2019) 223–231. https://doi.org/10.1016/j.carbpol.2018.10.012.

[27] S. Takeshita, A. Sadeghpour, W.J. Malfait, A. Konishi, K. Otake, S. Yoda, Formation of Nanofibrous Structure in Biopolymer Aerogel during Supercritical CO $_2$ Processing: The Case of Chitosan Aerogel, Biomacromolecules. 20 (2019) 2051–2057. https://doi.org/10.1021/acs.biomac.9b00246.

[28] F. Quignard, R. Valentin, F. Di Renzo, Aerogel materials from marine polysaccharides, New J. Chem. 32 (2008) 1300. https://doi.org/10.1039/b808218a.

[29] C. Chartier, S. Buwalda, H. Van Den Berghe, B. Nottelet, T. Budtova, Tuning the properties of porous chitosan: Aerogels and cryogels, Int. J. Biol. Macromol. 202 (2022) 215–223. https://doi.org/10.1016/j.ijbiomac.2022.01.042.

[30] S. Groult, T. Budtova, Tuning structure and properties of pectin aerogels, Eur. Polym. J. 108 (2018) 250–261. https://doi.org/10.1016/j.eurpolymj.2018.08.048.

[31] R. Valentin, B. Bonelli, E. Garrone, F. Di Renzo, F. Quignard, Accessibility of the Functional Groups of Chitosan Aerogel Probed by FT-IR-Monitored Deuteration, Biomacromolecules. 8 (2007) 3646–3650. https://doi.org/10.1021/bm070391a.

[32] G.T. Grant, E.R. Morris, D.A. Rees, P.J.C. Smith, D. Thom, Biological interactions between polysaccharides and divalent cations: The egg-box model, FEBS Lett. 32 (1973) 195–198. https://doi.org/10.1016/0014-5793(73)80770-7.

[33] F. Di Renzo, R. Valentin, M. Boissière, A. Tourrette, G. Sparapano, K. Molvinger, J.-M. Devoisselle, C. Gérardin, F. Quignard, Hierarchical Macroporosity Induced by Constrained Syneresis in Core−Shell Polysaccharide Composites, Chem. Mater. 17 (2005) 4693–4699. https://doi.org/10.1021/cm0503477.

[34] G. Conzatti, D. Faucon, M. Castel, F. Ayadi, S. Cavalie, A. Tourrette, Alginate/chitosan polyelectrolyte complexes: A comparative study of the influence of the drying step on physicochemical properties, Carbohydr. Polym. 172 (2017) 142–151. https://doi.org/10.1016/j.carbpol.2017.05.023.

[35] C.A. García-González, M. Alnaief, I. Smirnova, Polysaccharide-based aerogels—Promising biodegradable carriers for drug delivery systems, Carbohydr. Polym. 86 (2011) 1425–1438. https://doi.org/10.1016/j.carbpol.2011.06.066.

[36] T. Mehling, I. Smirnova, U. Guenther, R.H.H. Neubert, Polysaccharide-based aerogels as drug carriers, J. Non-Cryst. Solids. 355 (2009) 2472–2479. https://doi.org/10.1016/j.jnoncrysol.2009.08.038.
[37] C.A. García-González, I. Smirnova, Use of supercritical fluid technology for the production of tailor-made aerogel particles for delivery systems, J. Supercrit. Fluids. 79 (2013) 152–158. https://doi.org/10.1016/j.supflu.2013.03.001.
[38] L. Druel, R. Bardl, W. Vorwerg, T. Budtova, Starch Aerogels: A Member of the Family of Thermal Superinsulating Materials, Biomacromolecules. 18 (2017) 4232–4239. https://doi.org/10.1021/acs.biomac.7b01272.
[39] C.A. García-González, J.J. Uy, M. Alnaief, I. Smirnova, Preparation of tailor-made starch-based aerogel microspheres by the emulsion-gelation method, Carbohydr. Polym. 88 (2012) 1378–1386. https://doi.org/10.1016/j.carbpol.2012.02.023.
[40] I. De Marco, E. Reverchon, Starch aerogel loaded with poorly water-soluble vitamins through supercritical CO 2 adsorption, Chem. Eng. Res. Des. 119 (2017) 221–230. https://doi.org/10.1016/j.cherd.2017.01.024.
[41] Y. Kobayashi, T. Saito, A. Isogai, Aerogels with 3D Ordered Nanofiber Skeletons of Liquid-Crystalline Nanocellulose Derivatives as Tough and Transparent Insulators, Angew. Chem. Int. Ed. 53 (2014) 10394–10397. https://doi.org/10.1002/anie.201405123.
[42] S. Groult, T. Budtova, Thermal conductivity/structure correlations in thermal super-insulating pectin aerogels, Carbohydr. Polym. 196 (2018) 73–81. https://doi.org/10.1016/j.carbpol.2018.05.026.
[43] C. Rudaz, R. Courson, L. Bonnet, S. Calas-Etienne, H. Sallée, T. Budtova, Aeropectin: Fully Biomass-Based Mechanically Strong and Thermal Superinsulating Aerogel, Biomacromolecules. 15 (2014) 2188–2195. https://doi.org/10.1021/bm500345u.
[44] S. Groult, S. Buwalda, T. Budtova, Tuning bio-aerogel properties for controlling theophylline delivery. Part 1: Pectin aerogels, Mater. Sci. Eng. C. 126 (2021) 112148. https://doi.org/10.1016/j.msec.2021.112148.
[45] A. Veronovski, G. Tkalec, Ž. Knez, Z. Novak, Characterisation of biodegradable pectin aerogels and their potential use as drug carriers, Carbohydr. Polym. 113 (2014) 272–278. https://doi.org/10.1016/j.carbpol.2014.06.054.
[46] A. Nešić, M. Gordić, S. Davidović, Ž. Radovanović, J. Nedeljković, I. Smirnova, P. Gurikov, Pectin-based nanocomposite aerogels for potential insulated food packaging application, Carbohydr. Polym. 195 (2018) 128–135. https://doi.org/10.1016/j.carbpol.2018.04.076.
[47] W. Paul, C. Sharma, Chitosan, a drug carrier for the 21st century: A review, STP Pharma Sci. 10 (2000) 5–22.
[48] P. Broussignac, Chitosan, a natural polymer not well known by the industry, Chim. Ind. Génie Chim. 99 (1968) 1241–1247.
[49] K. Kurita, K. Tomita, T. Tada, S. Ishii, S.-I. Nishimura, K. Shimoda, Squid chitin as a potential alternative chitin source: Deacetylation behavior and characteristic properties, J. Polym. Sci. Part Polym. Chem. 31 (1993) 485–491. https://doi.org/10.1002/pola.1993.080310220.
[50] I. Bano, M. Arshad, T. Yasin, M.A. Ghauri, M. Younus, Chitosan: A potential biopolymer for wound management, Int. J. Biol. Macromol. 102 (2017) 380–383. https://doi.org/10.1016/j.ijbiomac.2017.04.047.
[51] M.A. Brown, M.R. Daya, J.A. Worley, Experience with Chitosan Dressings in a Civilian EMS System, J. Emerg. Med. 37 (2009) 1–7. https://doi.org/10.1016/j.jemermed.2007.05.043.
[52] M. Rinaudo, Properties and degradation of selected polysaccharides: hyaluronan and chitosan, Corros. Eng. Sci. Technol. 42 (2007) 324–334. https://doi.org/10.1179/174327807X238945.
[53] H. Zhang, S.H. Neau, In vitro degradation of chitosan by a commercial enzyme preparation: effect of molecular weight and degree of deacetylation, Biomaterials. 22 (2001) 1653–1658. https://doi.org/10.1016/S0142-9612(00)00326-4.
[54] S.B. Rao, C.P. Sharma, Use of chitosan as a biomaterial: studies on its safety and hemostatic potential, J. Biomed. Mater. Res. Off. J. Soc. Biomater. Jpn. Soc. Biomater. 34 (1997) 21–28.

[55] T. Jiang, R. James, S.G. Kumbar, C.T. Laurencin, Chitosan as a biomaterial: structure, properties, and applications in tissue engineering and drug delivery, in: Nat. Synth. Biomed. Polym., Elsevier, 2014: pp. 91–113.
[56] G. Lamarque, C. Viton, A. Domard, Comparative Study of the First Heterogeneous Deacetylation of α- and β-Chitins in a Multistep Process, Biomacromolecules. 5 (2004) 992–1001. https://doi.org/10.1021/bm034498j.
[57] M. Ioelovich, Crystallinity and Hydrophility of Chitin and Chitosan, J. Chem. 3 (2014) 7–14.
[58] C.K.S. Pillai, W. Paul, C.P. Sharma, Chitin and chitosan polymers: Chemistry, solubility and fiber formation, Prog. Polym. Sci. 34 (2009) 641–678. https://doi.org/10.1016/j.progpolymsci.2009.04.001.
[59] N. Islam, I. Dmour, M.O. Taha, Degradability of chitosan micro/nanoparticles for pulmonary drug delivery, Heliyon. 5 (2019) e01684. https://doi.org/10.1016/j.heliyon.2019.e01684.
[60] K.V. Harish Prashanth, R.N. Tharanathan, Chitin/chitosan: modifications and their unlimited application potential—an overview, Trends Food Sci. Technol. 18 (2007) 117–131. https://doi.org/10.1016/j.tifs.2006.10.022.
[61] N.A. Negm, H.H.H. Hefni, A.A.A. Abd-Elaal, E.A. Badr, M.T.H. Abou Kana, Advancement on modification of chitosan biopolymer and its potential applications, Int. J. Biol. Macromol. 152 (2020) 681–702. https://doi.org/10.1016/j.ijbiomac.2020.02.196.
[62] M.J. Zohuriaan-Mehr, Advances in chitin and chitosan modification through graft copolymerization: A comprehensive review, Iran. Polym. J. 14 (2005) 235–265.
[63] H. Caner, H. Hasipoglu, O. Yilmaz, E. Yilmaz, Graft copolymerization of 4-vinylpyridine on to chitosan - 1. By ceric ion initiation, Eur. Polym. J. 34 (1998) 493–497.
[64] X. Wang, X. Li, E. Stride, M. Edirisinghe, Fabrication of nanoporous chitosan membranes, Nano. 05 (2010) 53–60. https://doi.org/10.1142/S1793292010001846.
[65] E. Gossla, R. Tonndorf, A. Bernhardt, M. Kirsten, R.-D. Hund, D. Aibibu, C. Cherif, M. Gelinsky, Electrostatic flocking of chitosan fibres leads to highly porous, elastic and fully biodegradable anisotropic scaffolds, Acta Biomater. 44 (2016) 267–276. https://doi.org/10.1016/j.actbio.2016.08.022.
[66] W. Han, R. Bai, A novel method for obtaining a high-concentration chitosan solution and preparing a high-strength chitosan hollow-fiber membrane with an excellent adsorption capacity, J. Appl. Polym. Sci. 115 (2010) 1913–1921. https://doi.org/10.1002/app.31167.
[67] H. Avci, H. Ghorbanpoor, M. Nurbas, Preparation of origanum minutiflorum oil-loaded core–shell structured chitosan nanofibers with tunable properties, Polym. Bull. 75 (2018) 4129–4144. https://doi.org/10.1007/s00289-017-2257-y.
[68] Y.Z. Yu, Z.Z. Han, Y. Liu, S.H. Fang, Y.Y. Liu, Q.X. Hu, Fabrication of 3D Hierarchical Scaffolds by a Hybrid Process Combining Low-Temperature Deposition and Electrospinning, Key Eng. Mater. 522 (2012) 117–122. https://doi.org/10.4028/www.scientific.net/KEM.522.117.
[69] H. Geng, Q. Dai, H. Sun, L. Zhuang, A. Song, F. Caruso, J. Hao, J. Cui, Injectable and Sprayable Polyphenol-Based Hydrogels for Controlling Hemostasis, ACS Appl. Bio Mater. 3 (2020) 1258–1266. https://doi.org/10.1021/acsabm.9b01138.
[70] V. Asadian-Ardakani, S. Saber-Samandari, S. Saber-Samandari, The effect of hydroxyapatite in biopolymer-based scaffolds on release of naproxen sodium: Chitosan-graft-Poly(acrylic acid)/n-HAP as drug carrier for bone tissue engineering, J. Biomed. Mater. Res. A. 104 (2016) 2992–3003. https://doi.org/10.1002/jbm.a.35838.
[71] C. López-Iglesias, J. Barros, I. Ardao, P. Gurikov, F.J. Monteiro, I. Smirnova, C. Alvarez-Lorenzo, C.A. García-González, Jet Cutting Technique for the Production of Chitosan Aerogel Microparticles Loaded with Vancomycin, Polymers. 12 (2020) 273. https://doi.org/10.3390/polym12020273.
[72] Q. Wu, M. Maire, S. Lerouge, D. Therriault, M.-C. Heuzey, 3D Printing of Microstructured and Stretchable Chitosan Hydrogel for Guided Cell Growth, Adv. Biosyst. 1 (2017) 1700058. https://doi.org/10.1002/adbi.201700058.

[73] L. Baldino, S. Cardea, E. Reverchon, Nanostructured chitosan-gelatin hybrid aerogels produced by supercritical gel drying: Nanostructured Chitosan-Gelatin Hybrid Aerogels Produced by Supercritical Gel Drying, Polym. Eng. Sci. 58 (2018) 1494–1499. https://doi.org/10.1002/pen.24719.

[74] S. Saeedi Garakani, M. Khanmohammadi, Z. Atoufi, S.K. Kamrava, M. Setayeshmehr, R. Alizadeh, F. Faghihi, Z. Bagher, S.M. Davachi, A. Abbaspourrad, Fabrication of chitosan/agarose scaffolds containing extracellular matrix for tissue engineering applications, Int. J. Biol. Macromol. 143 (2020) 533–545. https://doi.org/10.1016/j.ijbiomac.2019.12.040.

[75] R.M. Obaidat, B.M. Tashtoush, M.F. Bayan, R. T. Al Bustami, M. Alnaief, Drying Using Supercritical Fluid Technology as a Potential Method for Preparation of Chitosan Aerogel Microparticles, AAPS PharmSciTech. 16 (2015) 1235–1244. https://doi.org/10.1208/s12249-015-0312-2.

[76] A. Tabernero, L. Baldino, A. Misol, S. Cardea, E.M.M. del Valle, Role of rheological properties on physical chitosan aerogels obtained by supercritical drying, Carbohydr. Polym. 233 (2020) 115850. https://doi.org/10.1016/j.carbpol.2020.115850.

[77] M.-H. Ho, P.-Y. Kuo, H.-J. Hsieh, T.-Y. Hsien, L.-T. Hou, J.-Y. Lai, D.-M. Wang, Preparation of porous scaffolds by using freeze-extraction and freeze-gelation methods, Biomaterials. 25 (2004) 129–138. https://doi.org/10.1016/S0142-9612(03)00483-6.

[78] A.S. Álvarez-Suarez, E.A. López-Maldonado, O.A. Graeve, F. Martinez-Pallares, L.E. Gómez-Pineda, M.T. Oropeza-Guzmán, A.L. Iglesias, T. Ng, E. Serena-Gómez, L.J. Villarreal-Gómez, Fabrication of porous polymeric structures using a simple sonication technique for tissue engineering, J. Polym. Eng. 37 (2017) 943–951. https://doi.org/10.1515/polyeng-2016-0423.

[79] S. Takeshita, S. Zhao, W.J. Malfait, Transparent, Aldehyde-Free Chitosan Aerogel, Carbohydr. Polym. 251 (2021) 117089. https://doi.org/10.1016/j.carbpol.2020.117089.

[80] S. Takeshita, S. Zhao, W.J. Malfait, M.M. Koebel, Chemistry of Chitosan Aerogels: Three-Dimensional Pore Control for Tailored Applications, Angew. Chem. Int. Ed. (2020). https://doi.org/10.1002/anie.202003053.

[81] S. Takeshita, S. Akasaka, S. Yoda, Structural and acoustic properties of transparent chitosan aerogel, Mater. Lett. 254 (2019) 258–261. https://doi.org/10.1016/j.matlet.2019.07.064.

[82] V. Gold, ed., The IUPAC Compendium of Chemical Terminology: The Gold Book, 4th ed., International Union of Pure and Applied Chemistry (IUPAC), Research Triangle Park, NC, 2019. https://doi.org/10.1351/goldbook.

[83] T. Budtova, D.A. Aguilera, S. Beluns, L. Berglund, C. Chartier, E. Espinosa, S. Gaidukovs, A. Klimek-Kopyra, A. Kmita, D. Lachowicz, F. Liebner, O. Platnieks, A. Rodríguez, L.K. Tinoco Navarro, F. Zou, S.J. Buwalda, Biorefinery Approach for Aerogels, Polymers. 12 (2020) 2779. https://doi.org/10.3390/polym12122779.

[84] ISO 10993-1: Biological evaluation of medical devices — Part 1: Evaluation and testing within a risk management process, 2018. https://www.iso.org/obp/ui#iso:std:iso:10993:-1:ed-5:v2:en.

[85] ISO 10993-5: Biological evaluation of medical devices — Part 5: Tests for in vitro cytotoxicity, 2009.

[86] A. Rogina, P. Rico, G. Gallego Ferrer, M. Ivanković, H. Ivanković, In Situ Hydroxyapatite Content Affects the Cell Differentiation on Porous Chitosan/Hydroxyapatite Scaffolds, Ann. Biomed. Eng. 44 (2016) 1107–1119. https://doi.org/10.1007/s10439-015-1418-0.

[87] D. Griffon, M. Sedighi, D. Schaeffer, J. Eurell, A. Johnson, Chitosan scaffolds: Interconnective pore size and cartilage engineering, Acta Biomater. 2 (2006) 313–320. https://doi.org/10.1016/j.actbio.2005.12.007.

[88] A. Barbetta, A. Carrino, M. Costantini, M. Dentini, Polysaccharide based scaffolds obtained by freezing the external phase of gas-in-liquid foams, Soft Matter. 6 (2010) 5213. https://doi.org/10.1039/c0sm00616e.

[89] V. Zubillaga, A.M. Salaberria, T. Palomares, A. Alonso-Varona, S. Kootala, J. Labidi, S.C.M. Fernandes, Chitin Nanoforms Provide Mechanical and Topological Cues to Support Growth of Human Adipose Stem Cells in Chitosan Matrices, Biomacromolecules. 19 (2018) 3000–3012. https://doi.org/10.1021/acs.biomac.8b00570.

[90] M.P. Nikolova, M.S. Chavali, Recent advances in biomaterials for 3D scaffolds: A review, Bioact. Mater. 4 (2019) 271–292. https://doi.org/10.1016/j.bioactmat.2019.10.005.
[91] S. Bose, M. Roy, A. Bandyopadhyay, Recent advances in bone tissue engineering scaffolds, Trends Biotechnol. 30 (2012) 546–554. https://doi.org/10.1016/j.tibtech.2012.07.005.
[92] A.S. Sumayya, G. Muraleedhara Kurup, Marine macromolecules cross-linked hydrogel scaffolds as physiochemically and biologically favorable entities for tissue engineering applications, J. Biomater. Sci. Polym. Ed. 28 (2017) 807–825. https://doi.org/10.1080/09205063.2017.1303119.
[93] Y.-C. Wang, M.-C. Lin, D.-M. Wang, H.-J. Hsieh, Fabrication of a novel porous PGA-chitosan hybrid matrix for tissue engineering, Biomaterials. 24 (2003) 1047–1057.
[94] J. Li, J. Pan, L. Zhang, X. Guo, Y. Yu, Culture of primary rat hepatocytes within porous chitosan scaffolds, J. Biomed. Mater. Res. Part Off. J. Soc. Biomater. Jpn. Soc. Biomater. Aust. Soc. Biomater. Korean Soc. Biomater. 67 (2003) 938–943.
[95] J. Kim, Z. Cai, Y. Chen, Biocompatible Bacterial Cellulose Composites for Biomedical Application, J. Nanotechnol. Eng. Med. 1 (2010). https://doi.org/10.1115/1.4000062.
[96] P. Coimbra, P. Alves, T.A.M. Valente, R. Santos, I.J. Correia, P. Ferreira, Sodium hyaluronate/chitosan polyelectrolyte complex scaffolds for dental pulp regeneration: Synthesis and characterization, Int. J. Biol. Macromol. 49 (2011) 573–579. https://doi.org/10.1016/j.ijbiomac.2011.06.011.
[97] D. Puppi, C. Migone, A. Morelli, C. Bartoli, M. Gazzarri, D. Pasini, F. Chiellini, Microstructured chitosan/poly(γ-glutamic acid) polyelectrolyte complex hydrogels by computer-aided wet-spinning for biomedical three-dimensional scaffolds, J. Bioact. Compat. Polym. 31 (2016) 531–549. https://doi.org/10.1177/0883911516631355.
[98] U. Adhikari, N.P. Rijal, S. Khanal, D. Pai, J. Sankar, N. Bhattarai, Magnesium incorporated chitosan based scaffolds for tissue engineering applications, Bioact. Mater. 1 (2016) 132–139. https://doi.org/10.1016/j.bioactmat.2016.11.003.
[99] I. Aranaz, E. Martínez-Campos, C. Moreno-Vicente, A. Civantos, S. García-Arguelles, F. del Monte, Macroporous Calcium Phosphate/Chitosan Composites Prepared via Unidirectional Ice Segregation and Subsequent Freeze-Drying, Materials. 10 (2017) 516. https://doi.org/10.3390/ma10050516.
[100] H.S. Kim, J.T. Kim, Y.J. Jung, S.C. Ryu, H.J. Son, Y.G. Kim, Preparation of a porous chitosan/fibroin-hydroxyapatite composite matrix for tissue engineering, Macromol. Res. 15 (2007) 65–73. https://doi.org/10.1007/BF03218754.
[101] Y. Xu, D. Xia, J. Han, S. Yuan, H. Lin, C. Zhao, Design and fabrication of porous chitosan scaffolds with tunable structures and mechanical properties, Carbohydr. Polym. 177 (2017) 210–216. https://doi.org/10.1016/j.carbpol.2017.08.069.
[102] D.P. Vasconcelos, M. Costa, N. Neves, J.H. Teixeira, D.M. Vasconcelos, S.G. Santos, A.P. Águas, M.A. Barbosa, J.N. Barbosa, Chitosan porous 3D scaffolds embedded with resolvin D1 to improve in vivo bone healing, J. Biomed. Mater. Res. A. 106 (2018) 1626–1633. https://doi.org/10.1002/jbm.a.36370.
[103] T.-W. Sun, W.-L. Yu, Y.-J. Zhu, F. Chen, Y.-G. Zhang, Y.-Y. Jiang, Y.-H. He, Porous Nanocomposite Comprising Ultralong Hydroxyapatite Nanowires Decorated with Zinc-Containing Nanoparticles and Chitosan: Synthesis and Application in Bone Defect Repair, Chem. - Eur. J. 24 (2018) 8809–8821. https://doi.org/10.1002/chem.201800425.
[104] A.K. Mahanta, S. Senapati, P. Paliwal, S. Krishnamurthy, S. Hemalatha, P. Maiti, Nanoparticle-Induced Controlled Drug Delivery Using Chitosan-Based Hydrogel and Scaffold: Application to Bone Regeneration, Mol. Pharm. 16 (2019) 327–338. https://doi.org/10.1021/acs.molpharmaceut.8b00995.
[105] Y. Zhang, C. Yin, Y. Cheng, X. Huang, K. Liu, G. Cheng, Z. Li, Electrospinning Nanofiber-Reinforced Aerogels for the Treatment of Bone Defects, Adv. Wound Care. 9 (2020) 441–452. https://doi.org/10.1089/wound.2018.0879.

[106] S. Rizal, E.B. Yahya, H.P.S. Abdul Khalil, C.K. Abdullah, M. Marwan, I. Ikramullah, U. Muksin, Preparation and Characterization of Nanocellulose/Chitosan Aerogel Scaffolds Using Chemical-Free Approach, Gels. 7 (2021) 246. https://doi.org/10.3390/gels7040246.

[107] A. Perez-Moreno, M. de las V. Reyes-Peces, D.M. de los Santos, G. Pinaglia-Tobaruela, E. de la Orden, J.I. Vilches-Pérez, M. Salido, M. Piñero, N. de la Rosa-Fox, Hydroxyl Groups Induce Bioactivity in Silica/Chitosan Aerogels Designed for Bone Tissue Engineering. In Vitro Model for the Assessment of Osteoblasts Behavior, Polymers. 12 (2020) 2802. https://doi.org/10.3390/polym12122802.

[108] M.V. Reyes-Peces, A. Pérez-Moreno, D.M. de-los-Santos, M. del M. Mesa-Díaz, G. Pinaglia-Tobaruela, J.I. Vilches-Pérez, R. Fernández-Montesinos, M. Salido, N. de la Rosa-Fox, M. Piñero, Chitosan-GPTMS-Silica Hybrid Mesoporous Aerogels for Bone Tissue Engineering, Polymers. 12 (2020) 2723. https://doi.org/10.3390/polym12112723.

[109] A.-M. Wu, C. Bisignano, S.L. James, G.G. Abady, A. Abedi, E. Abu-Gharbieh, R.K. Alhassan, V. Alipour, J. Arabloo, M. Asaad, W.N. Asmare, A.F. Awedew, M. Banach, S.K. Banerjee, A. Bijani, T.T.M. Birhanu, S.R. Bolla, L.A. Cámera, J.-C. Chang, D.Y. Cho, M.T. Chung, R.A.S. Couto, X. Dai, L. Dandona, R. Dandona, F. Farzadfar, I. Filip, F. Fischer, A.A. Fomenkov, T.K. Gill, B. Gupta, J.A. Haagsma, A. Haj-Mirzaian, S. Hamidi, S.I. Hay, I.M. Ilic, M.D. Ilic, R.Q. Ivers, M. Jürisson, R. Kalhor, T. Kanchan, T. Kavetskyy, R. Khalilov, E.A. Khan, M. Khan, C.J. Kneib, V. Krishnamoorthy, G.A. Kumar, N. Kumar, R. Lalloo, S. Lasrado, S.S. Lim, Z. Liu, A. Manafi, N. Manafi, R.G. Menezes, T.J. Meretoja, B. Miazgowski, T.R. Miller, Y. Mohammad, A. Mohammadian-Hafshejani, A.H. Mokdad, C.J.L. Murray, M. Naderi, M.D. Naimzada, V.C. Nayak, C.T. Nguyen, R. Nikbakhsh, A.T. Olagunju, N. Otstavnov, S.S. Otstavnov, J.R. Padubidri, J. Pereira, H.Q. Pham, M. Pinheiro, S. Polinder, H. Pourchamani, N. Rabiee, A. Radfar, M.H.U. Rahman, D.L. Rawaf, S. Rawaf, M.R. Saeb, A.M. Samy, L. Sanchez Riera, D.C. Schwebel, S. Shahabi, M.A. Shaikh, A. Soheili, R. Tabarés-Seisdedos, M.R. Tovani-Palone, B.X. Tran, R.S. Travillian, P.R. Valdez, T.J. Vasankari, D.Z. Velazquez, N. Venketasubramanian, G.T. Vu, Z.-J. Zhang, T. Vos, Global, regional, and national burden of bone fractures in 204 countries and territories, 1990–2019: a systematic analysis from the Global Burden of Disease Study 2019, Lancet Healthy Longev. 2 (2021) e580–e592. https://doi.org/10.1016/S2666-7568(21)00172-0.

[110] L. Esquivias, M. Piñero, V. Morales-Flórez, N. de la Rosa-Fox, Aerogels Synthesis by Sonocatalysis: Sonogels, in: M.A. Aegerter, N. Leventis, M.M. Koebel (Eds.), Aerogels Handb., Springer New York, New York, NY, 2011: pp. 419–445. https://doi.org/10.1007/978-1-4419-7589-8_20.

[111] S. Balaji, R. Kumar, R. Sripriya, P. Kakkar, D.V. Ramesh, P.N.K. Reddy, P.K. Sehgal, Preparation and comparative characterization of keratin–chitosan and keratin–gelatin composite scaffolds for tissue engineering applications, Mater. Sci. Eng. C. 32 (2012) 975–982. https://doi.org/10.1016/j.msec.2012.02.023.

[112] Q. He, Q. Ao, K. Gong, L. Zhang, M. Hu, Y. Gong, X. Zhang, Preparation and characterization of chitosan–heparin composite matrices for blood contacting tissue engineering, Biomed. Mater. 5 (2010) 055001. https://doi.org/10.1088/1748-6041/5/5/055001.

[113] V.G. Correia, M. Coelho, T. Barroso, V.P. Raje, V.D.B. Bonifácio, T. Casimiro, M.G. Pinho, A. Aguiar-Ricardo, Anti-biofouling 3D porous systems: the blend effect of oxazoline-based oligomers on chitosan scaffolds, Biofouling. 29 (2013) 273–282. https://doi.org/10.1080/08927014.2013.766172.

[114] T.-W. Sun, W.-L. Yu, Y.-J. Zhu, R.-L. Yang, Y.-Q. Shen, D.-Y. Chen, Y.-H. He, F. Chen, Hydroxyapatite Nanowire@Magnesium Silicate Core–Shell Hierarchical Nanocomposite: Synthesis and Application in Bone Regeneration, ACS Appl. Mater. Interfaces. 9 (2017) 16435–16447. https://doi.org/10.1021/acsami.7b03532.

[115] X. Hu, W. Li, L. Li, Y. Lu, Y. Wang, R. Parungao, S. Zheng, T. Liu, Y. Nie, H. Wang, K. Song, A biomimetic cartilage gradient hybrid scaffold for functional tissue engineering of cartilage, Tissue Cell. 58 (2019) 84–92. https://doi.org/10.1016/j.tice.2019.05.001.

[116] X.-N. Qi, Z.-L. Mou, J. Zhang, Z.-Q. Zhang, Preparation of chitosan/silk fibroin/hydroxyapatite porous scaffold and its characteristics in comparison to bi-component scaffolds: Preparation and

Characteristics of Composite Porous Scaffold, J. Biomed. Mater. Res. A. 102 (2014) 366–372. https://doi.org/10.1002/jbm.a.34710.

[117] J. Zhang, A. Deng, Y. Yang, L. Gao, A. Zhou, Z. Zhong, S. Yang, Evaluation of recombinant human collagen-peptide based porous scaffolds and molecular interaction with chitosan, Mater. Technol. 31 (2016) 307–314. https://doi.org/10.1179/17535557B15Y.000000001.

[118] D. Bhowmik, H. Gopinath, B.P. Kumar, S. Duraivel, K.S. Kumar, Controlled release drug delivery systems, Pharma Innov. 1 (2012) 24.

[119] J. Movaffagh, A. Ghodsi, B.S. Fazly Bazzaz, S.A. Sajadi Tabassi, H. Ghodrati Azadi, The Use of Natural Biopolymer of Chitosan as Biodegradable Beads for Local Antibiotic Delivery: Release Studies, Jundishapur J. Nat. Pharm. Prod. 8 (2013). https://doi.org/10.5812/jjnpp.7532.

[120] S. Kumari, R.P. Singh, Glycolic acid functionalized chitosan–Au–Fe3O4 hybrid nanoparticle based nanohybrid scaffold for drug delivery, Int. J. Biol. Macromol. 54 (2013) 244–249. https://doi.org/10.1016/j.ijbiomac.2012.12.001.

[121] T. Barroso, R. Viveiros, T. Casimiro, A. Aguiar-Ricardo, Development of dual-responsive chitosan–collagen scaffolds for pulsatile release of bioactive molecules, J. Supercrit. Fluids. 94 (2014) 102–112. https://doi.org/10.1016/j.supflu.2014.07.005.

[122] L. Guo, J. Xia, S. Yu, J. Yan, F. He, M. Zhang, Q. Fan, R. Yang, W. Zhao, Natural edible materials made of protein-functionalized aerogel particles for postprandial hyperglycemia management, Int. J. Biol. Macromol. 167 (2021) 279–288. https://doi.org/10.1016/j.ijbiomac.2020.11.186.

[123] M.M. Alsmadi, R.M. Obaidat, M. Alnaief, B.A. Albiss, N. Hailat, Development, In Vitro Characterization, and In Vivo Toxicity Evaluation of Chitosan-Alginate Nanoporous Carriers Loaded with Cisplatin for Lung Cancer Treatment, AAPS PharmSciTech. 21 (2020) 191. https://doi.org/10.1208/s12249-020-01735-8.

[124] J. Diosa, F. Guzman, C. Bernal, M. Mesa, Formation mechanisms of chitosan-silica hybrid materials and its performance as solid support for KR-12 peptide adsorption: Impact on KR-12 antimicrobial activity and proteolytic stability, J. Mater. Res. Technol. 9 (2020) 890–901. https://doi.org/10.1016/j.jmrt.2019.11.029.

[125] N. Gorshkova, O. Brovko, I. Palamarchuk, K. Bogolitsyn, A. Ivakhnov, Preparation of bioactive aerogel material based on sodium alginate and chitosan for controlled release of levomycetin, Polym. Adv. Technol. 32 (2021) 3474–3482. https://doi.org/10.1002/pat.5358.

[126] N.A. Valchuk, O.S. Brovko, I.A. Palamarchuk, T.A. Boitsova, K.G. Bogolitsyn, A.D. Ivakhnov, D.G. Chukhchin, N.I. Bogdanovich, Preparation of Aerogel Materials Based on Alginate–Chitosan Interpolymer Complex Using Supercritical Fluids, Russ. J. Phys. Chem. B. 13 (2019) 1121–1124. https://doi.org/10.1134/S1990793119070224.

[127] G.D. Winter, Formation of the Scab and the Rate of Epithelization of Superficial Wounds in the Skin of the Young Domestic Pig, Nature. 193 (1962) 293–294. https://doi.org/10.1038/193293a0.

[128] T.D. Turner, Hospital usage of absorbent dressings, Pharm. J. 222 (1979) 421–424.

[129] K. Vowden, P. Vowden, Wound dressings: principles and practice, Surg. Oxf. 32 (2014) 462–467. https://doi.org/10.1016/j.mpsur.2014.07.001.

[130] A.E. Pusateri, J.B. Holcomb, B.S. Kheirabadi, H.B. Alam, C.E. Wade, K.L. Ryan, Making Sense of the Preclinical Literature on Advanced Hemostatic Products:, J. Trauma Inj. Infect. Crit. Care. 60 (2006) 674–682. https://doi.org/10.1097/01.ta.0000196672.47783.fd.

[131] F.-L. Mi, S.-S. Shyu, Y.-B. Wu, S.-T. Lee, J.-Y. Shyong, R.-N. Huang, Fabrication and characterization of a sponge-like asymmetric chitosan membrane as a wound dressing, Biomaterials. 22 (2001) 165–173. https://doi.org/10.1016/S0142-9612(00)00167-8.

[132] E.C. Wu, S. Zhang, C.A.E. Hauser, Self-Assembling Peptides as Cell-Interactive Scaffolds, Adv. Funct. Mater. 22 (2012) 456–468. https://doi.org/10.1002/adfm.201101905.

[133] ISO 10993-4: Biological evaluation of medical devices — Part 4: Selection of tests for interactions with blood, 2004.

[134] French High Authority of Health, Dispositifs : articles pour pansements, 7AD.

[135] Y. Zhou, D. Yang, X. Gao, X. Chen, Q. Xu, F. Lu, J. Nie, Semi-interpenetrating polymer network hydrogels based on water-soluble N-carboxylethyl chitosan and photopolymerized poly (2-hydroxyethyl methacrylate), Carbohydr. Polym. 75 (2009) 293–298.

[136] G. Gorczyca, R. Tylingo, P. Szweda, E. Augustin, M. Sadowska, S. Milewski, Preparation and characterization of genipin cross-linked porous chitosan–collagen–gelatin scaffolds using chitosan–CO2 solution, Carbohydr. Polym. 102 (2014) 901–911. https://doi.org/10.1016/j.carbpol.2013.10.060.

[137] H.B. Tan, F.Y. Wang, W. Ding, Y. Zhang, J. Ding, D.X. Cai, K.F. Yu, J. Yang, L. Yang, Y.Q. Xu, Fabrication and evaluation of porous keratin/chitosan (KCS) scaffolds for effectively accelerating wound healing, Biomed Env. Sci. 28 (2015) 178–89.

[138] M. Davoodbasha, S.-C. Kim, S.-Y. Lee, J.-W. Kim, The facile synthesis of chitosan-based silver nano-biocomposites via a solution plasma process and their potential antimicrobial efficacy, Arch. Biochem. Biophys. 605 (2016) 49–58. https://doi.org/10.1016/j.abb.2016.01.013.

[139] S. Mania, R. Tylingo, E. Augustin, K. Gucwa, J. Szwacki, H. Staroszczyk, Investigation of an elutable N-propylphosphonic acid chitosan derivative composition with a chitosan matrix prepared from carbonic acid solution, Carbohydr. Polym. 179 (2018) 196–206. https://doi.org/10.1016/j.carbpol.2017.09.082.

[140] W. Sun, G. Chen, F. Wang, Y. Qin, Z. Wang, J. Nie, G. Ma, Polyelectrolyte-complex multilayer membrane with gradient porous structure based on natural polymers for wound care, Carbohydr. Polym. 181 (2018) 183–190. https://doi.org/10.1016/j.carbpol.2017.10.068.

[141] Y. Zhang, Y. Liu, Z. Guo, F. Li, H. Zhang, F. Bai, L. Wang, Chitosan-based bifunctional composite aerogel combining absorption and phototherapy for bacteria elimination, Carbohydr. Polym. 247 (2020) 116739. https://doi.org/10.1016/j.carbpol.2020.116739.

[142] A. Vidal, A. Giacaman, S.S. Orellana, S. Jofré, I. Moreno-Villoslada, F. Oyarzún-Ampuero, M. Concha, Application of Chitosan and Chondroitin Sulphate Aerogels in a Patient With Diabetes With an Open Forefoot Transmetatarsal Amputation, Wounds Compend. Clin. Res. Pract. 32 (2020) E14–E18.

[143] M. Concha, A. Vidal, A. Giacaman, J. Ojeda, F. Pavicic, F.A. Oyarzun-Ampuero, C. Torres, M. Cabrera, I. Moreno-Villoslada, S.L. Orellana, Aerogels made of chitosan and chondroitin sulfate at high degree of neutralization: Biological properties toward wound healing: AEROGELS OF CS AND ChS NANOCOMPLEXES, J. Biomed. Mater. Res. B Appl. Biomater. 106 (2018) 2464–2471. https://doi.org/10.1002/jbm.b.34038.

[144] Y. Fan, Q. Lu, W. Liang, Y. Wang, Y. Zhou, M. Lang, Preparation and characterization of antibacterial polyvinyl alcohol/chitosan sponge and potential applied for wound dressing, Eur. Polym. J. 157 (2021) 110619. https://doi.org/10.1016/j.eurpolymj.2021.110619.

[145] M.P. Batista, V.S.S. Gonçalves, F.B. Gaspar, I.D. Nogueira, A.A. Matias, P. Gurikov, Novel alginate-chitosan aerogel fibres for potential wound healing applications, Int. J. Biol. Macromol. 156 (2020) 773–782. https://doi.org/10.1016/j.ijbiomac.2020.04.089.

[146] N.A. Gorshkova, O.S. Brovko, I.A. Palamarchuk, K.G. Bogolitsyn, Influence of the Structure of Alginate-Chitosan Materials on the Kinetics of Usnic Acid Release, Appl. Biochem. Microbiol. 58 (2022) 110–117. https://doi.org/10.1134/S0003683822020089.

[147] LUNA, ChitoSeal™: Hemostatic sealants, 2013. https://lunainc.com/wp-content/uploads/2014/04/Hemostatic-Agents-August-2013.pdf.

[148] K. Inaba, B.C. Branco, P. Rhee, B. Putty, O. Okoye, G. Barmparas, P. Talving, D. Demetriades, Long-term preclinical evaluation of the intracorporeal use of advanced local hemostatics in a damage-control swine model of grade IV liver injury:, J. Trauma Acute Care Surg. 74 (2013) 538–545. https://doi.org/10.1097/TA.0b013e31827d5f5f.

[149] A. Mogrovejo-Valdivia, Conception et évaluation d'un pansement à libération de deux principes actifs pour le traitement des plaies chroniques, Université de Lille, 2018.

[150] R.S. Ambekar, B. Kandasubramanian, Advancements in nanofibers for wound dressing: A review, Eur. Polym. J. 117 (2019) 304–336. https://doi.org/10.1016/j.eurpolymj.2019.05.020.

[151] French High Authority of Health, Les pansements: Indications et utilisations recommandées, HAS, 2011. https://www.has-sante.fr/ (accessed January 7, 2020).

Chapter II. Materials and methods

List of abbreviations:

AAP: Ascorbic acid 2-phosphate

BET: Brunauer, Emmett and Teller method

DA: Degree of acetylation

Dex-P: Dexamethasone phosphate

DIC: Digital image correlation

DLC: Drug loading capacity

DLE: Drug loading efficiency

DMTA: Dynamical thermal analysis

Ea: Activation energy

HDF: Human dermal fibroblast

S/E: Solvent exchange

ScD: Drying with supercritical CO_2

SWE: Simulated wound exudate

Content

1. Materials

Chitosan of high molecular weight were purchased from Acros. Molecular weight of 600 – 800 KDa was given by the manufacturer, no precision on the determination method was given, and the degree of acetylation (DA) is in the range 10 ±2 % as determined by FTIR.

Glacial acetic acid, ethanol (≥ 99%), acetone (≥ 99%), isopropanol (≥ 99.5%) and sodium hydroxide pellets (analytical reagent grade) were supplied by Fisher Chemical. 10X PBS was supplied by Fisher bioreagents (Pittsburgh, PA, USA). All chemicals were used as received. Water was distilled. L-Ascorbic acid 2-phosphate sesquimagnesium salt hydrate (AAP) and dexamethasone phosphate (Dex-P) were supplied by Sigma. The solutions used for biological in vitro are listed in the corresponding section.

2. Methods

2.1. Preparation of chitosan aerogels

The Figure II.1 is the general scheme of the preparation of aerogels, xerogels and cryogels. This figure will help to understand the following parts.

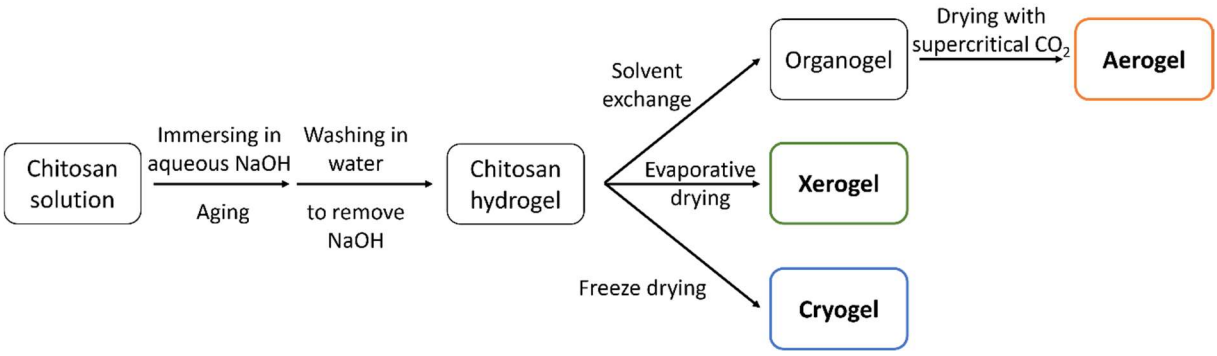

Figure II.1: Schematic representation of the preparation of chitosan aerogels and cryogels

2.1.1. Chitosan dissolution

Chitosan was dissolved in a solution of 2% v/v of acetic acid under mechanical stirring for several hours. The concentration of chitosan was varied from 1 to 10% wt/v. Chitosan solution was cast into plastic molds of 27.5 mm in diameter and 68 mm of height with 1 mm holes drilled in the walls. The molds filled with chitosan solution were immersed in NaOH-water solution (0.1 – 4 M) for non-solvent precipitation to fix sample shape. This coagulation step takes 24h.

2.1.2. Solvent exchange step

To perform drying with supercritical CO_2, solvent exchange must be done as water is not miscible with CO_2. Therefore, coagulated chitosan was carefully demolded, washed in water to remove the NaOH and immersed in solutions of organic solvent/distilled water. The organic solvent ratio was gradually increased from 0/100, 10/90, 25/75, 50/50, 75/25, 90/10 to 100/0 to slowly replace water by the non-solvent. This solvent exchange step resulted in a chitosan organogel. To ensure a complete solvent exchange, several “washing” steps with the organic solvent were performed.

2.1.3. Supercritical drying using CO_2

Organogels were dried with supercritical CO_2 in the center PERSEE of Mines ParisTech in Sophia Antipolis. The laboratory scale device is shown in Figure II.2. Organogels are placed in a 1 L autoclave and immersed in ethanol. The system is closed and pressurized at 50 bars and 37 °C with gaseous CO_2. The pressure is increased to 80 bars making the CO_2 supercritical ($ScCO_2$ is obtained at a pressure of 72.8 bar and T=31.1 °C). This $scCO_2$ solubilized the residual liquid inside the sample. A dynamic washing

step at 80 bars, 37°C with an output of 5 kg CO_2/h is carried out for 1 hour, then the system is put in static mode to allow $ScCO_2$ to diffuse and solubilize ethanol in nanopores for 1-2 hours. Dynamic washing is performed again in the same conditions for 2 h. Finally, the system is slowly depressurized at 4 bar/h and 37 °C and cooled to room temperature.

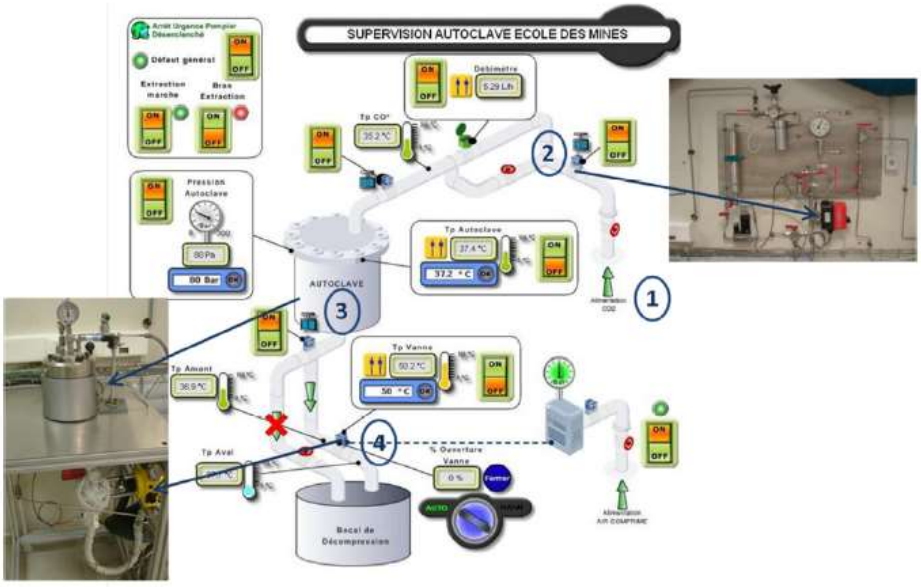

Figure II.2: Laboratory-scale supercritical CO_2 drying device in PERSEE Mines Paris. (1) CO_2 supply, (2) feeding valve, (3) autoclave, (4) depressurization valve. Courtesy of Pierre Ilbizian, PERSEE Mines Paris

2.1.4. Alternative drying method

a. Freeze drying

To obtain "cryogels", hydrogels were freeze-dried by immersion in liquid nitrogen (- 196°C) for 5 min and then freeze-drying (in Cryotec Cosmos 80 equipment) for 48 h.

b. Evaporative drying

"Xerogel" was obtained from a hydrogel made from 5% wt/v chitosan solution coagulated in 4 M NaOH, aged for 24 h and dried at 55 ◦C under vacuum until constant weight.

2.2. Characterization methods

2.2.1. Viscometry

The viscosity of solvent and dilute chitosan solution was measured using a LAUDA iVisc viscometer equipped with an Ubbelohde-type viscometer capillary at 10 °C and 50 °C and using the Mark-Houwink equation with 0.1M of acetic acid and 0.2M of NaCl at 25°C. Flow time for the solvent -2% of acetic acid is 115.4 s and 54.5 s at 10 °C and 50 °C, respectively.

$$[\eta] = K_m M_w^a \qquad \text{II.1}$$

with K = 1.81 x10^5 dL/g and a = 0.93 Roberts and Domzy.

2.2.2. Rheological tests

Solution behavior was studied with a Gemini rotational rheometer with Peltier temperature control system using a 2° cone-plate geometry of 60 mm in diameter at 20 °C in the linear viscoelastic domain at 5% of strain.

2.2.3. Fourier Transformed Infrared spectroscopy (FTIR)

Chitosan degree of acetylation (DA) was determined by infrared spectroscopy with the method described by Moore and Roberts [1]. The chitosan powder (4 mg) and 100 mg of KBr were dried for 4h at 80 °C and mechanically blended to make a disk. Then the degree of DA was determined with the equation:

$$DA\ (\%) = (A_{1655}/A_{3450}) \times (100/1.33) \quad \text{II.2}$$

with A_{1655} the absorption at 1655 cm^{-1} of the amide I band and A_{3450} the absorption at 3450 cm^{-1} of the hydroxyl groups.

2.2.4. Sample shrinkage, bulk density, and porosity

The evolution of sample volume at each processing step (for aerogels: from solution to alcogel and from alcogel to aerogel; for cryogels: from solution to hydrogel and from hydrogel to cryogel) and total shrinkage (from solution to dry material, see Figure II.1) was monitored. As samples were of cylindrical shape, their diameter and height were measured, and volume shrinkage was calculated according to the following equation:

$$Shrinkage\ (\%) = \left(V_i - V_f\right) \times 100/V_i \quad \text{II.3}$$

where Vi and Vf are sample volumes before and after the step, respectively.

The bulk density ρ_{bulk} was measured with an Envelope Density Analyzer Geopyc 1360 (Micromeritics) with a calibrated chamber using DryFlo fine powder. Porosity was calculated from bulk and skeletal density ($\rho_{skeletal}$, 1.446 ± 0.116 g/cm^3 for chitosan [2]) with Eq.II.4.

$$Porosity\ (\%) = \frac{(\rho_{skeletal} - \rho_{bulk})}{\rho_{skeletal}} \times 100 \quad \text{II.4}$$

2.2.5. Pore specific volume

Pore specific volume was estimated using bulk and skeletal densities:

$$V_{pore} = (1/\rho_{bulk}) - (1/\rho_{skeletal}) \quad \text{II.5}$$

2.2.6. Specific surface area measurement (BET method)

The specific surface area was measured using a Micromeritics ASAP 2020 employing the Brunauer, Emmett et Teller (BET) method. Prior to measurement the samples were degassed in a high vacuum at 70 °C for 10 h.

2.2.7. Scanning electron microscopy

The morphology of the aerogels was studied with a scanning electron microscope (SEM) field emission gun (FEG) MAIA at an accelerating voltage of 3 keV after platinum coating (14 nm) with Q150T Quarum rotating metallizer.

2.2.8. X-Ray diffraction

X-ray diffraction patterns were obtained on powder samples with a 'XPERT-PRO' diffractometer from PANalytical equipped with a θ/θ 3050/60 goniometer, a CuKα source operated at 40 kV and 30 mA, and the measurement program 'ScanPixcel'. The diffraction angle 2θ was from 5° to 40° with a 0.08° step.

2.2.9. Fluid sorption

Dried samples were immersed in simulated wound exudate (SWE) composed of 8.3 g/L of NaCl and 0.37 g/L of $CaCl_2$ at 31 °C (no viscosity modifier was used in agreement with the EN 13726-1

standard). The evolution of sample weight with time (w_t) was measured during 48 h, and SWE absorption was calculated with the following equation:

$$Absorption(\%) = \left((w_t - w_i) \times 100\right)/w_i \quad \text{II.6}$$

where w_i is sample initial weight.

2.2.10. Shore hardness measurements

The shore hardness measurements were done with a durometer Sauter HBA 100-0, type shore A.

2.2.11. Uniaxial compression measurements

Uniaxial compression tests were performed on 3400 Serie Instron (Norwood, MA, USA) electromechanical device equipped with a 30 kN load cell. The samples were in the shape of cylinders with length to diameter ratio below 2 to avoid buckling. The upper and lower surfaces of cylinders were polished with P320 sandpaper to be parallel and planar. The sensor was calibrated as follows: in class 0.5 - 0.5 % error above 100 N, and less than 1% error between 10 N-100 N. The tests were performed with a 5.0×10^{-2} s^{-1} strain rate with a pre-loading of 1N and 3 cycles of loading at 5, 10 and 15% of strain to a minimum of 0.5 N to keep the contact with the sample. A digital image correlation (DIC) system was used to track the true displacement of the plateau over time. The DIC system was composed of two cameras in stereo-correlation. The side of each plateau was speckled with black and white paints. The displacement was calculated by analyzing the evolution of the random speckle patterns with the analysis software VIC-3D—Correlated Solutions. A tracking line was then positioned between each plateau. The mechanical behavior was investigated by measuring the strain at the tracking point, i.e., at the maximum of the strain field. The setup is shown on Figure II.3a and a typical strain field, and the location of the tracking line are depicted in Figure II.3b. The engineering strain, stress and the specific stress were calculated according to the following equations:

$$Engineering\ strain = \varepsilon_{yy} = \Delta L/h_0 \quad \text{II.7}$$

$$Engineering\ stress = \sigma_N = F/A_0 \quad \text{II.8}$$

$$Specific\ stress = \sigma_N/\rho \quad \text{II.9}$$

With ε_{yy} the vertical strain, ΔL the difference of length between two tracking points from the start and the time t of the test, h_0 is the initial height of the sample. σ_N is the nominal or engineering strain in MPa, F is the strength in newton, A_0 is the initial surface of the sample in m², and ρ is the density of the sample.

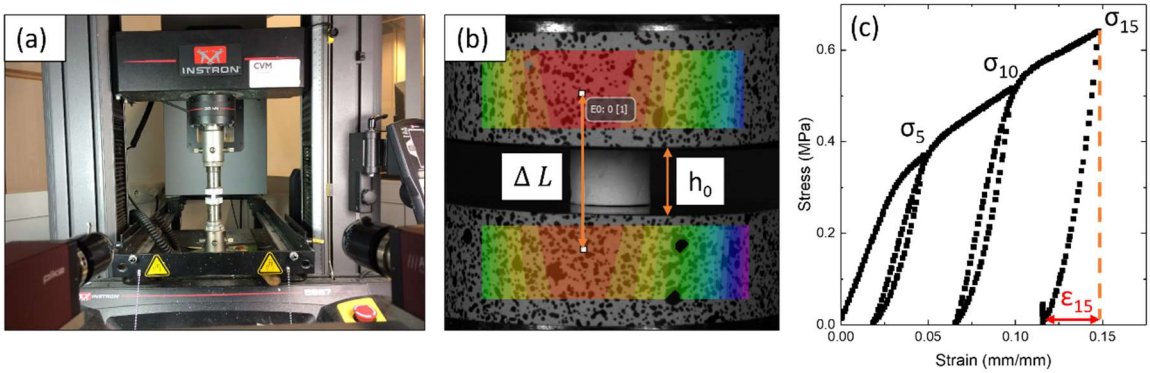

Figure II.3: (a) Set up of the uniaxial compression tests, (b) Typical analysis of a compression test with strain fields measured by DIC with tracking point between the plateau, (c) typical curve of engineering stress vs strain obtained σ_5, σ_{10} and σ_{15} the stress at 5, 10 and 15% of strain respectively and ε_{15} the elastic recovery for an unloading from 15% of strain.

2.2.12. Dynamic thermal mechanical analysis (DMTA)

a. Preparation of the samples:

Chitosan aerogels at different concentrations 4 to 8 %wt/v were used to perform the mechanical tests. Three kinds of molds were used to prepare the samples depending on the experiment:

- One mold was a long cylinder tube of polypropylene of 14 mm in diameter and 15 cm of length. The chitosan solution was poured in this mold filling half of the tube and the 4M NaOH solution was used to fill the tube. The samples obtained from these tubes are named UDT (for undrilled tubes).
- The second kind of mold was the same plastic tube but with holes of 1 mm in diameter in the wall. The samples obtained from these tubes are named DT (for drilled tubes).
- The last one was plastic spectrometer cell of 10.5 mm square and 44 mm of height, 2/3 of the cell was filled with chitosan solution and the top with NaOH solution. Cubic gels were obtained.

The 4M NaOH solution was renewed 3 times per day until complete coagulation (maximum 2 days for the long tubes), the coagulated gels were demolded and went through the whole process of aerogel preparation. The non-solvent used during ScD was ethanol. The DT and UDT aerogels were cut in small discs and the upper and lower surfaces of discs were polished with P320 sandpaper to be parallel and planar. The samples DT and UDT were used to see the influence of the propagation of coagulation on the mechanical properties of the network. The cubic aerogels obtained from the spectrometer cells were polished and used to test the anisotropy of the network.

b. DMA protocol for mechanical tests:

All DMTA experiments were conducted in compression using a Mettler-Toledo® DMA 1, Greifensee, Switzerland. Two measurements have been performed for each formulation on aerogels. A preloading was used to avoid losing contact during oscillation.

Protocol to investigate the influence of the water content on the mechanical behavior of UDT samples:

At a frequency of 1 Hz, two heating runs from 10 to 80°C are realized successively with an increase of 1°C per minute. The evolution of the elastic modulus as a function of the temperature is observed.

Protocol to investigate the influence of the humidity uptake and the influence of the coagulation direction on the mechanical behavior of DT and UDT samples:

1. Heating run in the DMTA with a temperature scan at 1Hz from 10 to 80°C at 1°C per minute
2. Frequency scan from 0.1 to 10 Hz every 10°C from 10 to 80°C
3. Heating run scan from 10 to 80°C at 1°C per minute and 1 Hz.
4. Humidity uptake in a climatic chamber Binder KBF 115 at 30°C and 50% of relative humidity (%RH) for a week
5. Redo the steps 1 till 3

Frequency and temperature scans are launched as soon as possible after drying to prevent humidity uptake.

Protocol to investigate the influence of the anisotropy on the cubic aerogels:

All samples were dried at 80°C until no evolution of the modulus was visible. At a frequency of 1 Hz, one temperature scan from 10 to 80°C is performed with an increase of 1°C per minute in the same direction as the coagulation front (longitudinal direction) and another one is performed

perpendicular to this direction in the transversal way. The evolution of the modulus as a function of the temperature is observed.

c. Protocol to follow coagulation kinetics

All DMTA experiments were conducted in compression mode using a Mettler-Toledo® DMA 1, Greifensee, Switzerland, at room temperature. A chitosan droplet was placed in-between the plates of 10 mm diameter with a gap of 1 mm. A displacement amplitude of 10 µm (i.e. strain of 1%), was applied during the whole duration of the experiment at a frequency of 1 Hz. This strain was checked to be within the linear visco-elastic region. The plates together with chitosan solution were gently immersed in a 4M NaOH-water bath (Figure II.4), and the elastic modulus evolution was recorded in time. Each formulation was tested in triplicate. Compressive modulus evolution in time during the coagulation was recorded.

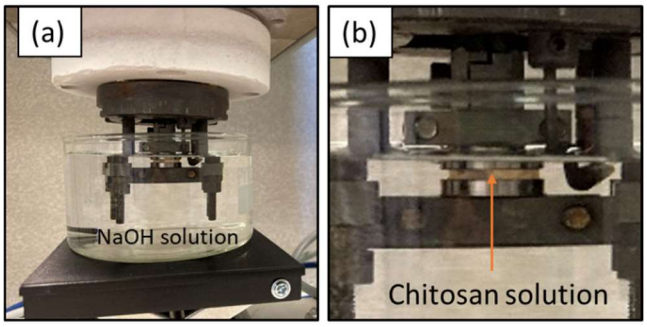

Figure II.4: Photos of the set up (a) and zoom on the sample (b)

2.2.13. Coagulation kinetics monitored by optical observations

A droplet of chitosan solution was placed between a microscope slide and a coverslip. A spacer of 1 mm was used to maintain a height similar to the one in the coagulation kinetics monitored by DMTA. The sample was placed on a transparent table and illuminated from below. Some droplets of 4M NaOH-water solution were deposited on the microscope slide entering by capillary forces the space between the slide and coverslip and surrounding the chitosan droplet. A camera (AVT PIKE 5 Megapixels with 2/3' CCD sensors and 50 mm Schneider Kreuzwach objectives) was recording droplet evolution in time at 1 fps from the top side, as shown in Figure II.5. The experiments were performed at room temperature. Each formulation was recorded in triplicate.

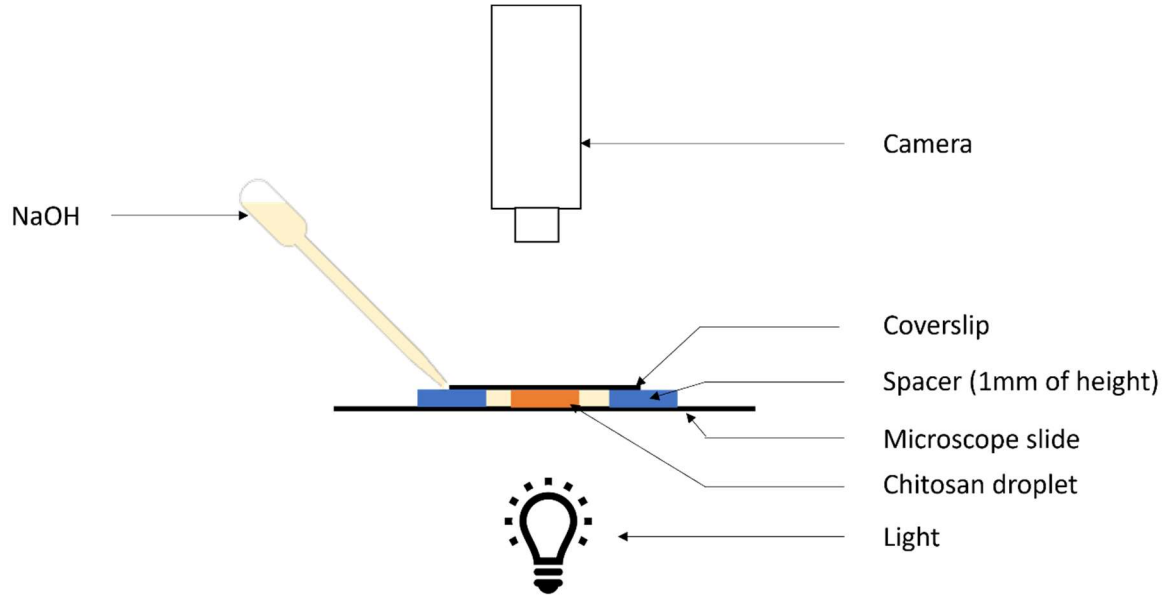

Figure II.5: Scheme of the optical experimental set-up.

The kinetics of chitosan coagulation in time was analyzed as follows: the snapshots were taken, and the total surface of the droplet and the surface of uncoagulated region were measured with ImageJ (Figure II.7). Each was assumed to be spherical and the corresponding radii were calculated. The width of coagulated layer L was taken as the difference between the two radii values (Figure II.7a). In this method, the error is determined by the quality of the optical contrast between coagulated and uncoagulated chitosan as well as the camera resolution. This error was estimated as the length needed for the camera to detect a variation between the grey levels; it corresponds to 0.026 cm as shown in Figure II.6. The peaks correspond to the bright areas (higher grey values) so either the NaOH solution either the non-coagulated chitosan solution. The valleys are the coagulated areas (darker areas, lower grey values).

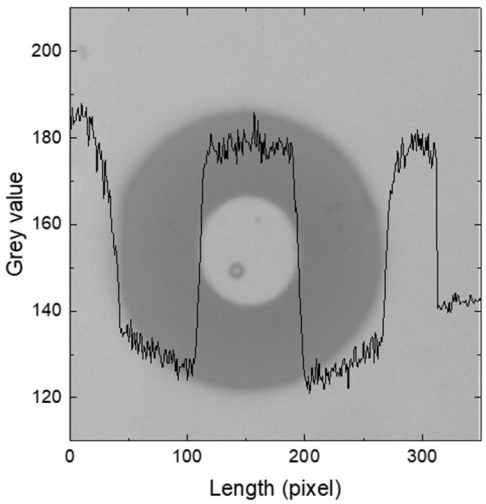

Figure II.6: Grey scale profile during coagulation for a 6%wt/v chitosan solution. The picture in the back show to which part of the picture the grey level corresponds.

Another method to evaluate the thickness of the coagulation layer was to measure it directly on the snapshots using ImageJ (Figure II.7); the average of five values was taken. An example of the comparison of L values obtained with both methods is shown in Figure II.8; both present very similar values. To have a consistent error for all measurements, the “surface” approach was chosen.

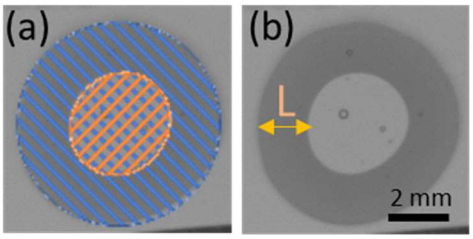

Figure II.7: Two methods showing the determination of the coagulated length (a) by “surface approach”, (b) by direct measurement. The example shown corresponds to a droplet of 6% wt/v chitosan.

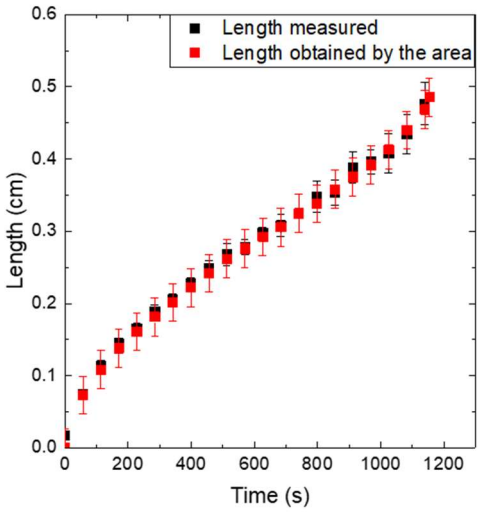

Figure II.8: Comparison of the evolution of the coagulated layer L in time calculated using “surface approach” (in red) and measured directly (in black). The droplet was from a 3% wt/v chitosan solution. The error for the “surface approach” originates from the optical contrast at the border, and for the direct measurement from five values taken at different places on the snapshot.

2.2.14. Preparation and characterization of drug loaded chitosan aerogels and cryogels

For a Galenician, the word "drug" defines an active ingredient and its excipient. In this work, to be consistent with the literature and the vocabulary commonly used in materials science, we use the word "drug" to designate only the active ingredient.

a. Drug incorporation into chitosan matrices

The hydrogels, washed from NaOH were loaded with the drug by immersing in 100 mL of 0.5 g/L Dex-P for 3 days or 450 mL of 0.5 g/L of AAP for 10 days under magnetic stirring at 100 rpm. For AAP impregnation, the solution was replaced by a fresh one after 48h. These drugs are well soluble in water, poorly soluble in ethanol and insoluble in CO_2 [3].

b. Aerogels and cryogels' drug loading capacity and specific loading

The drug loading efficiency (DLE) and the drug loading capacity (DLC) were calculated as follows:

$$DLE\ (\%) = \frac{Actual\ drug\ dose\ (g)}{Theoretical\ drug\ dose\ (g)} \times 100 \qquad \text{II.10}$$

$$DLC\ (\%) = \frac{Actual\ drug\ dose\ (g)}{Sample\ mass\ (g)} \times 100 \qquad \text{II.11}$$

The theoretical drug dose was determined as the corresponding amount of drug when the concentration of drug inside the sample and the one of the impregnation media are at the equilibrium.

2.2.15. In vitro drug release experiments

AAP release was performed in sink condition in 500 mL of PBS at pH 7.4 and 8.9 at 30°C with a magnetic stirring of 100 rpm. This temperature was selected in accordance with the skin temperature to perform the release at conditions close to the application. These two values of pH were selected as the pH of a chronic wound decreases from 8.9 (inflammation stage) to 7.2 (healing stage) [4–6]. The dried gel was placed in a tee-ball and immersed in the AAP solution and the release was followed by UV until constant concentration. The gel was then crushed with mortar and pestle in 20 mL PBS solution and placed in a sonicated bath for 30 min to ensure a complete release. After filtrating with a regenerated 0.45 µm nylon filter, a last UV measure was performed to quantify any traces of trapped drug.

Release kinetics of the AAP were followed using a Scanning Spectrophotometer UV-1800 UV/Visible (Shimadzu) coupled with a Peristaltic Sipper Pump 206-23790-91 (Shimadzu) and a Sipper Unit 160C (Shimadzu) with glass cell presenting an optical path length of 10 mm. Every 10 min a spectrophotometric measurement from 200 to 800 nm was performed on a freshly collected solution which was put back in the bath after the measurement. The molar extinction coefficient has been determined to be 35.72 g/L at pH 7.4 and 33.22 g/L at pH 8.9 for AAP at 30°C. The curves are shown in Figure II.9.

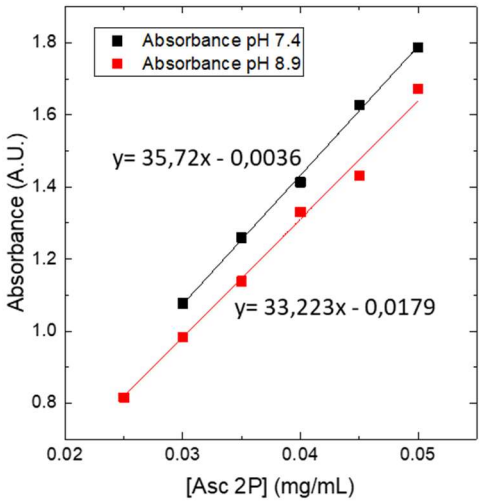

Figure II.9: Calibration curves at 260 nm of ascorbic acid 2-phosphate dissolved in PBS at 30°C. Straight lines are linear regressions of the data

The release of Dex-P was performed at the Division of Pharmaceutics of Utrecht Institute for Pharmaceutical Sciences (UIPS) in Utrecht University at Utrecht in The Netherlands. First, the calibration curve to be used for the determination of Dex-P concentration in the release bath (phosphate buffered saline, PBS) was established using an Acquity ultra high-performance liquid chromatography system (Waters Corporation, Milford, USA) operated by Empower software (Version 3-FRS, Waters Corporation). A BEH C18 column was used at 50°C. The injection volume was 10 µL, with 25 %ACN/75 % MilliQ water as eluent, acidified with 0.1% perchloric acid to yield pH 2.2. The run time was 5 min, the retention time 0.6 min and the flow rate 1 mL/min. The wavelength was 254 nm. The peak area was plotted as a function of the known Dex-P concentration (Figure II.10).

Dex-P release kinetics was monitored under sink conditions in 150 mL of PBS under magnetic stirring at 100 rpm at 30°C and at pH 7.4 or 8.9. The sample was placed in a tea-bag and immersed in release medium. 1 mL of the release medium was taken out regularly and replaced by 1 mL of fresh medium; the dilution was taken into account when calculating the Dex-P concentration. The release was followed until no evolution of the concentration occurred for several hours. Then, the sample was crushed with a mortar and pestle and dispersed in 20 mL PBS solution. The dispersion was sonicated for 30 min to ensure a complete release of the drug from the sample, filtered through a 0.22 µm cellulose acetate filter and the Dex-P concentration was determined using the calibration curve. As no drug remained in the chitosan matrix, the Dex-P concentration in the matrix before release was considered to be the one obtained after complete release. All measurements were performed in duplicate.

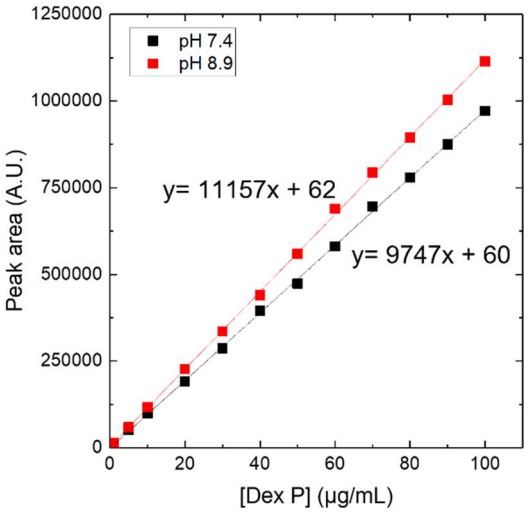

Figure II.10: Calibration curves (absorbance at 254 nm) for dexamethasone phosphate dissolved in PBS. Straight lines are linear regressions of the data.

2.3. Biological *in vitro* tests

2.3.1. Sample preparation

Two cell lines were used, the Human Dermal Fibroblasts (HDF) cell lines at passages 2 and 3 (GIBCO, C-013-5C) and the murine fibroblasts (L929) (ECACC 85011425). The cells were maintained in DMEM (Sigma Aldrich, D6546) supplemented with foetal bovine serum (5%, v/v) (Gibco, 10270106), glutaMAX 1X (Gibco, 35050061) and 1% penicillin/streptomycin (Sigma Aldrich, P0781) at 37°C in a humidified atmosphere containing 5% CO_2. All tests, except cytotoxicity assay, were performed with aerogel extracts made as followed. Aerogels made from 5%wt/v chitosan solution and dried in ethanol

were used for all the biological tests. The samples were decontaminated with UV-C irradiation at λ = 254 nm for several minutes. Extraction was done in a complete cell culture medium at 37°C under stirring for 3 days and filtrated to remove the aerogel pieces.

2.3.2. Cytotoxicity tests

Cytotoxicity was evaluated on, HDF and L929, using CellTiter Glo assay (Promega G7571). Extracts of unloaded chitosan were used to perform this test. The extraction ratio was done at 0.1 g/mL for 72h following NF EN ISO 10993 parts 5 and 12 guidance (2010 and 2021 respectively). Negative RM-C was high density polyethylene film and positive RM-A was a polyurethane film containing 0.1% zinc diethyldithiocarbamate supplied as reference materials by Hatano Research Institute, Food and Drug Safety Center, Japan. Cells were seeded at 1.10^4 cells per well (96-well plate) and allowed to adhere overnight. Then extracts were added to L929 and HDF cell monolayers and incubated for 24h at 37°C under a humidified atmosphere with 5% CO_2. An equivalent volume of CellTiter Glo was added to each well, and the luminescence was measured using CLARIOstar (BMG LABTECH) plate reader after 10 minutes of incubation.

2.3.3. Collagen detection

The AAP concentration in the aerogel extracts was measured in a UV spectrophotometer and diluted to the concentrations determined by experiments detailed in Supporting Data (Figure II.11). Cells were plated without serum in a 96-well plate in amount of 1.10^4 cells per well and allowed to attach overnight. Chitosan extracts and free AAP at 100, 300, 500, and 750 µg/mL were added to the wells. Medium without drug was used as a control. Collagen was detected at the different steps of its secretion after 6 and 13 days: insoluble extracellular collagen *via* Direct Red 80 (Sigma Aldrich, 365548), and extracellular soluble collagen *via* sircol assay (Biocolor, S5000). For each assay, cell number quantification was performed using PrestoBlue (Invitrogen, P50201). The reactant was added into each well at 10% in complete growth medium and the fluorescence at 590 nm was measured using CLARIOstar (BMG LABTECH) plate reader after 45 minutes incubation. Briefly, after cell fixation with paraformaldehyde 4% for 30 minutes, 0.1% direct red 80 solubilized in picric acid saturated 1.3% was applied for 30min then washed with acetic acid 0.5M and NaOH 0.1N was applied, finally the absorbance was measured after 15 min at 550nm. Sircol assay started with extraction and isolation of collagen, Sircol dye reagent was added to bind with the collagen and precipitate. After de-binding the dye, washing sodium hydroxide was added and absorbance was measured at 555 nm.

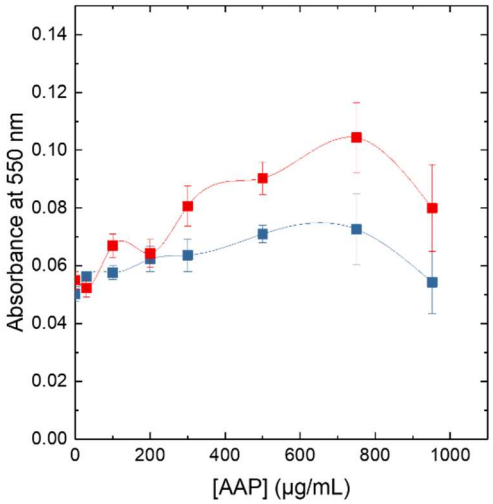

Figure II.11: Intracellular collagen detection after AAP treatment at 6 days (red) and 9 days (bleu) on HDF P4 fibroblasts seeded at 10 000 cells/well with 5% of FBS (FBS starvation 24h before treatment).

2.3.4. Scratch test

Scratch test was performed in a 24-well plate after cells seeding at $2.5.10^4$ cells per well and allowed them to attach and grow until confluence was reached. When the desired confluence is reached, a linear scratch was made in each well with the tip of a micropipette. After 24h, chitosan extracts and free AAP at 100, 350, and 750 µg/mL were added to the wells. Medium without drug and extract of unloaded aerogels were used as a control. Pictures of each well were taken over the time, and the width of the scratch was measured with ImageJ software. Each point on the graph count between 80 to 90 measurements.

References

[1] G.K. Moore, G.A.F. Roberts, Determination of the degree of N-acetylation of chitosan, 2 (n.d.).
[2] C. López-Iglesias, J. Barros, I. Ardao, F.J. Monteiro, C. Alvarez-Lorenzo, J.L. Gómez-Amoza, C.A. García-González, Vancomycin-loaded chitosan aerogel particles for chronic wound applications, Carbohydr. Polym. 204 (2019) 223–231. https://doi.org/10.1016/j.carbpol.2018.10.012.
[3] H. Hao, J. Wang, Y. Wang, Solubility of Dexamethasone Sodium Phosphate in Different Solvents, J. Chem. Eng. Data. 49 (2004) 1697–1698. https://doi.org/10.1021/je0498412.
[4] L.A. Schneider, A. Korber, S. Grabbe, J. Dissemond, Influence of pH on wound-healing: a new perspective for wound-therapy?, Arch. Dermatol. Res. 298 (2007) 413–420. https://doi.org/10.1007/s00403-006-0713-x.
[5] G. Gethin, The significance of surface pH in chronic wounds, Wounds UK. 3 (2007) 53.
[6] S.L. Percival, S. McCarty, J.A. Hunt, E.J. Woods, The effects of pH on wound healing, biofilms, and antimicrobial efficacy: pH and wound repair, Wound Repair Regen. 22 (2014) 174–186. https://doi.org/10.1111/wrr.12125.

Chapter III. Probing kinetics of chitosan coagulation: optical and mechanical testing

List of abbreviations:

C_E: coagulation coefficient obtained from DMTA data in MPa^2/s

DMTA: Dynamic mechanical thermal analysis

E: Elastic modulus obtained by DMTA measurements

G': Elastic modulus or storage modulus obtained by rheological measurements

G'': Viscous modulus or loss modulus obtained by rheological measurements

L: coagulated width

ω: Angular frequency (rad/s)

Content

Introduction

Coagulation is an important step in the preparation of precursors of porous dry materials. It allows to transform a solution into a polymer network. It is thus critical to control and understand coagulation in order to have a better control over the final structure of the material. To induce coagulation of polysaccharides, a mixture of solvent/non solvent can be placed on top of the polymer solution leading to a non-solvent induced phase separation, also called immersion-precipitation [1]. The solubility of the polymer decreases with the increase of the non-solvent proportion leading to a porous network for bio-based polymers. Indeed, synthetic flexible polymers often collapse during this step as their chains lack rigidity.

The network morphologies obtained via non-solvent phase separation are more or less well understood [2–8], but not much is known about coagulation kinetics [9–11] and very few papers report on this topic. Enache et al. [9] followed the NaOH induced coagulation of chitosan via recording the hydrogel volume and the thickness of the coagulation front. Smith et al. [10] looked at the radial progression of the coagulation front on a gelled rod of cellulose. Knaul and Creber [11] extruded a chitosan solution into a different coagulation baths (NaOH, NaOH/ethanol, NH_4OH, Na_3PO_4, KOH, LiOH) at different temperatures. After different coagulation times, the coagulated rods were removed from the solution, frozen in liquid nitrogen and the cross-section of the sample was observed microscope to measure the width of the coagulated layer. But to the best of our knowledge, the evolution of the mechanical properties during the coagulation has not been investigated yet.

In the present work, for the first time, we looked at the coagulation kinetics of chitosan solutions via the evolution of the mechanical properties and compared these data with coagulation kinetics followed by an optical camera. We also analyzed the influence of the chitosan concentration on the coagulation.

This study was performed in view of processing polysaccharide-based solutions, for example by additive manufacturing. Indeed, coagulation leads to a structuration of the network inducing specific morphology and drastically modifying the macro- and microscopic aspect of the gel and the mechanical properties. The evolution of these mechanical properties plays a critical role when polymer processing and coagulation occur at the same time. For example, during additive manufacturing, control over the coagulation kinetics may help to overlay polymer layers without crushing the bottom layer and without having independent coagulated layers. This study may therefore help in the rational design of e.g., polysaccharide-based bio-inks.

Résumé

La coagulation est une étape importante dans la préparation des précurseurs de matériaux poreux secs. Cette étape permet de passer d'une solution à un réseau de polymère. Il est crucial de comprendre et maîtriser ce processus afin de pouvoir mieux contrôler la structure finale du matériau. Pour coaguler les polysaccharides, un mélange de solvant/non-solvant peut être déposé à la surface de la solution de polymère menant à une séparation de phase induite par le non-solvant, aussi appelée immersion-précipitation [1]. La solubilité du polymère diminue avec l'augmentation de la proportion de non-solvant conduisant à un réseau poreux pour les polymères biosourcés. En effet, les polymères synthétiques flexibles s'écrasent généralement durant cette étape à cause du manque de rigidité des chaînes.

La morphologie du réseau obtenu par la séparation de phase induite par le non-solvant est plus ou moins bien comprise [2–8], mais la cinétique de coagulation est peu connue [9–11] et très peu d'articles abordent ce sujet. Enache et al. [9] a étudié la coagulation du chitosane induite par l'ajout de soude en suivant l'évolution du volume de l'hydrogel et l'épaisseur du front de coagulation. Smith et al. [10] a observé la progression radiale du front de coagulation sur un bâton de cellulose gélifiée. Knaul et Creber [11] ont extrudé une solution de chitosane dans des bains de coagulation de différentes natures (NaOH, NaOH/ethanol, NH_4OH, Na_3PO_4, KOH, LiOH) à différentes températures. Après différents temps de coagulation, les bâtons coagulés étaient sortis de la solution et gelés dans l'azote liquide puis la section du bâton était observée au microscope pour mesurer l'épaisseur de polymère coagulé. Cependant, d'après nos connaissances, l'évolution des propriétés mécaniques au cours de la coagulation n'a pas encore été étudiée.

Dans ce chapitre, pour la première fois, nous avons suivi la cinétique de coagulation des solutions de chitosane par le biais de l'évolution des propriétés mécaniques et nous avons comparé ces données avec celles obtenues via caméra optique. Nous avons également analysé l'influence de la concentration de chitosane sur la coagulation.

Cette étude a été réalisée afin de mettre en forme la solution de polysaccharide, par exemple par fabrication additive. En effet, la coagulation mène à une structuration du réseau qui induit une morphologie spécifique et modifie drastiquement les aspects macro et microscopique du gel et ses propriétés mécaniques. L'évolution de ces propriétés mécaniques joue un rôle important lorsque la mise en forme du polymère et la coagulation se déroulent en même temps. Par exemple, pendant un procédé de fabrication additive, un contrôle poussé de la cinétique de coagulation devrait aider à superposer les couches de polymères sans écraser les couches inférieures, ni avoir des couches indépendantes les unes des autres. Cette étude peut donc aider à la conception rationnelle d'encre à base de polysaccharide.

1. Coagulation recorded by optics

An example of the evolution of the width *L* of coagulated layer in time is shown in Figure III.1 for a droplet of 6% wt/v chitosan solution (see details of the experimental set-up in chapter II.2.2.11). Similar images were obtained for the droplets of other dimensions and other chitosan concentrations. The chitosan solution is transparent, and the coagulated layer is optically dark as in reality it is opaque. This layer consists of coagulated chitosan macromolecules assembled in a 3D network with NaOH-water in the pores. The total surface of the droplet did not change during the experiment within the experimental errors (Figure III.2); this correlated well with practically no volume shrinkage of chitosan during coagulation in NaOH-water of various NaOH concentrations [9,12].

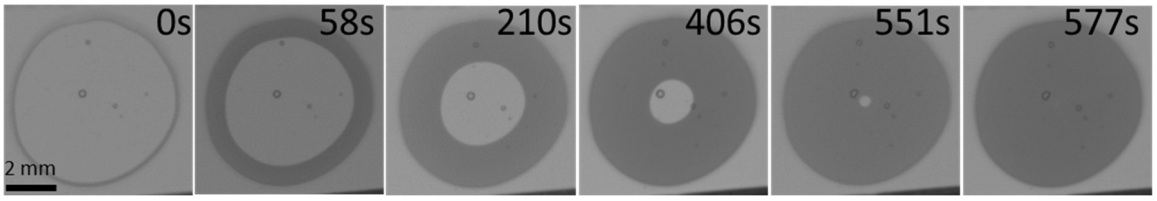

Figure III.1: Example of the evolution of the coagulated phase in a droplet of 6% chitosan solution coagulated with 4M NaOH

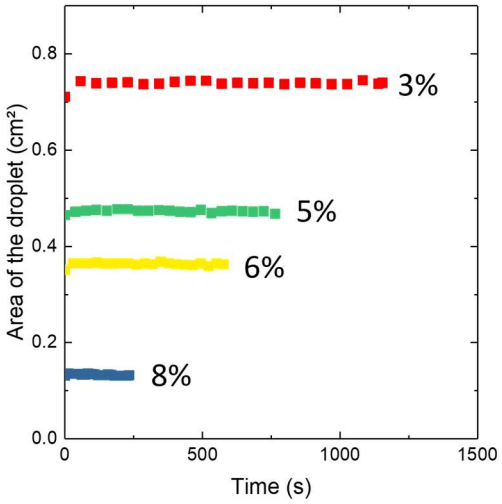

Figure III.2: Examples of the evolution of the droplet area during the coagulation performed with 4M NaOH follows by optical approach

Figure III.3 shows the dependence of the width *L* of coagulated layer on time for droplets of the same chitosan concentration, 3 %wt/v, but of different sizes. Larger is droplet diameter, longer is total coagulation time, as expected (Figure III.3a). Each curve has three regions: a) an initiation region with a high coagulation rate which decreases in time, b) the second region with approximately constant rate and c) “acceleration” region at the end of coagulation. The same trend was obtained for all coagulating chitosan solutions of other concentrations.

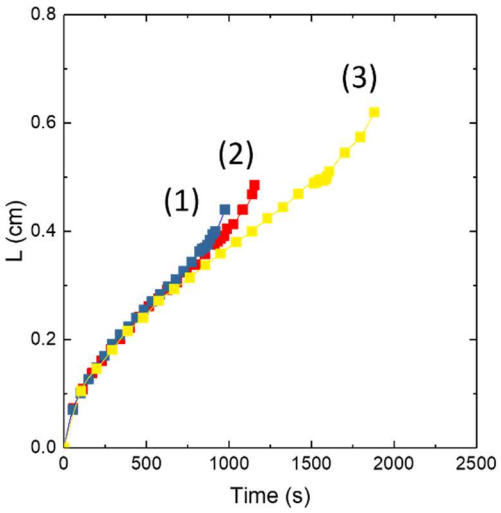

Figure III.3: Evolution of the width of coagulated layer as a function of time for droplets of various dimensions for 3%wt/v chitosan solution coagulated with 4M NaOH: total droplet surface 0.61 cm² – radius 0.44 cm (1), surface 0.71 cm² – radius 0.49 cm (2) and surface 1.1 cm² – radius 0.62 cm (3)

The first two regions are typical for diffusion-controlled processes (here, NaOH-water diffusion inside chitosan solution and coagulating chitosan) and have been reported for various coagulating synthetic and natural polymers [9,13–17]. Fick approach (Equation III.1) can be used until 60% of coagulation, an example for each concentration is shown in Figure III.4a. What is different is the final "acceleration" region which was not reported for coagulating chitosan solution [9] but shown for cylindrical filaments of coagulating acrylonitrile/vinyl acetate copolymer [17] and for the diffusion of $Na_2S_2O_3$ into gelatin/starch gels with iodine or copper ions into cellulose xanthate [18]. In fact, this acceleration region is due to the geometry of the sample: the increase of the width of coagulated layer is accompanied by a continuous decrease of the inner interface between the coagulated and non-coagulated phases (or of the area of coagulating front). The upward trend of the displacement of coagulation front vs time at the end of coagulation for an infinite cylinder was demonstrated experimentally and confirmed theoretically by Paul [17]. No acceleration was reported for sample geometry approximated, for example, by an infinite plane in which the area of coagulating front remains constant during the whole process [9,13–15].

$$Fick\ law\text{:}\ L_t/L_{max} = K \times t^{0.5} \qquad \text{III.1}$$

where L_t is the width of coagulated layer at time t, L_{max} the radius of the droplet, K the diffusion coefficient and t the time. The diffusion coefficient K was plotted as a function of the chitosan concentration on Figure III.4b and a proportional evolution of this coefficient was observed. This coefficient only considers the diffusion of the molecules but not the effects of chain organization nor the effects of NaOH concentration.

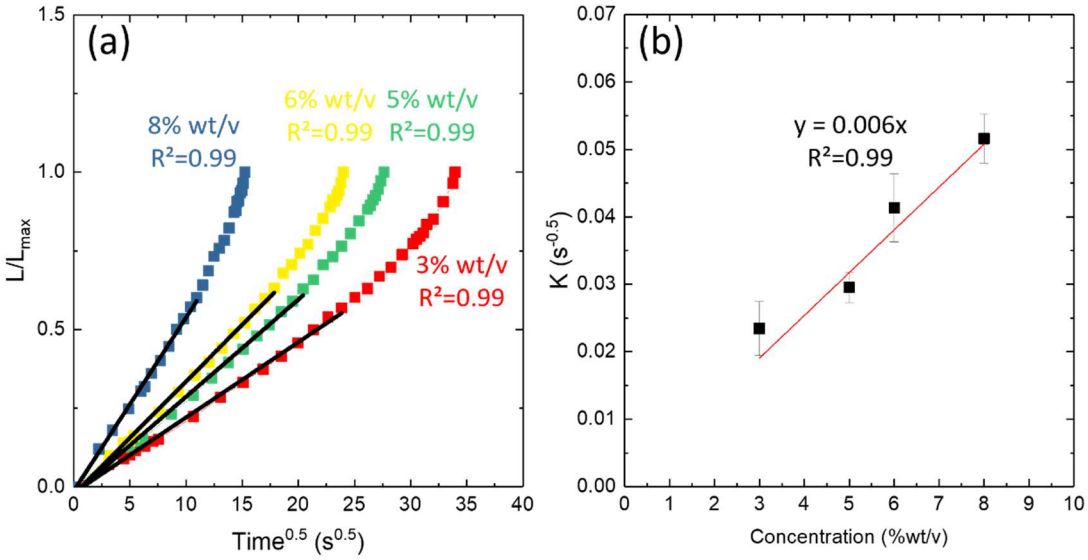

Figure III.4: (a) Evolution of the normalized width as a function of time$^{0.5}$ for all concentrations. The dark lines are the linear regressions of the curves up to 60% of coagulation, the R^2 for each line is indicated on the graph. (b) evolution of the diffusion coefficient as a function of the chitosan concentration. The red line is a linear regression, its equation is written on the graphic.

In addition to the geometrical considerations, the acceleration of coagulation layer width may be explained by "squeezing-out" the solvent of the minor liquid phase (10 to 20% of the total droplet diameter) by the increasing "dominating" gel-like coagulated phase, thus accelerating the expulsion of the rest of the solvent. The expulsion of the solvent is visible at the interface between NaOH and the coagulated chitosan. The coexistence of different chitosan states in the same droplet, dissolved and coagulated, could induce the development of internal stresses. This is what was recorded when observing a coagulating chitosan droplet between crossed polarizers (Figure III.5): a birefringent layer corresponding to coagulated chitosan appears with a sequence of colors. The latter correspond to highly oriented polymer chains. It is supposed that the colors are induced by the stresses at the interfaces of different phases and different level of stress are visible as the color is not the same depending on the interface: green for the interface NaOH/chitosan coagulated and red for the interface between coagulated and uncoagulated chitosan. A similar phenomenon was reported for sodium polyacrylate microgel particle swelling and contracting in polyvalent metal salt aqueous solutions: a birefringent layer (sodium polyacrylate crosslinked by metal ions) was formed on the surface of a microgel [19,20]. After 24 h of chitosan coagulation the colors in the coagulated area remain and a Maltese cross is visible at the center of the droplet, indicating that stresses are still present. A similar result was observed for cellulose coagulated in ionic liquid by Plappert et al. [21].

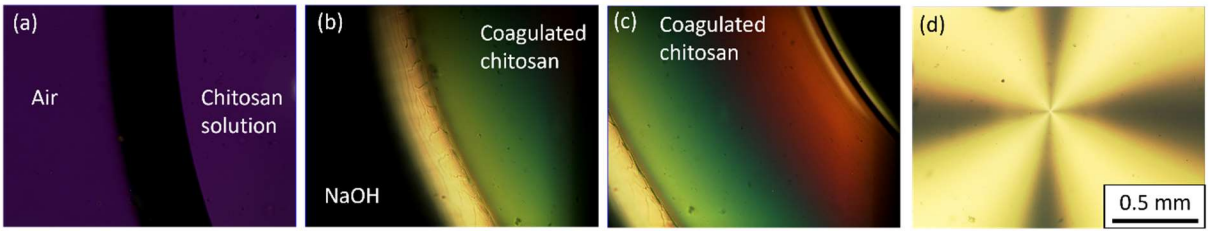

Figure III.5: Images of coagulating chitosan droplet between crossed polarizers. (a) Before the addition of 4M NaOH, (b) coagulated layer on the surface of chitosan solution droplet, (c) zoom on the birefringent zone in chitosan solution and (d) Maltese cross observed in the center of the droplet after coagulation

2. Coagulation followed by DMTA

Chitosan coagulation was also probed by following the evolution of the elastic modulus *E* as a function of time for different chitosan concentrations, see Figure III.6a (the details of experimental set-up are provided in chapter II.2.2.10.c). With the progress of coagulation, the modulus increases until it stabilizes to a plateau. The modulus at plateau is plotted vs chitosan concentration in Figure III.6b. As expected, higher is the chitosan concentration, higher is the plateau modulus. The evolution of the plateau modulus as a function of chitosan concentration *C* was approximated with a power law $E \sim C^n$ with n = 2.3. For gelling polysaccharides, the elastic modulus is usually proportional to polymer concentration in power 2 [22]; for gelling cellulose dissolved in 8%NaOH-water the exponent varies from 2 to 3.6 [23]. For solid open pores materials such as foams *n* = 2 [24–27], and for inorganic and organic aerogels *n* varies from 2 to 4 [1]. Despite that in the case studied here chitosan is a network of coagulated polymer with non-solvent in the pores, the exponent correlating the elastic modulus and polymer concentration fits well the prediction for polysaccharide gels.

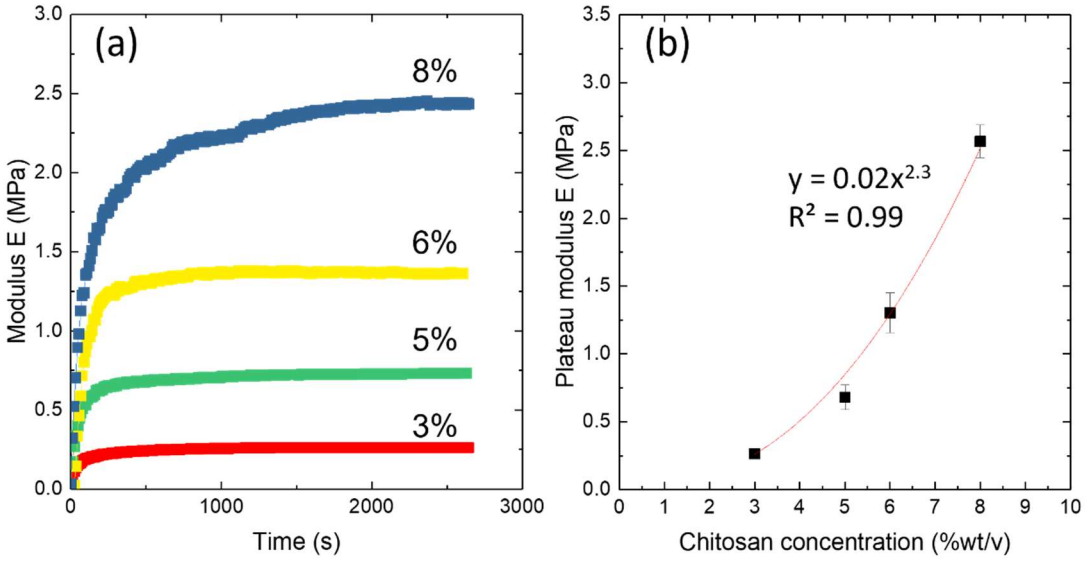

Figure III.6: (a) Examples of the modulus evolution as a function of the time during the coagulation of chitosan solutions by 4M NaOH of different concentrations (%wt/v) and (b) elastic modulus at plateau as a function of chitosan concentration.

Following the approach similar to the optical part, Fick equation was applied until 60% of the normalized modulus, as shown on Figure III.7. All the curves are superimposed with an exception for 8% wt/v chitosan solution. This difference may be induced by the initial concentration of chitosan being higher than the entanglement concentration as shown with the rheology data on Figure III.8. On Figure III.8A (3wt% chitosan solution), the elastic G' and viscous G" moduli obtained from dynamic rheological experiments reasonably well follow the Maxwell approach at low frequency with $G' \sim \omega^2$ and $G'' \sim \omega$. The Figure III.8B (6% solution) and C (7% solution) show the deviation from this approach and on Figure III.8C, G' is overlapping G" with almost the same power law dependence on frequency. It indicates either solutions are gelling or the chains become strongly entangled. In the view of the difference in the rheological response of chitosan solutions that undergo coagulation and complexity of the phenomenon, further analysis using Fick approach was not performed.

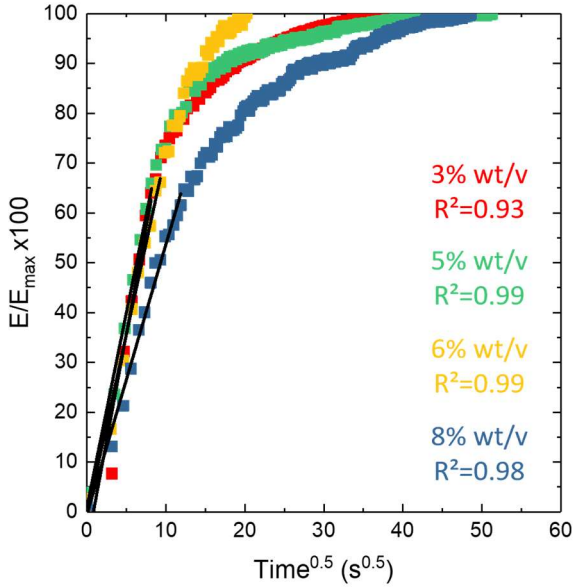

Figure III.7: Evolution of the normalized modulus as a function of time$^{0.5}$ for all concentrations. The dark lines are the linear regressions of the curves up to 60% of the normalize modulus, the R² for each line is indicated on the graph.

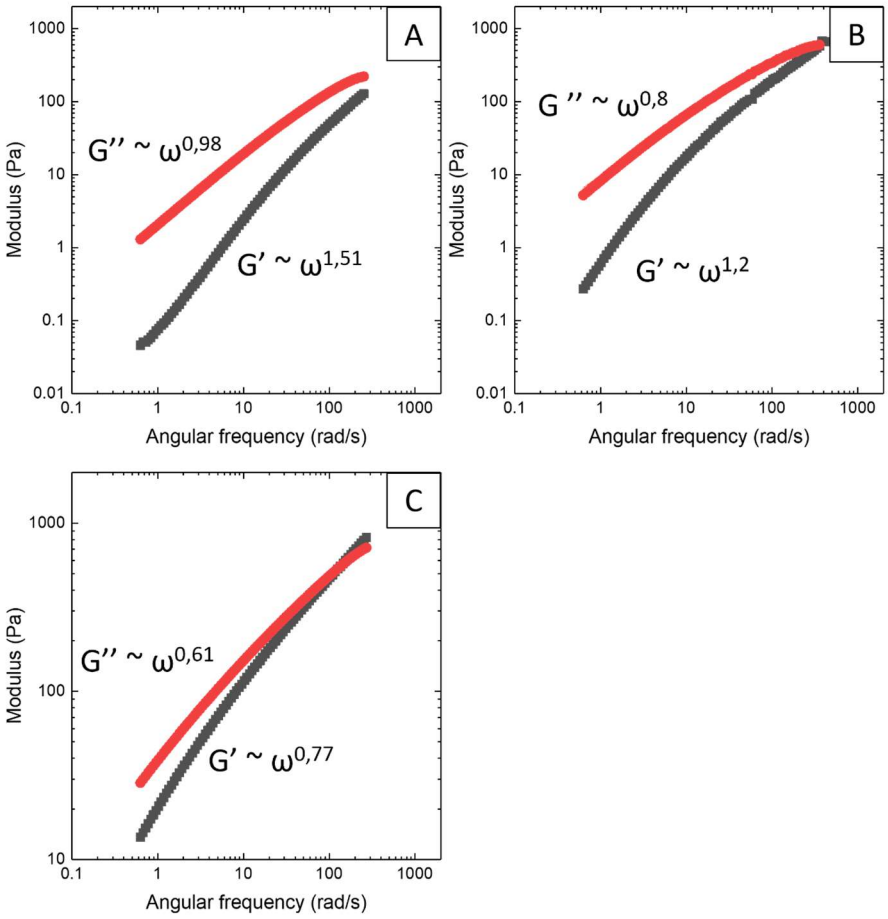

Figure III.8: G' (grey) and G" (red) at 20 °C for (A) 5%wt/v solution and (B) 6%wt/v solution of 600K and (C) 7%wt/v solution. Strain: 5%.

To further analyze the data obtained with DMTA, a theorical modulus was determined by interpolation of the modulus curves as a function of the time by the following function

$$E = \sqrt{C_E \times t} \qquad \text{III.2}$$

with C_E a "coagulation coefficient". The fit with experimental data was performed up to 70% of plateau moduli value. The Figure III.9a shows the experimental curve and the calculated one are well superposed. C_E increases with the chitosan concentration (Figure III.9b). It is increasing as the chains are closer, resulting in a faster coagulation.

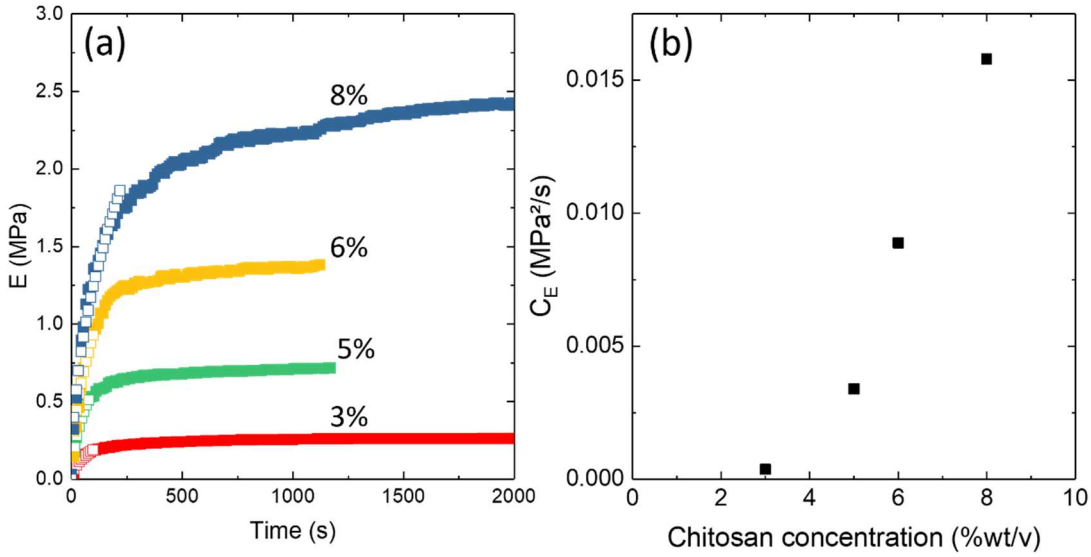

Figure III.9. (a) Comparison of the modulus as a function of time obtained experimentally (close points) and by interpolation (open points) up to 70% of the maximum modulus according to eq. III.2. (b) Coagulation coefficient C_E as a function of the chitosan concentration.

3. Discussion

The coagulation of chitosan was followed by two methods: by optics based on the contrast between the coagulated and solution phases and by DMTA based on the evolution of the elastic modulus. These two processes are compared in Figure III.10 for 8% solutions by plotting the normalized modulus $E(t)/E_{max}$ and normalized coagulated width $L(t)/L_{max}$ as a function of time. The maximum of coagulation is reached faster when followed by optical method than by DMTA: the deviation occurs when "acceleration" (final) phase starts on the optically followed coagulation (recall Figure 3.2). As explained in Section 1, the "acceleration" phase in $L(t)/L_{max}$ is due to sample spherical geometry; visual observations thus do not coincide with $E(t)/E_{max}$ recorded by DMTA which provides modulus value averaged over the sample. Thus, despite a visual complete coagulation, the chains are still being organized improving the mechanical response of the network.

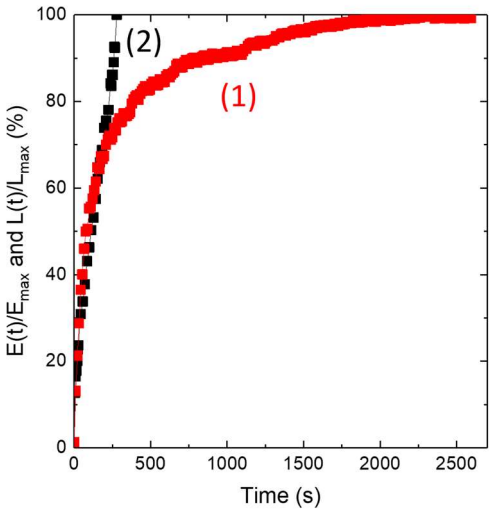

Figure III.10. Normalized modulus (1) and normalized coagulated width (2) as a function of time for 8%wt/v chitosan solution.

Next, using the evolution in time of the normalized width $L(t)/L_{max}$ and approach developed in the work of Paul et al. [17] on coagulation during wet spinning, an equation III.3 correlating elastic modulus and $L(t)/L_{max}$ was derived:

$$E_{predicted}(MPa) = C^A \times E_{max} \times \left(\ln\left(\frac{L(t)}{L_{max}} + 1\right)\right)^B \qquad \text{III.3}$$

with E_{max} = 9.63 MPa, A = 1.97 and B = 2.30 being the optimized parameters obtained with the least squares method, and C the chitosan concentration in g/mL. This calculated elastic modulus fits reasonably well the experimental data as shown in Figure III.11.

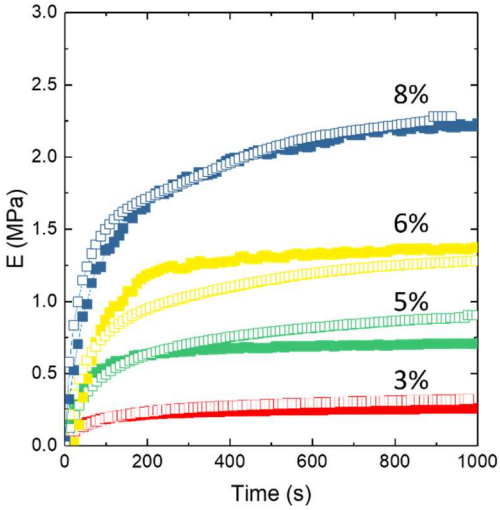

Figure III.11: Experimental modulus (closed points) recorded during coagulation and predicted modulus (open points) for different chitosan concentrations.

Conclusions

The kinetics of coagulation of chitosan solution was studied via observations of the coagulation front in a circular droplet and by the evolution of the elastic modulus. The influence of chitosan concentration was observed. Optical observations show 3 phases during the coagulation: an initiation phase, a phase with more or less constant coagulation speed and an acceleration phase due to the geometry of the sample. Larger droplet volume increases the whole duration of coagulation, as expected. The acceleration phase was not observed during the DMTA analysis as the elastic modulus is averaged over droplet volume. For both methods a higher chitosan concentration results in an increased coagulation rate probably thanks to a closer chain proximity. For the optically followed coagulation, Fick approach was shown to be applicable for the first 60-70% of the whole coagulation process. For DMTA-followed coagulation, a coagulation coefficient was introduced.

Lastly, we were able to predict the evolution of the elastic modulus in time using the data obtained from the optical observations. This prediction opens the way to a better control of the mechanical properties of a system when processing and coagulation occur at the same time and thus, for example, a better control during additive manufacturing.

References

[1] M.A. Aegerter, N. Leventis, M. Koebel, S.A. Steiner III, Handbook of Aerogels, 2nd edition, Springer Nature Switzerland, 2023.

[2] S. Mazinani, S. Darvishmanesh, A. Ehsanzadeh, B. Van der Bruggen, Phase separation analysis of Extem/solvent/non-solvent systems and relation with membrane morphology, J. Membr. Sci. 526 (2017) 301–314. https://doi.org/10.1016/j.memsci.2016.12.031.

[3] S.M. Ghasemi, N. Mohammadi, The prediction of polymeric membrane characteristics prepared via nonsolvent induced phase separation by the apparent coagulation time, Polymer. 54 (2013) 4675–4685. https://doi.org/10.1016/j.polymer.2013.06.046.

[4] J.T. Jung, J.F. Kim, H.H. Wang, E. di Nicolo, E. Drioli, Y.M. Lee, Understanding the non-solvent induced phase separation (NIPS) effect during the fabrication of microporous PVDF membranes via thermally induced phase separation (TIPS), J. Membr. Sci. 514 (2016) 250–263. https://doi.org/10.1016/j.memsci.2016.04.069.

[5] D.M. Koenhen, M.H.V. Mulder, C.A. Smolders, Phase separation phenomena during the formation of asymmetric membranes, J. Appl. Polym. Sci. 21 (1977) 199–215. https://doi.org/10.1002/app.1977.070210118.

[6] L. Li, C. Miesch, P.K. Sudeep, A.C. Balazs, T. Emrick, T.P. Russell, R.C. Hayward, Kinetically Trapped Co-continuous Polymer Morphologies through Intraphase Gelation of Nanoparticles, Nano Lett. 11 (2011) 1997–2003. https://doi.org/10.1021/nl200366z.

[7] S.P. Nunes, T. Inoue, Evidence for spinodal decomposition and nucleation and growth mechanisms during membrane formation, J. Membr. Sci. 111 (1996) 93–103. https://doi.org/10.1016/0376-7388(95)00281-2.

[8] R.X. Suzuki, Y. Nagatsu, M. Mishra, T. Ban, Phase separation effects on a partially miscible viscous fingering dynamics, J. Fluid Mech. 898 (2020) A11. https://doi.org/10.1017/jfm.2020.406.

[9] A.A. Enache, L. David, J.-P. Puaux, I. Banu, G. Bozga, Kinetics of chitosan coagulation from aqueous solutions, J. Appl. Polym. Sci. 135 (2018) 46062. https://doi.org/10.1002/app.46062.

[10] C. Liu, J.A. Cuculo, B. Smith, Coagulation studies for cellulose in the ammonia/ammonium thiocyanate (NH3/NH4SCN) direct solvent system, J. Polym. Sci. Part B Polym. Phys. 27 (1989) 2493–2511. https://doi.org/10.1002/polb.1989.090271208.

[11] J.Z. Knaul, K.A.M. Creber, Coagulation rate studies of spinnable chitosan solutions, J. Appl. Polym. Sci. 66 (1997) 117–127. https://doi.org/10.1002/(SICI)1097-4628(19971003)66:1<117::AID-APP14>3.0.CO;2-Z.

[12] C. Chartier, S. Buwalda, H. Van Den Berghe, B. Nottelet, T. Budtova, Tuning the properties of porous chitosan: Aerogels and cryogels, Int. J. Biol. Macromol. 202 (2022) 215–223. https://doi.org/10.1016/j.ijbiomac.2022.01.042.

[13] O. Biganska, P. Navard, Kinetics of Precipitation of Cellulose from Cellulose−NMMO−Water Solutions, Biomacromolecules. 6 (2005) 1948–1953. https://doi.org/10.1021/bm040079q.

[14] R. Sescousse, R. Gavillon, T. Budtova, Aerocellulose from cellulose–ionic liquid solutions: Preparation, properties and comparison with cellulose–NaOH and cellulose–NMMO routes, Carbohydr. Polym. 83 (2011) 1766–1774. https://doi.org/10.1016/j.carbpol.2010.10.043.

[15] R. Sescousse, T. Budtova, Influence of processing parameters on regeneration kinetics and morphology of porous cellulose from cellulose–NaOH–water solutions, Cellulose. 16 (2009) 417–426. https://doi.org/10.1007/s10570-009-9287-z.

[16] A. Hedlund, T. Köhnke, H. Theliander, Diffusion in Ionic Liquid–Cellulose Solutions during Coagulation in Water: Mass Transport and Coagulation Rate Measurements, Macromolecules. 50 (2017) 8707–8719. https://doi.org/10.1021/acs.macromol.7b01594.

[17] D.R. Paul, Diffusion during the coagulation step of wet-spinning, J. Appl. Polym. Sci. 12 (1968) 383–402. https://doi.org/10.1002/app.1968.070120301.

[18] J.J. Hermans, Diffusion with discontinuous boundary (1), J. Colloid Sci. 2 (1947) 387–398. https://doi.org/10.1016/0095-8522(47)90042-1.
[19] T. Budtova, P. Navard, Swelling-Induced Birefringence of a Polyelectrolyte Gel Strongly Interacting with Metal Ions, Macromolecules. 30 (1997) 6556–6558. https://doi.org/10.1021/ma970304e.
[20] T. Budtova, Absorption/release of polyvalent metal ions by a polyelectrolyte gel, J. Controlled Release. 54 (1998) 305–312. https://doi.org/10.1016/S0168-3659(98)00011-X.
[21] S.F. Plappert, J.-M. Nedelec, H. Rennhofer, H.C. Lichtenegger, S. Bernstorff, F.W. Liebner, Self-Assembly of Cellulose in Super-Cooled Ionic Liquid under the Impact of Decelerated Antisolvent Infusion: An Approach toward Anisotropic Gels and Aerogels, Biomacromolecules. 19 (2018) 4411–4422. https://doi.org/10.1021/acs.biomac.8b01278.
[22] K. Nijenhuis, Thermoreversible Networks, Springer Berlin Heidelberg, Berlin, Heidelberg, 1997. https://doi.org/10.1007/BFb0008699.
[23] W. Liu, T. Budtova, P. Navard, Influence of ZnO on the properties of dilute and semi-dilute cellulose-NaOH-water solutions, Cellulose. 18 (2011) 911–920. https://doi.org/10.1007/s10570-011-9552-9.
[24] L.J. Gibson, M.F. Ashby, Cellular Solids: Structure and Properties, 2nd ed., Cambridge University Press, 1997. https://doi.org/10.1017/CBO9781139878326.
[25] J.C.H. Wong, H. Kaymak, S. Brunner, M.M. Koebel, Mechanical properties of monolithic silica aerogels made from polyethoxydisiloxanes, Microporous Mesoporous Mater. 183 (2014) 23–29. https://doi.org/10.1016/j.micromeso.2013.08.029.
[26] N. Buchtová, C. Pradille, J.-L. Bouvard, T. Budtova, Mechanical properties of cellulose aerogels and cryogels, Soft Matter. 15 (2019) 7901–7908. https://doi.org/10.1039/C9SM01028A.
[27] N. Diascorn, S. Calas, H. Sallée, P. Achard, A. Rigacci, Polyurethane aerogels synthesis for thermal insulation – textural, thermal and mechanical properties, J. Supercrit. Fluids. 106 (2015) 76–84. https://doi.org/10.1016/j.supflu.2015.05.012.

Chapter IV. Tuning properties of chitosan aerogels and cryogels

List of abbreviations:

DIC: Digital image correlation

DMTA: Dynamical mechanical thermal analysis

DT: drilled tube

Ea: Activation energy

FzD: Freeze drying

RH: Relative humidity

S/E: Solvent exchange

Sc: supercritical

ScD: Drying with supercritical CO_2

SEM: Scanning electron microscopy

SWE: Simulated wound exudate

UDT: Undrilled tube

XRD: X-ray diffraction

Content

Introduction

A porous 3D biomaterial can be generated by removing the solvent from a "wet" polymer network. The properties of the porous material depend greatly on the drying method of the precursor [1,2]. Aerogels are obtained *via* drying under supercritical (sc) conditions, most often using sc CO_2. Since no liquid-vapor meniscus exists under sc conditions, capillary pressure, which usually leads to collapse of pore walls under ambient pressure drying, are no longer acting. The structure of the gel is therefore theoretically kept intact, leading to a nanostructured material with high porosity and high internal pores' surface area. This is in contrast with freeze-drying (for simplicity we will call such materials cryogels), where the growth of ice crystals may distort the network structure and lead to the formation of larger pores and a lower internal surface area. Aside few exceptional cases such as silylated silica gels, materials obtained via ambient pressure or vacuum drying, so-called xerogels, often have a high density and low porosity due to the collapse of pore walls. Both aerogels and cryogels possess specific properties in terms of density, morphology, pore size distribution and surface area. The understanding of processing-structure-properties correlations is therefore essential for matching the requested application.

Several examples of porous chitosan-based biomaterials, including cryogels and aerogels, exist in literature, as reviewed recently [3,4]. For example, pH-responsive chitosan [5] and hybrid chitosan-cellulose-graphene oxide [6] cryogels were developed for drug delivery applications. Drug-loaded chitosan aerogel particles prepared via the dropping [7] or jet cutting method [8] were suggested for wound healing applications.

In order to obtain chitosan aerogels or cryogels, various approaches exist. In all cases chitosan is first dissolved, usually in acidic medium. In order to form a network, chitosan can then be either crosslinked via its amino groups (using formaldehyde [9], urea [10], glutaraldehyde [11] or sodium tripolyphosphate [12]), or directly coagulated in a non-solvent (for example, in a basic solution). In the latter case non-solvent induced phase separation (or immersion precipitation) occurs: chitosan forms a network with non-solvent in the pores. The structure obtained mainly depends of the ratio of the rate of solvent "out" over the rate of non-solvent "in" as demonstrate for cellulose [13–17] and of the coagulation orientation [18] between the polymer solution and the non-solvent. Many articles studied the structure formation and evolution of crosslinked chitosan [11,19,20], but no work has been done on the coagulation orientation and its effect on chitosan aerogels properties.

To use drying with sc CO_2, the liquid in the pores of a network (crosslinked or not) must be miscible with CO_2, and thus solvent exchange step is often applied. Quignard et al. used the non-solvent induced phase separation method for the preparation of chitosan beads in NaOH-water; NaOH was then removed by washing the beads in water followed by exchange of water to ethanol and sc CO_2 drying, resulting in chitosan aerogel beads [21]. The same approach was used in refs. [7,8]. Chemical crosslinking is supposed to lead to better mechanical properties and a more homogeneous network structure [11], but the use of toxic crosslinkers (e.g. glutaraldehyde) may lead to adverse effects in biomedical applications.

In the vast majority of publications only one method of drying is used for the preparation of the chitosan porous material, which impedes the in-depth understanding of processing-structure-properties correlations of chitosan porous materials. To the best of our knowledge, only two articles compare the properties of sc dried and freeze-dried chitosan starting from the same precursor, and in both cases chitosan was crosslinked. Obaidat et al. prepared sc CO_2 and freeze-dried beads based on chitosan crosslinked with sodium tripolyphosphate [12]. The specific surface area of aerogels was 70 – 100 m^2/g and for cryogels it was not detectable. Takeshita et al. made sc CO_2 and freeze-dried (from water and from tert-butanol) chitosan crosslinked with formaldehyde and reported a much higher

value for the specific surface area of aerogels, almost 500 m^2/g. For the cryogel, as in the case above, the surface area was not detectable [19].

The structure can also be modified after drying with for example the humidity uptake. Aerogels are known to be highly sensitive to humidity [22] due to the small pore size leading to water condensation or important capillary forces like for silica aerogels [23]. The hygroscopicity inherent of biobased polymers increases this sensibility, changing the morphology or the mechanical properties.

The first part of this chapter is devoted to the understanding of the influence of drying conditions (freeze-drying versus sc drying) on the structural and physico-chemical properties of non-crosslinked chitosan porous materials starting from the same chitosan precursor. We also analyzed the influence of chitosan and NaOH concentrations in the coagulation bath, of aging time and of the non-solvent used during solvent exchange. In the view of potential biomedical applications of these porous chitosan materials, the absorption of simulated wound exudate was evaluated. In a second part, mechanical characterization of the sample was performed and an analysis of the influence of humidity on the mechanical properties of aerogels and the structure modifications induced were assessed by dynamic mechanical thermal analysis (DMTA). The influence of the coagulation direction was evaluated, and the resulting anisotropy of the samples characterized for non-crosslinked chitosan aerogels.

Introduction (FR)

Un biomatériau poreux est obtenu en retirant le solvant d'un réseau de polymère humide. Les propriétés des matériaux poreux dépendent grandement de la méthode de séchage du précurseur [1,2]. Les aérogels sont obtenus via séchage en condition supercritique (sc), en utilisant le plus souvent du CO_2 supercritique. Sous conditions supercritiques il n'y a pas d'interface liquide/gaz, la tension superficielle qui entraine un écrasement des pores lors du séchage à pression ambiante, n'existe plus. La structure du gel est donc en théorie gardée intacte, donnant un matériau nanostructuré avec une haute porosité et une grande surface interne des pores. C'est en contraste avec la lyophilisation (par simplicité, les matériaux obtenus par cette méthode sont appelés cryogels), où la croissance des cristaux de glace peut déformer le réseau et mener à la formation de pores plus larges et à une surface de pore interne plus faible. Les matériaux séchés à pression ambiante ou sous-vide sont appelés xerogels, ils ont souvent une haute densité et une faible porosité à cause de l'écrasement des pores. Les aérogels et cryogels possèdent des propriétés particulières en termes de densité, morphologie, distribution des tailles de pores et surface spécifique. Il est crucial de comprendre la relation entre le procédé de fabrication, la structure obtenue et les propriétés du matériau afin de répondre aux exigences des applications.

Le chitosane est un polymère semi-naturel qui peut être obtenu après dé-acétylation de la chitine extraite des coquilles de crustacées. C'est un polymère cationique composé de D-glucosamine et de N-acétyle-D-glucosamine lié par des liaisons glycosidique en β (1→4). Grâce à ses propriétés antivirales, antibactériennes et antifongiques ainsi que sa biocompatibilité, le chitosane est fréquemment employé pour des applications biomédicales comme les pansements et système de libération de médicament [24–26]. Plusieurs exemples de biomatériaux poreux à partir de chitosane, incluant des cryogels et aérogels, existent dans la littérature comme le montre de récentes revues [3,4]. Par exemple, un chitosane sensible au pH [5] et un cryogel hybride composé de chitosane, cellulose et oxyde de graphène [6] ont été développés pour de la libération de principe actif. Des particules d'aérogels de chitosane chargée en médicament ont été préparées par goutte-à-goutte [7] ou jet cutting [8] et proposées pour la cicatrisation de plaies.

Pour obtenir des aérogels ou cryogels de chitosane, différentes approches existent. Dans tous les cas, le chitosane est dans un premier temps dissout, habituellement dans un milieu acide. Pour obtenir un réseau, le chitosane peut être soit réticulé par le biais de ses groupes amines (en utilisant du formaldéhyde [9], de l'urée [10], du glutaraldéhyde [11] ou du sodium tripolyphosphate [12]), ou directement coagulé dans un non-solvant (par exemple en milieu basique). Dans le dernier cas une séparation de phase induite par la présence de non-solvant (ou immersion précipitation) a lieu : le chitosane forme un réseau et le non-solvant se situe dans les pores. Pour utiliser le séchage avec le CO_2 sc, le liquide dans les pores du réseau (réticulé ou non) doit être miscible avec le CO_2, une étape d'échange de solvant est donc souvent nécessaire. Quignard et al. a utilisé la méthode de séparation de phase induite par le non-solvant pour la préparation de billes de chitosane dans une solution de NaOH-eau ; la soude était enlevée des billes par de l'eau suivit par un remplacement de cette dernière par l'éthanol puis un séchage au CO_2 sc, donnant des billes d'aérogels de chitosane [21]. Une approche similaire a été utilisée dans les références [7,8]. La réticulation chimique est censée donner de meilleures propriétés mécaniques et une structure plus homogène [11], mais l'utilisation de réticulants toxiques (comme le glutaraldéhyde) peut entrainer des effets indésirables pour les applications biomédicales.

Dans la plupart des publications seul une méthode de séchage est utilisée pour la préparation de chitosane poreux, ce qui limite la compréhension de la corrélation entre procédé, structure et propriétés des matériaux poreux à base de chitosane. D'après nos connaissances, seuls deux articles comparent les propriétés d'aérogels et cryogels de chitosane obtenus à partir du même précurseur,

mais dans chaque cas le chitosane était réticulé. Obaidat et al. ont préparé par séchage supercritique et lyophilisation des billes à partir de chitosane réticulé avec du sodium tripolyphosphate [12]. La surface spécifique des aérogels était de 70 – 100 m^2/g, cependant celle des cryogels n'était pas détectable. Takeshita et al. ont obtenu des aerogels et cryogels par séchage supercritique ou lyophilisation (depuis l'eau ou du tert-butanol) de chitosane réticulé avec du formaldéhyde et ont reporté une valeur de surface spécifique très supérieure aux précédentes, presque 500 m^2/g. Pour les cryogels, comme dans le cas précédent, la surface spécifique n'était pas détectable [19].

La structure peut être modifiée après séchage avec par exemple l'absorption d'eau liée à l'humidité ambiante. Les aérogels sont connus pour être très sensibles à l'humidité [22] à cause de la faible taille des pores induisant une condensation de l'eau menant à des forces capillaires importantes comme pour les aérogels de silice [23]. L'hygroscopie inhérente aux polymères biosourcés augmente cette sensibilité, changeant la morphologie ou les propriétés mécaniques.

Cette étude présente pour la première fois l'influence des conditions de séchage (lyophilisation versus séchage supercritique) sur la structure et les propriétés physico-chimiques du chitosane poreux non réticulé a été étudiée à partir du même précurseur. Nous avons aussi analysé l'influence du chitosane, de la concentration de NaOH dans le bain de coagulation et du temps de coagulation mais également du solvant utilisé pour le séchage supercritique. Dans l'optique d'une potentielle application biomédicale de ces matériaux poreux, l'absorption d'exsudat simulé de plaie a été évaluée. Dans un second temps, la caractérisation mécanique des matériaux obtenus a été réalisée et les modifications de structure induites ont été étudiées par analyse mécanique dynamique en température (DMTA). D'après nos connaissances, c'est la première fois que l'influence de la direction de coagulation et l'anisotropie en résultant a été évaluée pour les aérogels de chitosane non réticulés.

1. Physico-chemical properties of chitosan aerogels and cryogels

This part was the subject of a publication: Chartier, C.; Buwalda, S.; Van Den Berghe, H.; Nottelet, B.; Budtova, T. Tuning the Properties of Porous Chitosan: Aerogels and Cryogels. Int. J. Biol. Macromol. 2022, 202, 215–223. https://doi.org/10.1016/j.ijbiomac.2022.01.042.

The results are presented as follows. First, the determination of the molecular weight and degree of acetylation of chitosan will be shown. Then, each material property, namely volume shrinkage, density, porosity, morphology, specific surface area and absorption of simulated wound exudate (SWE) will be presented and discussed for aerogels and cryogels as a function of various parameters such as the chitosan concentration, the concentration of NaOH in the coagulation bath, the aging time and the method of drying. In this part if the solvent used for Sc drying is not stated, it means it is ethanol.

1.1. Determination of chitosan molecular weight and degree of acetylation

The intrinsic viscosity of chitosan was determined as described in the Methods section [27] and found to be 4.87 dL/g. The molecular weight was estimated to be around 691 000 g/mol, which is in the range of the molecular weight given by the manufacturer, 600 – 800 kg/mol.

The degree of acetylation was determined as described in the Methods section [28] and found to be 10 ± 2 %.

1.2. Visual appearance of chitosan aerogels and cryogels

Photos of chitosan aerogels and cryogels made under different conditions are presented in Figure IV.1 Higher is the concentration of chitosan, more stable is the shape of the hydrogel (and of the corresponding aerogel or cryogel), as seen in Figure IV.1. For example, for 1 % wt/v of dissolved chitosan coagulated in 4 M NaOH, a fluffy aerogel with no distinct shape was obtained, and no adequate characterization of this sample was possible. A minimum of 3 % wt/v chitosan is necessary for the sample to keep the shape of the mold upon coagulation; a similar result was observed for cellulose aerogels despite that the molecular weight of cellulose was much lower, around 30-35 kDa [2]. No influence on the aerogel shape of NaOH concentration in the coagulation bath above 1 M was observed. Below 1 M NaOH, the hydrogel was soft and weak and the corresponding aerogel as well.

Figure IV.1: Photos of chitosan aerogels and cryogels.
Top line: aerogels made from solutions of chitosan of various concentrations (1 % wt/v, 3 % wt/v, 5 % wt/v and 7 % wt/v), coagulated in 4 M NaOH and aged for 24 h, ethanol was used as non-solvent.
Middle line: aerogels from solutions of 5 % wt/v chitosan coagulated in 0.1 M, 1 M and 4 M of NaOH and aged for 24 h, , ethanol was used as non-solvent.
Bottom line: cryogels from solutions of chitosan of various concentrations (5 % wt/v, 6 % wt/v, 7 % wt/v and 8 % wt/v) coagulated in 4 M NaOH and aged for 24 h.

The cryogels have a similar visual appearance as aerogels (Figure IV.1), but cracks are visible along the samples. They were formed during freezing because of the growing ice crystals. At higher chitosan concentrations, the samples present less cracks and are harder.

Xerogel picture is shown on Figure IV.2. The xerogel is brownish and partly translucent, with distorted shape and cracks most probably because of the significant and heterogeneous shrinkage.

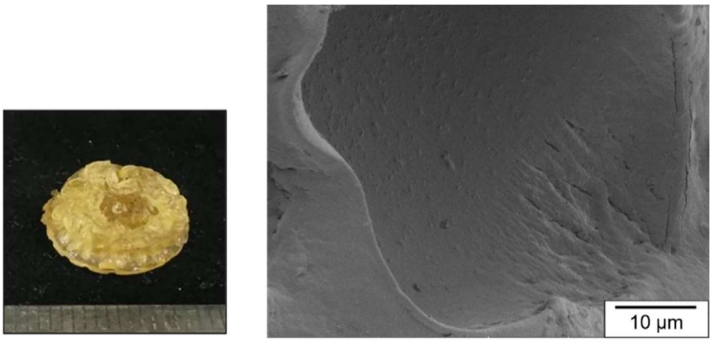

Figure IV.2: Photo and SEM image of chitosan xerogel made from 5% wt/v chitosan solution, coagulated in 4 M of NaOH solution and aged for 24 h.

1.3. Shrinkage during solvent exchange and drying

Volume shrinkage at different steps of the process and total shrinkage (eq. II.2 in Materials and Methods) are presented in Figure IV.3 for aerogels and cryogels as a function of the chitosan concentration in the initial solution (Figure IV.3a), of the NaOH concentration in the coagulation bath (Figure IV.3b) and of the aging time (Figure IV.3c). Because of a significant total shrinkage of the xerogel, around 80%, only one sample was prepared and analyzed. Data known from literature for chitosan aerogels and cryogels are also shown in Table IV.1 for comparison.

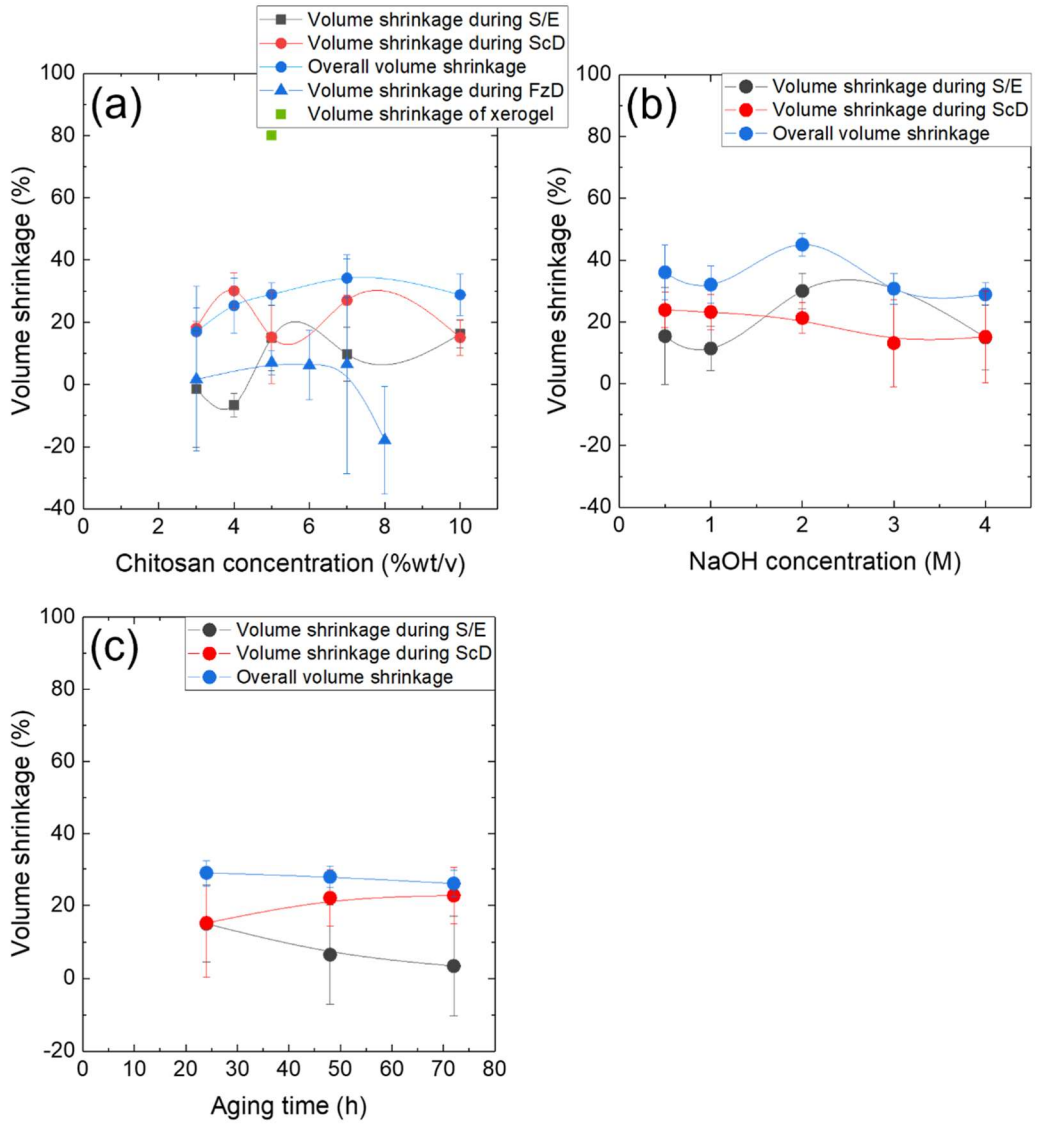

Figure IV.3: Volume shrinkage during the preparation of chitosan aerogels Sc dried, ethanol was used as a non-solvent, cryogels and xerogel as a function of:
(a) the chitosan concentration in solution (all samples coagulated in 4 M NaOH and aged for 24 h),
(b) NaOH concentration in coagulation bath (chitosan solution was 5 % wt /v, all samples aged during 24 h) and
(c) aging time (chitosan solution was 5 % wt/v, all samples coagulated in 4 M NaOH). Lines are given to guide the eye.

Table IV.1: Characteristics of aerogels and cryogels as a function of processing parameters, taken from literature. Density values marked with "" were calculated from the data reported for porosity, with ρs = 1.446 g/cm³ [7]. FzD: freeze-drying, ScD: supercritical drying.*

Chitosan concentration (%wt/v)	DA	Molecular weight (kDa)	Acetic acid concentration	Aging time (h)	NaOH concentration (M)	Drying method	Volume shrinkage (%)	Bulk density (g/cm^3)	Porosity (%)	Specific surface area (m^2/g)	Absorption (%)	Reference
2.5	10	200 - 400	1%	0.5	0.1	ScD	55.8	0.046	96.8	360	N.A.	[7]
2.5	10	200 - 400	1%	1	0.1	ScD	53.3	0.046	96.8	343	380% of PBS in 24 h	[7]
2.5	10	200 - 400	1%	2	0.1	ScD	52.6	0.049	96.6	386	N.A.	[7]
2.5	10	200 - 400	1%	4	0.1	ScD	41.3	0.041	97.2	479	N.A.	[7]
2.5	10	200 - 400	1%	10	0.1	ScD	38.3	0.041	97.2	257	N.A.	[7]
2.5	10	200 - 400	1%	24	0.1	ScD	35.0	0.042	97.1	324	N.A.	[7]
2.5	10	200 - 400	1%	N.A.	0.1	FzD	95.9	0.535	63.0	N.A.	N.A.	[7]
2	10	200 - 400	1%	1	0.2	ScD	N.A.	N.A.	N.A.	N.A.	900% of PBS in 24 h	[8]
2.5	5	200	0.055 M	N.A.	4	ScD	60	N.A.	N.A.	330	N.A.	[21]
1	10	500	0.055 M	N.A.	4	ScD	N.A.	0.0289*	98	175	N.A.	[29]
1	15	350	2%	N.A.	1.25	ScD	N.A.	0.1605*	88.9	111	N.A.	[30]
1	15	350	2%	N.A.	1.25	FzD	N.A.	0.0216*	98.3	3.6	N.A.	[30]
1	N.A.	111	0.1 M	12	4	ScD	N.A.	0.0488	97.94	301	963% of water in 30 min	[31]

1	N.A.	125	0.1 M	12	4	ScD	N.A.	0.0569	96.77	262	740% of water in 30 min	[31]
1	N.A.	294	0.1 M	12	4	ScD	N.A.	0.0761	95.89	254	589% of water in 30 min	[31]
1	N.A.	343	0.1 M	12	4	ScD	N.A.	0.0802	96.16	243	483% of water in 30 min	[31]
1	N.A.	250	3%	N.A.	1	ScD	N.A.	0.090	94	115	N.A.	[32]
2	N.A.	250	3%	N.A.	1	ScD	N.A.	0.112	92	125	N.A.	[32]
3	N.A.	250	3%	N.A.	1	ScD	N.A.	0.137	90	110	N.A.	[32]
3	N.A.	N.A.	1%	12	1	FzD	N.A.	0.1414*	90.22	N.A.	1365% of water in 24 h	[33]
3	6	440	0.2M	0.5	1	FzD	N.A.	0.3326	77	N.A.	310% of PBS in 13 h	[34]
N.A.	10	100	N.A	N.A.	N.A.	FzD	N.A.	0.1446	90	N.A.	250% of PBS in 2h	[35]
2	10	50	1%	N.A.	N.A.	FzD	N.A.	0.2169*	85	N.A.	900% of water in 24 h	[36]

During coagulation and solvent exchange, a small volume decrease within 20 % was observed (Figure IV.3). Polymer chains are supposed to strongly contract when a solvent is replaced by a non-solvent; this is well known for synthetic polyelectrolyte polymer gels [37]. Interestingly, chitosan is not shrinking much, most probably because the non-solvent used is an aqueous medium which has a high affinity for chitosan, and also because of polysaccharide chain rigidity. Rather low shrinkage in a non-solvent was also observed for cellulose, pectin and high-amylose starch [2,38,39]. Shrinkage during sc CO_2 drying is similar to the one during coagulation and solvent exchange, leading to a total shrinkage around 30 - 40 % which does not depend on process parameters within the intervals studied and experimental errors. Neither polymer concentration (Figure IV.3a), which usually strengthens the network to better resist the shrinkage [2,39], nor NaOH concentration (above 0.5 M NaOH) (Figure IV.3b) or aging time (Figure IV.3c) influence shrinkage, within experimental errors. At 0.1 M NaOH, despite that the amount of NaOH is superior to chitosan cationic groups, shrinkage is heterogeneous not allowing adequate determination of sample volume, see the photo and SEM image in Figure IV.4. We suppose that at low NaOH concentrations the chitosan network was not well "stabilized" during coagulation and partially collapsed. We hypothesize that the time needed for complete gel coagulation, which is governed by diffusion and polymer/non-solvent interactions, is an important parameter influencing shrinkage and aerogel properties. Thus the 0.1 M NaOH concentration will not be used in the following.

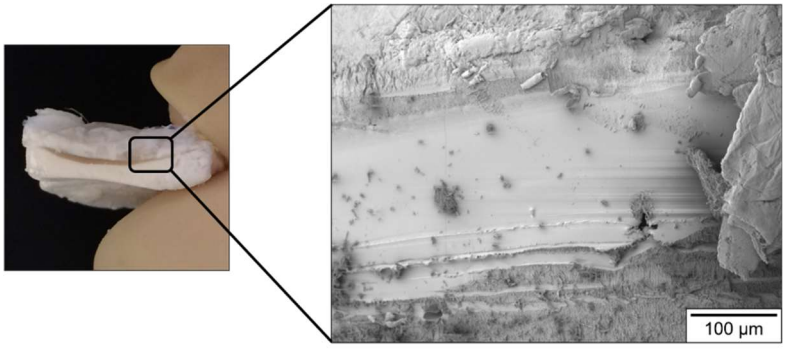

Figure IV.4: Photo and SEM image of a chitosan aerogel sample made from 5% wt/v of chitosan solution, coagulated in 0.1M of NaOH and aged for 24 h.

It should be noted that our data follow the trend of shrinkage vs aging time reported in [8]: higher the aging time, lower the shrinkage with no further dependence when aging is longer than 24 h. In the following, aging time is kept at 24 h. Overall, the shrinkage obtained is moderate compared to that reported for some chitosan aerogels (Table IV.1) which can be up to 60 % [7,21] and even 90 % [19], or for some other bio-aerogels, between 50 – 95 % [21]. However, because of the numerous parameters involved in the preparation of bio-aerogels (polymer molecular weight, charge and chain flexibility, solvent pH, ionic strength, way of structure formation (via non-solvent induced phase separation or gelation induced by crosslinking), type of non-solvent, way of coagulation, etc.), there is still no clear understanding and control of volume shrinkage, and as a consequence, of aerogel bulk density (see next section).

Cryogels showed no volume shrinkage during freezing and drying, within the experimental errors (Figure IV.3a). Lower shrinkage for cryogels as compared to that for aerogels has been reported for cellulose and starch [2,40]. This is an expected result as in the preparation of cryogels there is no step of hydrogel immersion in ethanol and in CO_2, both being non-solvents of native polysaccharides.

1.4. Density, porosity, specific surface area and morphology of aerogels and cryogels

Bulk density and porosity of aerogels and cryogels are shown in Figure IV.5a, b and c as a function of chitosan concentration in the initial solution, NaOH concentration in the coagulation bath and aging time, respectively. The theoretical density, calculated for a hypothetical case of zero shrinkage, is also shown for comparison. Bulk density of aerogels was between 0.07 and 0.26 g/cm^3, similar to the values reported in literature (Table IV.1) [7,8,21,29–32]. The density of aerogels is higher than the theoretical density due to the volume shrinkage during solvent exchange and drying. The bulk density of cryogels is lower than that of aerogels when made from the same chitosan concentration in solution (Figure IV.5), it is between 0.03 and 0.12 g/cm^3 and is almost equal to the theoretical density thanks to the negligible volume shrinkage (Figure IV.3a). As expected, higher is the chitosan concentration, higher is aerogel and cryogel density and lower is the porosity. The density of chitosan xerogel is around 1.30 ±0.15 g/cm^3 and thus porosity is very low, around 10% (Figure IV.5a).

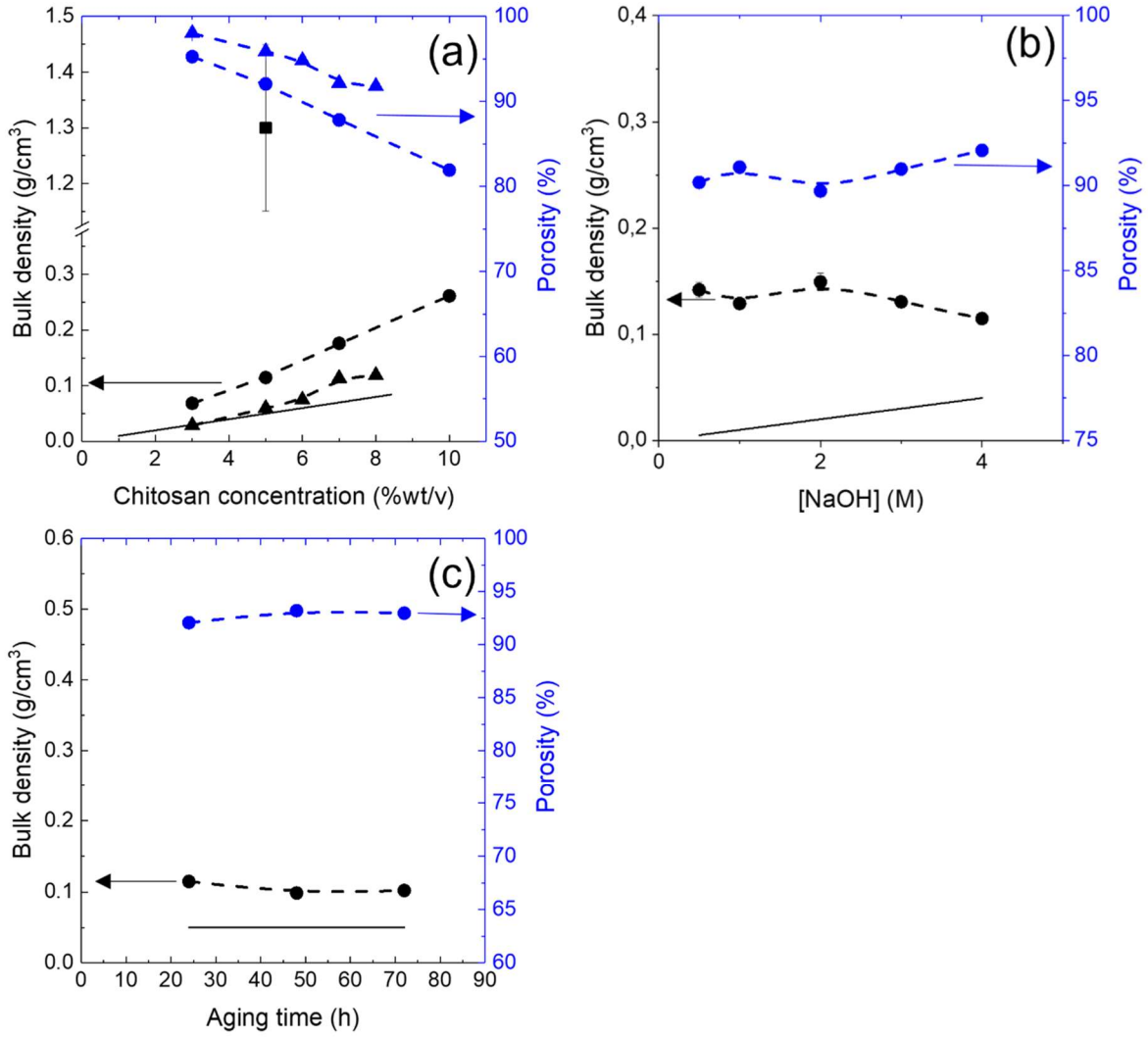

Figure IV.5: Bulk density (in black) and porosity (in blue) of chitosan aerogels (filled circles), cryogels (filled triangles) and xerogel (filled square) as a function of:
(a) the chitosan concentration in solution (coagulation in 4 M NaOH, 24 h aging, non-solvent: ethanol),
(b) NaOH concentration in the coagulation bath (5% wt/v chitosan solution, 24 h aging, non-solvent: ethanol)
(c) aging time (5% wt/v chitosan solution, 4 M NaOH, non-solvent: ethanol). Solid lines correspond to theoretical density in case of no shrinkage.

Dashed lines are given to guide the eye. If error bars are not seen, they are smaller than the symbol.

The sodium hydroxide concentration does not influence density and porosity of aerogels above 0.5 M NaOH (Figure IV.5b). At 4 M NaOH aging time also does not influence the density and the porosity (Figure IV.5c), confirming the observations reported in the literature [7].

The specific surface area of chitosan aerogels varies within 200 – 270 m^2/g (Figure IV.6); it slightly increases with the chitosan concentration (Figure IV.6a). The values obtained are similar to those reported in literature (Table IV.1) [7,8,21,29–32]. An increase in NaOH concentration in the coagulation bath slightly increases specific surface area (Figure IV.6b).

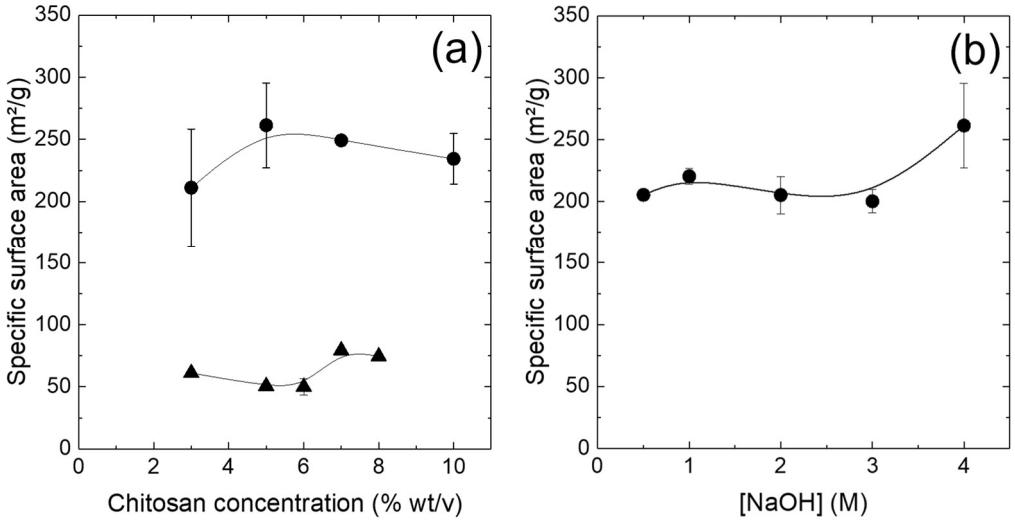

Figure IV.6: Specific surface area of aerogels Sc dried with ethanol as non-solvent (filled circles) and cryogels (filled triangles) as a function of:
(a) chitosan concentration in solution (coagulation in 4 M NaOH, 24 h aging)
(b) NaOH concentration (5 wt% chitosan solution, 24 h aging).
Lines are given to guide the eye.

The surface area of cryogels is much lower, around 50 – 70 m^2/g (Figure IV.6a). The reason is that pores in cryogels are larger as they constitute the space left by sublimated ice crystals. Nevertheless, the specific surface area of as-prepared chitosan cryogels is higher than that reported in literature (few m^2/g) [7,8,30,34,35,41], and of cellulose II and starch cryogels, being within 10 – 60 m^2/g and below 20 m^2/g, respectively [2,39].

The density and specific surface area of aerogel obtained from ScD with acetone or isopropanol as non-solvent are plotted on Figure IV.7. As observed for the previous materials, the density increases with the chitosan concentration. The specific surface area remains stable with the increase of the concentration. With similar densities for aerogels made using ethanol as non-solvent, the isopropanol and acetone aerogels present lower specific surface area, indicating a larger pore size. SEM images on Figure IV.7b show entangled chitosan fibers forming meso- and macroporosities.

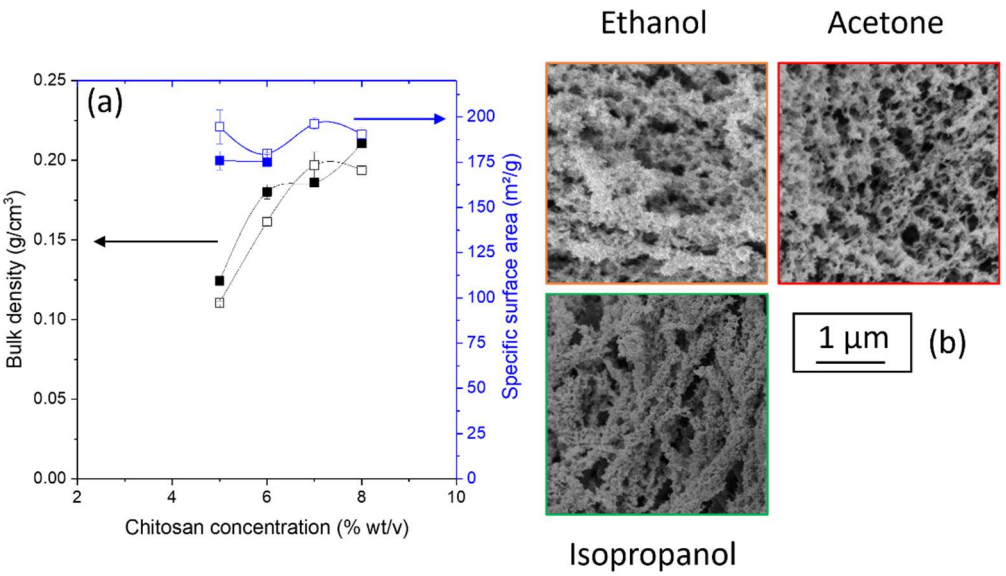

Figure IV.7: (a) Bulk density (in black) and specific surface area (in blue) of chitosan aerogels Sc dried with isopropanol as non-solvent (filled squares), and aerogels Sc dried with acetone as non-solvent (open squares) as a function of the chitosan concentration in solution (coagulation in 4 M NaOH, 24 h aging) (b) SEM images of chitosan aerogels from 5%wt/v solution with different non-solvents.

The inner morphology of chitosan aerogels and cryogels was studied by SEM, representative examples for each type of material made from chitosan solutions of the same concentration are shown in Figure IV.8 at different magnifications. The morphology depends on the drying technique: larger pores were obtained with freeze-drying confirming the lower specific surface area of cryogels as compared to that of aerogels. Similar results have been reported for cellulose II and starch-based aerogels and cryogels [2,40,42]. A SEM image of the xerogel morphology (Figure IV.4) shows the absence of pores, as expected from its very low porosity.

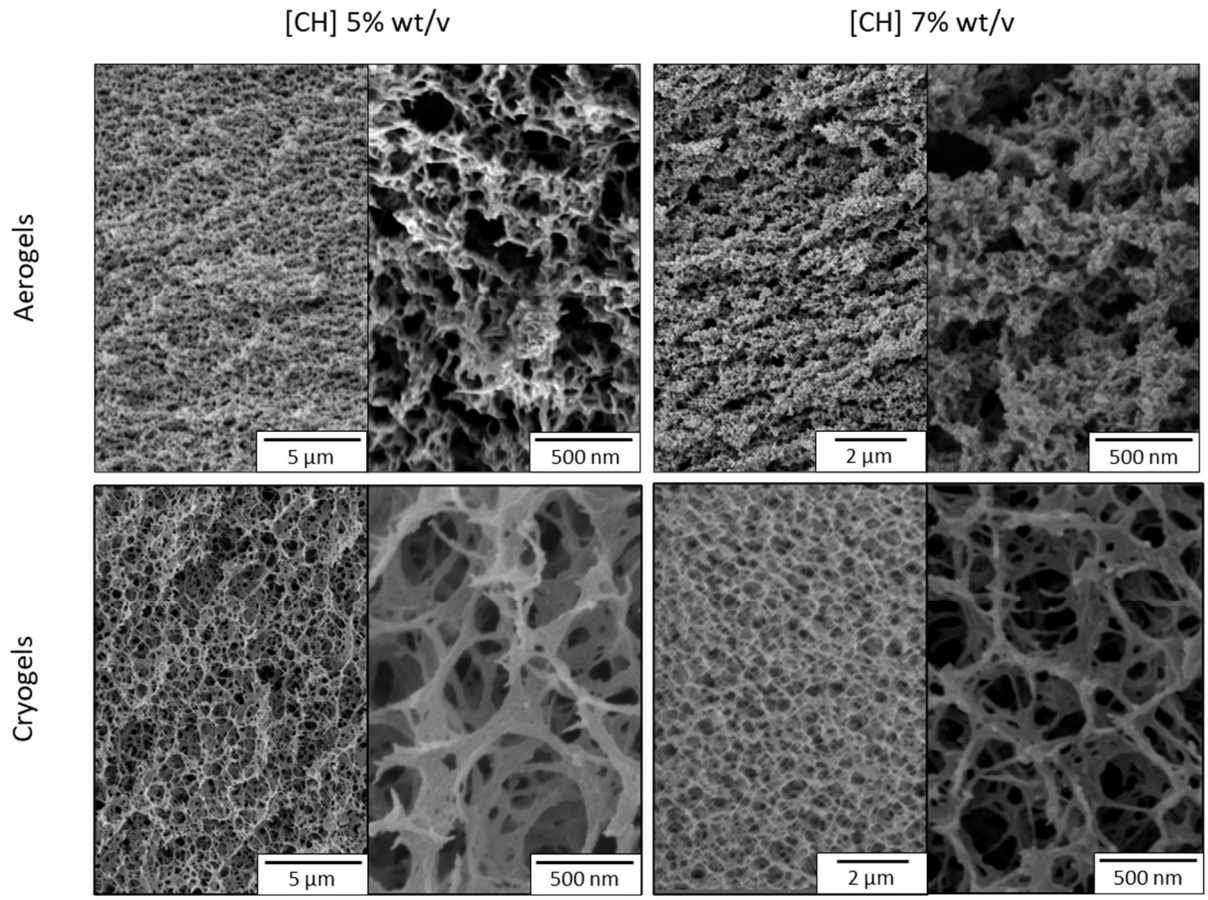

Figure IV.8: SEM images of chitosan aerogels (top line) and cryogels (bottom line). The chitosan concentration was 5 %wt/v (left column) and 7 %wt/v (right column). Samples were coagulated in 4 M NaOH, and aged for 24 h. The non-solvent used for solvent exchange was ethanol.

We roughly estimated the pore size of aerogels and cryogels from SEM images; the results are shown in Figure IV.9. In both aerogels and cryogels, the pore size is slightly decreasing with the increase of polymer concentration; the same trend was reported for cellulose aerogels and cryogels [2]. Interestingly, the sizes of the pores in cryogels are rather low, from several hundreds of nanometers to few microns which is much smaller compared to other non-crosslinked chitosan-based materials which underwent freeze-drying (pores of several tens up to few hundreds of microns [43]). The smaller pore size of the chitosan cryogels in the current study compared to many other chitosan freeze-dried materials can be explained as follows. The size of the pores in a freeze-dried material strongly depends on the state of the matter before drying. For example, a polysaccharide solution (agarose [44], hyaluronic acid [45]) can undergo cryogelation during freezing resulting in very large macropores of several tens of microns. Pores and channels from few to several tens of microns were reported for a freeze-dried nanocellulose suspension [46]. Freeze-dried ultrasonicated chitosan-alginate, chitosan-collagen and chitosan-gelatin blends also possess pores of several tens of microns [47]. The evolution of the morphology of a chitosan network (chitosan solution was dropped in tripolyphosphate solution for different duration, beads post-crosslinked with ethylene glycol diglycidyl ether and freeze-dried) at different stages of coagulation was demonstrated in ref. [48]. Ionic bonds are formed between phosphate groups of tripolyphosphate and amine groups of chitosan. At the early stage of coagulation (or phase inversion), when the network is not yet formed, large pores and channels of several hundreds of microns were obtained; with the progress of coagulation pores became smaller and channels disappeared. All examples given above demonstrate that in weak gels the morphology of freeze-dried

matter is adapting to the shape of growing ice crystals. In our case, the network morphology in the hydrogel is fixed before freezing as coagulation is completed, and growing ice crystals are deforming and enlarging the pores but not destroying them. Similar results were obtained for cellulose II and starch hydrogels: the network is formed either during coagulation for cellulose [2], or during retrogradation for starch [39].

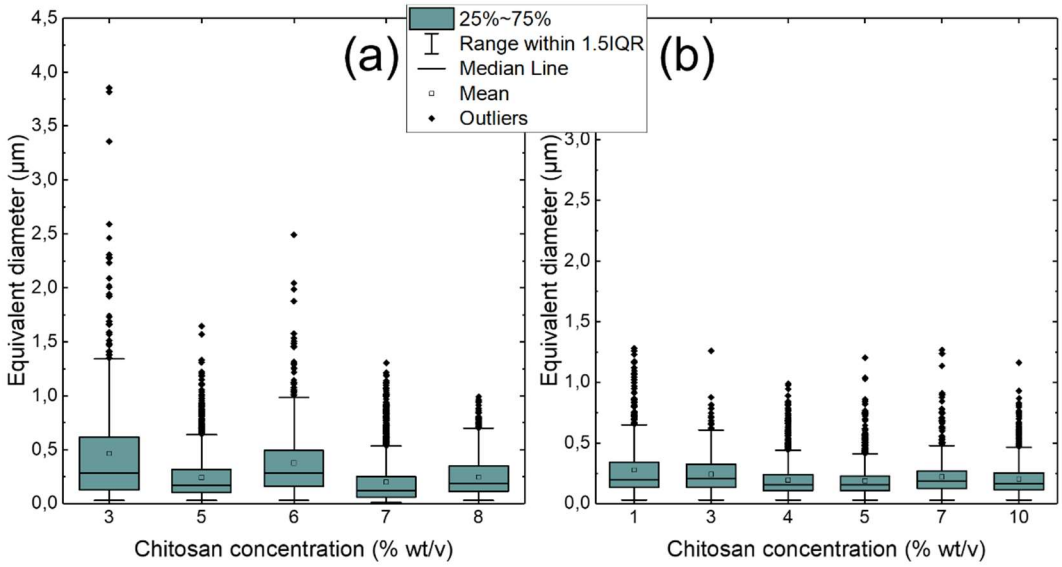

Figure IV.9: Box plot of the pore size distribution in chitosan cryogels (a) and aerogels (b) (values obtained from the analysis of SEM images at 10000x magnification). Samples were coagulated in 4 M NaOH and aged for 24 h. Solvent exchange, for aerogel precursors, was performed with ethanol.

Buchtová et al. [2] suggested that an increase of the concentration in a cellulose aerogel decreases the pore size thus increasing the specific surface area supposing that pore wall thickness remains the same. A very minor decrease in the pore size of aerogels can be seen (Figure IV.9), which corroborates the slight increase in specific surface area observed in Figure IV.6a, but no particular trend can be deduced considering a large dispersion of data and the roughness of the approach.

The average size of pore walls in aerogels and cryogels was also estimated from SEM images: the values are 14.4 ±3.9 nm and 32 ±14 nm, respectively, which results in approximately 1 nm and 18 nm after subtracting the thickness (14 nm) of the layer of sputtered platinum. These results were compared with the calculated pore wall thickness D assuming the pore walls are ideal rods of uniform thickness and having the same skeletal density as chitosan:

$$D = 4/(\rho_{bulk} \times S_A) \quad \text{IV.1}$$

The pore wall thickness for aerogels and cryogels was calculated to be around 1.3 nm and 13 nm, respectively, which fits well with the experimental observation.

The XRD pattern of the initial chitosan powder and of grinded aerogel and cryogel are presented in Figure IV.10. The initial powder shows a very broad peak around 10° and a sharper peak centered around 20°, similar to the ones reported for chitins and chitosan of various degrees of acetylation and typical for a semi-crystalline chitosan [49–52]. Aerogels and cryogels show peaks at the same angles but the one at 10° is sharper than that of chitosan powder. This sharp peak is characteristic of a hydrated crystalline chitosan [50]. As cryogels and aerogels present a higher specific surface area than that of the powder, we suppose that these porous materials may adsorb more water

vapours than chitosan powder explaining the sharper peak. Aging time and sodium hydroxide concentration do not influence the XRD pattern (data not shown) within the experimental errors.

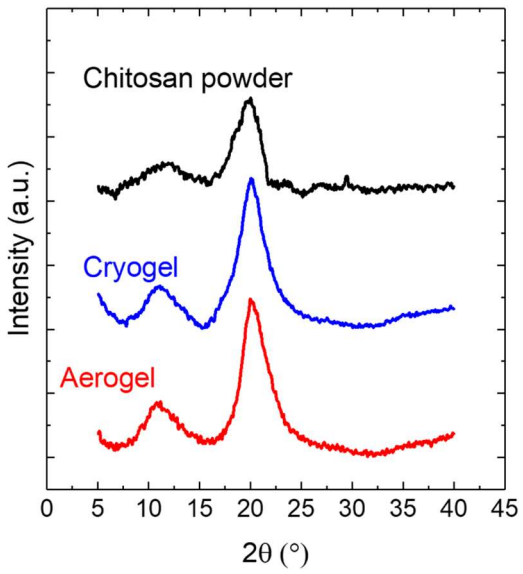

Figure IV.10: XRD diffraction patterns of the initial chitosan powder, cryogel and aerogel. The cryogel and aerogel were made from 5 %wt/v dissolved chitosan, coagulated in 4 M NaOH and aged for 24 h. The non-solvent used for solvent exchange was ethanol.

1.5. Absorption of simulated wound exudate (SWE)

In view of the potential application of chitosan aerogels and cryogels as wound dressings, the absorption of SWE was studied as a function of the chitosan concentration. Moisture balance is important to guarantee a good healing process and limit infections [53]. The absorption was monitored during 48 h, which is the duration a dressing is typically used before being replaced [54]. Figure IV.11a shows that higher is the concentration of chitosan in the initial solution, and thus lower the porosity (Figure IV.5) and pore volume (Figure IV.12), lower is the absorption of SWE by both aerogels and cryogels. In all cases, a plateau value is reached within one hour. The absorption values obtained correspond to the higher values of chitosan cryogels and aerogels reported in the literature [7,8,31,34,35,41,43] (Table IV.1). Because of their high absorption capacity, these materials seem suitable for healing of moist wounds where fluid absorption is necessary to limit bacterial proliferation. In Figure IV.11b, the amount of fluid absorbed after one hour shows that higher is the porosity, higher is the absorption, as expected. Cryogels and aerogels of similar porosity show similar values of absorption.

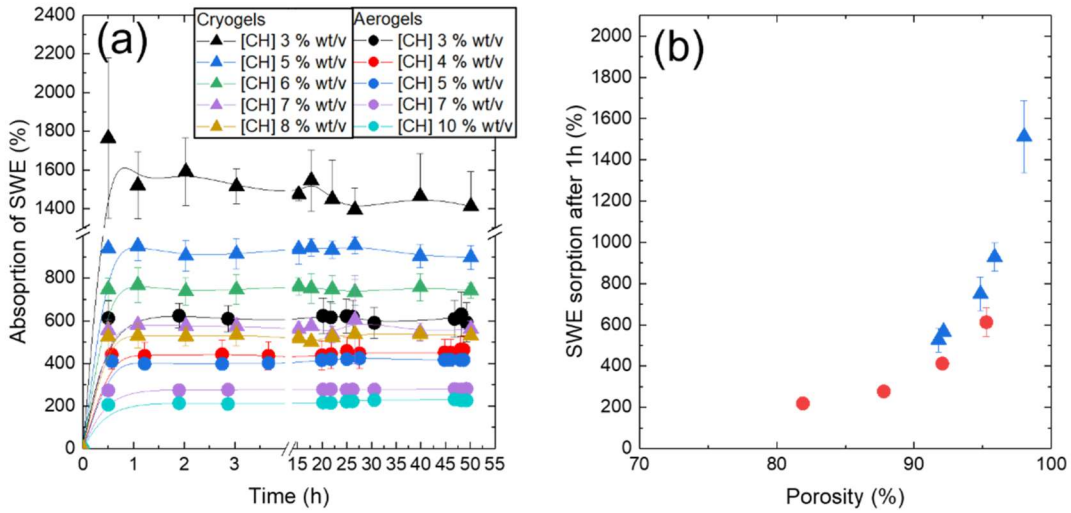

Figure IV.11: (a) Absorption kinetics of SWE at 30 °C for cryogels and aerogels made from 3, 4, 5, 6, 7, 8 and 10 % of chitosan solutions (aging for 24 h in 4 M NaOH), (b) SWE sorption after 1 h as a function of material porosity: blue triangles are for cryogels and red circles are for aerogels. The non-solvent used for solvent exchange was ethanol.

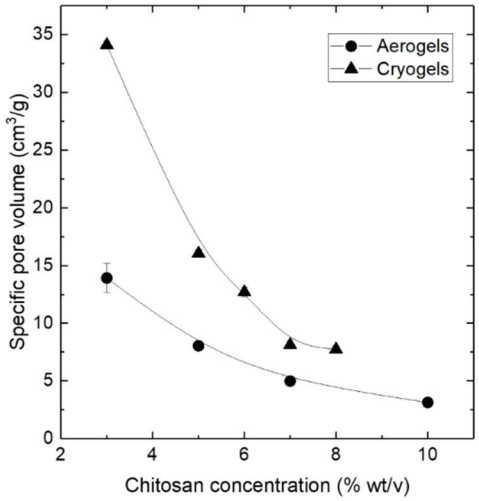

Figure IV.12: Specific pore volume in chitosan aerogels (circles) and cryogels (triangles). Samples were coagulated in 4 M NaOH and aged for 24 h. Solvent exchange, for aerogel precursors, was performed with ethanol. Lines are given to guide the eye.

2. Mechanical properties of porous dried chitosan-based materials

2.1. Influence of the chitosan concentration and drying method on mechanical properties

Cyclic uniaxial compression tests were performed on aerogels and cryogels monoliths made in drilled tubes. The compression was performed with 3 cycles up to 5, 10 and 15% of strain. The cycles were performed keeping in mind that the aerogels should be evaluated for potential dressing applications and thus be manipulated and slightly compressed when hold or put in the wound. The dressing should be able to be slightly viscoelastic to be comfortable for the patient. Compression tests were performed on aerogels obtained from ScD performed with ethanol as non-solvent (Figure IV.13b) and on cryogels (Figure IV.13c) and the mechanical properties are shown in Table IV.2. A full compression curve is shown on Figure IV.13a. We decided to work with the engineering stress and

strain instead of the true stress and strain because the Poisson's ratio (calculated with the equation IV.2) is around 0 for all the samples.

$$\upsilon = \frac{(l_0 - l)/l_0}{(L - L_0)/L_0} \qquad \text{IV.2}$$

with l_0 and L_0 the initial width and length respectively, and l and L the final width and length.

Despite a careful preparation of the sample and surface sanding, the surfaces presented some defects with faces not totally parallel or with small cavities. In some cases, the samples were too soft to be firmly handled for sanding. A pre-loading (1 N) was therefore applied but was sometimes not sufficient to compensate these defects. Thus, the very beginning of the curve (up to 1% of strain) (Figure IV.13) does not always reflect the real properties of the material. To have a consistent and coherent measure of the modulus, it was calculated for all samples from the first hysteresis to minimize the influence of these defects, indeed, the small deformation already applied had solve parallelism problems and eventually reduced or suppress the small cavities. The strain applied being low, it does not modify drastically the material and thus the modulus. An increase of the stress is observed with the strain and with the chitosan concentration for aerogels and aerogels, the latter due to the increase in material density. The samples did not break until 80% of strain (data not shown). Higher density induces a higher modulus for aerogels and cryogels as expected and observed in literature for cellulose porous materials [42]. The moduli obtained for aerogels between 1-4 MPa are similar to the one observed in the literature for chitosan aerogel composites ([55] (mixed with sodium silicate and trimethylsilyl), and [9](crosslinked with urea and mixed cetylmethylammonium chloride)), higher than starch aerogels (0.3-2.5 MPa) [56], but usually lower than cellulose aerogels (0.1-50 MPa) [42] for similar density. The modulus of chitosan cryogel is in the range of the cellulose one's (0.1-20 MPa) [42] for similar density. Cryogels presented an increase of the modulus up to samples made from solutions of 6%wt/v (0.07 g/cm^3) and then a limited decrease with the increase of the chitosan density from 0.06 to 0.1 g/cm^3 (Table IV.2). This behavior does not seem logical, but one explanation may be the inhomogeneity of the cryogel samples. It was discovered later that some cryogels exhibited an extremely hard center (shore 70-80 hardness) compared to the outside layer (shore 54 hardness) which may be ascribed to a too slow freezing resulting in more important water crystal growth pushing the chitosan fibers toward the center of the monolith. This was not known when the mechanical tests were performed, and this morphology may have not been noticed at the time. Overall, it should be noted that although an impact of chitosan aerogel and cryogel density was obtained for both aerogels and cryogels on the modulus (Table IV.2), conclusions should be considered with care as large standard deviations were obtained for some samples.

The shape of the loading-unloading cycle gives information on the elastic behavior of the material: if loading/unloading curves are not superimposed, it indicates that the viscous term (in viscoelastic solid) dominates the elastic term. This effect is more pronounced at higher strain (Figure IV.13), and higher material density indicating that densification of the material tends to decrease the elastic term.

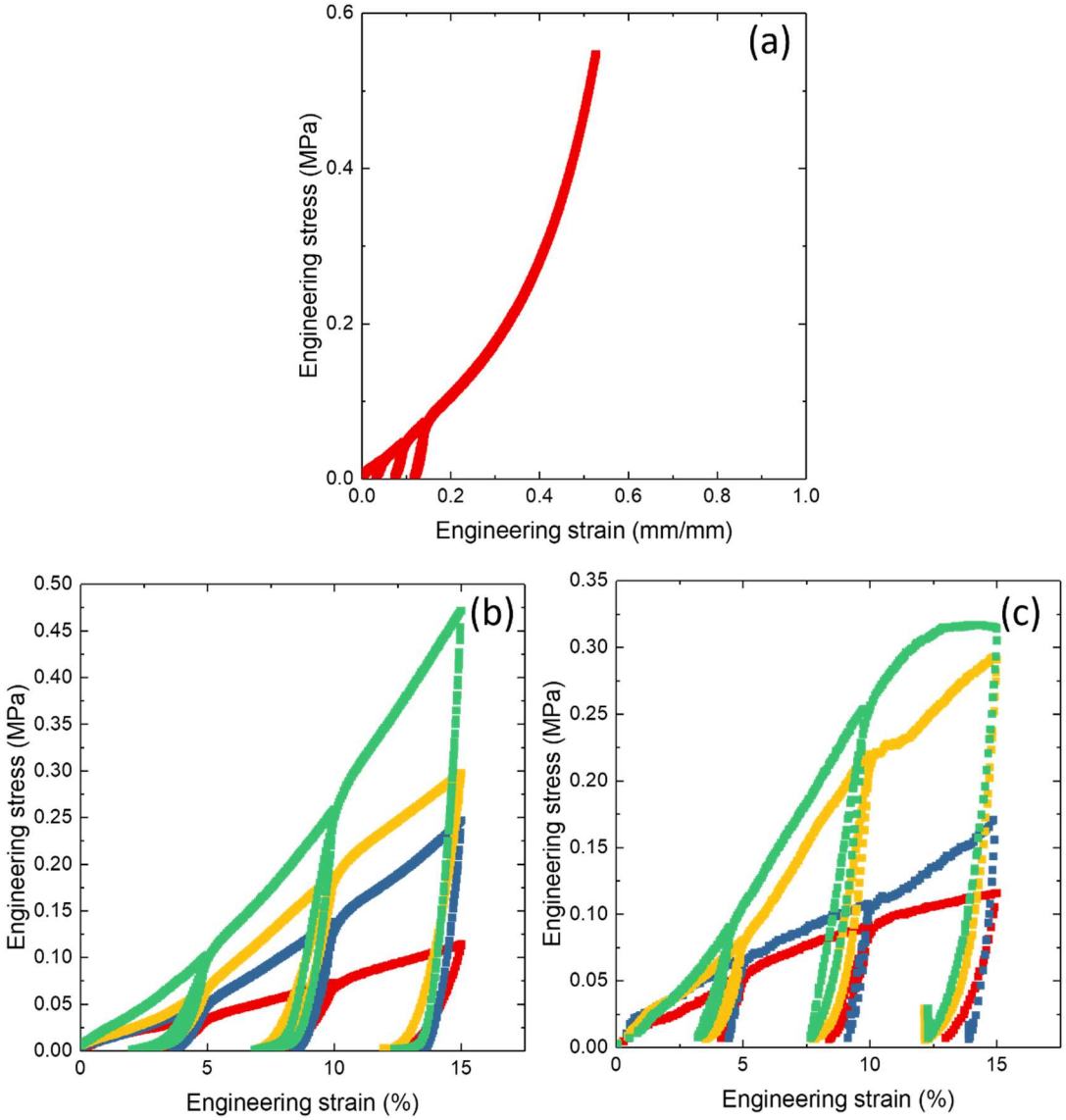

Figure IV.13: Influence of the chitosan concentration 5%wt/v in red, 6%wt/v in blue, 7%wt/v in yellow and 8%wt/v in green, on engineering stress for:
(a) aerogel Sc dried with acetone as non-solvent, full compression curve
(b) aerogels Sc dried with ethanol as non-solvent,
(c) cryogels on compression tests.

*Table IV.2: Mechanical properties of porous chitosan materials as a function of drying (ScD for aerogels, FzD for cryogels) and of the non-solvent used. (*no duplicate)*

Drying	Non-solvent before drying with CO_2	Chitosan concentration (%Wt/v)	Density (g/cm^3)	Modulus (MPa)	Elastic recovery at 5% of strain (%)
ScD	Ethanol	5	0.080 ± 0.003	1.20 ± 0.04	3.2 ± 0.7
ScD	Ethanol	6	0.097 ± 0.005	1.11 ± 0.38	4.0 ± 1.2

ScD	Ethanol	7	0.126 ± 0.009	2.53 ± 0.94	3.9 ± 0.5
ScD	Ethanol	8	0.150 ± 0.008	1.82 ± 0.44	4.5 ± 0.6
ScD	Isopropanol	5	0.126 ± 0.012	0.84 ± 0.58	2.9 ± 0.8
ScD	Isopropanol	6	0.144 ± 0.011	1.56 ± 0.67	2.7 ± 0.1
ScD	Isopropanol	7	0.156 ± 0.006	1.41 ± 0.62	1.8 ± 0.2
ScD	Isopropanol	8	0.192 ± 0.020	4.14 ± 1.30	1.6 ± 0.1
ScD	Acetone	5	0.109 ± 0.003	2.10 ± 0.02	1.5 ± 0.5
ScD	Acetone	6	0.076*	1.14*	2.6*
ScD	Acetone	7	0.160 ± 0.006	2.08 ± 1.56	1.8 ± 0.4
ScD	Acetone	8	0.189 ± 0.017	3.78 ± 3.50	2.0 ± 0.2
FzD	Water	5	0.062 ± 0.036	1.35 ± 1.55	1.2±0.8
FzD	Water	6	0.071 ± 0.005	9.86 ± 0.33	0.6 ± 0.1
FzD	Water	7	0.080 ± 0.040	7.00 ± 3.56	1.1 ± 0.6
FzD	Water	8	0.095 ± 0.006	5.03 ± 1.21	1.7 ± 0.6

Elastic recovery was determined by looking at the difference of strain between the maximum and the minimum value of a hysteresis. An elastic recovery from 1 to 4% was calculated for all materials from the first hysteresis. The recovery is low but an increase might be possible with the addition of crosslinked points in the network via crosslinking with genipin [57,58], for example. However, this recovery may be enough for the targeted application, we can suppose that patients presenting chronic wounds limit their movements due to the pain caused by the wound thus the elasticity required for the dressing may be, in fact, low. One way to approximate the elasticity needed is to look at the deformation applied on the skin during movements of the joint. Local deformations of the skin during foot movements were quantified with digital image correlation (DIC) on a healthy foot of a 30- and 60-years-old person on Figure IV.14. The color indicates the range of deformation. Depending on the movement, the skin undergoes anisotropic strains under tensile tension and compression. Tensile tension up to 12% of strain and compression of 9% were observed. These values, higher than the elastic recovery of the aerogels (2-4%), are still close to the aerogels' ones and indicate that the elastic recovery of the material proposed, despite being a bit low, could be suitable for an application as a dressing. Cryogels, made during this work, may not be suitable for wound dressing applications due to their low elasticity. In any case, improvements on elasticity by crosslinking or complexation with another material should be made to ensure a better comfort for patients.

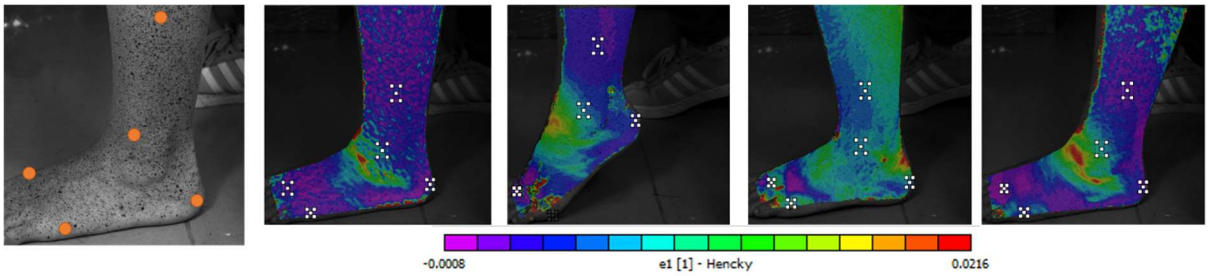

Figure IV.14: Left picture: Foot with the points indicating the different areas of interest for chronic wound; right pictures: local deformations obtained by DIC on a foot during movement.

The influence of the type of non-solvent used to be miscible with CO_2 (final non-solvent before drying) was investigated on aerogels obtained from ScD with isopropanol used as non-solvent (Figure IV.15a) and acetone (Figure IV.15b). The aerogels present a higher stress with higher material density whatever the non-solvent. The curves present a similar behavior than the ones obtained when ethanol is used. To be able to compare all the results together and see the influence of the non-solvent on the

mechanical properties, specific stress (engineering stress divided by the density, Eq. II.8) was calculated to consider the different densities between the samples [59]. The specific stress was plotted as a function of the strain and a typical plot is shown for aerogels made from 5wt/v% chitosan solutions (Figure IV.16). For all chitosan concentrations, the specific stress was decreased when changing the non-solvent from ethanol to acetone and last isopropanol. No chemical modification of chitosan can occur with these non-solvents, thus we can hypothesize that this difference is likely due to the chitosan network morphology. The higher specific surface area of ethanol's aerogels compared to the acetone's or isopropanol's aerogels, but with the same density, indicates a higher number of smaller pores as observed on SEM images on Figure IV.7b More walls are available to share the load applied on the sample and thus the force is applied on a larger surface making ethanol's samples more resistant. The engineering stress plotted cannot account for this difference of internal surface area as it only considers the external surface of the sample.

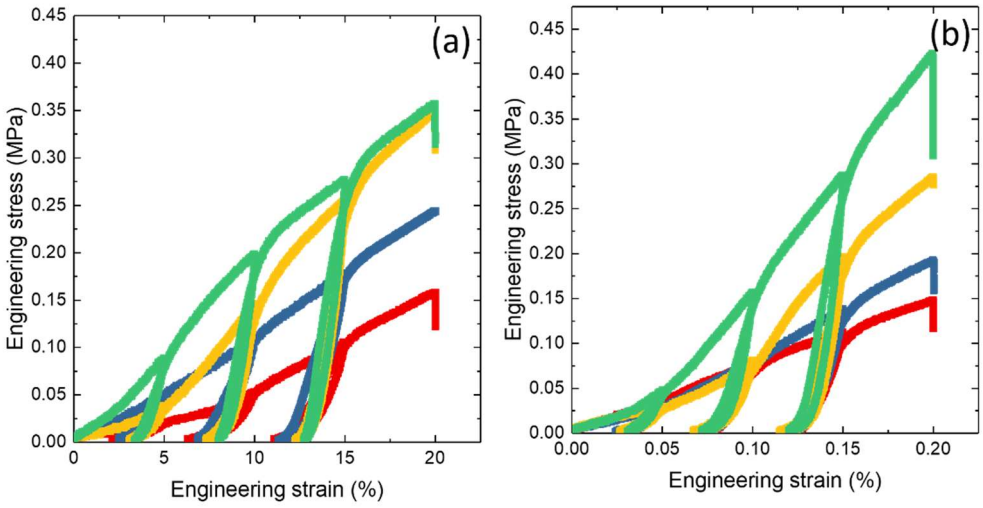

Figure IV.15: Influence of the chitosan concentration in the initial solution, 5%wt/v in red, 6%wt/v in blue, 7%wt/v in yellow and 8%wt/v in green, on engineering stress for:
(a) aerogels Sc dried with isopropanol as non-solvent
(b) aerogels Sc dried with acetone as non-solvent on aerogel mechanical properties.

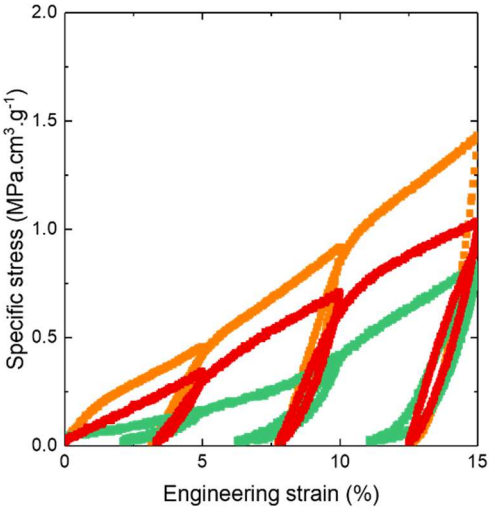

Figure IV.16: Specific stress of chitosan aerogel made from solutions of 5%wt/v, Sc dried using as non-solvent ethanol in orange, acetone in red or isopropanol in green.

2.2. Influence of the coagulation orientation, water content and humidity uptake on mechanical properties

2.2.1. Influence of the temperature and water content on mechanical behavior

The evolution of the modulus as a function of the temperature has been followed on two consecutive heating runs between 10 and 90°C, Figure IV.17a (the details of experimental set-up are provided in Chapter II.2.2.11.b 'Protocol to investigate the influence of the water content on the mechanical behavior of UDT samples'). Of notice, our experiments were carried out below Tg (reported for chitosan at ~ 140-150°C [60]) in the glassy state which may limit the impact of the temperature on the modulus. On the first run, the modulus increases. This was an unexpected behavior as the modulus is supposed to decrease with the temperature even in the glassy state. However, on the 2nd run, the modulus is decreasing with the temperature, showing the expected behavior. It is higher than the modulus on the 1st run indicating modifications of the network upon the first ramp of heating. An increase of the modulus with the temperature is often associated to crosslinking; however, in our case, no compound in the aerogel can crosslink. The results obtained for aerogels of other densities (made from solutions of different concentrations) were similar. The modulus of the 2nd run of aerogels from different chitosan concentrations was compared on Figure IV.17b. and show an expected result: the higher the chitosan aerogel density, the higher the modulus.

In the following part we will try to analyze and understand the influence of temperature increase on the mechanical response of chitosan aerogels. During temperature increase, at least three phenomena should be considered that are acting at the same time:

1) as it will be shown below, sample volume is changing: it decreases when temperature increases (i.e. drying and water evaporation),

2) sample mass also changes because of the evaporation of residual (adsorbed) water,

3) plasticizing effect [61] of water on chitosan is reduced

4) increasing the temperature increases the chain mobility, and thus decreases the modulus.

Because all phenomena are acting at the same time and may counterbalance each other, only qualitative considerations will be presented.

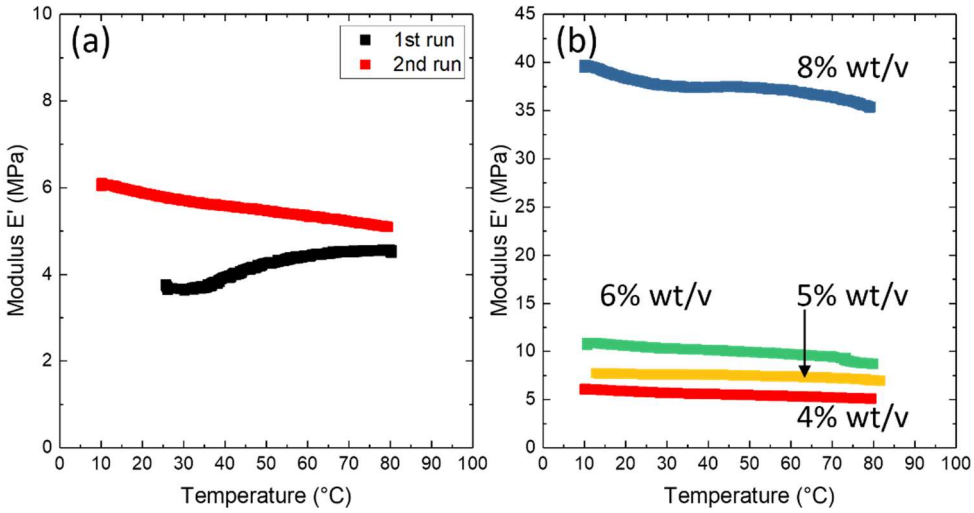

Figure IV.17: (a) Evolution of the modulus E' as a function of the temperature during two consecutive runs for aerogels made from solutions of 4 %wt/v chitosan concentration. (b) Evolution of the modulus E' during the 2nd run for different aerogel densities (4%-0.13 g/cm³; 5% - 0.13g/cm³; 6%-0.11g/cm³; 8%-0.16g/cm³). Samples were made in undrilled tubes (UDT).

The evolution of the static displacement on Figure IV.18a gives a hint for the increase of the modulus during the drying. The static displacement is the position of the plate to be in contact with the sample, it is automatically adjusted by the machine to keep a constant 'static force' on the sample. Modification of static displacement during the experiment indicates changes of sample size. The static displacement tends to increase with the temperature, decreasing the distance between the static and moving plate. It indicates a contraction of the sample and, as a consequence, the decrease of sample volume (Poisson's ratio is around 0) and, potentially, an increase of density (if the volume loss is more significant than the weight loss). This explains why the modulus of the second run is higher than that of the first one. This contraction is more important during the 1st run than the 2nd one for all concentrations. The results obtained for aerogels of other densities show the same trend.

To compare the difference of the evolution of the static displacement between the runs, a static displacement difference between the 2 runs was calculated according to Eq. IV.3 and plotted on Figure IV.18b:

$$x_0(\%) = \frac{(\Delta_1 - \Delta_2)}{\Delta_1} \times 100 \qquad \text{IV.3}$$

with Δ_1 and Δ_2 the static displacement observed for the first and second run, respectively.

The static displacement difference increases from 80 to 90% for aerogels made from 4 to 6%wt/v of chitosan, and stabilizes for higher concentrations. Biopolymers are well known to be hydrophilic, the evaporation of water from the aerogel with temperature increase could induce this shrinkage. Evaporation leads to pore collapsing [23] due to capillary pressure leading to aerogel densification and thus inducing modification of the mechanical properties. For example, samples with collapsed porosity like xerogels present drastically different properties as shown on cellulose [2].

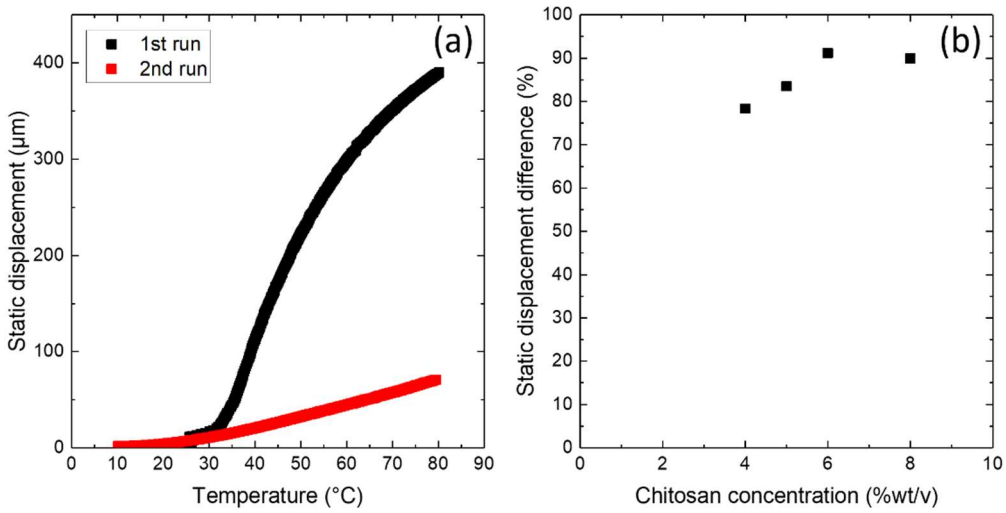

Figure IV.18: (a) Evolution of the static displacement as a function of the temperature during two consecutive runs for aerogels made from 4 %wt/v chitosan solution (density 0.13 g/cm³). (b) Static displacement shrinkage between the 1st run and the 2nd run for each concentration. Samples were made in UDT.

2.2.2. Influence of the humidity uptake on the mechanical behavior

To verify our hypothesis of water evaporation, the influence of humidity on the mechanical properties was checked. Mechanical properties were studied before and after humidity uptake and drying to check the possible structural modifications.

(1) Drying cycles and humidity uptake of aerogels

Figure IV.19 shows the evolution of the modulus as a function of the temperature during an entire cycle (the details of experimental set-up are provided in Chapter II.2.2.11.b 'Protocol to investigate the influence of the humidity uptake and the influence of the coagulation direction on the mechanical behavior of DT and UDT samples'). During the first heating run (grey curve), the modulus increases (Figure IV.17a), indicating a possible physical crosslinking or loss of plasticizing effect of water. When the sample is dried, a second heating run is performed (orange curve). These two curves are the same step already presented in Figure IV.17a. As previously observed, the modulus of the 2nd run is higher than the modulus of the first run (grey curve) and decreases to reach a modulus at 80°C equal to the one of the first run at the same temperature.

As water evaporation was suspected to be responsible for the increase of modulus during the first drying, the same samples were put in a climatic chamber at 30°C, the temperature of the skin, and 50%RH for a week. The heating run after this treatment (n°3) (black curve) shows a modulus starting at the same value as the one of 2nd heating run at 80°C, probably because the network reinforcement by water condensation was compensate by the plasticization, and increasing strongly with the temperature. The modulus value is doubled during this run which shows that during the stay in the climatic chamber the water absorbed lead to a reorganization of the chitosan network due to water condensation. The last heating run (n°4) (red curve) shows a decrease of the modulus with the temperature similar to the one observed during the 2nd heating run (orange curve) with a final modulus equal to the one measured at the end of the 3rd run. This increase of the modulus confirms the presence of water in our sample and its impact during drying on the mechanical properties. Other chitosan concentrations showed similar trend.

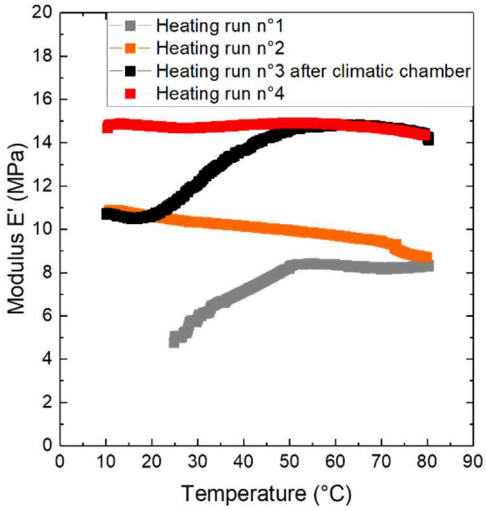

Figure IV.19: Aerogels modulus evolution as a function of the temperature during all the drying cycle for chitosan aerogels made from solution of 5 %wt/v (density 0.13g/cm³) made with UDT.

The volume shrinkage and the weight loss after each step of the experiment are shown on Figure IV.20. Weight decreases during drying due to the water evaporation and increases when the sample is placed in the climatic chamber due to the absorption of the humidity (Figure IV.20a). Volume shrinkage was observed during each step and was more significant during the first drying and the humidity uptake (Figure IV.20b). Volume shrinkage can be explained by two phenomena: capillary pressure (during aerogel "drying" because of temperature increase) and water condensation (due to water vapour uptake when aerogel is placed in a chamber at 30°C and 50%RH). It is known that hydrogels show pore collapsing due to the capillary pressure during water evaporation leading to a shrinkage. Water condensation [23,62] can also lead to a shrinkage because of the capillary pressure applied on the pores walls closing the porosity. The RH needed to have condensation can be calculated with the Kelvin equation IV.4:

$$\ln\frac{P}{P_s} = \frac{-2\gamma V_m}{RT} \times \frac{1}{r_m} \qquad \text{IV.4}$$

with $\frac{P}{P_s}$ the relative vapor pressure in equilibrium with a meniscus having a radius of curvature r_m, V_m is the molar volume of the liquid (1.8 .10^{-5} m^3/mol at 30°C for water [63]), γ is the surface tension between the liquid and gas (0.0712 N/m for liquid/air at 30°C [64]), R the universal gas constant and T the temperature in kelvin. The polymer nature should have an impact on the affinity between the polymer and the water and thus be considered as we are at the interfaces between 3 media (air/water/chitosan). To take into account the interface liquid/solid, the contact angle is needed, however, this angle is impossible to measure directly on mesopore range, hence it is assumed by simplicity that the contact angle between the solid and the liquid is equal to 0 [65]. The water condensation explained the shrinkage around 40% observed on starch aerogels [22] after storage at 25°C in 65% of humidity for months, because pore diameters were between 2 and 100 nm according their BJH analysis. However, when using a radius meniscus of 15 nm, which is the radius of the smallest chitosan aerogel pores as shown in a previous paper [66], the %RH needed to have water condensation is around 94%. This value is far from the conditions applied and cannot explain the shrinkage. To observe condensation at 50 %RH and 30°C, radius of 1.4 nm is needed. It indicates that small porosity could not be seen with SEM because of the resolution on aerogel is limited by the 14 nm platinum coating used for metallization that are closing the small pores and by the charge effects making difficult the image acquisition at large magnification.

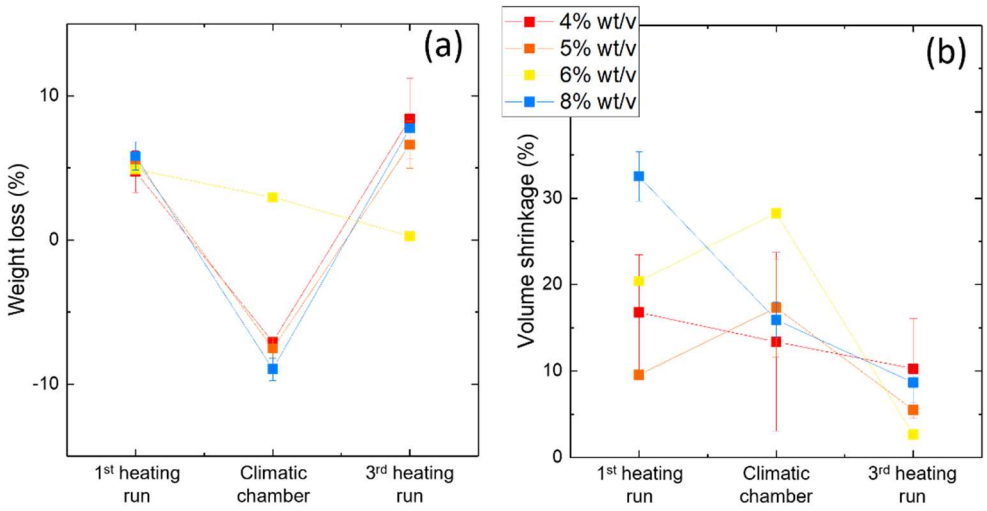

Figure IV.20: Weight loss (a) and volume shrinkage (b) as a function of the chitosan concentration after the 1st drying, the week in the climatic chamber and the 2nd drying. Negative values indicate a volume swelling or a weight intake. Lines are represented to guide the eyes.

The weight loss during each step (Figure IV.20a) is almost the same for all concentrations (except 6 %wt/v) so the relative amount of water in the aerogel whatever is the chitosan concentration is always the same but the variation of the absolute amount of water increases with chitosan concentration as shown on Figure IV.21. The total volume shrinkage, showed in Table IV.3, indicates a larger shrinkage for high chitosan concentrations. It means high chitosan concentrations are more sensitive to humidity as they can load larger amount of water.

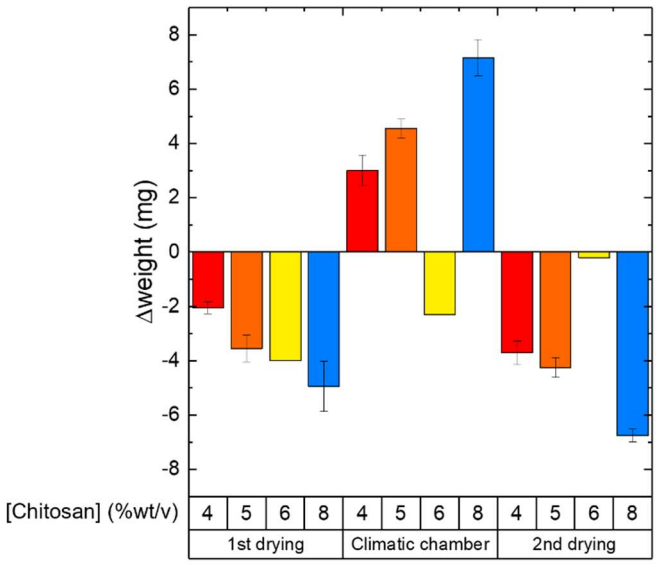

Figure IV.21: Variation of the amount of water in mg during each step for all chitosan concentrations.

Table IV.3 : Densities and total volume shrinkage as a function of the chitosan concentration for UDT samples

Chitosan concentration in the initial solution (%wt/v)	4	5	6	8
Initial density (g/cm^3)	0.133 ±0.023	0.130 ±0.001	0.0113	0.161 ±0.015
Density after the 1st heating run (g/cm^3)	0.153 ±0.036	0.136 ±0.002	0.135	0.225 ±0.029
Density after 1 week in climatic chamber (g/cm^3)	0.188 ±0.022	0.177 ±0.014	0.183	0.292 ±0.047
Final density after the 4th run (g/cm^3)	0.192 ±0.030	0.175 ±0.017	0.187	0.295 ±0.039
Initial porosity (%)	91	91	92	89
Total volume shrinkage (%)	36 ±2	29 ±5	44	48 ±2

The evolution of the modulus as a function of the temperature for different chitosan aerogels after the first drying and the second one after a week in a climatic chamber (t+1week) can be seen on Figure IV.17b and Figure IV.22 respectively. A logical order is found, with a higher modulus for higher aerogel density. An increase of the modulus was observed for all concentrations between t=0 and t+1week. For each aerogel, the modulus is almost doubled between t=0 and t+1week. In absolute value of modulus, 8 %wt/v chitosan aerogels show a higher increase due to the higher number of entanglement points as the rheology showed the entanglement point for 7 %wt/v (Figure III.8) indicating that critical concentration is exceeded.

The humidity uptake and the drying (due to temperature increases) increase the modulus indicating the water is at the origin of this increase. Drying leads to interactions in the network acting as “crosslinking points” because of pores closure. A hypothesis of the process is proposed on Figure IV.23: before drying, water is present at the entanglement points and the drying induces an evaporation of the water and a collapse of the pores where the water was. It creates connections between the chains mimicking a crosslinking. As these new connections cannot be removed, the modulus increases.

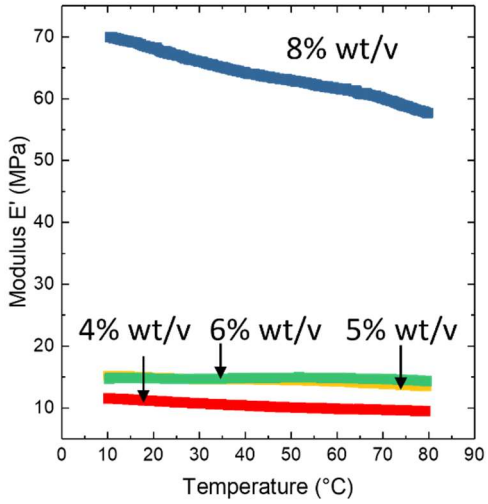

Figure IV.22: Evolution of the modulus during a temperature scan for chitosan aerogels made from solutions of different concentrations at t+1week. Samples were made in UDT.

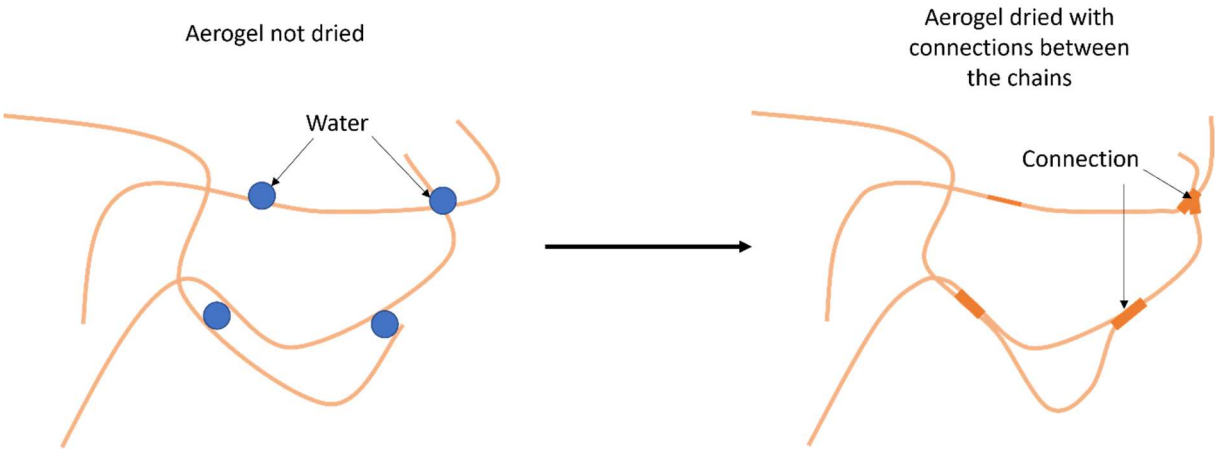

Figure IV.23: Hypothesis of the creation of network connections during drying

(2) Frequency scans

A frequency scan was performed after the 1st heating run to see the influence of the frequency on the modulus (Figure IV.22). As expected, the modulus increases with the frequency and decreases with the temperature. Frequency scans for other chitosan concentrations showed similar trends.

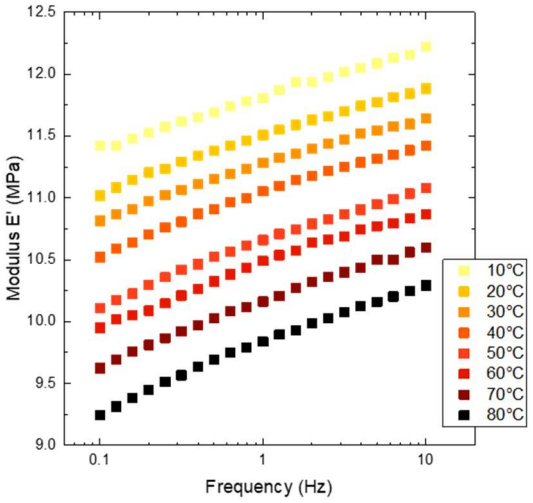

Figure IV.24: Frequency scan of a 6 %wt/v (density 0.011 g/cm³) sample after drying. Samples made in UDT.

When comparing the modulus at different temperatures during a frequency scan (Figure IV.25), the order is kept logical between the aerogels made from solutions of different concentrations, with a higher modulus for higher chitosan aerogel density. The modulus increases with the frequency. However, the value of the slope increases with the aerogel density showing a higher sensibility to the temperature for high chitosan concentration. This is confirmed with Figure IV.26 where all the evolution of the slopes as a function of the temperature is represented.

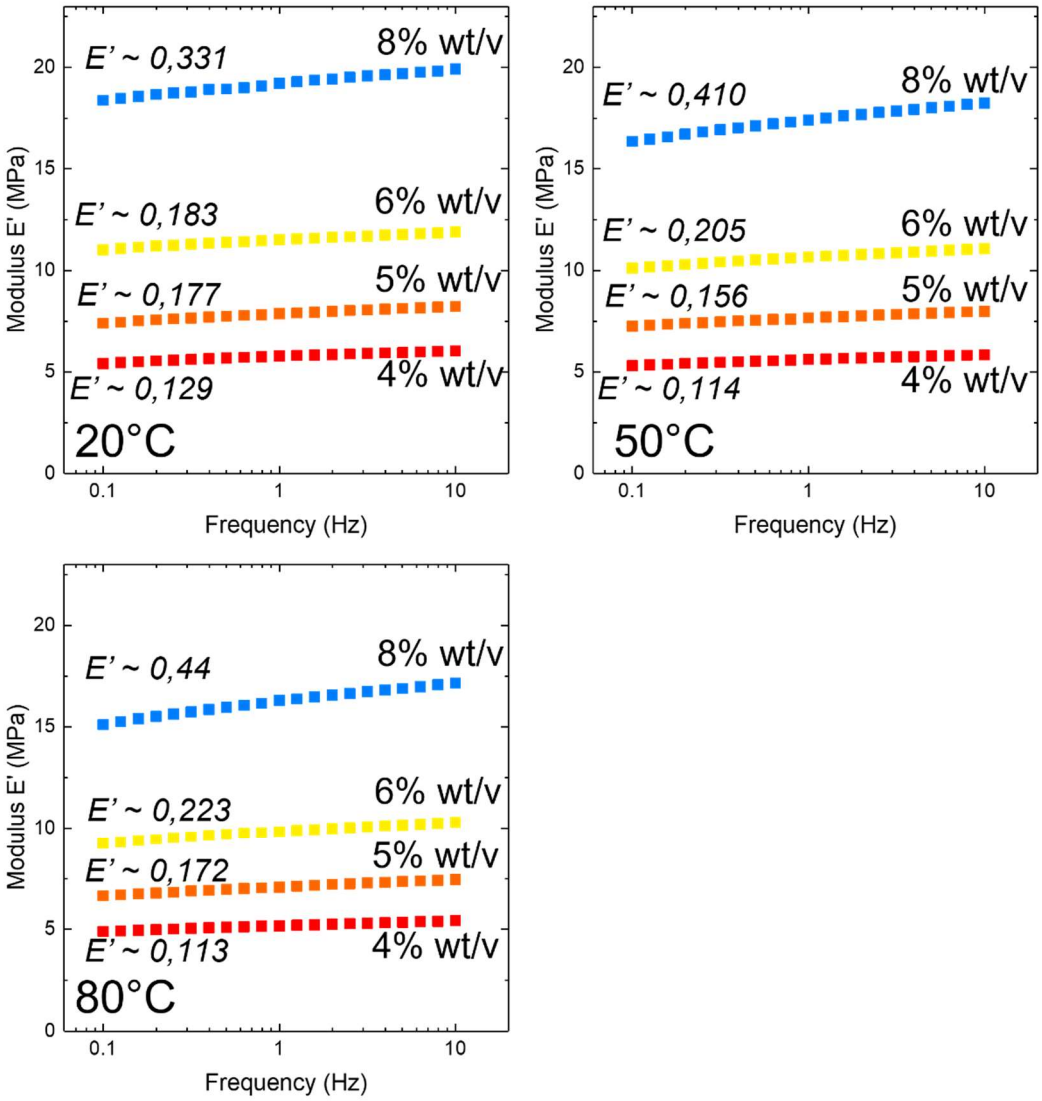

Figure IV.25: Comparison of the modulus evolution as a function of the frequency for 4 concentrations of chitosan (4, 5, 6 and 8 %wt/v) at 3 temperatures (20, 50 and 80°C). The slope is written for each curve. Samples made in UDT.

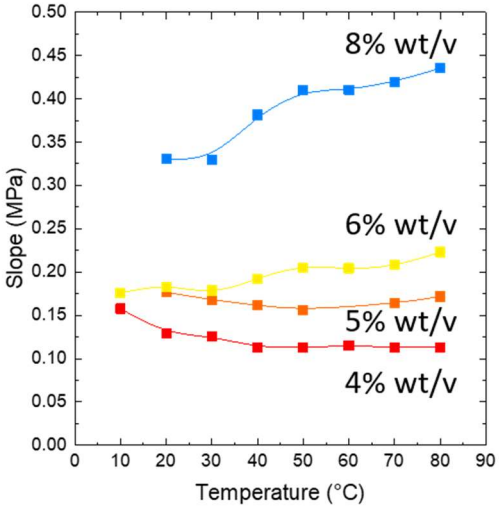

Figure IV.26: Slopes of the frequency scan for aerogels from four chitosan concentrations (4, 5, 6 and 8 %wt/v) and temperatures from 10 to 80°C. Lines are given to guide the eye. Samples made in UDT.

2.2.3. Influence of the coagulation direction with drilled and undrilled mold on mechanical properties

Coagulation direction may play an important role in the network formation. In many papers [8,21,30], chitosan solution is added dropwise into the NaOH bath to coagulate resulting in an isotropic structure. The structure formation has been studied for crosslinked chitosan [19,20], however, to the best of our knowledge, there is no literature reporting on the structure of non-crosslinked chitosan coagulated in one direction by NaOH. Plappert et al. [18] studied the impact of the coagulation direction on cellulose aerogels and obtained an isotropy in the aerogel.

The goal of these experiments was to check the influence of coagulation direction on the final material. For this purpose, two kinds of tubes were used during the coagulation. The undrilled tubes (UDT) allow a coagulation only from the top of the chitosan solution and the drilled tubes (DT) allow a coagulation from all the directions. The latter is supposed to give an anisotropic structure while the first one may induce an orientation. This difference in the morphology should result in different mechanical properties of the material. The Figure IV.27 is a schematic representation of the coagulation orientation and of the orientation of the mechanical tests performed.

As shown previously, the humidity is an important factor for mechanical properties. To perform all the following experiments, the samples were always dried at 80°C until no evolution of the modulus was observed.

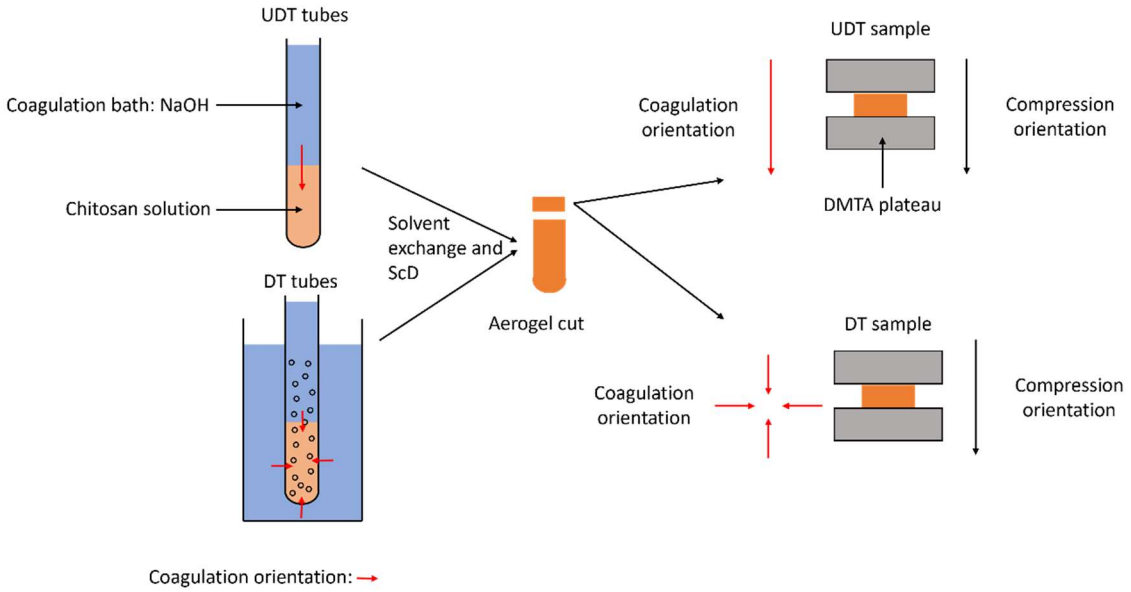

Figure IV.27: Scheme of the preparation of the samples with the coagulation orientation compared to the compression orientation.

The evolution of the modulus during a frequency scan on DT and UDT samples is shown in Figure IV.28. A higher modulus is observed for UDT samples at the same density. It indicates a different morphology between both samples indicating the influence of coagulation. Moreover, the modulus doubled after a week in climatic chamber for UDT samples demonstrating a higher sensibility to the humidity than DT samples as their modulus show almost no increase. It confirms that depending on the coagulation direction, the samples present different structures and thus different properties. Unidirectional coagulation is expected to lead to an anisotropic material thus anisotropic properties, this was evaluated in the next part.

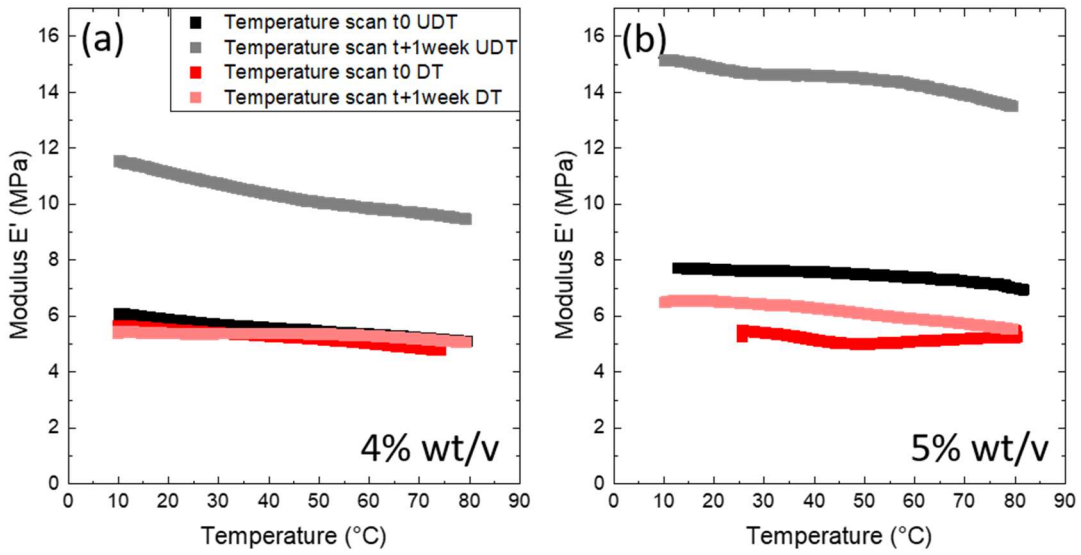

Figure IV.28: Comparison of the coagulation orientation on the modulus E' during a temperature scan for two chitosan concentrations at t0 and t+1week. The samples made in drilled tubes are represented in red/pink, in undrilled tubes in black/grey.

2.2.4. Anisotropy of chitosan aerogels

The influence of the coagulation direction was shown in the previous part. UDT samples are expected to present an anisotropic morphology as the coagulation only occurs from one direction. To check the anisotropy induced by one direction coagulation, cubic samples were prepared and tested in longitudinal direction (parallel to the coagulation) and transversal direction (perpendicular to the coagulation) (Figure IV.29 is a scheme of the coagulation and test directions, more details of experimental set-up are provided in Chapter II.2.2.11.b 'Protocol to investigate the influence of the anisotropy on the cubic aerogels'). Modulus obtained at 25°C for chitosan aerogels made from solutions of different chitosan concentrations in the 2 directions were plotted on Figure IV.30. As shown previously, the modulus increases with the chitosan concentration whatever the test direction. Modulus in the longitudinal direction is always higher than the transversal one for the samples of the same density. This is also observed at 50°C and 70°C (data not shown). This difference of modulus as a function of the test direction indicates an anisotropy of the morphology which is governed by the coagulation direction. The anisotropy is more important for high chitosan concentrations compared to lower ones as the difference of modulus between the 2 directions is more important.

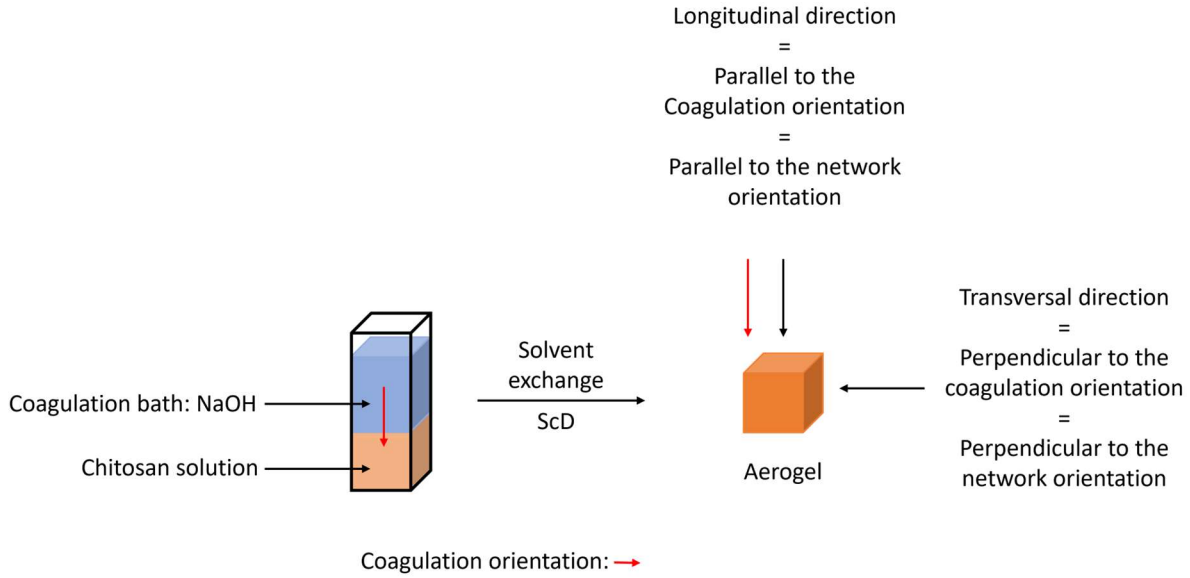

Figure IV.29: Scheme of the coagulation orientation and the compression directions of the sample.

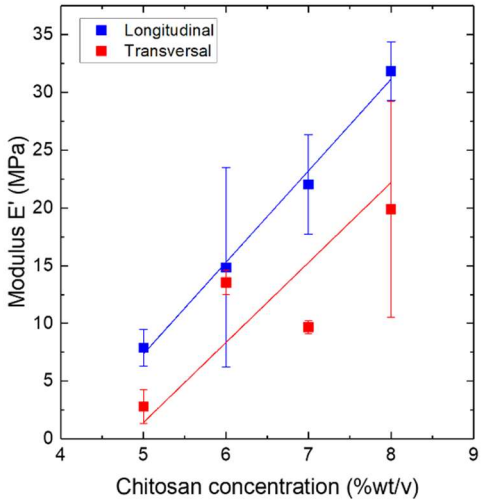

Figure IV.30: Modulus in measured in longitudinal and transversal direction at 25°C for aerogels from solutions of different chitosan concentrations. Lines are given to guide the eyes.

Conclusions

In this chapter, chitosan cryo- and aerogel monoliths were prepared by non-solvent induced phase separation (without crosslinker) and characterized. The influence of the process parameters (polymer concentration, first non-solvent (NaOH-water) concentration, time of aging, non-solvent before Sc drying and drying conditions) on the morphology and properties of the porous materials was studied. No influence of the aging time was observed within the time frame used. As long as the concentration of the coagulation bath is 0.5 M NaOH-water or higher, it also does not have a major impact on chitosan aerogel or cryogel properties. Chitosan concentration in solution increases density and decreases porosity of both types of materials, as expected.

The main parameter that changes the properties is the method of drying. Supercritical drying preserves in the best way the morphology of the hydrogels resulting in a specific surface area of 200-270 m^2/g. Due to the moderate shrinkage of the samples during solvent exchange and drying (within 30 %), the bulk density of aerogels is low, between 0.07 and 0.26 g/cm^3. Freeze-drying distorted the morphology of hydrogels due to the growth of ice crystals resulting in larger pores compared to aerogels and in a lower specific surface area (50 - 70 m^2/g). Furthermore, cryogels were of lower density than aerogels and thus of higher porosity. Nevertheless, the pore sizes in cryogels were surprisingly small (from a few hundreds of nanometers to a few microns) as compared to chitosan materials reported in literature which underwent freeze-drying. It indicates a strong capacity of the network to resist to deformations induced by growing ice crystals during freezing.

In view of the high and tunable simulated wound exudate absorption, the well-known biocompatibility of chitosan and the small pores which prevent cell ingrowth, these porous chitosan materials are promising materials for wound dressing applications.

Mechanical properties of chitosan aerogels and cryogels were assessed. Increase the chitosan concentration in the initial solution increases the resistance of the sample to the deformation: higher is the chitosan concentration in solution, higher is the modulus so stronger is the network. Density is the main parameter to tune the modulus. Elastic recovery of the aerogels was evaluated, it presents an elasticity in the same range as of the parts of the skin that are the most commonly affected by chronic wounds. The structure of the aerogel tuned by the non-solvent used for the solvent exchange modify the mechanical properties of the aerogels, more pores is leading to samples more resistant to the deformation.

The last section of this chapter was dedicated to the study of the influence of moisture and coagulation direction on the mechanical properties. First, the influence of humidity on mechanical properties was studied for chitosan aerogels for different aerogel densities. The drying leads to an increase of the modulus and decreases the sample's volume indicating the creation of new connections in the network because of the capillary pressure. After removing the water, the modulus decreases with the increase of the temperature. The hygroscopic properties of chitosan make chitosan aerogels sensible to humidity. The relative amount of water absorbed is the same for all aerogels, but it represents larger mass for higher chitosan concentration and thus, induces a larger sensibility to humidity compared to low chitosan concentration. Humidity intake leads to volume shrinkage due to water condensation leading to pore collapse.

Finally, the influence of the coagulation direction was assessed. Coagulation performed from all the sides or in the unidirectional way induces a different morphology in the final material. Homogeneous coagulation leads to an isotropic structure. Unidirectional coagulation makes the structure of the sample oriented with anisotropic mechanical properties. This anisotropy was demonstrated by DMTA compression tests parallel to the coagulation direction and in the transversal

way. Higher modulus was obtained in the longitudinal direction. Moreover, the anisotropic aerogels show a higher sensibility to the humidity uptake.

For application as wound dressing, the possibility to have anisotropic mechanical properties is interesting to orient the dressing according to the area of the wound in order to have properties that are closer to those of the original skin, making the dressing more comfortable even when the patient moves.

References

[1] S. Groult, S. Buwalda, T. Budtova, Pectin hydrogels, aerogels, cryogels and xerogels: Influence of drying on structural and release properties, Eur. Polym. J. 149 (2021) 110386. https://doi.org/10.1016/j.eurpolymj.2021.110386.

[2] N. Buchtová, T. Budtova, Cellulose aero-, cryo- and xerogels: towards understanding of morphology control, Cellulose. 23 (2016) 2585–2595. https://doi.org/10.1007/s10570-016-0960-8.

[3] S. Wei, Y.C. Ching, C.H. Chuah, Synthesis of chitosan aerogels as promising carriers for drug delivery: A review, Carbohydr. Polym. 231 (2020) 115744. https://doi.org/10.1016/j.carbpol.2019.115744.

[4] E.S. Dragan, M.V. Dinu, Advances in porous chitosan-based composite hydrogels: Synthesis and applications, React. Funct. Polym. (2019) 104372. https://doi.org/10.1016/j.reactfunctpolym.2019.104372.

[5] J. Radwan-Pragłowska, M. Piątkowski, ł. Janus, D. Bogdał, D. Matysek, Biodegradable, pH-responsive chitosan aerogels for biomedical applications, RSC Adv. 7 (2017) 32960–32965. https://doi.org/10.1039/C6RA27474A.

[6] R. Wang, D. Shou, O. Lv, Y. Kong, L. Deng, J. Shen, pH-Controlled drug delivery with hybrid aerogel of chitosan, carboxymethyl cellulose and graphene oxide as the carrier, Int. J. Biol. Macromol. 103 (2017) 248–253. https://doi.org/10.1016/j.ijbiomac.2017.05.064.

[7] C. López-Iglesias, J. Barros, I. Ardao, F.J. Monteiro, C. Alvarez-Lorenzo, J.L. Gómez-Amoza, C.A. García-González, Vancomycin-loaded chitosan aerogel particles for chronic wound applications, Carbohydr. Polym. 204 (2019) 223–231. https://doi.org/10.1016/j.carbpol.2018.10.012.

[8] C. López-Iglesias, J. Barros, I. Ardao, P. Gurikov, F.J. Monteiro, I. Smirnova, C. Alvarez-Lorenzo, C.A. García-González, Jet Cutting Technique for the Production of Chitosan Aerogel Microparticles Loaded with Vancomycin, Polymers. 12 (2020) 273. https://doi.org/10.3390/polym12020273.

[9] S. Takeshita, S. Yoda, Chitosan Aerogels: Transparent, Flexible Thermal Insulators, Chem. Mater. 27 (2015) 7569–7572. https://doi.org/10.1021/acs.chemmater.5b03610.

[10] S. Takeshita, S. Zhao, W.J. Malfait, Transparent, Aldehyde-Free Chitosan Aerogel, Carbohydr. Polym. 251 (2021) 117089. https://doi.org/10.1016/j.carbpol.2020.117089.

[11] S. Takeshita, S. Zhao, W.J. Malfait, M.M. Koebel, Chemistry of Chitosan Aerogels: Three-Dimensional Pore Control for Tailored Applications, Angew. Chem. Int. Ed. (2020). https://doi.org/10.1002/anie.202003053.

[12] R.M. Obaidat, B.M. Tashtoush, M.F. Bayan, R. T. Al Bustami, M. Alnaief, Drying Using Supercritical Fluid Technology as a Potential Method for Preparation of Chitosan Aerogel Microparticles, AAPS PharmSciTech. 16 (2015) 1235–1244. https://doi.org/10.1208/s12249-015-0312-2.

[13] R.B. Seymour, G.A. Stahl, Macromolecular Solutions: Solvent-property Relationships in Polymers, Elsevier, 2013.

[14] M. Guillotin, C. Lemoyne, C. Noel, L. Monnerie, Physicochemical processes occurring during the formation of cellulose diacetate membranes. Research of criteria for optimizing membrane performance. IV. Cellulose diacetate-acetone-organic additive casting solutions, Desalination. 21 (1977) 165–181. https://doi.org/10.1016/S0011-9164(00)80314-8.

[15] E. Klein, J.K. Smith, Asymmetric Membrane Formation. Solubility Parameters for Solvent Selection, Prod. RD. 11 (1972) 207–210. https://doi.org/10.1021/i360042a017.

[16] H. Strathmann, P. Scheible, R.W. Baker, A rationale for the preparation of Loeb-Sourirajan-type cellulose acetate membranes, J. Appl. Polym. Sci. 15 (1971) 811–828. https://doi.org/10.1002/app.1971.070150404.

[17] R.D. Sanderson, H.S. Pienaar, A morphological approach to desalination in hyperfiltration, Desalination. 25 (1978) 281–301. https://doi.org/10.1016/S0011-9164(00)80327-6.

[18] S.F. Plappert, J.-M. Nedelec, H. Rennhofer, H.C. Lichtenegger, S. Bernstorff, F.W. Liebner, Self-Assembly of Cellulose in Super-Cooled Ionic Liquid under the Impact of Decelerated Antisolvent Infusion: An Approach toward Anisotropic Gels and Aerogels, Biomacromolecules. 19 (2018) 4411–4422. https://doi.org/10.1021/acs.biomac.8b01278.

[19] S. Takeshita, A. Sadeghpour, W.J. Malfait, A. Konishi, K. Otake, S. Yoda, Formation of Nanofibrous Structure in Biopolymer Aerogel during Supercritical CO_2 Processing: The Case of Chitosan Aerogel, Biomacromolecules. 20 (2019) 2051–2057. https://doi.org/10.1021/acs.biomac.9b00246.

[20] S. Takeshita, A. Sadeghpour, D. Sivaraman, S. Zhao, W.J. Malfait, Solvents, CO2 and biopolymers: Structure formation in chitosan aerogel, Carbohydr. Polym. 247 (2020) 116680. https://doi.org/10.1016/j.carbpol.2020.116680.

[21] F. Quignard, R. Valentin, F. Di Renzo, Aerogel materials from marine polysaccharides, New J. Chem. 32 (2008) 1300. https://doi.org/10.1039/b808218a.

[22] V. Santos-Rosales, G. Alvarez-Rivera, M. Hillgärtner, A. Cifuentes, M. Itskov, C.A. García-González, A. Rege, Stability Studies of Starch Aerogel Formulations for Biomedical Applications, Biomacromolecules. 21 (2020) 5336–5344. https://doi.org/10.1021/acs.biomac.0c01414.

[23] M.R. Miner, B. Hosticka, P.M. Norris, The effects of ambient humidity on the mechanical properties and surface chemistry of hygroscopic silica aerogel, J. Non-Cryst. Solids. 350 (2004) 285–289. https://doi.org/10.1016/j.jnoncrysol.2004.06.023.

[24] M. Dash, F. Chiellini, R.M. Ottenbrite, E. Chiellini, Chitosan—A versatile semi-synthetic polymer in biomedical applications, Prog. Polym. Sci. 36 (2011) 981–1014. https://doi.org/10.1016/j.progpolymsci.2011.02.001.

[25] T. Jiang, R. James, S.G. Kumbar, C.T. Laurencin, Chitosan as a biomaterial: structure, properties, and applications in tissue engineering and drug delivery, in: Nat. Synth. Biomed. Polym., Elsevier, 2014: pp. 91–113.

[26] A. Anitha, S. Sowmya, P.T.S. Kumar, S. Deepthi, K.P. Chennazhi, H. Ehrlich, M. Tsurkan, R. Jayakumar, Chitin and chitosan in selected biomedical applications, Prog. Polym. Sci. 39 (2014) 1644–1667. https://doi.org/10.1016/j.progpolymsci.2014.02.008.

[27] G.A. Roberts, J.G. Domszy, Determination of the viscometric constants for chitosan, Int. J. Biol. Macromol. 4 (1982) 374–377.

[28] G.K. Moore, G.A.F. Roberts, Determination of the degree of N-acetylation of chitosan, 2 (n.d.).

[29] F. Di Renzo, R. Valentin, M. Boissière, A. Tourrette, G. Sparapano, K. Molvinger, J.-M. Devoisselle, C. Gérardin, F. Quignard, Hierarchical Macroporosity Induced by Constrained Syneresis in Core−Shell Polysaccharide Composites, Chem. Mater. 17 (2005) 4693–4699. https://doi.org/10.1021/cm0503477.

[30] M. Díez-Municio, A. Montilla, M. Herrero, A. Olano, E. Ibáñez, Supercritical CO2 impregnation of lactulose on chitosan: A comparison between scaffolds and microspheres form, J. Supercrit. Fluids. 57 (2011) 73–79. https://doi.org/10.1016/j.supflu.2011.02.001.

[31] D. Lovskaya, N. Menshutina, M. Mochalova, A. Nosov, A. Grebenyuk, Chitosan-Based Aerogel Particles as Highly Effective Local Hemostatic Agents. Production Process and In Vivo Evaluations, Polymers. 12 (2020) 2055. https://doi.org/10.3390/polym12092055.

[32] A. Tabernero, L. Baldino, A. Misol, S. Cardea, E.M.M. del Valle, Role of rheological properties on physical chitosan aerogels obtained by supercritical drying, Carbohydr. Polym. 233 (2020) 115850. https://doi.org/10.1016/j.carbpol.2020.115850.

[33] W. Sun, G. Chen, F. Wang, Y. Qin, Z. Wang, J. Nie, G. Ma, Polyelectrolyte-complex multilayer membrane with gradient porous structure based on natural polymers for wound care, Carbohydr. Polym. 181 (2018) 183–190. https://doi.org/10.1016/j.carbpol.2017.10.068.

[34] Y.-C. Wang, M.-C. Lin, D.-M. Wang, H.-J. Hsieh, Fabrication of a novel porous PGA-chitosan hybrid matrix for tissue engineering, Biomaterials. 24 (2003) 1047–1057.

[35] H.B. Tan, F.Y. Wang, W. Ding, Y. Zhang, J. Ding, D.X. Cai, K.F. Yu, J. Yang, L. Yang, Y.Q. Xu, Fabrication and evaluation of porous keratin/chitosan (KCS) scaffolds for effectively accelerating wound healing, Biomed Env. Sci. 28 (2015) 178–89.

[36] Y. Fan, Q. Lu, W. Liang, Y. Wang, Y. Zhou, M. Lang, Preparation and characterization of antibacterial polyvinyl alcohol/chitosan sponge and potential applied for wound dressing, Eur. Polym. J. 157 (2021) 110619. https://doi.org/10.1016/j.eurpolymj.2021.110619.
[37] T. Tanaka, Collapse of Gels and the Critical Endpoint, Phys. Rev. Lett. 40 (1978) 820–823. https://doi.org/10.1103/PhysRevLett.40.820.
[38] L. Druel, R. Bardl, W. Vorwerg, T. Budtova, Starch Aerogels: A Member of the Family of Thermal Superinsulating Materials, Biomacromolecules. 18 (2017) 4232–4239. https://doi.org/10.1021/acs.biomac.7b01272.
[39] S. Groult, T. Budtova, Tuning structure and properties of pectin aerogels, Eur. Polym. J. 108 (2018) 250–261. https://doi.org/10.1016/j.eurpolymj.2018.08.048.
[40] F. Zou, T. Budtova, Tailoring the morphology and properties of starch aerogels and cryogels via starch source and process parameter, Carbohydr. Polym. 255 (2021) 117344. https://doi.org/10.1016/j.carbpol.2020.117344.
[41] T.-W. Sun, W.-L. Yu, Y.-J. Zhu, F. Chen, Y.-G. Zhang, Y.-Y. Jiang, Y.-H. He, Porous Nanocomposite Comprising Ultralong Hydroxyapatite Nanowires Decorated with Zinc-Containing Nanoparticles and Chitosan: Synthesis and Application in Bone Defect Repair, Chem. - Eur. J. 24 (2018) 8809–8821. https://doi.org/10.1002/chem.201800425.
[42] N. Buchtová, C. Pradille, J.-L. Bouvard, T. Budtova, Mechanical properties of cellulose aerogels and cryogels, Soft Matter. 15 (2019) 7901–7908. https://doi.org/10.1039/C9SM01028A.
[43] Y. Fan, Q. Lu, W. Liang, Y. Wang, Y. Zhou, M. Lang, Preparation and characterization of antibacterial polyvinyl alcohol/chitosan sponge and potential applied for wound dressing, Eur. Polym. J. 157 (2021) 110619. https://doi.org/10.1016/j.eurpolymj.2021.110619.
[44] V.I. Lozinsky, L.G. Damshkaln, K.O. Bloch, P. Vardi, N.V. Grinberg, T.V. Burova, V.Y. Grinberg, Cryostructuring of polymer systems. XXIX. Preparation and characterization of supermacroporous (spongy) agarose-based cryogels used as three-dimensional scaffolds for culturing insulin-producing cell aggregates, J. Appl. Polym. Sci. 108 (2008) 3046–3062. https://doi.org/10.1002/app.27908.
[45] Z. Cai, F. Zhang, Y. Wei, H. Zhang, Freeze–Thaw-Induced Gelation of Hyaluronan: Physical Cryostructuration Correlated with Intermolecular Associations and Molecular Conformation, Macromolecules. 50 (2017) 6647–6658. https://doi.org/10.1021/acs.macromol.7b01264.
[46] F. Martoïa, T. Cochereau, P.J.J. Dumont, L. Orgéas, M. Terrien, M.N. Belgacem, Cellulose nanofibril foams: Links between ice-templating conditions, microstructures and mechanical properties, Mater. Des. 104 (2016) 376–391. https://doi.org/10.1016/j.matdes.2016.04.088.
[47] N. Naghshineh, K. Tahvildari, M. Nozari, Preparation of Chitosan, Sodium Alginate, Gelatin and Collagen Biodegradable Sponge Composites and their Application in Wound Healing and Curcumin Delivery, J. Polym. Environ. 27 (2019) 2819–2830. https://doi.org/10.1007/s10924-019-01559-z.
[48] F. Mi, Adsorption of indomethacin onto chemically modified chitosan beads, Polymer. 43 (2002) 757–765. https://doi.org/10.1016/S0032-3861(01)00580-8.
[49] Y.-W. Cho, J. Jang, C.R. Park, S.-W. Ko, Preparation and Solubility in Acid and Water of Partially Deacetylated Chitins, Biomacromolecules. 1 (2000) 609–614. https://doi.org/10.1021/bm000036j.
[50] R. Barreiro-Iglesias, R. Coronilla, A. Concheiro, C. Alvarez-Lorenzo, Preparation of chitosan beads by simultaneous cross-linking/insolubilisation in basic pH, Eur. J. Pharm. Sci. 24 (2005) 77–84. https://doi.org/10.1016/j.ejps.2004.09.013.
[51] M.-T. Yen, J.-H. Yang, J.-L. Mau, Physicochemical characterization of chitin and chitosan from crab shells, Carbohydr. Polym. 75 (2009) 15–21. https://doi.org/10.1016/j.carbpol.2008.06.006.
[52] K. Harish Prashanth, Solid state structure of chitosan prepared under different N-deacetylating conditions, Carbohydr. Polym. 50 (2002) 27–33. https://doi.org/10.1016/S0144-8617(01)00371-X.
[53] T.D. Turner, Hospital usage of absorbent dressings, Pharm. J. 222 (1979) 421–424.

[54] C. Lindholm, T.J. Styche, H.E. Horton, Diagnosis and treatment impacts on wound care efficiency drivers: real-world analysis, J. Wound Care. 30 (2021) 534–542. https://doi.org/10.12968/jowc.2021.30.7.534.
[55] L. Baldino, S. Cardea, E. Reverchon, Nanostructured chitosan-gelatin hybrid aerogels produced by supercritical gel drying: Nanostructured Chitosan-Gelatin Hybrid Aerogels Produced by Supercritical Gel Drying, Polym. Eng. Sci. 58 (2018) 1494–1499. https://doi.org/10.1002/pen.24719.
[56] T. Budtova, D.A. Aguilera, S. Beluns, L. Berglund, C. Chartier, E. Espinosa, S. Gaidukovs, A. Klimek-Kopyra, A. Kmita, D. Lachowicz, F. Liebner, O. Platnieks, A. Rodríguez, L.K. Tinoco Navarro, F. Zou, S.J. Buwalda, Biorefinery Approach for Aerogels, Polymers. 12 (2020) 2779. https://doi.org/10.3390/polym12122779.
[57] R. Muzzarelli, M. El Mehtedi, C. Bottegoni, A. Aquili, A. Gigante, Genipin-Crosslinked Chitosan Gels and Scaffolds for Tissue Engineering and Regeneration of Cartilage and Bone, Mar. Drugs. 13 (2015) 7314–7338. https://doi.org/10.3390/md13127068.
[58] J.R. Du, L.H. Hsu, E.S. Xiao, X. Guo, Y. Zhang, X. Feng, Using genipin as a “green” crosslinker to fabricate chitosan membranes for pervaporative dehydration of isopropanol, Sep. Purif. Technol. 244 (2020) 116843. https://doi.org/10.1016/j.seppur.2020.116843.
[59] S. Zhou, V. Apostolopoulou-Kalkavoura, M.V. Tavares da Costa, L. Bergström, M. Strømme, C. Xu, Elastic Aerogels of Cellulose Nanofibers@Metal–Organic Frameworks for Thermal Insulation and Fire Retardancy, Nano-Micro Lett. 12 (2020) 9. https://doi.org/10.1007/s40820-019-0343-4.
[60] Y. Dong, Y. Ruan, H. Wang, Y. Zhao, D. Bi, Studies on glass transition temperature of chitosan with four techniques, J. Appl. Polym. Sci. 93 (2004) 1553–1558. https://doi.org/10.1002/app.20630.
[61] M.G.A. Vieira, M.A. da Silva, L.O. dos Santos, M.M. Beppu, Natural-based plasticizers and biopolymer films: A review, Eur. Polym. J. 47 (2011) 254–263. https://doi.org/10.1016/j.eurpolymj.2010.12.011.
[62] S. Antonyuk, S. Heinrich, P. Gurikov, S. Raman, I. Smirnova, Influence of coating and wetting on the mechanical behaviour of highly porous cylindrical aerogel particles, Powder Technol. 285 (2015) 34–43. https://doi.org/10.1016/j.powtec.2015.05.004.
[63] CRC Handbook of Chemistry and Physics, CRC Press, 2022.
[64] N.B. Vargaftik, B.N. Volkov, L.D. Voljak, International Tables of the Surface Tension of Water, J. Phys. Chem. Ref. Data. 12 (1983) 817–820. https://doi.org/10.1063/1.555688.
[65] S.J. Gregg, K.S. Sing, Adsorption, surface area and porosity, 2. ed., 4. print, Academic Pr, London, 1997.
[66] C. Chartier, S. Buwalda, H. Van Den Berghe, B. Nottelet, T. Budtova, Tuning the properties of porous chitosan: Aerogels and cryogels, Int. J. Biol. Macromol. 202 (2022) 215–223. https://doi.org/10.1016/j.ijbiomac.2022.01.042.

Chapter V. Evaluation of drug loaded cryogels and aerogels

List of abbreviations:

AAP: Ascorbic acid 2-phosphate

Dex-P: Dexamethasone phosphate

DLC: Drug loading capacity

DLE: Drug loading efficiency

HDF: Human dermal fibroblast

Sc: Supercritical

S/E: Solvent exchange

TCPS: Tissue culture polystyrene

Content

Introduction

In general, drug release from a matrix depends on several material properties such as matrix solubility and the swelling ability in the release medium, potential interactions between the matrix and the drug, and, if the matrix is porous, on its density, morphology, pore size distribution and internal surface area. It is therefore important to establish processing-structure-property relationships, as they allow the design of chitosan materials with tailored characteristics and the desired release behavior.

Several articles reported the use of chitosan-based aerogels and cryogels as controlled drug delivery systems. For example, chitosan-collagen cryogels coated with poly(N,N'-diethylacrylamide) were developed for temperature- and pH-responsive delivery of the anti-inflammatory drug ibuprofen [1]. Furthermore, chitosan-alginate aerogel microparticles were developed for pulmonary delivery of the anticancer drug cisplatin [2]. The field of porous chitosan-based materials for drug delivery purposes was extensively reviewed in two recent publications [3,4]. In all articles related to porous chitosan-based drug delivery systems, only one drying method of chitosan solutions or gels was employed, which makes it complicated to develop correlations between the drying technique, the structural and morphological properties of the material and its release behavior.

In the previous chapter, we described the influence of drying conditions (sc drying *versus* freeze-drying) on the physico-chemical properties of non-crosslinked chitosan porous materials. In the current chapter, we investigate the incorporation and the release of two hydrophilic drugs from chitosan aerogels and cryogels prepared from the same chitosan hydrogel precursor: the dexamethasone sodium phosphate (Dex-P), a synthetic corticosteroid with anti-inflammatory effects, and the ascorbic acid-2-phosphate (AAP), which is a stable derivative of ascorbic acid, inducing angiogenesis and promoting collagen synthesis by fibroblasts [5,6]. For both drugs, the influence of the material preparation process and material properties on the drug loading and release kinetics from chitosan aerogels and cryogels is evaluated. The drug loading efficiency, the drug loading capacity and release kinetics are discussed with respect to the processing conditions, the network morphology of the materials, their physico-chemical properties, the interactions between the drug and chitosan and the pH of the release medium. The Korsemeyer-Peppas equation is used to identify the dominant physical mechanism controlling the release of Dex-P. Non-cytotoxicity of neat chitosan aerogel was checked on murine fibroblast L929 cell line and primary human dermal fibroblasts (HDF). The capacity of the AAP loaded aerogels to stimulate collagen expression was assessed during *in vitro* cell culture on HDF by quantification of extracellular collagen.

Some parts of this chapter are based on a paper submitted to Biomacromolecules: Chartier, C.; Buwalda S.; Ilochonwu B.C.; Van Den Berghe H.; Vermonden T.; Viola M.; Nottelet B.; Budtova T. Release kinetics of dexamethasone phosphate from porous chitosan: comparison of aerogels and cryogels.

Introduction (FR)

En général, la libération de principe actif depuis une matrice dépends des propriétés de la matrice comme sa solubilité et sa capacité à gonfler dans un milieu de libération, les potentielles interactions entre la matrice et le principe actif et, si la matrice est poreuse, sa densité, sa morphologie, sa distribution de la taille de pore et la surface interne. C'est pourquoi il est important d'établir les relations entre le procédé, la structure et les propriétés. Cela permet de développer un matériau à base de chitosane avec des propriétés sur-mesure et une cinétique de libération de principe actif souhaitée.

Plusieurs articles portent sur l'utilisation de d'aérogels et de cryogels à base de chitosane en tant que système de libération de principe actif contrôlé. Par exemple, des cryogels de chitosane-collagène recouvert avec du poly(N,N'-diethylacrylamide) ont été développés pour la libération contrôlée d'ibuprofène, un anti-inflammatoire, sur activation avec la température ou le pH [1]. Du plus, des microparticules d'aérogels de chitosane-alginate ont été développées pour la libération intrapulmonaire d'un anticancéreux, la cisplatine [2]. Le domaine des matériaux poreux à base de chitosane pour la libération de principes actifs a été largement décrite dans deux récentes publications [3,4]. Dans tous les articles traitant des matériaux poreux à base de chitosane en tant que système de libération de principe actif, seulement une méthode de séchage de la solution ou gel était employée par article, rendant compliqué d'établir la corrélation entre les méthodes de séchage, la structure et la morphologie du matériau, et sa cinétique de libération.

Dans le chapitre précédent, nous avons décrit l'influence des conditions de séchage (séchage supercritique *versus* lyophilisation) sur les propriétés physico-chimiques d'un matériau poreux à base de chitosane non réticulé. Dans ce chapitre, nous étudions l'incorporation et la libération de deux principes actifs hydrophiles d'aérogels et cryogels de chitosane préparés à partir du même précurseur : la dexaméthasone sodium phosphate (Dex-P), un corticostéroïde synthétique avec un effet anti-inflammatoire, et l'acide ascorbique 2-phosphate (AAP), un dérivé stable de l'acide ascorbique, induisant l'angiogenèse et promouvant la synthèse de collagène par les fibroblastes [5,6]. Pour les deux principes actifs, l'influence du procédé de préparation et les propriétés du matériau sur le chargement des principes actifs et la cinétique de libération depuis les aérogels et cryogels de chitosane sont évalués. L'efficacité de chargement, la capacité de chargement du principe actif et sa cinétique de libération sont évaluées en respect des conditions de préparations, de la morphologie du réseau du matériau, leur propriétés physico-chimiques, et les interactions entre le principe actif, le chitosane et le pH du milieu de libération. L'équation de Korsemeyer-Peppas est utilisée pour identifier le mécanisme dominant qui contrôle la libération de Dex-P. La non-cytotoxicité des aérogels de chitosane non chargés a été vérifiée sur lignées cellulaires de fibroblastes murins L929 et des fibroblastes humains dermiques primaires (HDF). La capacité d'aérogels chargés d'AAP à stimuler l'expression de collagène a été évaluée au travers de culture cellulaire *in vitro* d'HDF par quantification du collagène extracellulaire.

Certaines parties de ce chapitre sont basées sur un papier soumis à Biomacromolecules : Chartier, C.; Buwalda S.; Ilochonwu B.C.; Van Den Berghe H.; Vermonden T.; Viola M.; Nottelet B.; Budtova T. Release kinetics of dexamethasone phosphate from porous chitosan: comparison of aerogels and cryogels.

1. Drug loading and release kinetics

1.1. Influence of aero- and cryogel properties on drug loading efficiency and drug loading capacity

Addition of a drug in aerogel/cryogel can be performed at different steps of the preparation process. Each presents advantages and drawbacks and the selection of the addition step depends on the drug's solubility, its stability, and size. AAP and Dex-P are water-soluble drugs that are poorly soluble in ethanol and Sc CO_2, making these drugs good candidates to be added to aerogel or cryogel precursor without performing any chemical modifications or bonding to the polymer. Different ways can be considered to add AAP or Dex-P during the aerogel or cryogel preparation [7]. The easiest and fastest is to directly mix the drug with the polymer solution prior to gelation [8], allowing to load significant amounts of drug. For this, the drug must be soluble in the polymer solvent, and it should not be altered nor washed out during the subsequent steps of the process. But considering that this work includes a coagulation step in 4M NaOH solution, that could possibly degrade the drug, and that NaOH removal steps would also wash it out, this first strategy was not selected. Supercritical impregnation of the drug during the final drying step [2,9] is interesting to load aerogels as it avoids degradation/washing of the drug. However, it requires a drug soluble in $ScCO_2$ which is not the case of AAP and Dex-P, and this approach cannot be implemented for cryogels. As this work aims at comparing the two materials, this option was not chosen. Finally, addition of the drug to the network *via* impregnation [10,11], either to the hydrogel or to the alcogel, can be envisioned. Despite the long time required to impregnate the sample, an efficient impregnation can be achieved with small and highly soluble molecules. AAP and Dex-P being water-soluble, drugs will be impregnated into the hydrogel by diffusion (Figure V.1). The dimensions of the samples in this study being relatively small, thus limiting the time needed for diffusion.

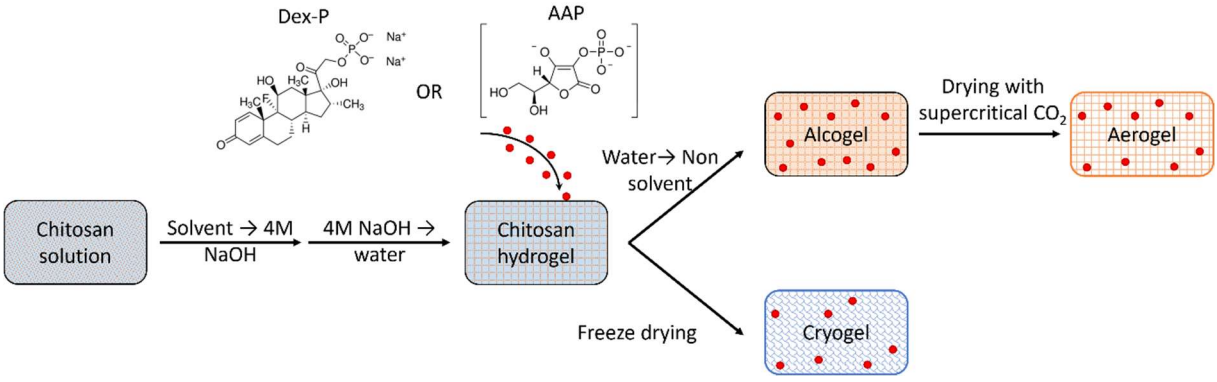

Figure V.1: Schematic representation of the preparation process of loaded chitosan cryogels and aerogels.

The time needed for impregnation was calculated using Fick diffusion approach with the following equation V.1:

$$t_{impregnation}(s) = \frac{L^2}{D_{Drug}} \qquad \text{V.1}$$

with L the half thickness of the gel to impregnate and D_{Drug} the drug diffusion coefficient. The diffusion coefficient of AAP (D_{AAP}) not being found in the literature, that of ascorbic acid, $D_{Ascorbic\ acid}$ = 1.055 .10^{-9} m^2/s, was used [12]. By analogy with previous work published on diffusion of molecules in cellulose matrices [10,11,13–15], the diffusion was divided by a factor of ten due to the difference between diffusion in water and diffusion through a matrix. The coefficient used was therefore 1.055 .10^{-10} m^2/s in chitosan matrices. Considering a half thickness of 0.5 cm for the matrix, the maximum time of impregnation needed to diffuse to the material center is around 3 days. To check if indeed the drug

completely diffused in chitosan hydrogel, preliminary studies were conducted on xerogels, *i.e.,* matrices loaded with AAP in water and dried in the open air, (Figure V.2.1). To check if any interactions occur between the AAP and the chitosan, neat alcogels were loaded in AAP-ethanol solution. The AAP, being poorly soluble, was mostly in suspension in ethanol. The drug loading efficiency (DLE) and the drug loading capacity (DLC) of xerogels were evaluated as a function of impregnation time. As no difference was observed between the times considered (Data not shown), 3 days of loading without renewing the impregnation solution was finally chosen to reduce the processing times.

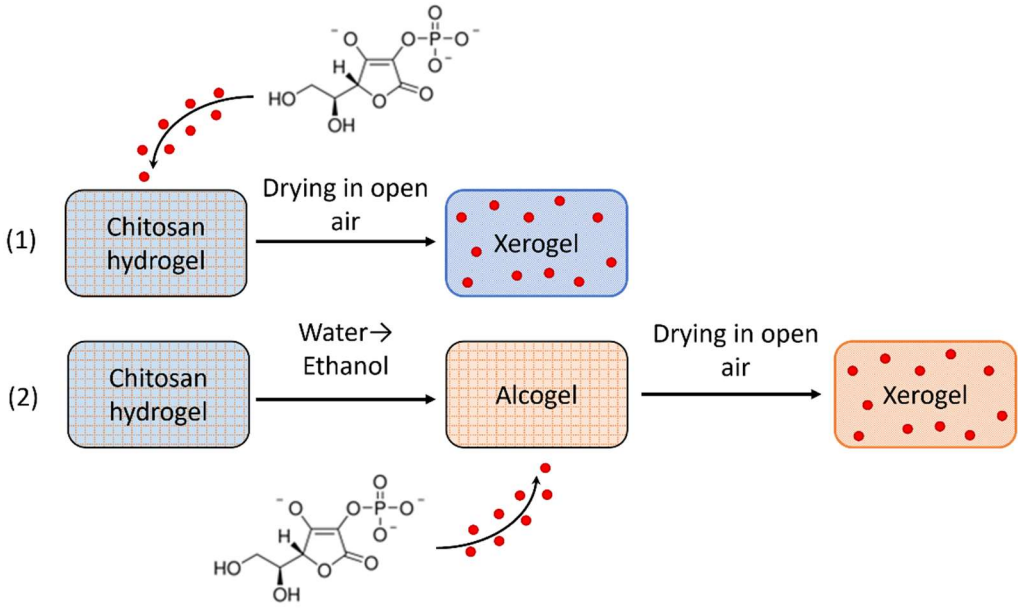

Figure V.2: Schematic representation of the preparation process of chitosan xerogels to test the impregnation of chitosan by AAP from different solvents: water (1) and ethanol (2).

Various aerogels/cryogels samples, loaded with either AAP or Dex-P, were prepared by varying three parameters: the chitosan concentration (5 or 8% wt/v), the non-solvent used for solvent exchange (S/E) in the case of aerogels, and the drying method (freeze drying or supercritical drying with CO_2). The influence of these parameters on material density, porosity and specific surface area have been extensively described in our previous work [16]. Briefly, a higher chitosan concentration resulted in a higher density and lower porosity; the surface area was not substantially influenced. Aerogels were of slightly higher density and with significantly higher surface area as compared to their cryogels counterparts (Table V.1). Examples of materials' morphology are shown in Figure V.3.

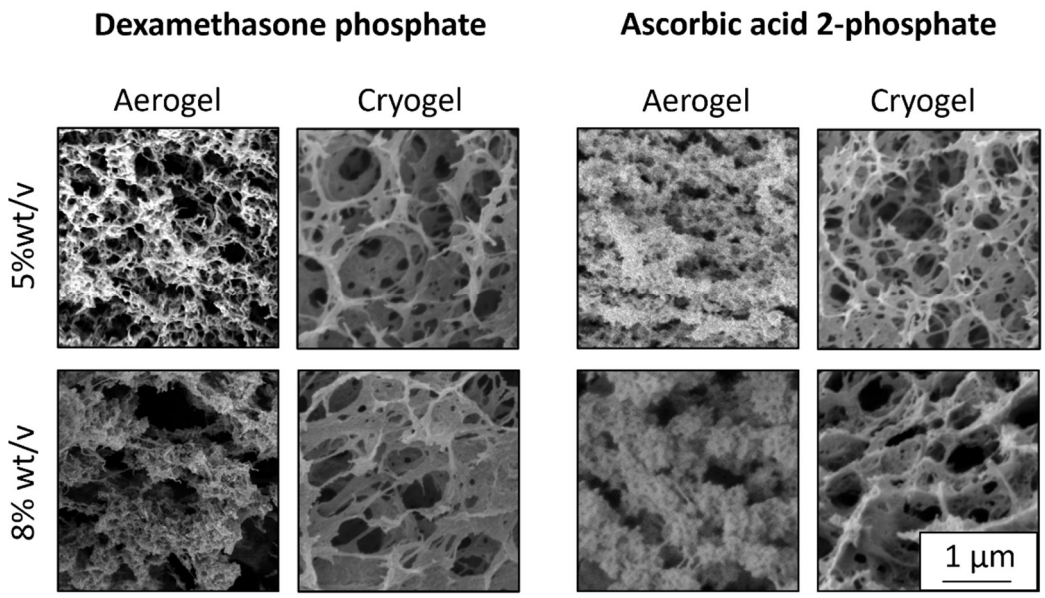

Figure V.3: SEM images of chitosan aerogels and cryogels made from 5 and 8 % wt/v chitosan solutions and loaded in water with either Dex-P or AAP. Non-solvent used for ScD of the presented aerogel is ethanol. Their corresponding characteristics are given in Table V.1.

DLE (eq. II.9) and DLC (eq. II.10) of these different aerogels and cryogels, were evaluated as a function of the material properties (density and surface area) and compared to DLE and DLC of AAP loaded xerogels (Table V.1).

*Table V.1 : Bulk density, specific surface area, drug loading efficiency (DLE), and drug loading capacity (DLC) for xerogels, cryogels, and aerogels after 3 days of impregnation. * Value obtained for unloaded aerogel, † Calculated using the density of a 5%wt/v chitosan aerogel.*

Drug used	Type of sample	Chitosan concentration in solution (%wt/v)	Density (g/cm^3)	Specific surface area (m^2/g)	DLE (%)	DLC (%)
AAP	Xerogel loaded in water	5	1.30	/	521 ± 58†	2.27 ± 0.25
	Xerogel loaded in ethanol	5	1.30	/	86 ± 16†	0.38 ± 0.07
	Aerogel S/E with acetone	5	0.076 ± 0.002	194 ± 9*	278 ± 3	1.83 ± 0.07
	Aerogel S/E with isopropanol	5	0.094 ± 0.020	175 ± 5*	305 ± 44	1.64 ± 0.11
	Aerogel S/E with ethanol	5	0.090 ± 0.029	248 ± 0.3	355 ± 146	1.95 ± 0.16
		8	0.15 ± 0.017	182 ± 2	453 ± 88	1.49 ± 0.27
	Cryogel	5	0.057 ± 0.010	51 ± 1	276 ± 72	2.49 ± 0.87
		8	0.10 ± 0.012	75 ± 2	329 ± 19	1.66 ± 0.18
Dex-P	Aerogel S/E with ethanol	5	0.064 ± 0.005	261 ± 34	67 ± 2	0.53 ± 0.04
		8	0.124 ± 0.006	245 ± 1.1	68 ± 6	0.28 ± 0.03
	Cryogel	5	0.058 ± 0.004	48 ± 4	252 ± 58	2.2 ± 0.45
		8	0.098 ± 0.017	51 ± 4	206 ± 27	1.05 ± 0.07

All materials, *i.e.,* cryogels, aerogels and xerogels, loaded with AAP in water presented DLE higher than 100% showing a good affinity between the drug and chitosan, and a good absorption of

the drug solution during the hydrogel impregnation. The higher DLE of xerogel loaded with AAP in water compared to cryogels and aerogels, indicates a loss of the drug during the solvent exchange or drying steps of the cryogels and aerogels preparation.

Aerogels loaded with Dex-P presented a lower DLE than that of Dex-P-loaded cryogels, around 70% *vs* 200 - 250%. Despite a poor solubility of the drug in ethanol [17], it was partly washed out during the step of water to ethanol exchange in the aerogel preparation, as the drugs may still be soluble in a water-ethanol mixture. Some washing out could have also occurred during supercritical drying of aerogel preparation. A similar phenomenon was observed for pectin aerogels loaded with theophylline [18]. However, this difference was not observed when AAP was loaded in the materials since the DLE of aerogels was similarly to that of cryogel. This can be explained by stronger ionic interactions between AAP and chitosan as compared to Dex-P and chitosan. AAP structure presents 3 anionic charges against only 2 for Dex-P, which favors interactions between AAP and chitosan when the latter is positively charged (pKa ~ 6.3-6.4 [19]). These interactions could counteract the AAP washing out phenomenon for aerogel preparation.

Regarding the loading efficiency of aerogels, 70% for Dex-P and 280 – 450% for AAP, values are high (in particular, for AAP) compared to those of other bio-aerogels reported in the literature for other drugs: 13-23% for alginate-based aerogels loaded with ketoprofen or benzoic acid [9], 16-80% for pectin-based aerogels loaded with ketoprofen or benzoic acid or theophylline [9,10], 15-27% for starch-based aerogels loaded with ketoprofen and benzoic acid [9] and 50-100% for cellulose-pectin aerogels loaded theophylline [11]. Neither density nor surface area of aerogels or cryogels had a marked influence on the loading efficiency within the intervals studied, but the latter are too narrow to deduce trends.

Finally, the impact of the non-solvents used for the solvent-exchange on the DLE was assessed on the APP-loaded aerogels. The DLE is similar whatever the non-solvent used (acetone, isopropanol, or ethanol), which seems logical considering that AAP has no particular affinity for any of them.

DLC (eq. II.10) follows the same trends as DLE (Table V.1), as expected. Dex-P-loaded aerogels presented a DLC around 0.25 – 0.50% lower than that of Dex-P-loaded cryogels 1.10 – 2.20%. AAP-loaded aerogels presented DLC between 1.49 and 1.95, similar to that of cryogels 1.66 and 2.49. A higher chitosan concentration results in a lower DLC due to a higher chitosan matrix mass. The obtained DLC of Dex-P are lower than that for other bio-aerogels, for example aerogels based on pectin (2-37%) [9,10,20], alginate (12-21%) [9,21], starch (10-25%) [9,21] or cellulose-pectin (2-4%) [11] due to the relatively low Dex-P concentration in the loading bath and relatively high concentrations of chitosan.

In an effort to limit the drug loss during the solvent exchange and Sc CO_2 drying steps, it was decided to add a step of pre-drying before the solvent exchange. The goal of this pre-drying step is to induce a small shrinkage of the network on the surface (inducing a pore size reduction and an increase of density) to limit the washing out of the drug, and possibly slow down the release of the AAP. Briefly, the AAP-loaded hydrogels were put in an oven at 60 °C and let drying for a defined time before applying the rest of the process. By changing the duration of pre-drying, the shrinkage could be controlled (Figure V.4). The shrinkage is induced by the collapse of the pores due to water evaporation. Of notice, the shrinkage should not be too high to avoid closing all pores which would result in trapping the drug inside chitosan sample. For this reason, the pre-drying time was not pushed over 17h as the resulting aerogel showed a morphology too close to the one of xerogel due to a loss of its mesoporous network. Different pre-drying times were evaluated, and the corresponding density, DLC and shrinkage obtained are summarized in Table V.2. As expected, the longer the pre-drying step, the higher the density as more shrinkage is observed, from 56 % for 4.5h to 92 % for 17h of pre-drying. Pictures of the samples in Figure V.4 show the color change from white to yellow and brown as the shrinkage increases. This

shrinkage indicates a collapse of the pores, thus a network densification and possibly a reduction of the pore size. As the DLE depends on the dried sample volume that highly depends on the pre-drying time, no comparison with the data without pre-drying could be made. Thus, only the DLC was calculated and compared with the one of aerogels prepared without pre-drying. The DLC seems to slightly increase with the pre-drying compared to the aerogel without pre-drying, confirming that this step allows to limit the drug loss during the solvent exchange and Sc CO_2 drying steps. No significant difference of DLC was observed between the pre-drying durations. This result may indicate that despite densification, the pores size is still too large to see an impact.

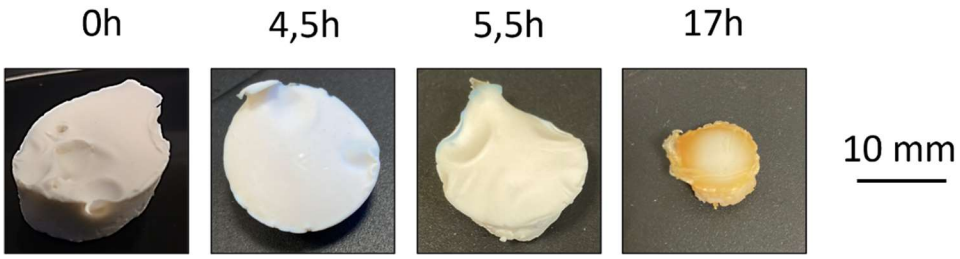

Figure V.4 : Pictures of the pre-dried aerogels as a function of pre-drying time.

*Table V.2: Bulk density, DLC and shrinkage rate of 6% AAP loaded aerogels with a step of pre-drying. * No duplicate*

Time of pre-drying (h)	Density (g/cm^3)	DLC (%)	Shrinkage (%)
0	0.12*	1.02*	22*
4.5	0.11 ± 0.015	1.26 ± 0.27	56 ± 14
6.5	0.14 ± 0.039	1.27 ± 0.19	51 ± 22
17	1.12 ± 0.68	1.17 ± 0.41	92 ± 6

1.2. Kinetics of dexamethasone sodium phosphate and ascorbic acid 2 phosphate release from chitosan aerogels and cryogels

Drug release studies were carried out for both drugs in PBS at pH 7.4 and 8.9, and 30°C (temperature of the skin). Of notice, in the first minutes after immersion of the samples in the buffer, a shrinkage of about 30% for aerogels and 20% for cryogels was observed, due to the pores collapse resulting from capillary pressure. No dissolution or erosion of the matrix was observed during all the release.

Figure V.5 shows Dex-P release kinetics, with Figure V.5a and b illustrating the Dex-P release as a function of the density of chitosan aerogels or cryogels, respectively. The comparison of Dex-P release from aerogel and cryogel of the same density is shown in Figure V.5c. The same is illustrated for AAP in Figure V.6.

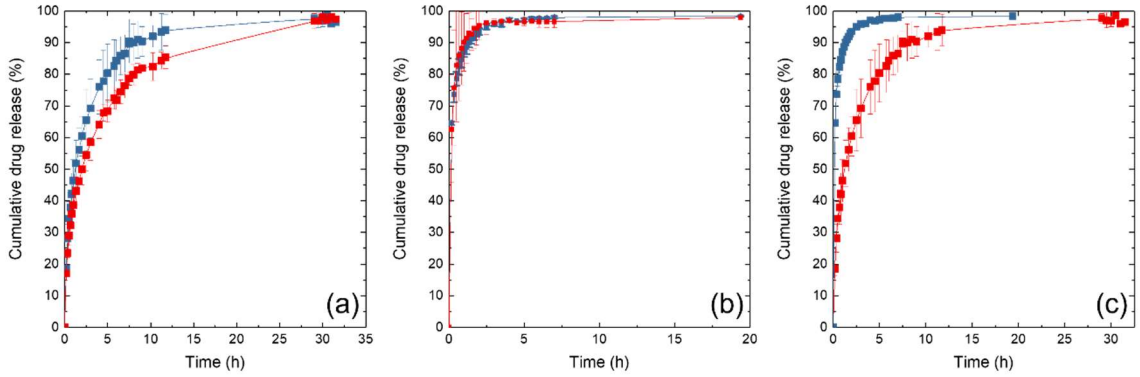

Figure V.5: The kinetics of Dex-P release in PBS at pH 7.4 and 30°C from:
(a) chitosan aerogels made with ethanol as non-solvent of density 0.06 g/cm³ (blue) and 0.11 g/cm³ (red),
(b) chitosan cryogels of density 0.06 g/cm³ (blue) and 0.09 g/cm³ (red),
(c) from aerogel (red) and cryogel (blue) of density 0.06 g/cm³.
Lines are given to guide the eye. Results are expressed as mean +/- standard deviation with n = 2. Corresponding error bars are provided and may be hidden by symbols in some cases.

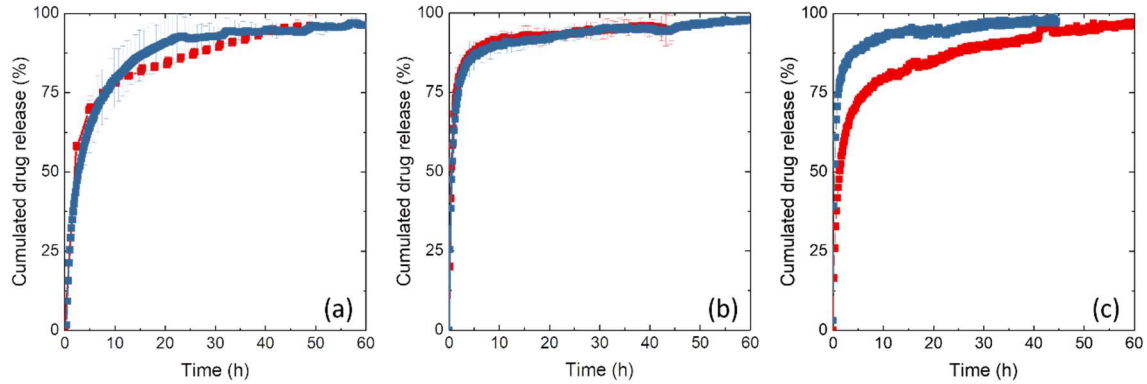

Figure V.6: Influence of the density ρ on the AAP release kinetics in PBS at pH 7.4 at 30°C:
(a) for aerogels with in blue a density of 0.16 g/cm³ and in red 0.084 g/cm³,
(b) for cryogels with a density of 0.10 in blue and 0.061 g/cm³ in red.
(c) Comparison of both materials: cryogels (ρ = 0.071 g/cm³) in blue and aerogel (ρ = 0.070 g/cm³) in red in PBS at pH 7.4 at 30°C.
Results are expressed as mean +/- standard deviation with n = 2. Corresponding error bars are provided and may be hidden by symbols in some cases.

The drugs release from aerogels and cryogels can be divided into two phases (Figure V.5, 6, 7a, 8, 9 and 10) with an initial burst release, followed by a slower release until plateauing. The duration of the burst stage is less than one hour for cryogels and lasts several hours (1.5 – 4h) for aerogels. On one hand, burst release is generally not desired as it can lead to high concentrations and thus toxicity for the surrounded tissues. It can also be an economical waste as it implies to change the dressing more frequently to preserve the drug effect [22]. On the other hand, a fast release may help reaching an effective concentration quickly, *e.g.,* for a pain-killer drug. In this respect, the toxicity and the efficiency of the drug-loaded materials will be studied (part 2. Biological *in vitro* tests).

Coming to the influence of the density, it can be observed that the higher the density of the aerogel, the slower the release, as expected [10], as drug diffusion is hindered by a denser network. However, density does not influence the release kinetics from chitosan cryogels in the interval studied

which may be the consequence of the very large macropores present in the cryogels. The influence of morphology on release kinetics is clearly visible in Figure V.5c and V.6c for aerogels and cryogels of the same density: the release is much faster from cryogels. This can be ascribed to the presence of smaller pores in aerogels (and thus higher tortuosity) in comparison with cryogels and as demonstrated in our previous work [16].

The influence of the non-solvent used during solvent exchange on AAP release kinetics from aerogels is shown in Figure V.7. Faster release was observed in the following order: ethanol, acetone, and isopropanol aerogel precursors, with 80% of the cumulated drug release achieved in 12h, 4h, and 3h, respectively. This difference in release kinetics cannot be explained by the density as all aerogels presented a similar density, but by the specific surface area S_A (Table V.1). The decrease in S_A for materials of the same density indicates an increase in the pore size as confirmed by the SEM images in Figure V.7, and thus faster AAP release kinetics. These differences in the structures are surprising as only a minimal impact of the non-solvent on the aerogel network was expected since the network is already coagulated when both are brought into contact.

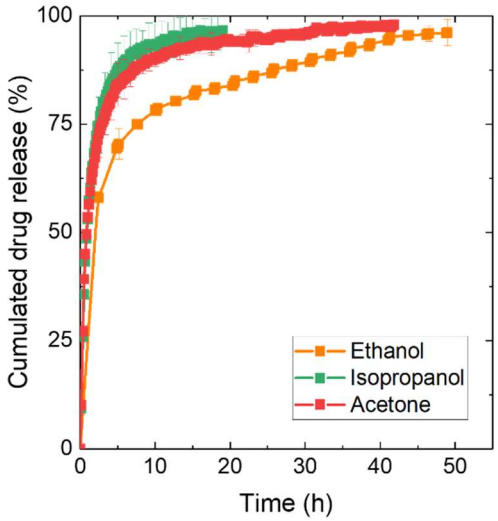

Figure V.7: Influence of non-solvent used for solvent exchange on the kinetics of the AAP release. Release in PBS at pH 7.4 and 30°C from chitosan aerogels made from solution at 5%wt/v chitosan. Results are expressed as mean +/- standard deviation with n = 2. Corresponding error bars are provided and may be hidden by symbols in some cases.

The influence of the pH of the release medium, 7.4 *vs* 8.9, on Dex-P release kinetics from aerogel and cryogel of the same density is illustrated in Figure V.8a and b. Similar results were obtained for AAP release, with the corresponding graphics shown in Figure V.9a and b. The drugs release from aerogels is slightly faster at pH 8.9 as compared to pH 7.4 (Figure V.8a and Figure V.9a): for example, 80% of Dex-P cumulative release from aerogels of density 0.06 g/cm^3 occurs in 3 h at pH 8.9 *vs* 5 h at pH 7.4. As mentioned above, due to the ionic interactions between protonated amino groups of chitosan and the negative charges of Dex-P and AAP, drugs are likely to be bound to the polymer. The higher the pH of the release medium, the weaker the ionic interactions and thus the faster the drug release. In contrast, the pH of the release medium practically does not influence the kinetics of Dex-P and AAP releases from cryogels (Figure V.8b and Figure V.9b). Although the same mechanism also occurs in cryogels, its effect on the drugs release is not noticeable because of the fast release caused by the large macropores and low specific surface area, making cryogels a less “sensitive” matrix. This

difference of pH sensitivity between cryogels and aerogels may be exploited for wound healing as for the latter, a faster release would be encountered during the inflammation step (pH 8.9) and a slower release in the healing stage (pH 7.4).

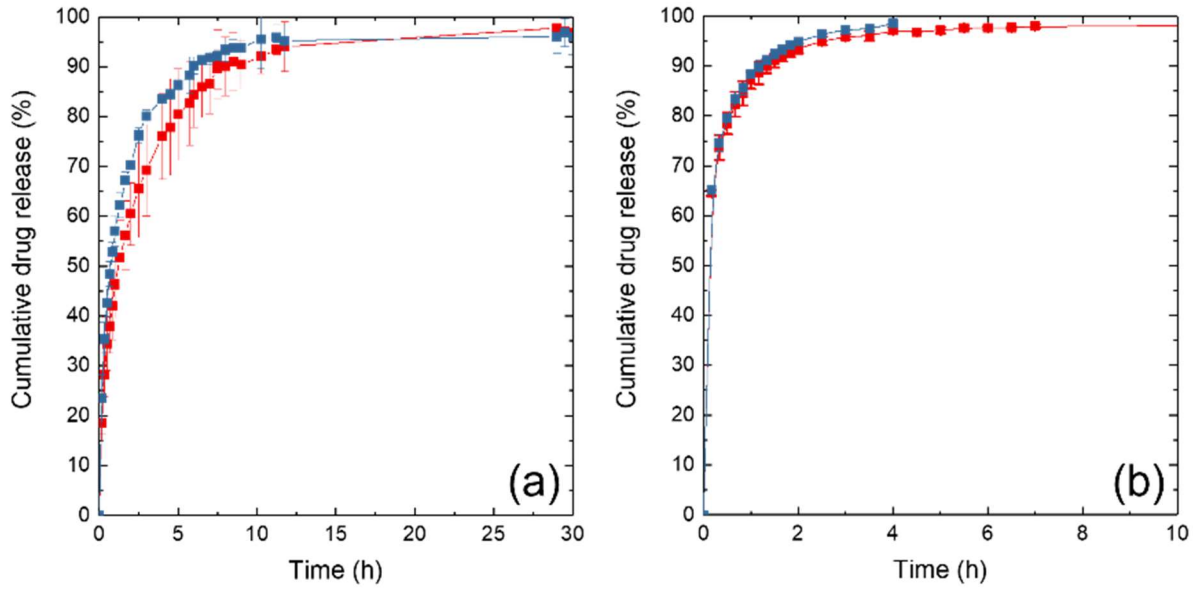

Figure V.8: Cumulative Dex-P release into PBS at 30°C as a function of time at pH 7.4 (red) and 8.9 (blue) from (a) chitosan aerogels (density 0.06 g/cm3) and (b) chitosan cryogels (density 0.06 g/cm3). Lines are given to guide the eye. Results are expressed as mean +/- standard deviation with n = 2. Corresponding error bars are provided and may be hidden by symbols in some cases.

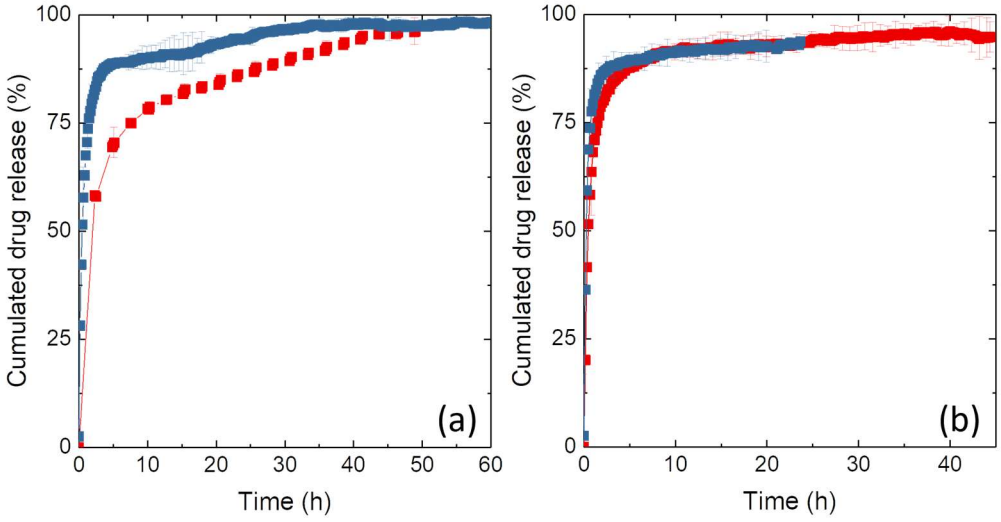

Figure V.9: Comparison of kinetics of AAP release for (a) aerogels (ρ = 0.084 g/cm³) and (b) cryogels (ρ = 0.057 g/cm³) in PBS at pH 7.4 (red) and 8.9 (blue) at 30°C. Results are expressed as mean +/- standard deviation with n = 2. Corresponding error bars are provided and may be hidden by symbols in some cases.

The addition of a pre-drying step modifies the kinetics of drug release as shown in Figure V.10 for AAP. The longer the pre-drying step duration, the slower the release, with 80% of the cumulated

AAP release reached in 6h without pre-drying against 7, 8 and 16 h for 4.5h, 6.5, and 17h of pre-drying, respectively. The slower release is induced by the higher density caused by the high shrinkage (Table V.2) and probably smaller pore size. A pre-drying step can therefore be added to slightly tune the kinetics of release, but as mentioned previously, drying should be limited to avoid drastic changes of the porosity and the risk of losing the advantage of having an aerogel.

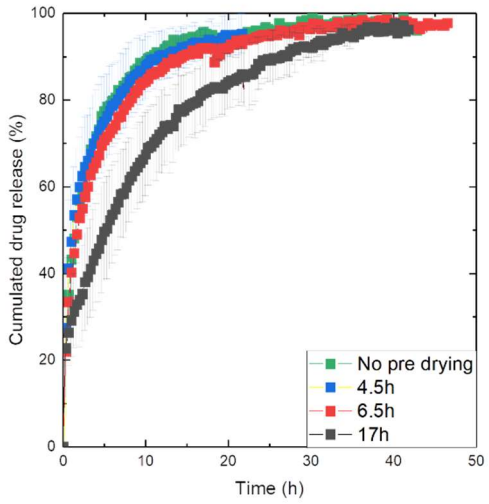

Figure V.10: Cumulated drug release for 6%wt/v aerogels loaded with AAP with pre-drying in PBS at pH 7.4 and 30°C. The pre-drying duration is indicated in the legend. Results are expressed as mean +/- standard deviation with n = 2. Corresponding error bars are provided and may be hidden by symbols in some cases.

1.3. Selection of a kinetics model to describe the release from chitosan aerogels and cryogels

It should be noted that when drug-loaded chitosan materials were immersed in the release medium, the samples were shrinking, and this occurred during the first few minutes after immersion. No dissolution of the matrix was observed, as expected in view of the insolubility of chitosan at pH 7.4 and 8.9. A sharp volume decrease can be one of the reasons for the fast increase of drug concentration in the release medium. Aerogels are shrinking more than cryogels, around 50 – 60% *vs* 10 – 40%, respectively (Figure V.11). The shrinkage is due to the capillary pressure occurring when a porous material is immersed in a liquid. Capillary pressure is defined by the Young-Laplace equation which predicts higher pressure, and thus enhanced pore collapse, for smaller pores. The difference in pore size explains why aerogels are shrinking more than cryogels.

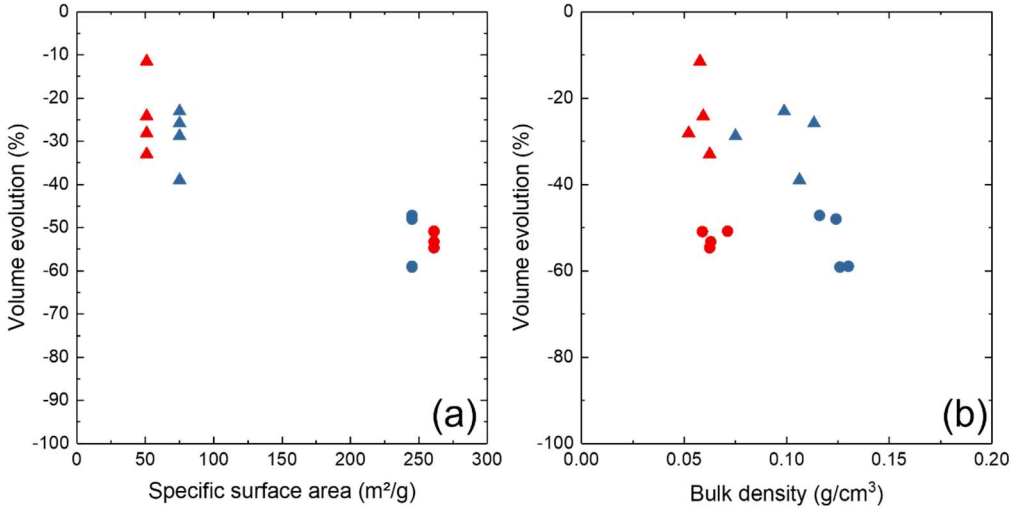

Figure V.11: Volume shrinkage of chitosan aerogels (circles) and cryogels (triangles) made from chitosan solutions of either 5 wt% (red) or 8 wt% (blue) as a function of (a) their specific surface area and (b) their density.

Various mathematical models are used to describe release kinetics from a solid polymer matrix [23]. Zero-order model is not applicable as the slope of cumulative release varies during the release. As chitosan aerogels are not swelling or dissolving in PBS, all models that consider polymer relaxation and/or erosion should not be considered, nor should be the Ritger-Korsmeyer-Peppas model which predicts an instantaneous burst release. The Higuchi model is not applicable either as the main requirement, *i.e.,* the initial drug concentration in the system to be higher than drug solubility, is not fulfilled. Thus, two models which may describe the first 60% of release were tested to fit experimental data of Dex-P and AAP release kinetics from chitosan aerogels: first-order kinetics and the Korsmeyer-Peppas approach. Both models were tested to describe the release kinetics of AAP but none of them presented a good fit. Regarding Dex-P release from cryogels, as 60 % of cumulated release from cryogels was reached very quickly, there were not sufficient data points for the modelling of the release kinetics. The two selected models were used to describe the Dex-P release from aerogels:

The first-order kinetic model predicts the following dependence of the cumulated release Q as a function of release time t:

$$\log(1 - Q) \sim A \times t \qquad \text{V.2}$$

where A is a constant. An example demonstrated in Figure V.12 shows that the fit of this model to experimental data is not good, and thus it will not be used.

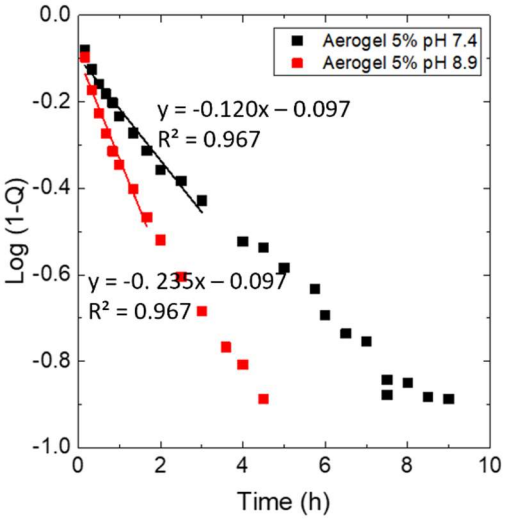

Figure V.12: Fit of experimental data by the first order model (lines) for Dex-P release into the bath at pH 7.4 (1) and 8.9 (2) from aerogels of density 0.064 g/cm³. Data correspond to mean values +/- standard deviations with n = 2.

Finally, the Korsmeyer-Peppas approach was applied to the first 60% of the cumulated Dex-P release:

$$Q \sim K \times t^n \qquad \text{V.3}$$

where *K* and *n* are constants. According to our experimental set-up (see Methods section), thin film approximation can be used. The results are shown in Figure V.13a, b and in Table V.3, demonstrating that Korsmeyer-Peppas approach provides the best fit to experimental data with the correlation coefficient R^2 = 0.99. In most cases the exponent *n* is around 0.45 corresponding to Fickian diffusion, as expected [23].

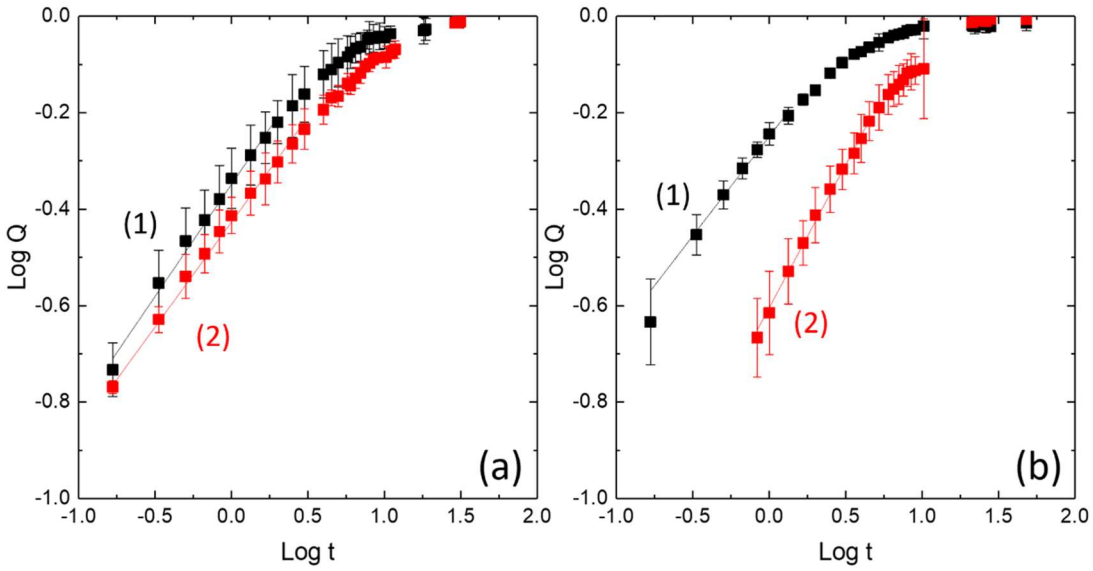

Figure V.13: Fit of experimental data by the Korsmeyer-Peppas model (lines) for Dex-P release into the bath of pH 7.4 (a) and 8.9 (b) from aerogels of density 0.064 (1) and 0.124 (2) g/cm³. Data correspond to mean values +/- standard deviations with n = 2).

Table V.3: Korsmeyer-Peppas fitting constants (eq.V.3) for the kinetics of Dex-P from chitosan aerogels into release media of different pH.

Chitosan aerogel density, g/cm^3	pH of release medium: 7.4			pH of release medium: 8.9		
	n	*K*	R^2	*n*	*K*	R^2
0.064	0.47	0.46	0.99	0.47	0.57	0.99
0.124	0.42	0.38	0.996	0.59	0.24	0.99

2. Biological in vitro tests

Having demonstrated that chitosan aerogels lead to longer release times with a pH dependence of potential interest for wound healing applications, they were further tested in terms of cytotoxicity. The non-cytotoxicity of chitosan itself is already clearly established [19,24], but considering that during the preparation of chitosan aerogels a solution of 4M NaOH and ethanol are used, the absence of cytotoxic effects needs to be checked.

Cytotoxicity of chitosan aerogels was assessed on the human dermal fibroblasts (HDF) and murine L929 fibroblasts. Controls were validated with no cytotoxicity for tissue culture polystyrene (TCPS) and the negative control material RM-C, but cytotoxicity for the positive control material RM-A (Figure V.14). For both cell lines, chitosan aerogels presented no cytotoxic effect with a cell viability above 70% which is the limit of cytotoxicity given by the norm NF EN ISO 10993-5 (2010), which confirms the results reported in the literature with similar process of aerogel preparation [8,25].

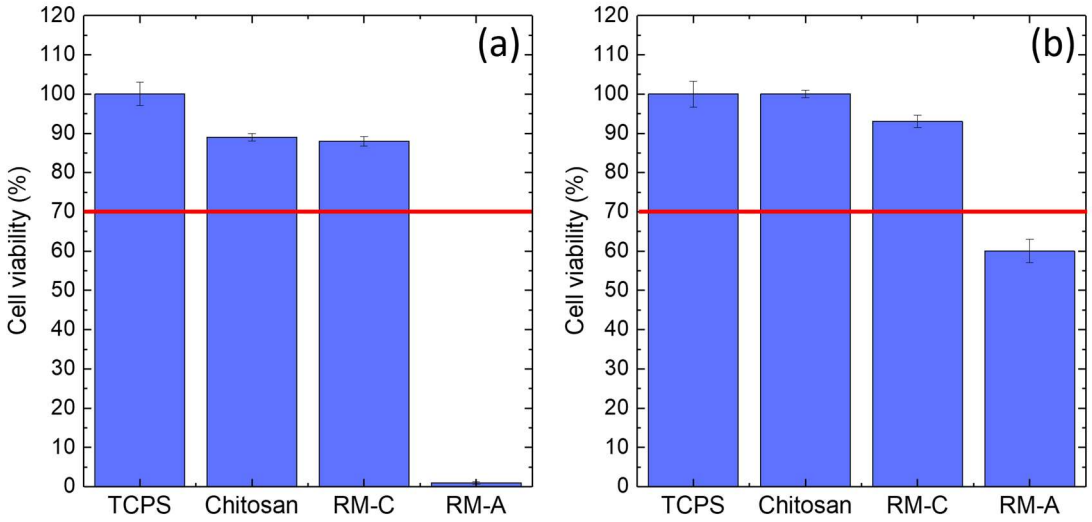

Figure V.14: CellTiter Glo assay of chitosan aerogels and controls on (a) L929 and (b) HDF. The red line is the limit of cytotoxicity given by the norm NF EN ISO 10993-5 (2010). Data correspond to mean values +/- standard deviations with n = 3).

AAP is expected to enhance healing through increased production of collagen [26], so the effect of AAP on collagen production by fibroblasts was evaluated through two tests, Sircol and Direct red 80, to detect the collagen at the different steps of its secretion by HDF cells. The tests were performed with extracts from AAP-loaded chitosan aerogels at different concentrations of AAP from 0 to 750 µg/mL. First, preliminary tests were carried out to establish the optimal concentration range of

free AAP able to induce collagen production (Figure V.15). An optimal range of 100 to 750 µg/mL was thus determined. All subsequent tests were therefore conducted in this range of concentration.

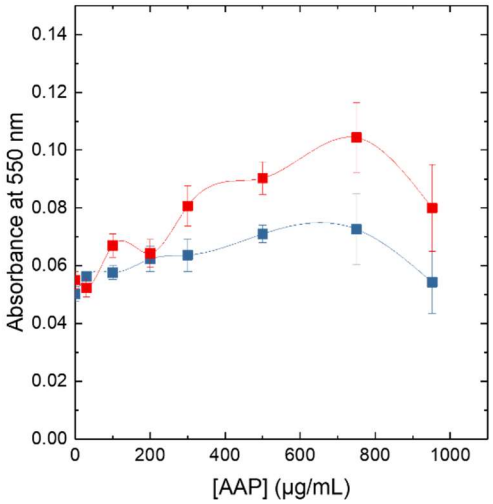

Figure V.15: Extracellular collagen detection after AAP treatment of 6 (blue) and 9 days (red) on HDF seeded at 10 000 cells/well with an FBS starvation of 24h before treatment. Data correspond to mean values +/- standard deviations with n = 3.

Sircol test was first used to quantify the extracellular soluble tropocollagen, the fundamental unit of collagen (Figure V.16a). Tropocollagen in contact with extracts of AAP-loaded aerogel or free AAP was quantified after 6 and 13 days. An increase of tropocollagen production with increasing concentrations of free AAP and with time was observed. A decrease of tropocollagen production at the highest AAP concentration after 13 days was observed. The scenario was rather different for the AAP released from the aerogel's extracts. At day 6, no increase of tropocollagen concentration was observed, whatever the concentration of AAP. After 13 days, tropocollagen production was higher for concentrations of released AAP superior to 300 µg/mL.

A Direct Red 80 test was run in parallel to detect and quantify extracellular collagen fibrils, formed from the association of tropocollagen in the collagen production process. HDF cells were put in contact with free AAP or AAP released from aerogels at different concentrations for 6 and 13 days (Figure V.16b). Below 300 µg/mL no impact of AAP, free or released form aerogels, was found on collagen production, for both times. For concentrations of AAP of 300 µg/mL or above, collagen production increased with increasing concentrations of AAP and increasing time, except for free AAP where the production of collagen decreased at with the highest AAP concentration (750 µg/mL) for both times. In this range of AAP concentrations, it was also found that collagen production was higher for cells in contact with AAP released from chitosan aerogels compared to free AAP. This result may indicate a possible beneficial effect of the combination of chitosan and AAP on collagen production.

Taken together, these results confirm that AAP released from aerogels is responsible for a higher production of collagen for AAP concentrations above 300 µg/mL.

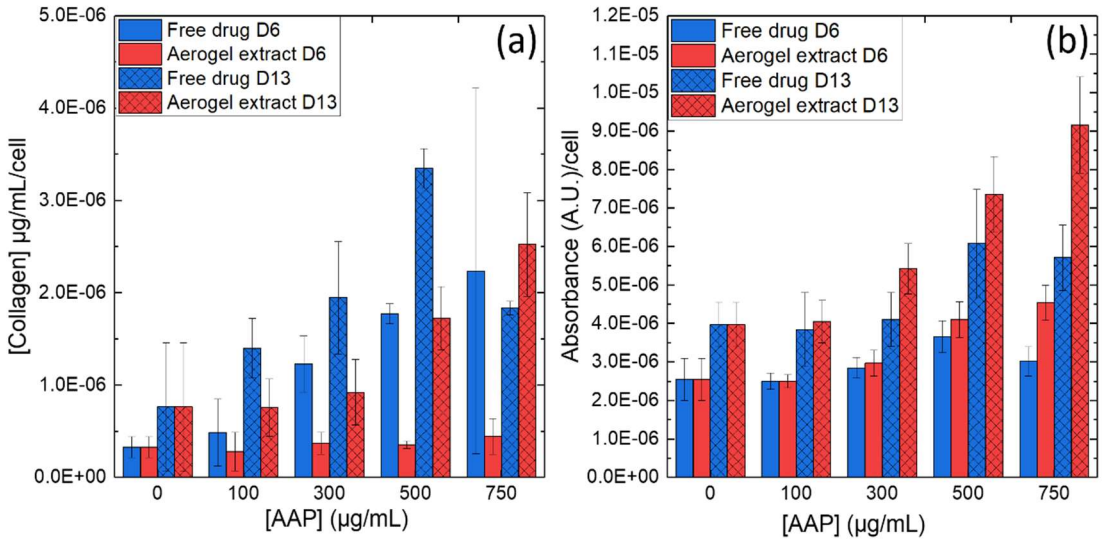

Figure V.16: Quantification of collagen by (a) Sircol assay (n=2) and (b) Direct Red 80 (n=3) on HDF cells after 6 and 13 days in contact with AAP-loaded chitosan aerogel extracts and free AAP.

Finally, a scratch test was performed on HDF cells to assess the ability of AAP-loaded aerogels to accelerate the cell migration and thus, the wound closure (Figure V.17). Whatever the conditions, cells were able to close the scratch, however, clear differences in the closure kinetics were observed. The cells in the absence of AAP (TCPS), in contact with pristine culture medium, or in contact with the extract from non-loaded aerogels, were slower to close the scratch compared to the medium with AAP. In more details, for AAP concentrations of 750 µg/ml, complete scratch closure was observed after 33 h for cells in contact with free AAP or with AAP from aerogel extracts, against 48 h for cells without AAP. No difference in wound closure was observed between free AAP and AAP from aerogels extracts, showing no benefice by the combination of chitosan and AAP contrary to what was observed for Direct Red 80 test.

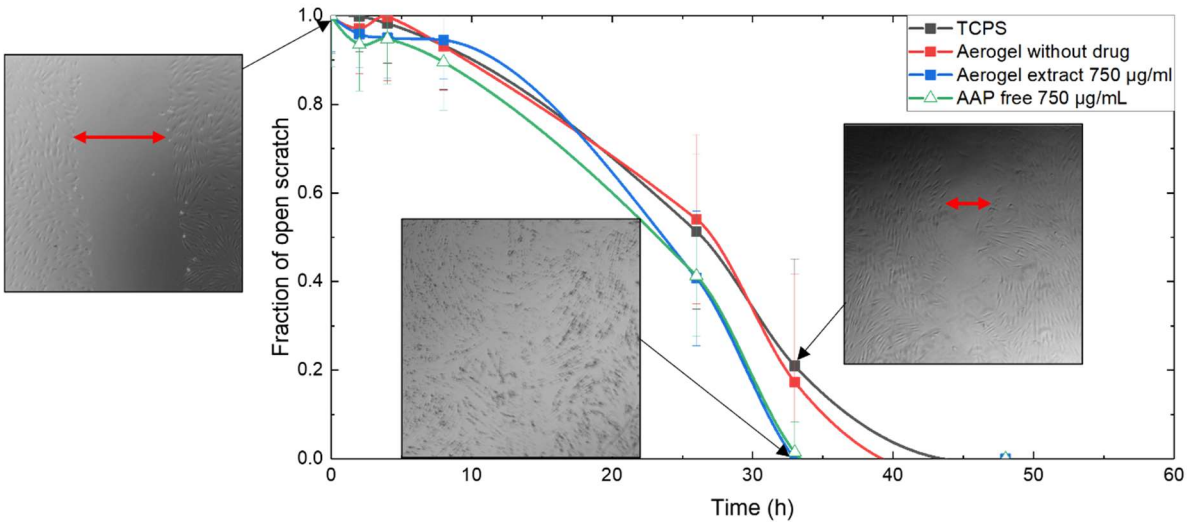

Figure V.17: Scratch test on HDF cells in contact with TCPS, non-loaded aerogels, 750 µg/mL of AAP loaded in aerogel and 750 µg/mL of free AAP, with pictures of the scratch (n=2). The red arrow indicates the width of the scratch. Standard deviation is the average of 18 to 30 measurements of the scratch width.

Conclusions

Chitosan aerogels and cryogels were loaded with Dex-P and AAP and the release kinetics from materials of different densities and in medium of pH 7.4 and 8.9 was studied. DLE in cryogels was three times higher than in aerogels and exceeded 200% for Dex-P loading. The DLE of AAP-loaded porous dried gels was between 280 and 450%. These high DLE are due to the ionic interactions between positively charged amino groups of chitosan and the negatively charged phosphate group of dexamethasone phosphate or ascorbic acid 2-phosphate. DLE of Dex-P-loaded aerogels is high, around 70%, but it is lower than 100%, likely due to: potential solubility of the drug in the water-ethanol mixture during the step of solvent exchange, “mechanical” washing-out during supercritical drying, and fewer interactions of chitosan with Dex-P compared to AAP.

The release of Dex-P and AAP from porous chitosan materials, aerogels and cryogels, were investigated in two buffer solutions: one at pH 7.4, approximating the pH value of a chronic wound in the healing stage, and one at pH 8.9, corresponding to the pH value of a chronic wound in the inflammation stage. The AAP and Dex-P release kinetics from chitosan aerogels and cryogels was shown to depend on material density and morphology. Slower release was recorded from aerogels of higher density, as expected; whereas cryogel density did not influence the release kinetics within the interval studied. At a same material density, the release of Dex-P and AAP from cryogels was faster than from aerogels, which was ascribed to the different material morphologies: large pores and channels in cryogels *vs* smaller pores with high tortuosity in aerogels. Aerogels exhibited a faster release at pH 8.9 than at pH 7.4 due to decreased ionic interactions between chitosan and the drugs. The Korsmeyer-Peppas model showed the best fit to experimental data for Dex-P release from aerogels, no model fitted AAP release from aerogel or both drugs release from cryogels.

Chitosan aerogels were non-cytotoxic towards HDF and L929 cells. Finally, it was shown that AAP loaded in aerogels can increase the production of collagen similarly to free AAP and lead to faster wound closure compared to non-loaded aerogel, making such AAP-loaded chitosan aerogels promising candidates as wound dressing.

Overall, it was demonstrated that Dex-P and AAP-loaded chitosan porous materials can be made with various porosity and morphology, which results in different release kinetics. Moreover, the absence of cytotoxicity, the improved collagen production and faster healing on scratch test are making these materials promising for biomedical applications.

References

[1] T. Barroso, R. Viveiros, T. Casimiro, A. Aguiar-Ricardo, Development of dual-responsive chitosan–collagen scaffolds for pulsatile release of bioactive molecules, J. Supercrit. Fluids. 94 (2014) 102–112. https://doi.org/10.1016/j.supflu.2014.07.005.

[2] M.M. Alsmadi, R.M. Obaidat, M. Alnaief, B.A. Albiss, N. Hailat, Development, In Vitro Characterization, and In Vivo Toxicity Evaluation of Chitosan-Alginate Nanoporous Carriers Loaded with Cisplatin for Lung Cancer Treatment, AAPS PharmSciTech. 21 (2020) 191. https://doi.org/10.1208/s12249-020-01735-8.

[3] S. Wei, Y.C. Ching, C.H. Chuah, Synthesis of chitosan aerogels as promising carriers for drug delivery: A review, Carbohydr. Polym. 231 (2020) 115744.

[4] E.S. Dragan, M.V. Dinu, Advances in porous chitosan-based composite hydrogels: Synthesis and applications, React. Funct. Polym. 146 (2020) 104372. https://doi.org/10.1016/j.reactfunctpolym.2019.104372.

[5] U. Stumpf, M. Michaelis, D. Klassert, J. Cinatl, J. Altrichter, J. Windolf, J. Hergenröther, M. Scholz, Selection of proangiogenic ascorbate derivatives and their exploitation in a novel drug-releasing system for wound healing: Pro wound healing effects of ascorbic acid-2-phosphate, Wound Repair Regen. 19 (2011) 597–607. https://doi.org/10.1111/j.1524-475X.2011.00718.x.

[6] S. Takamizawa, Effects of ascorbic acid and ascorbic acid 2-phosphate, a long-acting vitamin C derivative, on the proliferation and differentiation of human osteoblast-like cells, Cell Biol. Int. 28 (2004) 255–265. https://doi.org/10.1016/j.cellbi.2004.01.010.

[7] C.A. García-González, M. Alnaief, I. Smirnova, Polysaccharide-based aerogels—Promising biodegradable carriers for drug delivery systems, Carbohydr. Polym. 86 (2011) 1425–1438. https://doi.org/10.1016/j.carbpol.2011.06.066.

[8] C. López-Iglesias, J. Barros, I. Ardao, F.J. Monteiro, C. Alvarez-Lorenzo, J.L. Gómez-Amoza, C.A. García-González, Vancomycin-loaded chitosan aerogel particles for chronic wound applications, Carbohydr. Polym. 204 (2019) 223–231. https://doi.org/10.1016/j.carbpol.2018.10.012.

[9] C.A. García-González, M. Jin, J. Gerth, C. Alvarez-Lorenzo, I. Smirnova, Polysaccharide-based aerogel microspheres for oral drug delivery, Carbohydr. Polym. 117 (2015) 797–806. https://doi.org/10.1016/j.carbpol.2014.10.045.

[10] S. Groult, S. Buwalda, T. Budtova, Tuning bio-aerogel properties for controlling theophylline delivery. Part 1: Pectin aerogels, Mater. Sci. Eng. C. 126 (2021) 112148. https://doi.org/10.1016/j.msec.2021.112148.

[11] S. Groult, S. Buwalda, T. Budtova, Tuning bio-aerogel properties for controlling drug delivery. Part 2: Cellulose-pectin composite aerogels, Biomater. Adv. 135 (2022) 212732. https://doi.org/10.1016/j.bioadv.2022.212732.

[12] M. Shamim, S. Baki, Diffusion measurements in aqueous L-ascorbic acid solutions, Aust. J. Chem. 33 (1980) 1857. https://doi.org/10.1071/CH9801857.

[13] R. Gavillon, T. Budtova, Kinetics of Cellulose Regeneration from Cellulose−NaOH−Water Gels and Comparison with Cellulose− *N* -Methylmorpholine- *N* -Oxide−Water Solutions, Biomacromolecules. 8 (2007) 424–432. https://doi.org/10.1021/bm060376q.

[14] R. Sescousse, R. Gavillon, T. Budtova, Aerocellulose from cellulose–ionic liquid solutions: Preparation, properties and comparison with cellulose–NaOH and cellulose–NMMO routes, Carbohydr. Polym. 83 (2011) 1766–1774. https://doi.org/10.1016/j.carbpol.2010.10.043.

[15] S. Groult, Advanced materials for thermal insulation and drug delivery applications, Université PSL, 2019.

[16] C. Chartier, S. Buwalda, H. Van Den Berghe, B. Nottelet, T. Budtova, Tuning the properties of porous chitosan: Aerogels and cryogels, Int. J. Biol. Macromol. 202 (2022) 215–223. https://doi.org/10.1016/j.ijbiomac.2022.01.042.

[17] H. Hao, J. Wang, Y. Wang, Solubility of Dexamethasone Sodium Phosphate in Different Solvents, J. Chem. Eng. Data. 49 (2004) 1697–1698. https://doi.org/10.1021/je0498412.

[18] S. Groult, S. Buwalda, T. Budtova, Pectin hydrogels, aerogels, cryogels and xerogels: Influence of drying on structural and release properties, Eur. Polym. J. 149 (2021) 110386. https://doi.org/10.1016/j.eurpolymj.2021.110386.

[19] M.N.V.R. Kumar, R.A.A. Muzzarelli, C. Muzzarelli, H. Sashiwa, A.J. Domb, Chitosan Chemistry and Pharmaceutical Perspectives, Chem. Rev. 104 (2004) 6017–6084. https://doi.org/10.1021/cr030441b.

[20] A. Veronovski, G. Tkalec, Ž. Knez, Z. Novak, Characterisation of biodegradable pectin aerogels and their potential use as drug carriers, Carbohydr. Polym. 113 (2014) 272–278. https://doi.org/10.1016/j.carbpol.2014.06.054.

[21] T. Mehling, I. Smirnova, U. Guenther, R.H.H. Neubert, Polysaccharide-based aerogels as drug carriers, J. Non-Cryst. Solids. 355 (2009) 2472–2479. https://doi.org/10.1016/j.jnoncrysol.2009.08.038.

[22] D. Bhowmik, H. Gopinath, B.P. Kumar, S. Duraivel, K.S. Kumar, Controlled release drug delivery systems, Pharma Innov. 1 (2012) 24.

[23] J. Siepmann, F. Siepmann, Mathematical modeling of drug delivery, Int. J. Pharm. 364 (2008) 328–343. https://doi.org/10.1016/j.ijpharm.2008.09.004.

[24] M. Dash, F. Chiellini, R.M. Ottenbrite, E. Chiellini, Chitosan—A versatile semi-synthetic polymer in biomedical applications, Spec. Issue Biomater. 36 (2011) 981–1014. https://doi.org/10.1016/j.progpolymsci.2011.02.001.

[25] M. Alnaief, R.M. Obaidat, M.M. Alsmadi, Preparation of Hybrid Alginate-Chitosan Aerogel as Potential Carriers for Pulmonary Drug Delivery, Polymers. 12 (2020) 2223. https://doi.org/10.3390/polym12102223.

[26] R.-I. Hata, H. Senoo, L-ascorbic acid 2-phosphate stimulates collagen accumulation, cell proliferation, and formation of a three-dimensional tissuelike substance by skin fibroblasts, J. Cell. Physiol. 138 (1989) 8–16. https://doi.org/10.1002/jcp.1041380103.

Conclusions and perspectives

The aim of this work was to develop porous biobased dressings for chronic wounds. To fulfill this aim, we made chitosan porous materials, aerogels and cryogels, and tuned the parameters of their preparation and understood the correlation between these parameters and the final material structure and properties. These materials were made by chitosan dissolution followed by coagulation and drying in different conditions. We focused on a better understanding of coagulation process, which was required to give new opportunities in material processing. Finally, characterization of the materials for biomedical applications was needed, with the drug release kinetics and testing material biomedical properties. Three chapters in this manuscript present these results.

In the chapter 3, which is the first chapter devoted to the results obtained in this work, we studied the kinetics of coagulation of chitosan solutions in NaOH-water as a function of the chitosan concentration via i) optical observations of the evolution of the coagulation front in a droplet, and ii) by the evolution of the elastic modulus. Three phases were visible via optical observations, an initiation phase, a phase with more or less constant coagulation speed and an acceleration phase, the latter due to the geometry of the sample. Higher chitosan concentration induces an increase of the coagulation rate thanks to a closer chain proximity. Fick approach was applicable till 60% of the coagulation process with optical follow-up. Using DMTA, a coagulation coefficient was introduced. Using data obtained with optical observations, we were able to predict the evolution of the elastic modulus in time. This prediction allows having a better control of the mechanical properties of coagulating chitosan. Thus, it gives the possibility to control processing, like 3D printing, of chitosan solutions with non-optimized rheological properties.

Chapter 4 was dedicated to the preparation of chitosan cryo- and aerogels monoliths that were made by non-solvent induced phase separation, without any crosslinker, and characterization of the dry materials. The understanding of the correlation between the process parameters and the material properties is a key to tune the material properties. The main parameter to vary the properties is the drying mode: supercritical drying allows obtaining mesoporous materials with a high porosity and high specific surface area while lyophilization leads to materials with high porosity but low specific surface area. Aerogels seem to be more adapted for a wound dressing application as the small pore size prevents cell colonization.

Mechanical properties of materials were characterized. Density is the main parameter to tune the mechanical properties. Elasticity of aerogels and cryogels was reasonably close to skin but improvements still should be made. The influence of moisture on the mechanical properties was evaluated. The absorption of water molecules plays a plasticizer role; drying induces shrinkage and increases the density of the material. The coagulation “direction”, isotropic vs anisotropic, also influences aerogel mechanical properties.

In the last chapter, the release kinetics of dexamethasone-phosphate (Dex-P) and of ascorbic acid 2-phosphate (AAP) from porous chitosan materials, aerogels and cryogels, was investigated in two buffer solutions: at pH 7.4, approximating the pH value of a chronic wound in the healing stage, and at pH 8.9, corresponding to the pH value of a chronic wound in the inflammation stage. The drug loading efficiency was high, from 70% to 450%, in particular for aerogels. This large range can be explained by two factors:

- In aerogels, the drug is slightly washed out during the solvent exchange and the supercritical drying,
- Ionic interactions between the negatively charged phosphate group of the drugs and the positively charged amine groups of chitosan allows obtaining DLE above 100%.

The release kinetics from aerogels and cryogels depends on material density and morphology. Slower release was observed for aerogels of higher density, whereas cryogel density did not influence the release kinetics as the large pore size has a more important effect on the release. At the same material density, the important parameter is the morphology: cryogels possessed a faster release than aerogels thanks to their large pore size. The pH of medium has an influence on the release with a faster release from aerogel at pH 8.9 compared to pH 7.4 due to the decrease of ionic interactions between the drugs and the chitosan material at higher pH. It is possible to tune the release of a drug from chitosan aerogel by adding a pre-drying step, increasing the density of the material, and thus slowing the release. The Korsmeyer-Peppas model showed the best fit to experimental data for Dex-P release from aerogels, but no model fitted AAP release nor cryogels loaded with both drugs.

Chitosan aerogels presented no cytotoxicity towards HDF and L929 cells. Biological *in-vitro* tests showed that AAP-loaded aerogels increase the collagen production and lead to a faster wound closure compared to non-loaded aerogels, making these materials promising for biomedical applications.

Overall, we first improve the comprehension of the coagulation process of the chitosan solution by monitoring optical and mechanical properties in time. We proposed an equation to predict the mechanical properties of chitosan during coagulation. Then, we made chitosan aero- and cryogels without crosslinker and studied the influence of the process parameters on their final properties. The materials were suitable for drug delivery with the possibility to tune the release kinetics. Chitosan aerogels were non-cytotoxic, they can improve the wound healing and increase the collagen production. With a careful selection of the process parameters, we were able to make chitosan aerogels suitable for a wound dressing application.

A lot of perspectives can be drawn from this study. The chapter 3 gives a better understanding of the evolution of the mechanical properties during coagulation. Observations similar to those obtained with DMTA could be made with a rheometer to measure the viscosity and the moduli evolution during coagulation. 3D printing of chitosan solution with simultaneous coagulation could be performed to assess the validity of our results and identify the new problematics. These experiments were started but not completed because of time constraints. Another way to print chitosan solution would be to improve the rheological properties of the solution by mixing it with another polymer that can be easily removed afterward [1]. This work is ongoing in collaboration with colleagues from Helsinki university; aerogels obtained with this method should be characterized.

Mechanical properties of aerogels and cryogels could be improved to make them more elastic to be more comfortable for patients. To achieve this aim, reticulation could be made. The crosslinking rate should be well controlled, to be not too low to have enough reticulation points to make the material elastic, but not too high to completely block chain movements and obtain moduli values that are too high compared to the skin. However, the reticulation on chitosan amine groups may reduce the antibacterial properties of chitosan. To avoid this problem, genipin could be a good candidate for chitosan reticulation thanks to its antibacterial properties [2]. We tested the mechanical properties of chitosan cryogels and aerogels with uniaxial compression in dry state, however, in exudative wound, the dressing will absorb exudate, and this will change the mechanical properties of the material. Uniaxial compression could be performed on aerogels after absorption of simulated wound exudate to characterize the evolution of the mechanical properties and assess if the materials are still adapted to a wound healing application. A fundamental study on the local deformation at microscopic scale during indentation tests in SEM could be performed and the mechanical behavior of the material could be determine.

Following the *in vitro* biomedical tests, an *in vivo* study may be envisioned. This study could be performed on pigs to have a skin structure similar to the human one. Wound healing could be evaluated through different ways: the rate of closure of the wound with pictures of the wound taken at different times during healing, biological tests to detect the presence and to quantify proteins or immunomarkers characteristics of wound healing, and by the recovery of mechanical properties of the skin compared to a healthy one with biaxial tensile stress.

References

[1] C. Hu *et al.*, « A thermogelling organic-inorganic hybrid hydrogel with excellent printability, shape fidelity and cytocompatibility for 3D bioprinting », *Biofabrication*, vol. 14, n° 2, p. 025005, avr. 2022, doi: 10.1088/1758-5090/ac40ee.

[2] R. Muzzarelli, M. El Mehtedi, C. Bottegoni, A. Aquili, et A. Gigante, « Genipin-Crosslinked Chitosan Gels and Scaffolds for Tissue Engineering and Regeneration of Cartilage and Bone », *Mar. Drugs*, vol. 13, n° 12, p. 7314-7338, déc. 2015, doi: 10.3390/md13127068.

List of figures

List of tables

RÉSUMÉ

Le vieillissement de la population engendre des problèmes de santé majeurs, comme les plaies chroniques, pouvant engendrer la mort. Afin de traiter ces plaies, nous avons étudié deux types de matériaux poreux : les aérogels, obtenus par séchage au CO2 supercritique, qui ont une double porosité méso- et macro- (2 nm -2 µm) et une haute surface spécifique (>100 m²/g), et les cryogels, obtenus par lyophilisation, qui présentent des macropores (> 50 nm). Ces matériaux ont été obtenus à partir de chitosane, un polymère biosourcé, ayant des propriétés antibactériennes. Nous avons défini une gamme de propriétés à viser pour le traitement de plaies et nous avons étudié le lien entre le procédé de fabrication du matériau poreux et ses propriétés finales. Les matériaux optimisés ont ensuite été testés dans le contexte de l'application, avec un focus sur les aspects de chargement et de libération de principes actifs, ainsi que de l'impact de ces principes actifs sur la production de collagène.

MOTS CLÉS

Aérogel; cryogel; chitosane ; matériaux poreux; libération contrôlée de principes actifs ; pansements pour plaies

ABSTRACT

The aging of the population is leading to major health problems, such as chronic wounds, that can be fatal. To treat these wounds, 2 types of porous materials are studied: aerogels obtained by a drying with supercritical CO2, with a meso- and macroporosity (2 nm – 2 µm) and a high specific surface area (>100 m²/g), and cryogels, made via freeze-drying, and that are microporous material (> 50nm). These porous materials are based on chitosan, a biobased polymer with antibacterial properties. The goal of this work is to define a range of targeted properties and then understand the correlation between the process and the final material structure/properties to develop a porous material suitable for wound healing. Optimized materials are tested in relation with the targeted biomedical application in terms of drug loading and drug release, as well as collagen production.

KEYWORDS

Aerogel; cryogel; chitosan; porous materials; controlled drug release; wound dressing